RIDE VIBRATION AND COMPACTION DYNAMICS OF VIBRATORY SOIL COMPACTORS

Ario Kordestani, Eng.

A Thesis

in

the Department

of

Mechanical and Industrial Engineering

Presented in Partial Fulfillment of the Requirements

for the Degree of Master of Applied Science

in Mechanical Engineering at

Concordia University

Montreal, Quebec, Canada

April 2010

© Ario Kordestani, 2010

CONCORDIA UNIVERSITY

SCHOOL OF GRADUATE STUDIES

This is to certify that the Thesis prepared,

By: **Ario Kordestani**

Entitled: "**Ride Vibration and Compaction Dynamics of Vibratory**

Soil Compactors"

and submitted in partial fulfillment of the requirements for the Degree of

Master of Applied Science (Mechanical Engineering)

complies with the regulations of this University and meets the accepted standards

with respect to originality and quality.

Signed by the Final Examining Committee:

_____	Chair
Dr. R. Wuthrich	
_____	Examiner
Dr. A.K.W. Ahmed	
_____	Examiner
Dr. C. Alecsandru	External
Building, Civil and Environmental Engineering	
_____	Supervisor
Dr. S. Rakheja	
_____	Co-Supervisor
Dr. P. Marcotte	

Approved by: _____

Dr. A.K.W. Ahmed, MASc Program Director
Department of Mechanical and Industrial Engineering

_____
Dean Robin Drew
Faculty of Engineering & Computer Science

Date: _____

ABSTRACT

Ride Vibration and Compaction Dynamics of Vibratory Soil Compactors

Ario Kordestani, Eng.

This study explores the ride dynamics of typical North-American vibratory soil compactors via analytical and experimental methods. In-plane ride dynamic models of the vehicle are formulated to evaluate ride vibration responses of the vehicle in the transit mode on undeformable terrain surfaces with the roller vibrator off. An in-plane dynamic model is also formulated to study the compaction mode dynamics at lower speeds on elasto-plastic soil subject to roller induced vibration. Field measurements were conducted to characterize the ride vibration environments during the two modes of operations.

The ride dynamic models of the soil compactor are thus analyzed to study its whole-body vibration environment while operating on undeformable random terrain surfaces. The modeling of the equipment in compaction mode of operation, however, gives insight over the efficiency of the compactor as a tool aimed to perform compaction of soil layers by plastic deformation (compression). The ride vibration environment of the vehicle and its compaction capability is subsequently assessed using the ISO-2631-1 (1997) guidelines and commonly accepted compaction criteria, respectively. The validity of the proposed model is demonstrated by comparing the model responses with the measured data. Comprehensive parametric analyses were subsequently performed to study the influences of variations in various design and operating parameters on the ride quality and the compaction efficiency of the mobile equipment. The results of the study are utilized to propose desirable design and operating parameters of the vibratory soil compactor for enhancement of its ride vibration environment and compaction performance.

Acknowledgments

A ma moitié sans l'aide

de qui, rien de tout cela

n'aurait été possible

Table of contents

LIST OF TABLES

LIST OF FIGURES

xv

NOMENCLATURE

A_0 Nominal amplitude of the drum vibrator (mm)

$A(8)$ Eight-hour equivalent vibration exposure (m/s^2)

$a(t)$ Measured acceleration in time domain (m/s^2)

a_k rms acceleration along axis k (m/s^2)

a_{wk} Frequency-weighted acceleration due to vibration along axis k (m/s^2)

C_{sp} Constant of surface profile (*of variable units*)

c_a^z Vertical damping coefficient of axle suspension (Ns/m)

c_{cj}^k Damping coefficients of operator station (cab or open platform) mounts along axis k, with $j = f, r$ referring to the front and rear mounts (Ns/m)

c_d^k Damping coefficient of drum mounts along axis k (Ns/m)

c_{ej}^k Damping coefficients of engine mounts along axis k, with $j = f, r$ referring to the front and rear mounts (Ns/m)

c_h^z Damping coefficient of seat cushion along the vertical axis (Ns/m)

c_t^k Damping coefficient of rear tires along axis k (Ns/m)

c_{se} Equivalent viscous damping of the soil (Ns/m)

c_s^z Damping coefficient of seat suspension along the vertical axis (Ns/m)

e Eccentricity of the vibrator rotating mass (m)

$F(t)$ Vertical projection of vibrator centrifugal force, compaction model excitation (N)

F_a^z Vertical force developed by the axle suspension (N)

F_{cent} Centrifugal force of the drum vibrator (N)

F_{cj}^k Forces developed by the operator station (cab or open platform) mounts along axis k, with $j = f, r$ referring to the front and rear mounts (N)

F_d^k Force developed by the drum mounts along axis k (N)

F_{ej}^k Forces developed by the engine mounts along axis k, with $j = f, r$ referring to the front and rear mounts (N)

F_h^z Force due to seat cushion along the vertical axis (N)

F_s^k Soil reaction force along axis k (N)

F_s Dynamic reaction force of the soil under vibratory compaction (N)

$F_{s\,Tot}$ Total soil reaction force with dynamic and static components (N)

F_s^z Force due to seat suspension along the vertical axis (N)

F_t^k Force developed by the tires along axis k (N)

f Temporal vibration frequency (Hz)

$f_{n\,d}^*$ Natural frequency of the uncoupled 1-DOF drum

$f_{n\,s}^*$ Nominal natural frequency of the uncoupled 2-DOF suspension seat (Hz)

f_s^z Friction damping of seat suspension along the vertical axis (N)

f_v Frequency of drum vibrator (Hz)

h_a Vertical distance between the rear axle centre and the vehicle body c.g. (m)

h_b Vertical distance between the vehicle body c.g. and the ground (m)

h_b^* Vertical distance between equivalent vehicle body c.g. and ground (m)

h_c Vertical distance between the cab/platform c.g. and the vehicle body c.g. (m)

h_{cm} Vertical distance of the cab/platform c.g. from its isolation mounts (m)

h_d Vertical distance between the drum centre and the vehicle body c.g. (m)

h_e Vertical distance between the engine group c.g. and the vehicle body c.g. (m)

h_{em} Vertical distance of the engine group c.g. from its isolation mounts (m)

h_t Vertical distance between the tire-soil contact and the vehicle body c.g. (m)

I_b Vehicle body pitch moment of inertia (kgm^2)

I_b^* Equivalent vehicle body pitch moment of inertia in the 2-DOF ride model (kgm^2)

I_c Operator-station (cab or open platform) pitch moment of inertia (kgm^2)

I_e Engine group pitch moment of inertia (kgm^2)

K_k Multiplying factors, for assessment of vibration along axis k, per ISO 2631-1

k_a^z Vertical stiffness of axle suspension (N/m)

k_{cj}^k Stiffness of operator station (cab or open platform) mounts along axis k, with $j = f, r$ referring to the front and rear mounts (N/m)

k_d^k Stiffness of drum mounts along axis k (N/m)

k_{ej}^k Stiffness of engine mounts along axis k, with $j = f, r$ referring to the front and rear mounts (N/m)

k_h^z Stiffness of seat cushion along the vertical axis (N/m)

k_{se} Elastic stiffness of the soil (N/m)

k_{sp} Plastic stiffness of the soil (N/m)

k_s^* Equivalent stiffness of the soil (N/m)

k_s^z Stiffness of seat suspension along the vertical axis (N/m)

k_{st}^z Stiffness of seat stops along the vertical axis (N/m)

k_t^k Stiffness of rear tires along axis k (N/m)

l_c Longitudinal distance of the cab/platform c.g. from the vehicle body c.g. (m)

l_{cj} Longitudinal distances of cab/platform mounts from the cab/platform c.g. with $j = f, r$ referring to the front and rear mounts (m)

l_d Longitudinal distance of the drum c.g. from the vehicle body c.g. (m)

l_d^* Longitudinal distance of equivalent vehicle body c.g. from the drum c.g. (m)

l_e Longitudinal distance of the engine group c.g. from the vehicle body c.g. (m)

l_{ej} Longitudinal distances of engine mounts from the engine group c.g. with $j = f, r$ referring to the front and rear mounts (m)

l_s Longitudinal distance of seat from the cab/platform c.g. (m)

l_t Longitudinal distance of the rear tires c.g. from the vehicle body c.g. (m)

l_t^* Longitudinal distance of equivalent vehicle body c.g. from the rear tires c.g. (m)

$M_0(t)$ Moment of the engine excitation (Nm)

m_1 Front axle (drum) static load (kg)

m_2 Rear axle (tires) static load (kg)

m_b Vehicle body mass (kg)

m_b^* Equivalent vehicle mass in the 2-DOF compactor ride model (kg)

m_c Operator-station (cab or open platform) mass (kg)

m_d Drum mass (kg)

m_e Engine group mass (kg)

m_f^* Effective vehicle frame mass in one-dimensional compactor- soil models (kg)

m_{tot} Total vehicle mass (kg)

m_v Eccentric mass of the drum vibrator (kg)

m_w Unsprung mass (rear wheels) when considering the virtual axle suspension (kg)

N Number of frequency bands considered for weighted summation of accelerations

N_j Exponents in surface profile determination, with $j = \emptyset, 1\ or\ 2$

n Number of DOF in the Multi-Body System

T Exposure duration (s)

T_0 Reference duration of 8 hours

T_e Representative period of exposure (hours)

T_v Period of drum vibrator (s)

P_{avg} Power absorbed per AAP guideline (W)

$S_d(f)$ Temporal PSD of the drum displacement (m^2/Hz)

$S_g(\Omega)$ Spatial PSD of the ground surface profile ($\frac{m^2}{cycle/m}$)

$S_g(\omega)$ Temporal PSD of the ground surface profile ($\frac{m^2}{rad/s}$)

VDV Vibration dose value ($m/s^{1.75}$)

v Vehicle velocity (m/s)

W_d Weighting function for vibration along lateral and longitudinal axes

W_e Weighting function for rotational vibrations (roll, pitch and yaw)

W_k Weighting function for vibration along the vertical axis

X_a Longitudinal distance of the wheel-axle from the vehicle central articulation (m)

X_d Longitudinal distance of the drum axis from the vehicle central articulation (m)

x_b Longitudinal displacement of the vehicle body (m)

x_c Longitudinal displacement of the operator-station (cab or open-platform) (m)

x_e Longitudinal displacement of the engine group (m)

x_w Longitudinal displacement of wheels when considering axle suspension (m)

Z_0 Amplitude of assumed harmonic elevations of the terrain at a given frequency (m)

z_{0j} Elevations of the terrain surface at the axle-terrain interfaces with $j = f, r$ referring to front (drum) and rear (tires) (m)

z_b Vertical displacement of the vehicle body (m)

z_c Vertical displacement of the operator-station (cab or open-platform) (m)

z_d Vertical displacement of the drum (m)

z_e Vertical displacement of the engine group (m)

z_f Displacement of the effective vehicle frame in classic one-dimensional compactor models aimed for simulating the compaction process (m)

z_h Vertical displacement of the seated portion of the operator mass (m)

z_s Vertical displacement of suspension seat mass (m)

z_{se} Vertical elastic deformation of soil during vibratory compaction (m)

z_w Vertical displacement of wheels when considering axle suspension (m)

α_i Real part of the ith mode of the Multi-Body Systems (rad/s)

β_i Imaginary part of the ith mode of the Multi-Body Systems (rad/s)

γ Damping to plasticity ratio of the soil (s)

δ_s^{stat} Static deflection of the soil under the compactor front axle (drum) load (m)

δ_s^{plast} Plastic deformation of the soil resulting from a pass of the roller drum (m)

δ_s^z Seat suspension half travel (m)

ε Plasticity parameter

ζ_i Damping ratio associated with the ith mode of the Multi-Body Systems

ζ_s^* Nominal (uncoupled) damping ratio of suspension seat

λ_i i^{th} complex eigenvalue of the Multi-Body Systems

τ Lag between the ground excitations at the drum and the rear axle tire (s)

φ_b Pitch angular displacement of the vehicle body (rad)

φ_c Pitch angular displacement of the operator-station (cab or open-platform) (rad)

φ_e Pitch angular displacement of the engine group (rad)

ω_{di} i^{th} damped natural frequency of the Multi-Body Systems (rad/s)

ω_{ni} i^{th} natural frequency of the Multi-Body Systems (rad/s)

ω_v Angular velocity of drum vibrator (rad/s)

Ω Spatial frequency $(cycle/m)$

Ω_o Transition spatial frequency in road profiles classification (cycle/m)

CHAPTER 1 – INTRODUCTION AND LITERATURE REVIEW

1.1. Introduction

Construction equipments are a category of heavy equipments or industrial vehicles dedicated to civil application. The work presented in this dissertation concerns a special type of construction equipment, the soil compactors. A soil compactor is essentially a vibratory roller used for compaction of soils and road base layers. These articulated vehicles are designed with a vibratory drum (roller) as front unit linked to a single-axle tractor with off road capabilities as the rear unit. Soil compactors are mainly used in road building to compact the base grade of paved roads and streets or the core of dirt roads. Since the production of the first commercial vibratory rollers about 50 years ago, considerable efforts have been made to improve the compaction efficiency and safety of the equipment. Operation of such vehicles on unpaved terrains causes comprehensive magnitudes of ride vibration transmitted to the operators. The exposure to such vibration may impose adverse effects on the driver's health and safety. The ride vibration characteristic of the vehicle, however, has gained only minimal importance in the design of compactors. Traditionally, soil compactors have been seen as tools or equipments rather than vehicles and thereby lesser emphasis is placed on the ride dynamics and the effects on the operator. Owing to the increasing demand for operator comfort and concerns related to adverse health effects of vibration exposure, the future designs or design modifications are expected to emphasize the need for dynamic characteristics that allow safe and comfortable operation under the designated tasks. These would necessitate enhanced knowledge of dynamic properties and performances of the compactors.

The soil compactors are designed with intentional mass unbalances within the rolling drum to achieve efficient vibratory compaction of soils. The vehicle comprises a tire axle and a vibrating drum on the other axle (by opposition to a typical asphalt compactor employing drums as both axles) which results in asymmetric loading, and thereby considerable magnitudes of fore-aft and pitch motions of the chassis and the operator station, in addition to the vertical motions arising from interactions of the wheels and the rigid drum with the terrain.

Construction equipment tires are typically large and soft, which tend to attenuate the terrain-induced vibrations and shocks. Furthermore, these vehicles do not employ primary suspension at the wheels. The soil compactors rear axle is directly bolted to the vehicle frame, while the drum is supported through elastic mounts, which help suppress only high frequency vibration and noise. The light damping due to tires and natural rubber mounts, thus, yields high magnitude resonant vibration. The implementation of suspended operator station (cab) and seat is thus becoming increasingly popular, particularly in Europe, for reducing the vibration levels transmitted to the operator. In majority of the vehicles, the operator station is fastened to the frame through stiff rubber mounts, while a seat suspension could attenuate vibrations only in the vertical direction. The low frequency vibration arising from drum/terrain and wheel/terrain interactions are thus transmitted to the operator through the seat, which in the vast majority of vehicles in North America is limited to a polyurethane foam cushion. The vibration environment of such vehicles could thus be characterized by that of the resonance of a lightly damped system formed by the unsuspended vehicle and the tires.

The prolonged occupational exposure to low frequency Whole-Body Vibration (WBV) has been associated with increased risk of disorders in the lumbar spine and the connected nervous system (Seidel, 1993; Wikström, 1993; Griffin, 1990). These findings have also been supported by the reported epidemiologic studies, which suggest a strong association between the WBV exposure and the low back pain among the occupational vehicle drivers (Bongers, Boshuizen, Hulshof, & Koemeester, 1988; Bernard, 1997; Bovenzi & Hulshof, 1998; Bovenzi, et al., 2006). A field survey of heavy mobile equipments, including the vibratory compactors, defined the ranges of weighted root mean square (rms) accelerations (a_w) in vertical direction (Dupuis & Zerlett, 1987), and established that a_w lies in the 0.3 to 1.7 m/s^2 range for compactors. The study, however, did not attempt a distinction between the lighter utility compactors (less than 5 tons in weight), the heavier asphalt compactors (tandem-drums above 5 tons) or the more powerful soil compactors (single-drum above 5 tons). The study highlighted the fact that compactor operators could be exposed to levels of whole-body vibration in excess of what is considered to be safe by International Standards Organisation for an eight-hour working day (ISO 2631-1, 1997).

In Europe, where a constant pressure for almost two decades (Kittusamy & Buchholzb, 2004), not only through regulations but also from the users, has persuaded the manufacturers to offer equipment featuring improved operator comfort (Kittusamy N. , 2003), the measurements of whole-body vibration (WBV) have been performed on 16 machines between 1997 and 2005. The highest axis vibration values were reported jointly by INRS and RMS Vibration Test Laboratory (Griffin, et al., 2006) for the soil compactors. The average values were in the order of 0.6 m/s^2, which exceeded the

3

"exposure action level" of 0.5 m/s^2 defined by the European Directive (EN 2002/44/EC, 2002). The studies also reported the vibration levels of the worst machine as 1.2 m/s^2, which is beyond the European Directive defined "exposure limit level" of 1.15 m/s^2 (Daniere, et al., 1987; Boulanger, Donati, & Galmiche, 1996; Griffin, et al., 2006). Studies in USA performed mesurements on a Caterpillar CS-433B soil compactor and suggested WBV, characterized by vector summation of those measured along the vertical, fore-aft and lateral axes, in the order of 2.5 m/s^2 (Beck, et al., 2004). A recent Canadian study performed on 3 soil compactors in Ontario revealed WBV in vertical direction of an average of 0.91 m/s^2, while the worst machine revealed vertical vibration magnitude of 1.3 m/s^2 (Cann, Salmoni, Vi, & Eger, 2003).

The WBV environment of mobile equipment is in general strongly influenced by many design and operating factors (Donati, 2002). In case of vibratory compactors, the WBV environment is most significantly influenced by the mode of operation. In the transit mode, the vehicle vibration responses are attributable to the interactions of the pneumatic tires and the rigid drum with mostly undeformable terrain, and to occasional drum-hop. In the compaction mode, the interaction of the vibratory drum with deformable soil and drum hop motions, account for the major sources of vehicle vibration. The soil compactors are generally designed with elastic vibration isolation mounts between the drum and the chassis (vehicle main body), and between the operator cabin/platform and the chassis. Such mounts, generally provide attenuation of only high frequency vibration (Bertrand, Brzezinski, & Rocques, 1994). Some of the models, however, include a low natural frequency vertical suspension at the seat to limit the transmission of vertical vibration to the operator. The soil compactors may thus be considered as unsuspended

vehicles, with the exception of a suspension seat. The vibration arising from the above sources are thus mostly transmitted to the operator-station. The nature of WBV transmitted to drivers of various off-road vehicles have been extensively characterized in terms of frequencies of predominant vibration and frequency-weighted vibration magnitudes in order to assess potential health and safety risks (Daniere, et al., 1987; Boulanger, Donati, & Galmiche, 1996; Paddan & Griffin, 2002).

The interactions of drum/tire with the unpaved surfaces, coupled with the drum vibrator are known to impose severe levels of WBV. Considering that the health risks posed by WBV are related to exposure level and exposure duration, apart from the posture related factors, it is vital to control the levels of vibration for reducing the health and safety risks among the exposed operators. A number of approaches may be considered to reduce the exposure levels, such as implementation of adequately tuned suspension seat, operator station vibration isolation, wheel suspension and drum mounts. The design of such suspensions, however, necessitates total characterization of vibration properties of such vehicles under most representative operating conditions. Only a few studies have reported vibration levels of soil compactors, which were limited to measurements along the vertical direction alone at the operator seat level for the purpose of exposure assessments. Such measurements would thus be considered valid for the particular seat considered in the study. Moreover, the studies did not consider the equipments that are most commonly used in North America.

This thesis investigates the ride vibration properties of single-drum soil compactors during the transit and compaction tasks through field-measurements and analytical

methods. The reported results could be effectively applied for the design/selection of adequate secondary suspensions.

1.2. Literature Review

The analyses and assessments of ride vibration of compactors encompasses several challenges associated with mechanical characterisation of the vehicle, the drum with rotating eccentric masses, the drum- and tire-soil interactions, dynamic properties of the soil, assessment of vibration levels, etc. The reported studies in the related subjects are thus reviewed and briefly summarised in the following sections in order to build adequate background and formulate the scope of the study.

1.2.1. Assessment of Vehicle Ride Vibration Response

A number of standardised approaches have been proposed for assessment of ride vibration comfort vibration. Among these methods recommended by the International Organization for Standardization (ISO 2631-1, 1997), the British standard (BS 6841, 1987), the Society of German Engineers guideline (VDI 2057, 1987) and the Average Absorbed Power (AAP) method (Els, 2005) have been most widely used. Presently, the assessment guidelines in Europe mostly follow the directive 2002/44/EC (EN 2002/44/EC, 2002) that defines the limits on human occupational exposure to vibrations. Verein Deutscher Ingenieure (VDI), the Society of German Engineers was the first to release a method for ride comfort assessment (VDI, 1963). The method was based on empirical results from a large population of individuals exposed to sinusoidal vibrations of various frequencies and intensities. The VDI guideline defines a ride comfort index (K

factor) based on the frequency-weighted rms acceleration and provides a range of value to assess the ride comfort as subjectively perceived by humans (Hohl, 1984). The current guideline (VDI 2057, 1987) has adopted the tolerance curves released within an earlier version of the equivalent ISO standard (ISO 2631, 1978). In the vertical direction, the K values are determined from rms vertical acceleration a_z, as:

$$K_z = 10a_z\sqrt{f} \; ; \qquad \text{for} \qquad 1Hz \leq f \leq 4\,Hz$$

$$K_z = 20a_z \; ; \qquad \text{for} \qquad 4Hz \leq f \leq 8\,Hz$$

$$K_z = 160a_z f \; ; \qquad \text{for} \qquad 8Hz \leq f \leq 80\,Hz$$

(1.1)

where f is the vibration frequency.

The Average Absorbed Power (AAP) guideline was developed by the US Army in 1966 (Pradko & Lee, 1966). It is based on the human body elastic behaviour. Under vibrations the human body exhibits reaction forces as a function of the motions, which are expressed in terms of dissipated energy or absorbed power. The power (P_{avg}) absorbed by the exposed body is computed using empirical relations in the 1 and 80 Hz frequency range, given by:

$$P_{avg} = \sum_{i=0}^{N} K_i \cdot a(f_i)^2$$

(1.2)

Where K_i is the weighting factor and $a(f_i)$ the rms acceleration corresponding to frequency f_i.

The British Standard (BS 6841, 1987) defines a frequency weighting in the 0.5–80 Hz frequency range and the concept of vibration dose value (VDV) to assess exposure to high intensity vibration or shock motions. Different weight functions are defined for each axis of vibration in order to determine their specific ride value. The rms and VDV values are computed as follows:

$$rms = \sqrt{\frac{1}{T}\int_0^T a(t)^2\, dt} \qquad\qquad VDV = \left[\int_0^T a(t)^4\, dt\right]^{1/4}$$

<div align="right">(1.3)</div>

Where $a(t)$ is the measured acceleration along a given axis and T is the exposure duration considered.

Although the above-mentioned standardised methods continue to be used in some applications, the assessments of WBV exposure have mostly converged to the current equivalent and concurrent ISO standard (ISO 2631-1, 1997). The first part of this standard defines methods for measurement of periodic, random and transient WBV in the frequency range of 0.5–80 Hz, for assessment of health, comfort and perception, and in the 0.1–0.5 Hz range for assessing probability of motion sickness. The evaluation is based on frequency-weighted rms accelerations, while different frequency-weightings are defined for the evaluation of different effects. The different weighting functions are also defined for vibration along individual axes, which include W_k for vertical, W_d for lateral and longitudinal, and W_e for rotational vibrations (roll, pitch and yaw), as shown in Figure 1-1. The frequency-weights suggest a critical frequency range of 0.5–2 Hz for the horizontal and rotational vibration exposure, and 4–10 Hz for the vertical vibration. The frequency weighted rms acceleration along a particular axis is computed from:

$$a_{wk} = \sqrt{\sum_{i=1}^{N}\left[W_j(f_i) \cdot a_k(f_i)\right]^2}$$

<div align="right">(1.4)</div>

Where a_{wk} is the frequency-weighted rms acceleration due to vibration along axis k, $W_j(f_i)$ is the weighting factor and $a_k(f_i)$ the rms acceleration along axis k, corresponding to center frequency f_i (third-octave bands), with $j = k, d, e$ referring to the appropriate weighting function. The standard provides guidance for assessing the vibration comfort and human perception, and health effects in terms of a health caution guidance zone. The standard also recommends that the exposure be expressed by VDV, when the vibration comprises shock components. A vibration signal is judged to encompass shock components, when crest factor of vibration (ratio of instantaneous peak value of the frequency-weighted acceleration signal to its rms value) exceeds 9.

The assessment of vibration comfort considers translational vibrations that occur in all three axes on the seat pan, while the vibration total value is computed as the vector sum of vibration in orthogonal coordinates (x, y and z) with identical unit multiplying factors ($K = 1$) for each coordinate. In cases where the rotational vibrations are of considerable magnitude, the total rotational vibration value is also computed in a similar manner with different multiplying factors for each coordinate. For assessment of health effects, each axis of translational vibration is considered independently, applying higher weighting ($K = 1.4$) for the horizontal vibration components. The axis featuring the highest weighted acceleration is retained. When vibration in one axis is not dominant, the vector sum acceleration, could serve to assess of health effects.
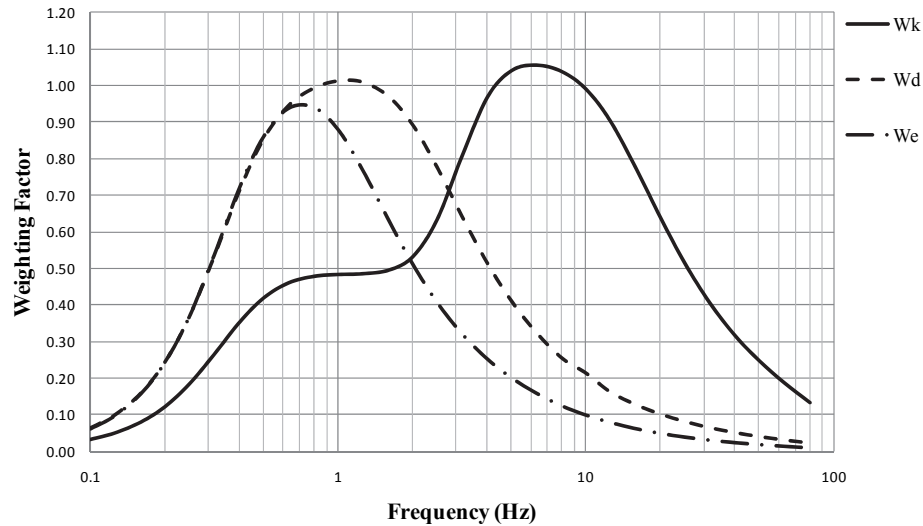
A Directive of the European Parliament on the minimum health and safety requirements regarding the exposure of workers to the risks arising from physical agents (vibration) was adopted in July 2002, and subsequently implemented in July 2005. It sets minimum standards for controlling the risks of whole-body vibration (WBV) exposure in terms of an "action value" beyond which the employer is required to take appropriate actions to control WBV exposure levels, and a "limit value" above which the workers must not be exposed (Griffin, et al., 2006). The directive defines the eight-hour equivalent, $A(8)$ exposure action value of 0.5 m/s² (alternatively VDV of 9.1 m/s$^{1.75}$), and a limit value of 1.15 m/s² (alternatively VDV of 21 m/s$^{1.75}$). The eight-hour equivalent $A(8)$ exposure is defined as the equivalent exposure to continuous acceleration over an eight-hour work period. Determination of $A(8)$ does not require the measurements over a continuous duration of 8 hours; it can be estimated from the measurements performed over a shorter period T_e, such that (Weber, 2008):

$$A(8) = a_w \sqrt{\frac{T_e}{T_0}}$$

<div align="right">(1.5)</div>

Where a_w is the weighted rms acceleration over the measurement duration or the total duration of exposure during one work day and T_0 is the reference duration of 8 hours.

The WBV exposure of seated operators is measured in terms of weighted rms accelerations a_w along the three orthogonal axes (ISO 2631-1, 1997), and the appropriate health assessment multiplying factors ($K_x = K_y = 1.4$ and $K_z = 1$) are applied. The highest of the frequency-weighted accelerations ($1.4a_{wx}$, $1.4a_{wy}$ or a_{wz}) or the vector sum could be applied to determine a_w and $A(8)$. The VDV values may also be applied in a similar manner to obtain an estimate of $A(8)$. In situations, where the daily exposure encompasses different levels of vibration encountered during different activities, the daily exposure is estimated from:

$$A(8) = \sqrt{\frac{1}{T_0} \sum_{i=1}^{n} a_{wi}^2 T_{ei}}$$

<div align="right">(1.6)</div>

where a_{wi} is the weighted rms acceleration of the ith activity and T_{ei} is its period of exposure; n is the number of activities representing the daily exposure.

The EU directive suggests that the exposure level may be limited to values below the action level by either limiting the exposure duration or the acceleration magnitude. The first approach, however, has severe economic consequences, while the latter method poses considerable challenge in the design of the vibration attenuation mechanisms.

1.2.2. **Modelling of Roller-Soil Interaction**

The ride vibrations of a soil compactor arise from two primary sources: (i) vehicle undeformable terrain interactions; (ii) interactions of the vibratory roller with the deformable soil, the material to compact. The vibration behaviour may thus be characterised by two distinct tasks associated with the transit mode involving low frequency vibration due to tire- and drum-terrain interactions and the compaction mode involving relatively higher frequency vibration attributed to the vibratory roller drum interactions with soils. The compaction mode vibrations are primarily associated with soil compaction by means of an eccentric mass (m_v) rotating around the axis of the drum, as shown in Figure 1-2. The magnitudes and frequencies of such vibration are selected to the design and operating speed of the vibrator, and the elasto-plastic properties of the soil.

(a)   (b)
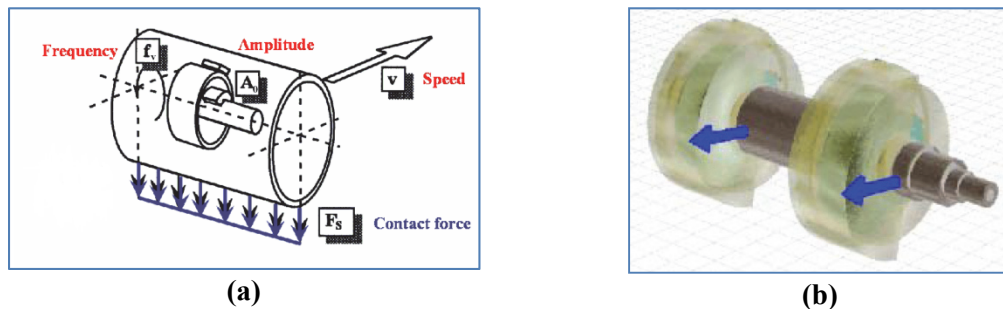
Figure 1-2: (a) Rotating mass vibrator mechanism (Anderegg, von Felten, & Kaufmann, 2006); and (b) rotary exciter by Bomag (Kloubert, 2004)

The studies on soil compactors have evolved into a wide-range of models for characterizing the elasto-plastic properties of the soils. A number of lumped-parameter and finite element models have been developed to predict the propagation of the compaction forces in the soil and the distribution of the stress in different soil layers (Farzaneh, 1983; Pietzsch & Poppy, 1992; Anderegg, 2000; Erdmann, Adam, & Kopf, 2006). While the finite-element models are most adequate for estimating the three-

dimensional stress distribution in the soil, the lumped-parameter models have been considered sufficiently accurate for analysis of in-plane or one-dimensional propagation of the compaction force and the drum-soil interaction (Pietzsch & Poppy, 1992; Adam & Kopf, 2000; Krober, Floss, & Wallrath, 2001; Anderegg & Kaufmann, 2004).
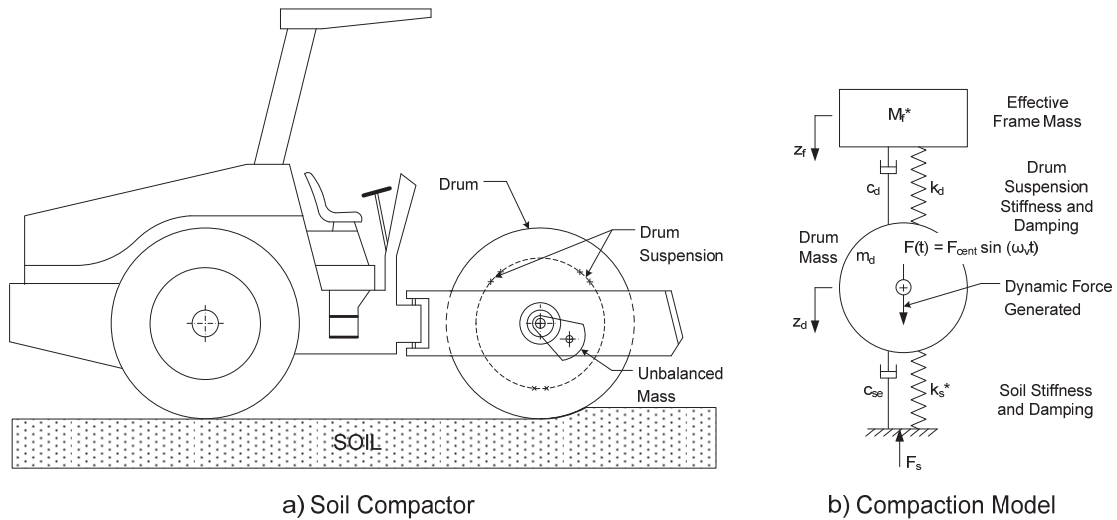
Figure 1-3: (a) Schematic of a vibratory soil compactor; and (b) A two-degrees-of-freedom soil - compactor model (Yoo & Selig, 1979)

The compactions models, invariably, consider the time variant properties of the soil. During a constant speed operation, the soil is deformed in the immediate vicinity of the drum-soil contact patch, and the compactor continuously interacts with the new or undeformed soil during a given compaction pass. Consequently, the observed force-deformation response of the soil exhibits closed-loop behaviour for every complete rotation of the eccentric mass. In its simplest form, the drum-soil interaction is characterised by a two-degree-of-freedom (DOF) model, as shown in Figure 1-3 where the soil under compaction is represented by its equivalent stiffness k_s^* and viscous damping c_{se}. The closed-loop force-deflection behaviour of the soil is significantly different from a stationary loading case (Figure 1-4 a), where the same soil elements

13

sustain the applied force and thus accumulation of soil deformation with the repetition of loading cycles. (Yoo & Selig, 1979). The compaction during forward motion, however, yields very different deformation behaviour as the drum interacts with undeformed soil during its rotation (Figure 1-4 b).
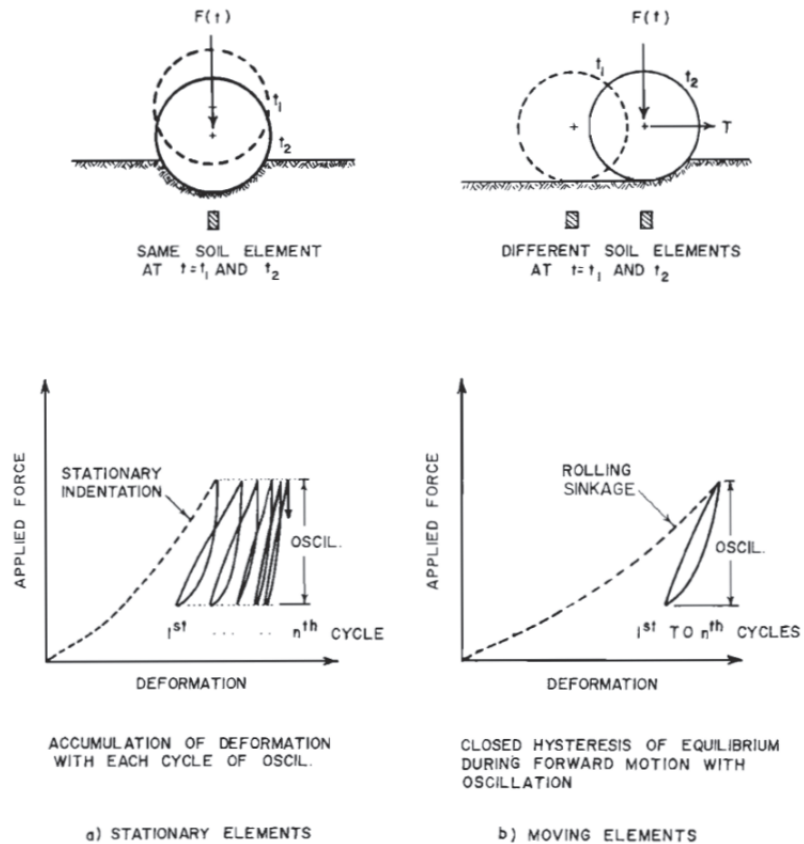
Figure 1-4: Force-deflection characteristics of (a) stationary; and (b) moving soil elements by the drum (Yoo & Selig, 1979)

Furthermore, the force-deflection properties of soil tend to vary under repeated compaction passes, since each pass of the vibratory drum alters the density and stress-strain properties of the soil elements. The soil may exhibit elastic and elastic-plastic deformation during a given compaction pass. The closed-loop force-deformation characteristics of the soil, during a given compaction pass, is often described by an indicator diagram representing the soil contact force F_s as function of the drum vertical

displacement z_d.(Sandström, 1994; Thurner, 2001; Floss & Kloubert, 2000). Figure 1-5 (a) illustrates the reaction force – drum displacement characteristics obtained during three consecutive passes of the compactor. The hysteretic force – deflection characteristics have been described in terms of the responses under loading and unloading, as seen in Figure 1-5 (b).
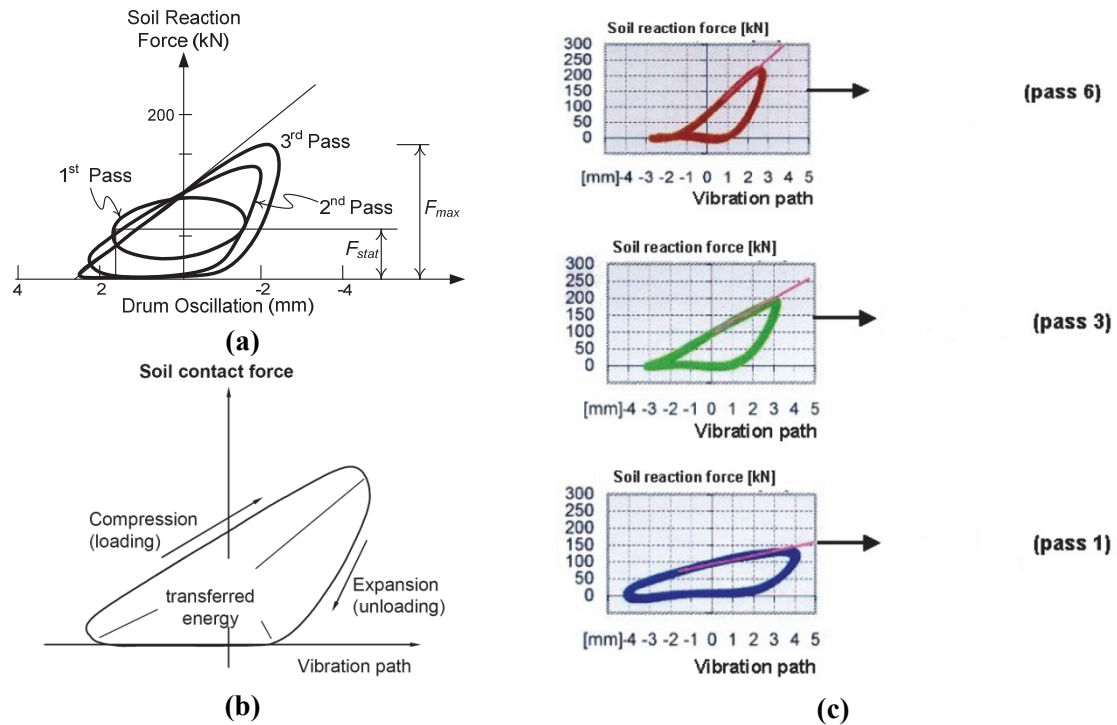
Figure 1-5: (a) Typical reaction force-drum displacement properties during repeated passes of the roller (Floss & Kloubert, 2000); (b) Reaction force-drum displacement under drum loading and unloading(Krober, Floss, & Wallrath, 2001); and (c) Typical force-displacement indicator diagrams for the 1st, 3rd and 6th passes of the compaction illustrating variations in the reaction force in the loading and unloading phases (Kloubert, 2004)
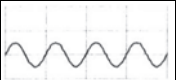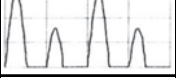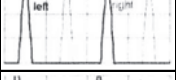
During the loading phase, the stress-strain properties of the soil exhibit both the elastic and plastic effects. Dominantly elastic energy however, is returned to the drum. During the unloading phase, while the remaining energy is effectively transferred into compaction and partly is attributed to radiation losses (material damping being negligible). Owing to the symmetric geometry of cylindrical drum, the plastic effects are noticeably quasi-linear, while the elastic effects are significantly non-linear (Adam &

15

Kopf, 2000; Thurner, 2001). The drum would lose contact with the soil, when the magnitude of total soil reaction force, comprising dynamic and static components, during unloading equals zero as the soil cannot exert any tension on the drum. A condition for retaining the drum-soil contact was established as (Anderegg & Kaufmann, 2004):

$$F_{s\,Tot}\Big|_{max} \leq 2\left(m_f^* + m_d\right)g$$

(1.7)

where $F_{s\,Tot}$ is the total vertical soil reaction force with dynamic and static components, m_d is the drum mass and m_f^* is the effective vehicle frame mass supported by the drum.

Table 1-1: Operating conditions and motion behaviours of a vibratory roller drum, and applicability of Continuous Compaction Control (Adam & Kopf, 2000)

Drum motion	Interaction drum-soil	Operating condition	Soil contact force	Application of CCC	Soil stiffness
Periodic	Continuous contact	CONT. CONTACT		Yes	Low
	Periodic loss of contact	PARTIAL UPLIFT		Yes	
		DOUBLE JUMP		Yes	
		ROCKING MOTION		No	
Chaotic	Non-periodic loss of contact	CHAOTIC MOTION		No	High

It has been suggested that the magnitude of the soil reaction force after the initial pass may become sufficiently important to cause partial lifting of the drum from soil (Floss & Kloubert, 2000). The magnitude of the reaction force and the duration of the loss of contact during a cycle, however, differ considerably over subsequent passes, as seen in Figure 1-5 (c), which lead to highly non-linear unloading behaviour (Anderegg & Wehrli, 1995). A few studies have also characterised the unloading behaviour in the frequency

16

domain suggesting the occurrence of harmonics of the excitation frequency (Mooney, Gorman, & Gonzalez, 2005; Tateyama, Ashida, Fukagawa, & Takahashi, 2006; Scherocman, Rakowski, & Uchiyama, 2007). Figure 1-6 illustrates the three elementary vibration states of vibrating drum during the unloading cycle (Andereg, 2000). The oscillations exhibit single harmonic component in the vicinity of the excitation frequency under continuous contact of the drum with the soil. After the first passes of compaction, a denser and consequently stiffer soil results in partial drum uplift. The motion occurs at the multiples of the excitation frequency, as seen in Figure 1-6 (b). Continued compaction of soil leads to higher density and soil stiffness, which has been associated with "double jumping" of the drum (sub-harmonic motion of the drum at half the excitation frequency as seen in Figure 1-6 (c)), rocking (a 180° phase lag between the sub-harmonics of the right and left sides of the drum) and ultimately a chaotic motion of the drum (Adam & Kopf, 2000; Anderegg & Kaufmann, 2004). These also suggested considerably high magnitudes of reaction force occurring at ½ the excitation frequency in addition to those at its multiples. These motions are further summarised in Table 1-1.

The partial loss of contact, corresponding to the partial drum uplift operating condition, has been considered as the most efficient drum behaviour for soil compaction (Andereg, 2000). Double jumping and rocking motions, however, should be typically avoided since they cause rapid machine wear and limit machine manoeuvrability (Adam & Kopf, 2000; Rinehart & Mooney, 2008). Furthermore, the associated high magnitude loading at a lower frequency also tends to loosen the top layer of the soil (Anderegg & Kaufmann, 2004). Consequently, the parameters of the compactor vibrator are modified during the final compaction passes in order to avoid double jumping and rocking motions. Typically

the nominal vibrator amplitude A_0 (eccentric moment $m_v\,e$, with e being the eccentricity) is decreased and the excitation frequency f_v (vibrator rotational velocity ω_v) may be increased either manually by the operator or automatically by the new Continuous Compaction Control systems (also referred to as "Intelligent Compaction").
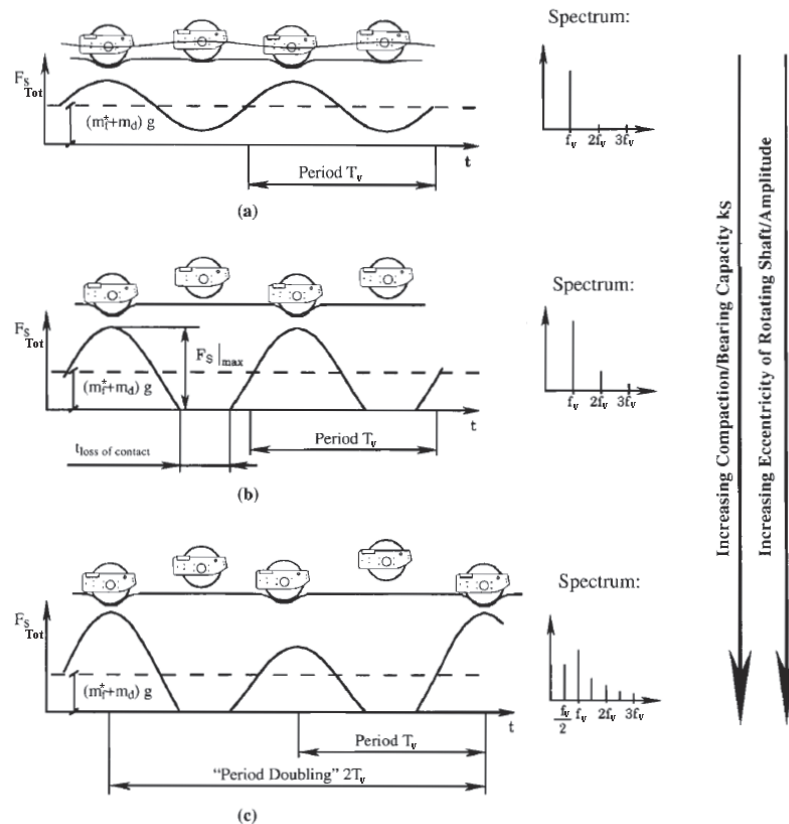
Figure 1-6: Oscillating motions of the drum during loading and unloading phases illustrating the harmonic components (Anderegg & Kaufmann, 2004)

The elasto-plastic behaviour of the soil observed during the loading and unloading phases of a compaction cycle have been effectively characterized by visco-elastic models of the soil in several studies (Pietzsch & Poppy, 1992; Anderegg & Wehrli, 1995; Adam & Kopf, 2000). The soil in some of these models is characterized by a linear stiffness k_{sp} describing the plastic behavior in series with the visco-elastic properties of the soil.

18

Figure 1-7 illustrates the idealization of the elasto-plastic properties of the soil, as reported in some studies (Adam & Kopf, 2000; Thurner, 2001), for analysing the one-dimensional soil compaction and propagation of the compaction force.
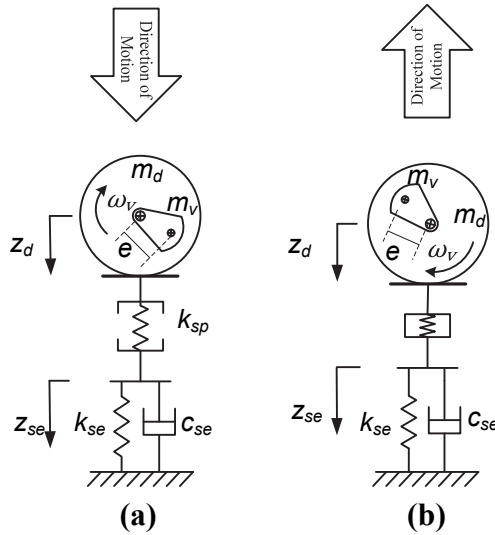
Figure 1-7: Elasto-plastic model of the soil: (a) loading phase with elasto-plastic behaviour; and (b) unloading phase with elastic behaviour

1.2.3. **Vehicle Models**

Ride dynamics of soil compactors have received only little attention. However, the wide range of models developed for various off-road vehicles could be applied to study the ride vibration characteristics of soil compactors.

The most commonly studied off-road mobile equipment, in the context of ride vibration, is perhaps the agricultural tractor. The earlier analytical models of the tractor were relatively simple linear Multi-Body Systems (Stayner, Hilton, & Moran, 1975), which were effectively applied in predicting the vehicle ride vibration levels under the defined ground surface profiles (Dale, 1978). The combination of an agricultural tractor and a trailer in a MBS ride model created an interesting articulated off-road vehicle model for

frequency response calculations and resulted in vibration levels higher than those of the tractor alone. This was primarily attributed to increased tractor pitch motion (Crolla, 1980). The coupled nature of the vibration modes of the unsuspended off-road vehicles further motivated the developments in multi-DOF two and three dimensional vehicle models and characterizations of suspension and low inflation-pressure tyres (Peng & Lines, 1997). The analytical ride dynamic models of the unsuspended tractor could also be applied to the compactor, when an appropriate drum-soil interaction model is integrated.

For the soil compactors, the modeling efforts have mostly focused on the roller drum - soil interactions and the soil compaction models in order to enhance the compaction efficiency of the vehicles. In such models, the vehicle is represented by an equivalent rigid body mass supported by the vibratory drum in contact with the deformable soil (Yoo & Selig, 1979; Andereg, 2000; Popa & Nicoara, 2002; Mooney, Gorman, & Gonzalez, 2005). This aspect of the modeling of compactors was reviewed in the previous sub-section. The first published attempt for modeling a compactor as a two-axle vehicle was made by building 3-D model in the MBS software SYMOS (Bertrand, Brzezinski, & Rocques, 1994) to explore the ride performance potential of a cab suspension. In this model, depicted in Figure 1-8 the compactor was represented by five rigid bodies including those of the rear-frame with its rigid wheel axle, the front frame, the vibratory drum, the engine group and the operator-station or cab. The model also defined soil forces acting on the drum by considering linear stiffness and damping properties of the soil.

The nonlinearities arising due to partial up-lift of the drum and even the double-jump of the drum under interaction with most severe soil parameters (soil of higher density) were also incorporated. The vehicle was assumed moving at constant low speed on graded soils; subsequently the compaction forces were simulated assuming the vehicle as static equipment continuously interacting with undeformed soil during the considered compaction pass. Furthermore, the analysis was limited to pitch plane dynamics alone, although the model was formulated in three dimensions. The validity or applicability of the vehicle model was not explored in the transit mode at higher speed with vibrator off, while operating on undeformable terrain. The study recommended a soft cab suspension with its natural modes occurring well below the double-jump frequency near 15 Hz.
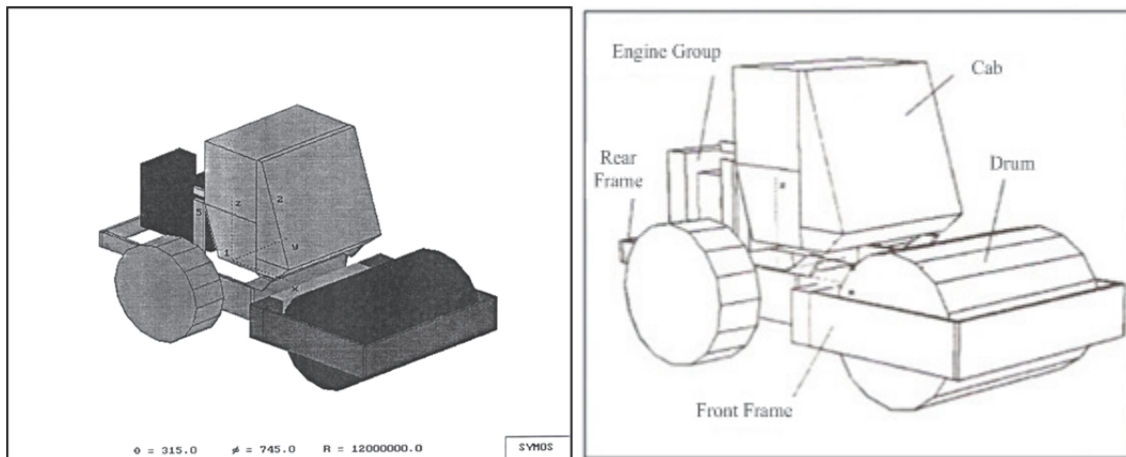
Figure 1-8: MBS model of a soil compactor (Bertrand, Brzezinski, & Rocques, 1994)

Recent efforts on modelling of compactors have focussed on path planning, automation and on-board compaction indicators (Guillo, Gautier, & Froumentin, 1999; Andereg, 2000; Delclos, Vandanjon, F., & M., 2001; Krober, Floss, & Wallrath, 2001; Kloubert, 2004). These studies also evaluate the rolling resistance and the motion resistances during compaction (Corcoran & Fernandez, 2001). Although these studies primarily focused on

the dynamics of the asphalt compaction by double-drum compactors (also called tandem rollers), the proposed modelling techniques would be equally applicable to single drum soil compactors.
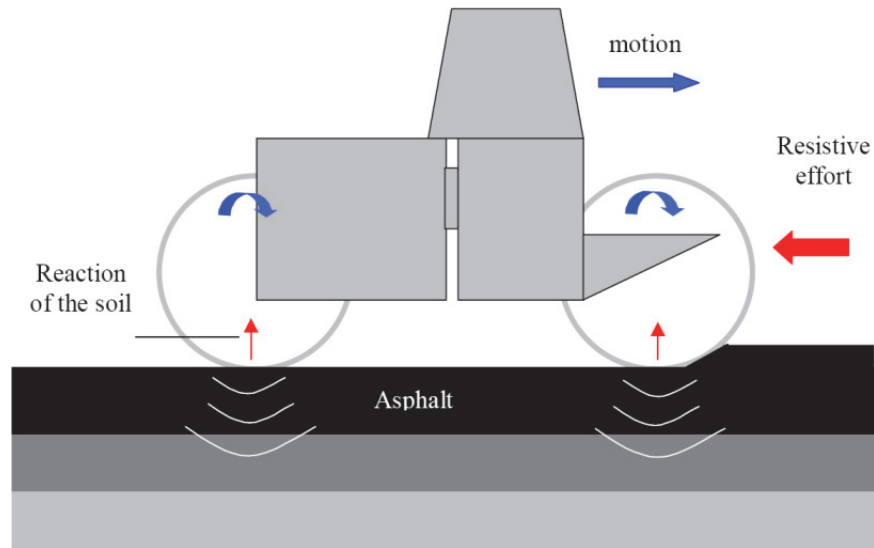
Figure 1-9: plane model by OSYRIS for estimating the degree of compaction by monitoring the resistive effort (Delclos, Vandanjon, Peyret, & Gautier, 2001)

A study indicated by the European project OSYRIS (Open System for Road Information Support) proposed a modelling techniques based upon various on-board measurements and a dynamic model of the machine (Delclos, Vandanjon, Peyret, & Gautier, 2001). Figure 1-9 illustrates the modelling concept of the study, which was primarily focused on the compaction effectiveness of the vehicle through analyses of motion resistance due to compacting materials. A horizontal plane kinematic model was also built incorporating the kinematic analysis of the articulated-frame steered vehicle as a mobile robot. The vehicle was represented by the kinematic chains as seen in Figure 1-10 (Guillo, Gautier, & Boyer, 1999), and its parameters were identified through solution of an over-determined linear system obtained from sampling of the dynamic model along a known

22

trajectory. The analyses identified drum slip in the horizontal plane as a major issue, which necessitates further developments in the 3-D modeling of the drum-soil contact (Lemaire, Vandanjon, & Gautier, 2003; Lemaire, Vandanjon, & Gautier, 2005). It was further suggested that the integration of the drum-soil contact model with the kinematic model of the vehicle would make the model more robust for motion planning as an effort toward road construction automation (Lemaire C.-E. , Vandanjon, Gautier, & Peyret, 2002).

(a) Bodies definition   (b) Equivalent tree structure   (c) Projection frames definition
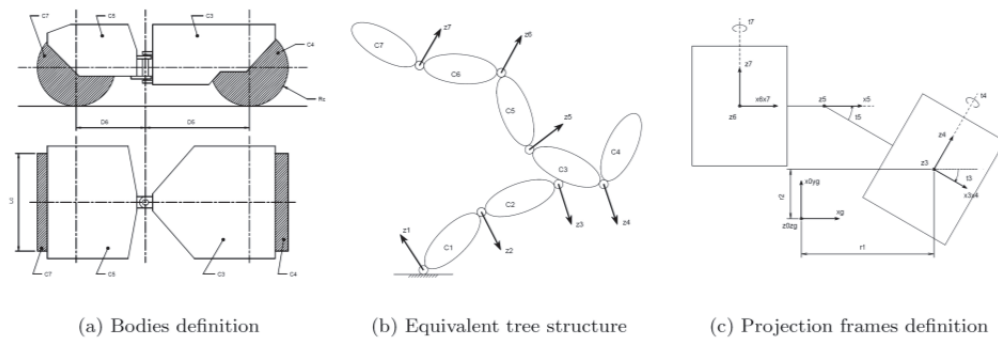
Figure 1-10: Kinematic model of a double-drum compactor as an articulated mechanical system (Lemaire C.-E. , Vandanjon, Gautier, & Peyret, 2002)

The above models considered the compactor as an articulated linkage mechanism, while the modeling efforts were mostly oriented toward estimating the contact forces between the compactor drums and the material (Lemaire C.-E. , Vandanjon, Gautier, & Lemaire, 2006). Although the models had been initially developed in the horizontal plane and later extended to include the vertical dynamics of the machine, the analyses or assessments of ride vibration characteristics were not attempted.

1.2.4. **Suspension Design**

Although a number of primary and secondary suspension designs have been developed for different wheeled off-road vehicles (Claar, Sheth, Buchele, & Marley, 1980; Crolla & MacLaurin, 1985; Hansson, 1996; Hansson, 2002), the implementations of such designs in soil compactors have been mostly limited to the low natural frequency vertical seat suspension. The suspension seats are designed with low natural frequency, in the order of 1.5 Hz, to attenuate terrain-induced ride vibration in the vertical axis alone, while the suspension travel is generally limited to ±5 cm by introducing elastic end-stops (Wu & Griffin, 1996; Wu & Griffin, 1998; Wu, Rakheja, & Boileau, 1999). The vehicle interaction with rough jobsite terrains may cause the suspension to exceed its free travel and transmit high intensity vibration or shock motions to the operator due to repeated end-stop impacts. Apart from the suspension seat, the low frequency terrain-induced translational and rotational vibrations are mostly transmitted to the operator through the relatively stiff cab and drum mounts. A number of rubber springs or hydro-pneumatic struts-based suspended axles have been developed for articulated dump trucks, and agricultural tractors (Bartlett & Brown, 1995), which may be applicable in soil compactors. The implementation of an axle suspension, however, is associated with many complexities, and would result in major design modifications. Furthermore, an axle suspension would alter the pitch and roll dynamics of the vehicle that may affect the compaction efficiency in an adverse manner. Above all, the axle suspension must be designed to yield low natural frequency of the vehicle, which would yield larger rattle space requirements and relative motion of the sprung frame.

1.2.5. **Characterizations of the terrain roughness**

The ride vibration responses of vehicles are strongly influenced by the terrain roughness apart from the various design and operating factors. Consequently, considerable efforts have been made in characterizing the roughness properties of roads and various off-road terrains such as pasture and plumed fields (Wong, 2001). The vibratory compactors are involved in transit operations over a substantial portion of the daily work hours. These include the vehicle motion to a jobsite and transit from one compaction zone to another within a jobsite. The transit mode is generally associated with relatively higher speeds (in the order of 10 km/h). The vehicle interaction with relatively rough terrains induces significant magnitudes of low frequency vibration.
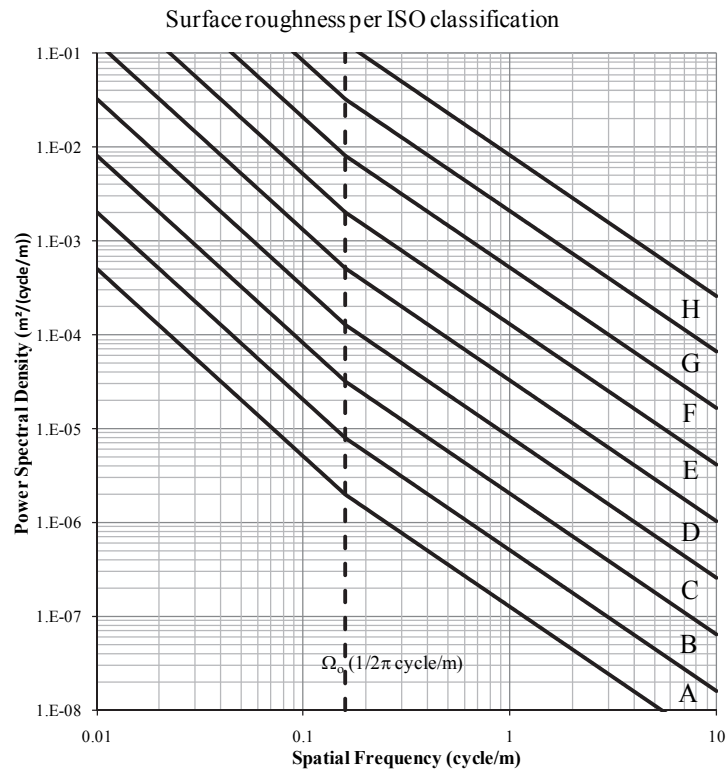
Figure 1-11: Spatial PSD of different road surface irregularities and their classification (ISO 8608, 1995)

The surface elevation is profiled by means of vehicle mounted devices. Most mechanical profiling devices consist of rolling rigid wheels that are loaded or towed at low speeds (Bekker, 1969). The reported studies have expressed the ground surface profile in terms of the Power Spectral Density (PSD) of its elevation as a function of spatial frequency (ISO 8608, 1995; Wong, 2001).

The spatial PSD of the surface profile $S_g(\Omega)$ is generally expressed as a function of the spatial frequency Ω. For off-road terrains, the spatial spectral density is related to the spatial frequency Ω as:

$$S_g(\Omega) = C_{sp}\Omega^{-N}$$

(1.8)

where C_{sp} is a constant and the exponent N ranges from 1.6 to 3.8 (Wong, 2001). ISO has also classified irregularities of road surfaces (ISO 8608, 1995). The spatial PSD of the road profile $S_g(\Omega)$ is defined over the different spatial frequency ranges as:

$$S_g(\Omega) = S_g(\Omega_o)\left(\Omega/\Omega_o\right)^{-N_1} ; \text{for } \Omega \leq \Omega_o$$

(1.9)

$$S_g(\Omega) = S_g(\Omega_o)\left(\Omega/\Omega_o\right)^{-N_2} ; \text{for } \Omega > \Omega_o$$

The resulting classification plot is illustrated in Figure 1-11. Where there is a defined range of transition value $S_g(\Omega_o)$ at a transition spatial frequency, $\Omega_o = {}^1/_{2\pi}$ (cycle/m) for different classes of road, and N_1 and N_2 are the constant exponents. The roughness properties of different roads have been classified on the basis of the magnitude of roughness, while the classification ranges from very good (A) to very rough (H), as shown in Figure 1-11.

1.3. Scope and objectives of the thesis

From the review of the literature, it is evident that ride vibration dynamics of soil compactors has received very little attention, while it may have significant impact on the derivers' perception of comfort, and health and safety. The primary goal of this work is to contribute towards enhancement of whole-body vibration environment of vibratory soil compactors used in the road building sector, in order to minimize the health and safety risks among the operators of such equipment, while preserving the essential compaction efficiency. The proposed thesis is concerned with the primary task of modeling and characterization of the vibration environment of soil compactors models most commonly used in North America, under a range of most representative operating conditions, and to provide guidance on selection of suspension seat and other potentially promising vibration mitigation concepts. The thesis research is particularly focused on development of vehicle models to predict its ride vibration during compaction and transit modes of operation, while field measurements are designed for characterization of vibration environment under simulated tasks. The proposed models could be applied for design of primary as well as secondary suspensions for enhancement of WBV environment. The models may also be applied to seek modifications of design and operating factors, namely be retrofitting of secondary suspensions, alternate drum and operator station mounts.

The specific objectives of the dissertation research include:

- Development of an in-plane multi-body dynamic model of a soil compactor incorporating non-linear drum - soil interactions during vibratory compaction;

- Development of a ride-dynamic model of the vehicle incorporating tire-and drum-terrain interactions;

- Characterisation of the vibratory environments of soil compactors during compaction and transit modes of operation;

- Identification of roughness properties of equivalent undeformable terrains;

- Analysis of ride vibration properties of the vehicle and role of various design and operating factors for identifying avenues for reducing the WBV exposure of the operators

1.4.   Layout of the Thesis

In CHAPTER 2, the compactor configuration adopted for this study and its specific properties are emphasised and justified. Ride models based on simplified yet credible mathematical formulations of subsystems are developed. The subsystem models of the vehicle frame, the suspended cab and the operator's seat as well as the subsystem model of the vibratory drum - deformable soil interaction, are detailed successively. The integration of the vibratory drum – deformable soil interaction into the developed ride models leads to a dynamic model of the equipment in compaction mode of operation.

In CHAPTER 3, field measurement protocol and instrumentation are described and followed by data analysis of the dynamic response of the vehicle in normal operations. These include passes over graded soils of various degrees of compaction and transit on random terrains. Measured data are presented in frequency domain.

In CHAPTER 4, ride and compaction models developed are validated with respect to the field measurement data and furthermore, in the particular case of compaction modelling, with respect to reported data.

In CHAPTER 5, the ride quality of compactors is evaluated based on ISO guidelines (ISO 2631-1, 1997) for different operating conditions. A parametric sensitivity analysis meant to study the influence of several design parameters is carried out. The compaction efficiency of the equipment is also evaluated, mostly based on the plastic deformation (compression) of the soil obtained by simulation. Similar sensitivity analysis highlighting the influence of operating and design parameters is carried out. The results are discussed and design changes proposed for enhanced ride quality.

Conclusions are summarised in CHAPTER 6 which also presents avenues relevant for future studies.

CHAPTER 2 – DEVELOPMENT OF ANALYTICAL MODELS OF THE VIBRATORY COMPACTOR

2.1. Introduction

The lumped-parameter and multi-body dynamic models of different off-road vehicles have been widely reported to study the influences of various designs and operating factors on the transmitted vibration and to seek designs of primary and secondary suspension systems (Laib, 1995; Soliman, 1995; Peng & Lines, 1997; Lehtonen, 2005). Such efforts for soil compactors, however, have been limited to only a few kinematic and dynamic models for motion planning of the compaction tasks (Guillo, Gautier, & Boyer, 1999; Lemaire C.-E. , Vandanjon, Gautier, & Peyret, 2002). A dynamic model of a soil compactor incorporating the drum vibrator and tire/drum-soil interactions could yield considerable insight into factors affecting the transmission of vibration to the operator, and the soil compaction efficiency. Furthermore, such a model could serve as an essential tool for the design and tuning of primary and secondary suspensions for the vehicle.

From preliminary measurements, it was concluded that the soil compactor vibrations are mostly attributed to the vertical, pitch, roll, lateral and longitudinal vibration modes. This suggests the need for developing a three dimensional vehicle model. This study, however, is limited to the analysis of the in-plane vibration along the vertical and pitch axis. The modeling effort may thus be considered as a preliminary work on characterization and analysis of ride vibration behaviour of a soil compactor. The in-plane models, however, are considered sufficient to study the vibration along the most important axes.

This chapter presents the formulation of in-plane dynamic models of soil compactors to predict the ride vibration responses during the transit and compaction modes of operation, respectively. The transit mode model is formulated considering the rigid steel drum as an extension of the terrain, point contact of the tire with the undeformable terrain surface, and linear visco-elastic properties of the cab and drum mounts. The compaction mode model considers the compaction of the deformable soil together with the eccentric mass-driven drum vibratory system. The major simplifying assumption and excitation due to soil/terrain roughness properties are described together with the methods of analyses.

2.2. Development of soil compactor model – Transit Mode

The ride vibration responses of a soil compactor arising from the interactions of the pneumatic tire and the rigid drum with undeformable terrain are strongly influenced by the weights and dimensions of the vehicle, in addition to many other design and operating conditions (Dynapac, 2000). In this thesis only planar dynamics of the vehicle are investigated. Three different pitch-plane models of the vehicle of varying degrees-of-freedom (DOF) are formulated to investigate different dynamic response aspects in a systematic manner. These include: (i) a two-DOF pitch plane model to investigate the primary bounce and pitch ride dynamic responses of the vehicle body supported on rear axle tires and the front drum suspension; (ii) a Seven-DOF model incorporating the engine group and the operator-station (cab or platform) supported on elastic mounts and an unsuspended seat (cushion); and (iii) a comprehensive 12-DOF model additionally comprising an idealized rear axle suspension and a two-DOF suspension seat. All the three models are formulated assuming linear stiffness and damping properties of the

mounts and the rear axle tires, and consider the weights and dimensions of the vehicles chosen for the field measurements studies (CHAPTER 3). The contribution due to articulated-frame steering to the ride vibration responses, however, is assumed negligible.

2.2.1. Two-DOF vehicle model

The soil compactor in the pitch plane, in the simplest form, may be represented by a two-DOF dynamic model comprising the primary vertical and pitch motions of the vehicle. The mass and moment of inertia of the vehicle body are significantly higher than those of the engine group and the cab. The vehicle can thus be represented by an equivalent single rigid body comprising the masses and moments of inertia of the unsprung body, cab and the engine group. The equivalent single rigid body is isolated from the ground by means of a pair of tires at the rear and drum suspension at the front; the drum being mounted onto the front frame through a number of rubber mounts, as shown in Figure 2-1.
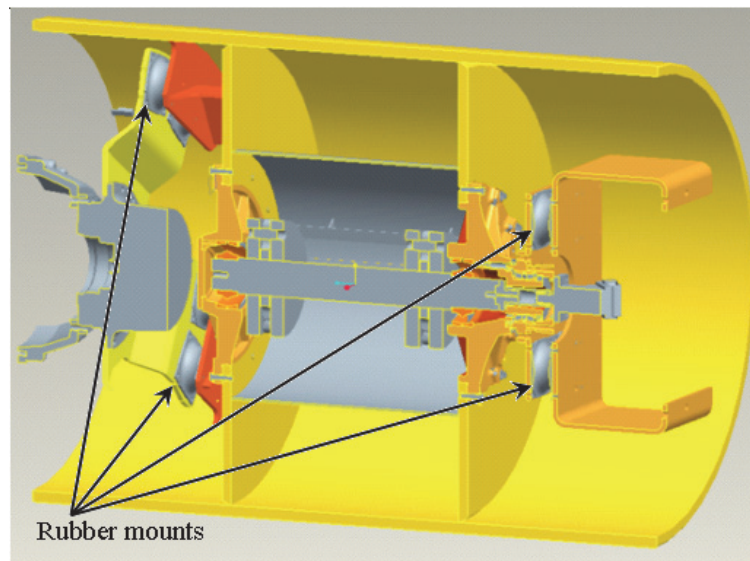
Figure 2-1: The vibratory drum with rubber mounts on the drum drive (left) and on the drum bearing bracket (right)
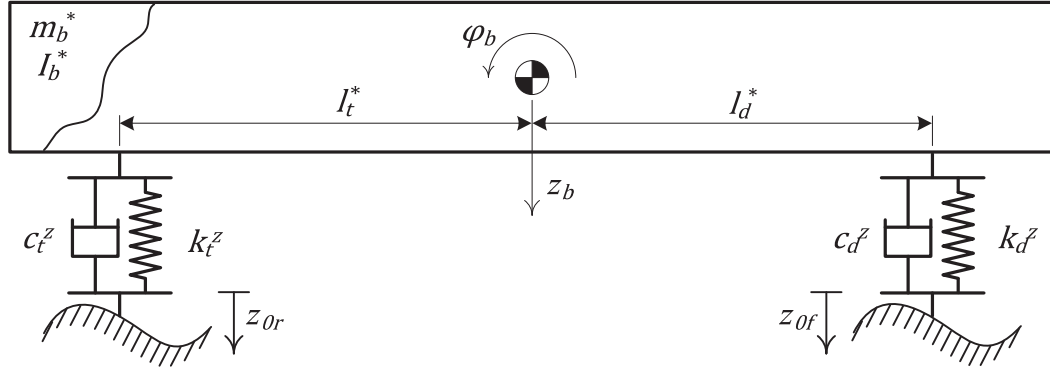
The rubber mounts are considered to serve as the front suspension in the simplified two-DOF model, as shown in Figure 2-2. The equivalent mass (m_b^*), pitch mass moment of inertia (I_b^*) and the coordinates of the center of mass (c.g.) are computed from the distributions of the cabin and engine group masses, as illustrated in Figure 2-3, such that:

$$m_b^* = m_b + m_c + m_e$$

$$I_b^* = I_b + m_b[(l_t - l_t^*)^2 + (h_b^* - h_b)^2]$$

$$+ I_c + m_c[(l_t + l_c - l_t^*)^2 + (h_b + h_c - h_b^*)^2]$$

$$+ I_e + m_e[(l_t^* - l_t + l_e)^2 + (h_b + h_e - h_b^*)^2]$$

$$(2.1)$$

In the above equations m_b, m_c and m_e are the masses due to actual vehicle body, cabin and engine group, respectively, and I_b, I_c and I_e are the respective pitch moments of inertia. The lengths l_t, l_d, l_e and l_c are distances of the rear-axle tires, the drum, engine group c.g. and the cab c.g. from the body c.g., respectively. h_b, h_c and h_e are the vertical distances of the body c.g. from the ground, and the cab and engine group c.g. from the body c.g., respectively. The longitudinal and vertical locations of equivalent vehicle mass (m_b^*) c.g. are described by l_t^* and h_b^*, which are derived as follows:

$$l_t^* = \frac{m_b l_t + m_c(l_t + l_c) + m_e(l_t - l_e)}{m_b^*}$$

$$h_b^* = \frac{m_b h_b + m_c(h_b + h_c) + m_e(h_b + h_e)}{m_b^*}$$

<div align="right">(2.2)</div>

The equations of motion of the simplified two-DOF model are derived as:

$$m_b^* \, \ddot{z}_b + F_d^z + F_t^z = 0$$

$$I_b^* \, \ddot{\varphi}_b - l_d^* \, F_d^z + l_t^* \, F_t^z = 0$$

<div align="right">(2.3)</div>
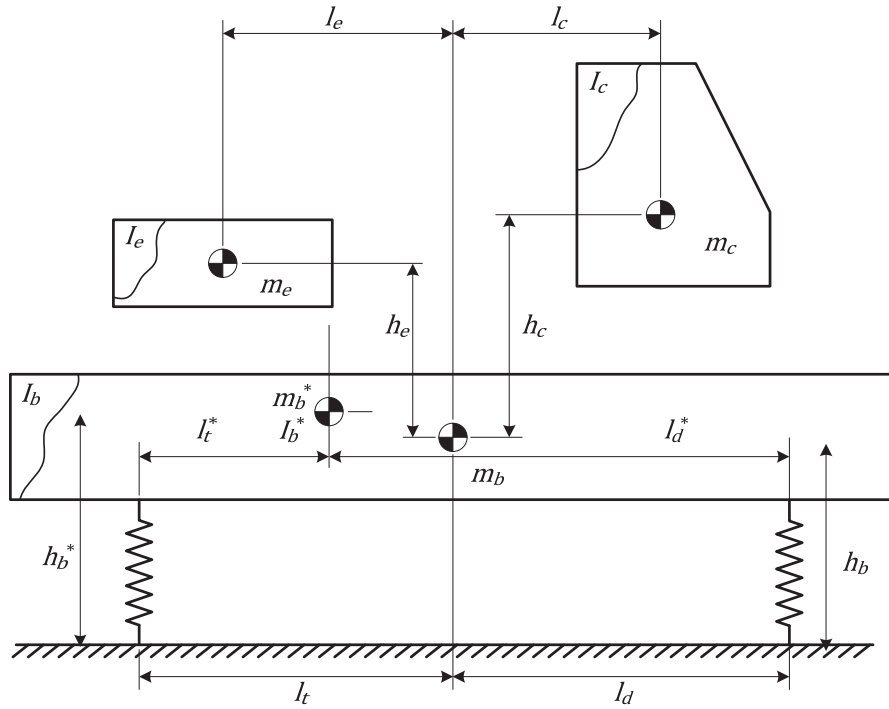
Figure 2-3: The two-DOF bounce/pitch model of a soil compactor illustrating the distribution of the cabin and the engine group masses

Assuming linear vertical stiffness and damping properties of the tires (k_t^z, c_t^z) and the drum mounts (k_d^z, c_d^z), the forces developed by the tire (F_t^z) and the drum mounts (F_d^z) are derived from:

$$F_d^z = k_d^z \left[z_b - l_d^* \varphi_b - z_{0f} \right] + c_d^z \left[\dot{z}_b - l_d^* \dot{\varphi}_b - \dot{z}_{0f} \right]$$

$$F_t^z = k_t^z \left[z_b + l_t^* \varphi_b - z_{0r} \right] + c_t^z \left[\dot{z}_b + l_t^* \dot{\varphi}_b - \dot{z}_{0r} \right]$$

<div align="right">(2.4)</div>

In the above equations, z_b and φ_b define the vertical and pitch DOF of the model, and z_{0f} and z_{0r} define the elevations of the terrain surface at the drum- and tire-terrain interfaces, respectively.
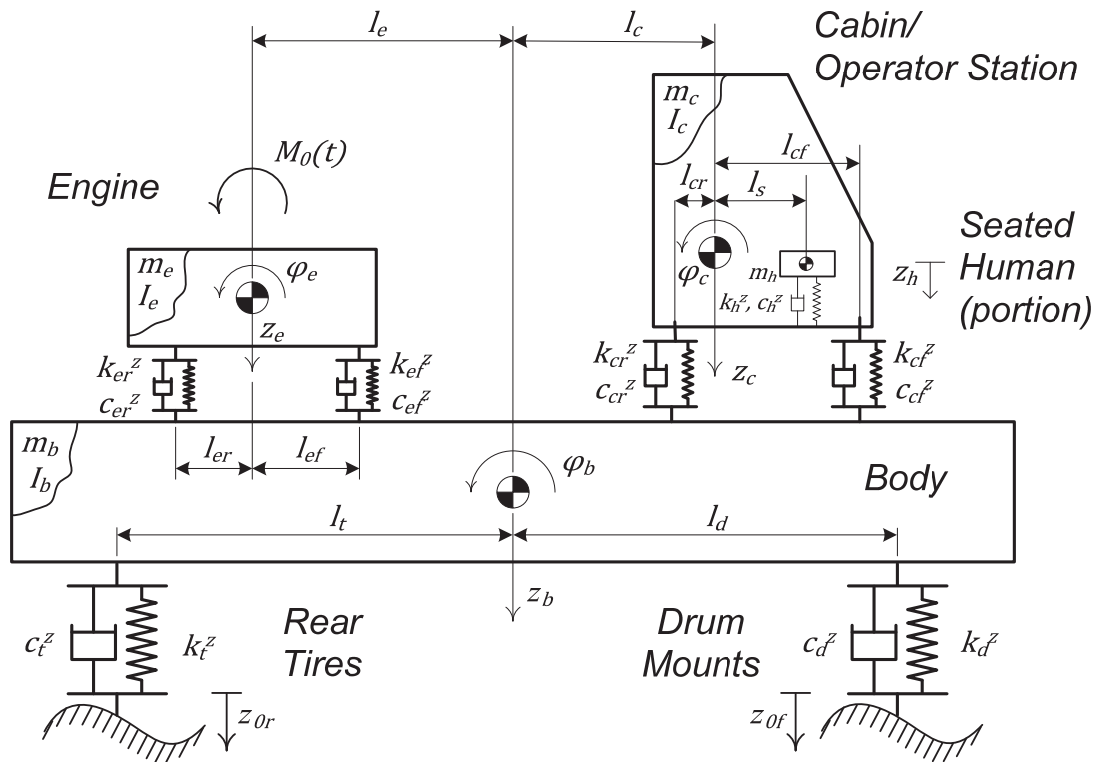
Figure 2-4: Seven-DOF pitch plane ride dynamic model of a soil compactor

2.2.2. Seven-DOF vehicle model

The simplified two-DOF can provide the bounce and pitch mode frequencies of the vehicle in a convenient manner, while it cannot describe the cab motions encountered by the operator. The contributions of the cab mounts, and engine mounts and vibration can

be adequately incorporated through formulation of a seven-DOF model, as shown in Figure 2-4 . The model incorporates the vertical and pitch motions of the vehicle body (z_b , φ_b), cab mass (z_c , φ_c), engine mass (z_e , φ_e) and the operator mass (z_h), while the engine excitation is represented by the moment $M_0(t)$. The engine and cab mounts, as well as the seat cushion, are represented by vertical linear stiffness and damping.

The equations of motion of the vehicle model are expressed as:

$$m_h \ddot{z}_h + F_h^z = 0$$

$$m_c \ddot{z}_c + F_{cf}^z + F_{cf}^z - F_h^z = 0$$

$$I_c \ddot{\varphi}_c - l_{cf} F_{cf}^z + l_{cr} F_{cr}^z + l_s F_h^z = 0$$

$$m_e \ddot{z}_e + F_{ef}^z + F_{er}^z = 0$$

$$I_e \ddot{\varphi}_e - l_{ef} F_{ef}^z + l_{er} F_{er}^z = M_0(t)$$

$$m_b \ddot{z}_b + F_d^z + F_t^z - F_{ef}^z - F_{er}^z - F_{cf}^z - F_{cr}^z = 0$$

$$I_b \ddot{\varphi}_b - l_d F_d^z + l_t F_t^z - \left(l_e - l_{ef}\right) F_{ef}^z - \left(l_e + l_{er}\right) F_{er}^z$$
$$+ \left(l_c + l_{cf}\right) F_{cf}^z + \left(l_c - l_{cr}\right) F_{cr}^z = 0$$

$$\text{(2.5)}$$

Where F_{ej}^z and F_{cj}^z are the vertical forces due to engine and cab mounts, where $j = f, r$ refers to the front and rear mounts and F_h^z the vertical forces due to seat cushion. Assuming linear stiffness (k_{ej}^z, k_{cj}^z and k_h^z) and damping (c_{ej}^z, c_{cj}^z and c_h^z) coefficients of the mounts and the cushion, these forces are expressed as:

$$F_{ef}^z = k_{ef}^z \left[z_e - l_{ef}\varphi_e - z_b - (l_e - l_{ef})\varphi_b \right]$$

$$+ c_{ef}^z \left[\dot{z}_e - l_{ef}\dot{\varphi}_e - \dot{z}_b - (l_e - l_{ef})\dot{\varphi}_b \right]$$

$$F_{er}^z = k_{er}^z \left[z_e + l_{er}\varphi_e - z_b - (l_e + l_{er})\varphi_b \right]$$

$$+ c_{er}^z \left[\dot{z}_e + l_{er}\dot{\varphi}_e - \dot{z}_b - (l_e + l_{er})\dot{\varphi}_b \right]$$

<div align="right">(2.6)</div>

and

$$F_{cf}^z = k_{cf}^z \left[z_c - l_{cf}\varphi_c - z_b + (l_c + l_{cf})\varphi_b \right]$$

$$+ c_{cf}^z \left[\dot{z}_c - l_{cf}\dot{\varphi}_c - \dot{z}_b + (l_c + l_{cf})\dot{\varphi}_b \right]$$

$$F_{cr}^z = k_{cr}^z \left[z_c + l_{cr}\varphi_c - z_b + (l_c - l_{cr})\varphi_b \right]$$

$$+ c_{cr}^z \left[\dot{z}_c + l_{cr}\dot{\varphi}_c - \dot{z}_b + (l_c - l_{cr})\dot{\varphi}_b \right]$$

$$F_h^z = k_h^z [z_h - z_c + l_s\varphi_c] + c_h^z [\dot{z}_h - \dot{z}_c + l_s\dot{\varphi}_c]$$

<div align="right">(2.7)</div>

In the above equations, l_{ef} and l_{er} are the longitudinal distances of the front and rear engine mounts, respectively, from the engine mass c.g. . In a similar manner, l_{cf} , l_{cr} and l_s are the respective distances of front and rear cab/platform mounts, and seat with respect to the cab mass c.g. , as seen in Figure 2-4. The forces developed by the linear tire and drum mounts, F_t^z and F_d^z, are described by Eq. (2.4), where $l_d^* = l_d$ and $l_t^* = l_t$.

2.2.3. Twelve-DOF vehicle model

The simplified two- and seven-DOF models, presented in the previous sections, consider negligible contributions of the shear properties of the mounts, which could lead to horizontal motion of the cabin, vehicle body and the engine mass. These models do not

permit the analysis of potential benefits of a suspension seat and a possible primary suspension at the rear axle. Consequently, a more detailed model is formulated with an objective to investigate potential ride performance benefits of a suspension seat and an axle suspension, which are assumed to possess linear properties, with the rear wheels considered as unsprung mass (m_w). The visco-elastic properties of the drum mounts are represented by lumped linear stiffness and damping constants in the vertical (k_d^z, c_d^z) and longitudinal (k_d^x, c_d^x) modes, as shown in Figure 2-6. In a similar manner, the shear properties of the engine and cab mounts are represented by linear stiffness (k_{ej}^x, k_{cj}^x) and damping (c_{ej}^x, c_{cj}^x) in the longitudinal direction. The tire interaction with the terrain surface in the shear direction is modeled by linear stiffness (k_t^x) and damping (c_t^x) elements, while the axle suspension is represented by its linear vertical stiffness and damping elements (k_a^z, c_a^z). The rear axle suspension representation by the vertical spring and damping elements is supported by an independent suspension design proposed by Timothy (Cashin, 2007) and shown in Figure 2-5.
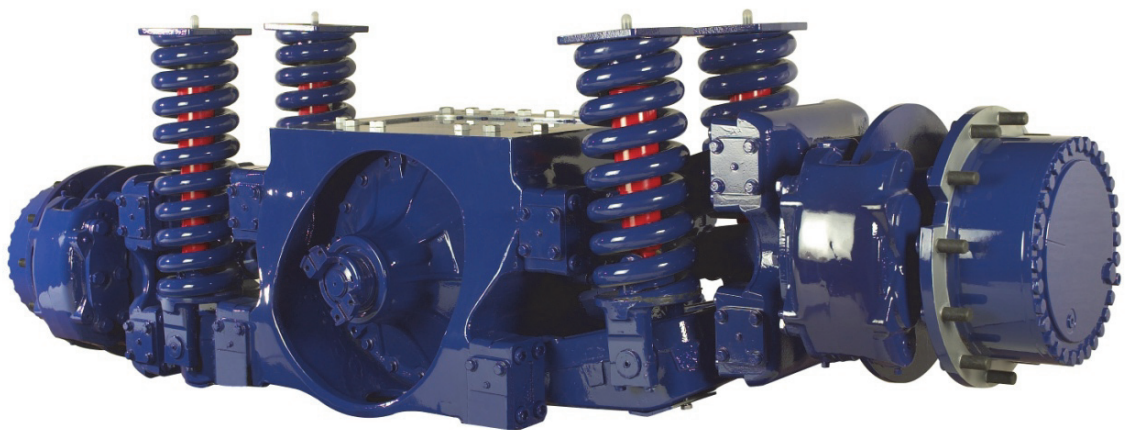
Figure 2-5: Pictorial view of an independent axle suspension for construction equipment (Timoney Mobility Systems)

38

The DOFs of the model include: the vertical, pitch and longitudinal motions of the vehicle body (z_b, φ_b, x_b), cabin (z_c, φ_c, x_c) and the engine group (z_e, φ_e, x_e); vertical motion of rear wheels mass m_w (z_w); and vertical motion of the suspension seat mass (z_s) and the operator mass (z_h). Axle suspension is assumed to be constrained along the vertical axis, and the longitudinal motion of the wheels x_w is assumed to be equal to x_b. As for the previous models, the rigid drum is considered as an extension of the terrain.

The heights h_a, h_t and h_d are the distances between the axle centre, tire-soil contact and the drum centre from the body c.g., respectively. Similarly, h_{cm} and h_{em} are the vertical distances of the cab and engine mass c.g. from their isolation mounts, respectively.
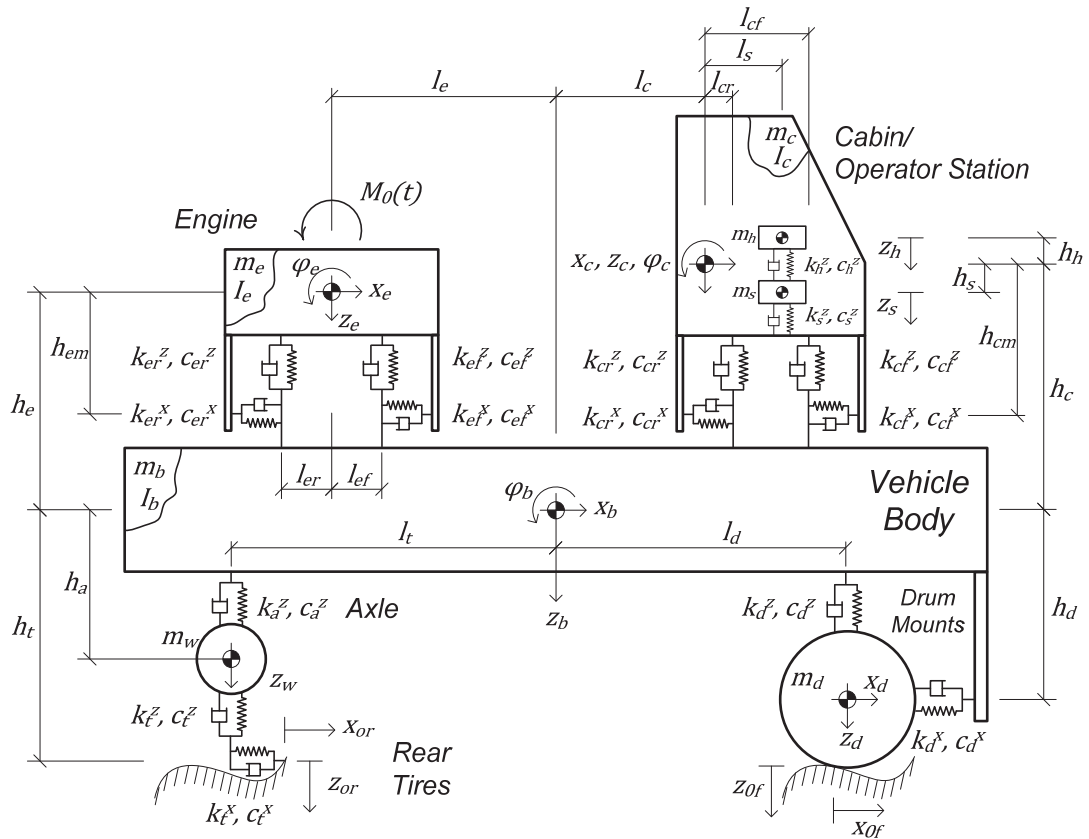
Figure 2-6: The twelve-DOF pitch-plane model of the soil compactor

39

The visco-elastic properties of the seat suspension are represented by lumped linear stiffness and damping constants in the vertical (k_s^z, c_s^z) modes, as are represented the elastic properties of the seat stops (k_{st}^z) and the seat friction damping (f_s^z) as shown in Figure 2-7.
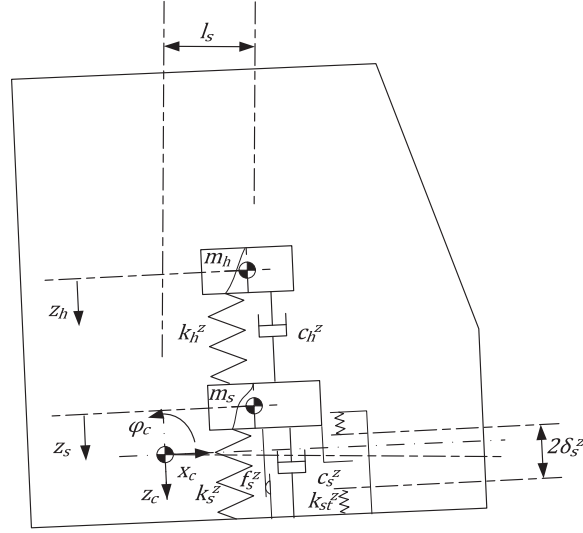
Figure 2-7: suspension seat model

The vertical forces due to the seat suspension (F_s^z) and cushion (F_h^z) are derived from:

$$F_s^z = k_s^z[z_s - z_c + l_s \, \varphi_c] + c_s^z[\dot{z}_s - \dot{z}_c + l_s \, \dot{\varphi}_c]$$

$$+ f_s^z \, sgn[\dot{z}_s - \dot{z}_c + l_s \, \dot{\varphi}_c] + k_{st}^z[z_s - z_c + l_s \, \varphi_c - \delta_s^z]S$$

with
$$sgn[\dot{z}_s - \dot{z}_c + \dot{\varphi}_c l_s] = \begin{cases} +1; & [\dot{z}_s - \dot{z}_c + l_s \, \dot{\varphi}_c] > 0 \\ -1; & [\dot{z}_s - \dot{z}_c + l_s \, \dot{\varphi}_c] < 0 \end{cases}$$

and
$$S = \begin{cases} 1; & |z_s - z_c + l_s \, \varphi_c| > \delta_s^z \\ 0; & Else \end{cases}$$

$$F_h^z = k_h^z[z_h - z_s] + c_h^z[\dot{z}_h - \dot{z}_s]$$

(2.8)

In the above equations δ_s^z is the seat suspension half travel, as seen in Figure 2-7.

The nonlinear suspension seat model could be approximated by a simplified linear model (Allen, 1978), as illustrated by the twelve-DOF idealisation of the compactor depicted in Figure 2-6, in order to drive a system of linear coupled differential equations of motion for the vehicle model. This yields the vertical force due to the seat suspension as:

$$F_s^z \cong k_s^z[z_s - z_c + l_s \, \varphi_c] + c_s^z[\dot{z}_s - \dot{z}_c + l_s \, \dot{\varphi}_c]$$

(2.9)

The equations of motion of the vehicle model are derived using the Lagrange's energy method and summarized below.

Suspension Seat and Occupant:

$$m_s \ddot{z}_s + F_s^z - F_h^z = 0 \qquad\qquad m_h \ddot{z}_h + F_h^z = 0$$

(2.10)

Cabin:

$$m_c \ddot{x}_c + F_c^x = 0$$

$$m_c \ddot{z}_c + F_{cf}^z + F_{cr}^z - F_s^z = 0$$

$$I_c \ddot{\varphi}_c + h_{cm} F_c^x - l_{cf} \, F_{cf}^z + l_{cr} \, F_{cr}^z + l_s \, F_s^z = 0$$

(2.11)

Engine Group:

$$m_e \ddot{x}_e + F_e^x = 0$$

$$m_e \ddot{z}_e + F_{ef}^z + F_{er}^z = 0$$

$$I_e \ddot{\varphi}_e + h_{em} \, F_e^x - l_{ef} \, F_{ef}^z + l_{er} \, F_{er}^z = M_0(t)$$

(2.12)

41

Vehicle Body:

$$(m_b + m_w)\,\ddot{x}_b + F_d^x + F_t^x - F_e^x - F_c^x = 0$$

$$m_b\ddot{z}_b + F_d^z + F_a^z - F_{ef}^z - F_{er}^z - F_{cf}^z - F_{cr}^z = 0$$

$$I_b\ddot{\varphi}_b + h_d F_d^x + h_t\, F_t^x - l_d F_d^z + l_t\, F_a^z$$

$$+ (h_e - h_{em})\, F_e^x - (l_e - l_{ef})\, F_{ef}^z - (l_e + l_{er})\, F_{er}^z$$

$$+ (h_c - h_{cm}) F_c^x + (l_c + l_{cf})\, F_{cf}^z + (l_c - l_{cr})\, F_{cr}^z = 0$$

$$(2.13)$$

Rear Axle:

$$m_w\ddot{z}_w + F_t^z - F_a^z = 0$$

$$(2.14)$$

where F_t^x and F_d^x are the longitudinal forces due to tires and drum mounts. These forces are expressed as:

$$F_t^x = k_t^x[x_b + h_t\varphi_b - x_{0r}] + c_t^x[\dot{x}_b + h_t\dot{\varphi}_b - \dot{x}_{0r}]$$

$$F_d^x = k_d^x[\, x_b + h_d\varphi_b - x_d] + c_d^x[\dot{x}_b + h_d\dot{\varphi}_b - \dot{x}_d]; \qquad \text{with } x_d \approx x_{0f}$$

$$(2.15)$$

The vertical forces developed by the tires (F_t^z), the axle suspension (F_a^z) and the drum mounts (F_d^z) are derived from:

$$F_t^z = k_t^z\, [z_w - z_{0r}] + c_t^z\, [\dot{z}_w - \dot{z}_{0r}]$$

$$F_a^z = k_a^z\, [z_b + l_t\varphi_b - z_w] + c_a^z\, [\dot{z}_b + l_t\dot{\varphi}_b - \dot{z}_w]$$

$$F_d^z = k_d^z\, [z_b - l_d\varphi_b - z_d] + c_d^z\, [\dot{z}_b - l_d\dot{\varphi}_b - \dot{z}_d]; \qquad \text{with } z_d = z_{0f}$$

$$(2.16)$$

The longitudinal forces developed by the engine (F_e^x) and cab mounts (F_c^x) are derived from:

$$F_e^x = \left(k_{ef}^x + k_{er}^x\right)[x_e + h_{em}\,\varphi_e - x_b + (h_e - h_{em})\varphi_b]$$

$$+ \left(c_{ef}^x + c_{er}^x\right)[\dot{x}_e + h_{em}\,\dot{\varphi}_e - \dot{x}_b + (h_e - h_{em})\,\dot{\varphi}_b]$$

$$(2.17)$$

$$F_c^x = \left(k_{cf}^x + k_{cr}^x\right)[x_c + h_{cm}\,\varphi_c - x_b + (h_c - h_{cm})\,\varphi_b]$$

$$+ \left(c_{cf}^x + c_{cr}^x\right)[\dot{x}_c + h_{cm}\dot{\varphi}_c - \dot{x}_b + (h_c - h_{cm})\,\dot{\varphi}_b]$$

$$(2.18)$$

The vertical forces due to engine and cab mounts, F_{ej}^z and F_{cj}^z, where $j = f, r$ refers to the front and rear mounts, are described by Eq. (2.6) and Eq. (2.7).

The system of linear coupled differential equations of motion for the vehicle models can be represented in the matrix form as:

$$[M]\{\ddot{Z}\} + [C]\{\dot{Z}\} + [K]\{Z\} = \{F(t)\}$$

$$(2.19)$$

Where $[M]$, $[C]$ and $[K]$ are $(n \times n)$ mass, damping and stiffness matrices, respectively; n is the number of DOF and $\{F(t)\}$ is the $(n \times 1)$ forcing vector.

2.3. Development of soil compactor model–Compaction Mode

In the compaction mode, the terrain can no longer be considered undeformable. The vibration responses of a soil compactor arising from the interaction of the rigid vibratory drum with elasto-plastic soils are strongly influenced by the nature and grade of the soil as well as its moisture content in addition to many other widely-studied road design and construction parameters (Quibel & Corte, 1994; Terzaghi, Peck, & Mesri, 1996; Akanda,

43

1999; Lay, 2009). The stress-strain properties of the soils have been extensively investigated analytically and experimentally (Kabré, 1991; Quibel & Corte, 1994; Valeux & Feistenauer, 1995; Adam & Kopf, 2000). A number of studies have also proposed the lumped-parameter and finite element models of the soils for predicting propagation of the loading forces applied at the soil surface (Farzaneh, 1983; Pietzsch & Poppy, 1992, Anderegg, 2000; Erdmann, Adam, & Kopf, 2006). The models based on the finite-element method have been shown to be more appropriate for predicting stress distributions in three dimensions, while the lumped parameters describing the elasto-plastic properties of the soil are considered adequate for study of one-dimensional compaction, which is considered well-suited for the in-plane vehicle model in this study. The soil compaction and the drum-soil interactions are thus characterized by formulating a simple elasto-plastic model of the soil to drive the equations of motion of the vehicle. In the modeling process, the vibratory drum and the soil are considered to form a closed-loop system (Thurner, 2001; Krober, Floss, & Wallrath, 2001; Anderegg & Kaufmann, 2004). The soil may be considered to behave as an elastic-plastic medium during initial loading by the drum (Pietzsch & Poppy, 1992; Adam & Kopf, 2000). The propagation of the drum forces to the soil tends to enhance the density of the soil (Yoo & Selig, 1979; Quibel & Corte, 1994; Adam & Kopf, 2000). In the initial passes, the soil thus poses elasto-plastic reaction forces in the compression axis. The soil behaviour tends to become increasingly elastic as the compaction process progresses, with subsequent compactor passes, as a result of the increased soil density. The denser, thus stiffer, soil poses a greater demand on the drum forces. The dynamic behaviour of a vibratory compactor is thus determined by the properties of both the vehicle and the soil, and the interaction

44

between the two. The drum-soil model is subsequently integrated into the planar vehicular models, developed in the previous section, to study the dynamic responses of the vehicle in the compaction phase.

2.3.1. Single-DOF drum - soil compaction model

In this study, a drum-soil interaction model is formulated considering the vertical dynamics of the drum alone coupled with a visco-elastic model describing the elasto-plastic behaviour of the soil. The resulting model could be described by a third-order differential equation.
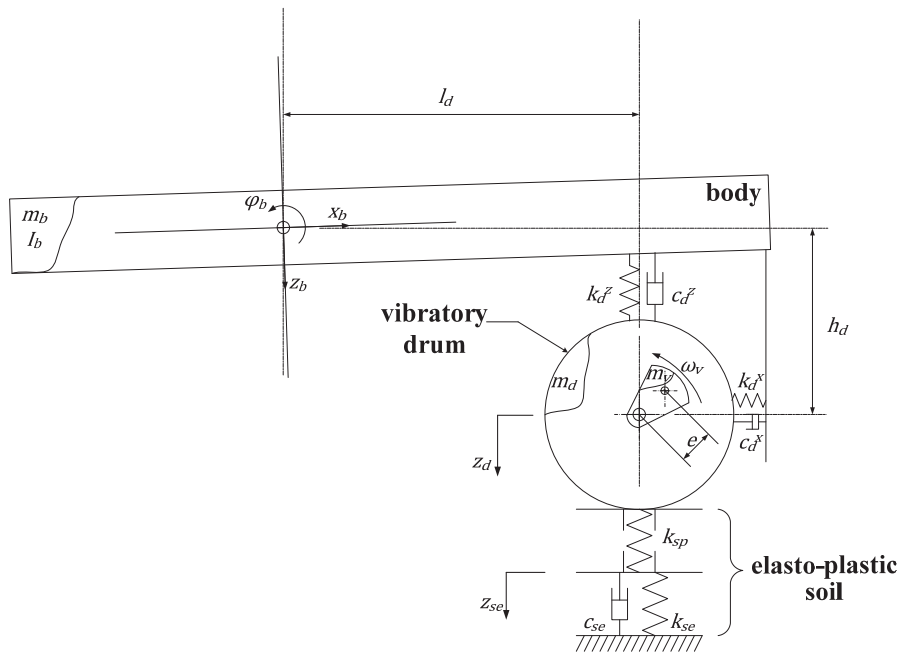
Figure 2-8: model of the vibratory drum with elasto-plastic soil interaction

The drum-soil model is formulated assuming constant stiffness and damping properties of the elasto-plastic soil model. The contributions of the drum cylindrical geometry and its penetration into the soil to variations in the soil stiffness and damping properties are assumed negligible. A simple model of the vibratory drum coupled to the main body

through its rubber mounts (drum suspension) is depicted in Figure 2-8. The drum mounts are represented by their effective stiffness and damping constants along the vertical (k_d^z, c_d^z) and the horizontal (k_d^x, c_d^x) axes, as shown. The model features an unbalance mass that constitutes its vibrator to generate forced vibration or dynamic loading of the soil at frequencies around 30 Hz. The soil is dynamically modeled as being the juxtaposition of a linearly plastic zone embedded in a wider and deeper visco-elastic body (Pietzsch & Poppy, 1992; Adam & Kopf, 2000; Thurner, 2001).

When the vibratory drum is in contact with the elasto-plastic soil, the equation of motion of the drum can be expressed as:

$$m_d \ddot{z}_d + F_s - F_d^z = F(t)$$

(2.20)

Where F_d^z is the vertical force developed due to the drum mounts, as described by Eq. (2.16) and F_s is the dynamic force developed by the surface layer of the soil due to its plastic deformation, given by:

$$F_s = k_{sp}(z_d - z_{se})$$

(2.21)

Where k_{sp} is the idealized stiffness associated with the soil plastic behaviour ($k_{sp} \rightarrow \infty$ when the soil is unloaded) and z_{se} is the soil elastic deformation. The propagation of the above soil force, attributed to the plastic deformation yields elasto-plastic deformation of the subsequent layers of the soil. From the elasto-plastic soil model, shown in Figure 2-8, the force due to soil can also be expressed as:

$$F_s = c_{se}\dot{z}_{se} + k_{se}z_{se}$$

(2.22)

where k_{se} and c_{se} are the elastic stiffness and damping properties of the soil model shown in Figure 2-8.

Eq. (2.21) and (2.22) yield following relationship between the soil deformation and the drum motion, z_d:

$$c_{se}\dot{z}_{se} + (k_{se} + k_{sp})z_{se} = k_{sp}z_d$$

(2.23)

Also $F(t)$ in Eq. (2.20), is the vertical projection of the centrifugal force F_{cent} developed by the rotating eccentric mass m_v, given by:

$$F(t) = F_{cent} \sin(\omega_v t) \qquad \text{with} \qquad F_{cent} = m_v\, e\, \omega_v{}^2$$

(2.24)

where ω_v is the angular frequency of the vibrator, and e is the eccentricity of the rotating mass. Considering the static equilibrium as the reference point for the vertical displacement coordinates of the model, the portion of the total vehicle mass supported at the drum - soil interface (front axle static load) m_1 is balanced by the soil force due to its static compression, such that:

$$\delta_s^{stat} = \frac{m_1\, g}{k_s^*} \quad ; \text{where} \quad k_s^* = \frac{k_{se}\, k_{sp}}{k_{se} + k_{sp}}$$

(2.25)

The total compaction or soil reaction force $F_{s\,Tot}$ is thus the sum of the front axle static load and the soil dynamic force F_s, such that:

$$F_{s\,Tot} = F_s + m_1\, g$$

(2.26)

The elastic-plastic behaviour of the soil has been described (Adam & Kopf, 2000) by a plasticity parameter ε:

$$\varepsilon = \frac{k_{sp}}{k_{sp} + k_{se}}$$

<div align="right">(2.27)</div>

The parameter ε varies between 0 and 1, where $\varepsilon = 1$ refers to an ideal elastic behaviour that is achieved as $k_{sp} \to \infty$. The value $\varepsilon = 0$ refers to purely plastic property characterised by $k_{sp} = 0$, which also qualifies the loss of contact between the drum and the soil. The motion of the vibratory drum on a soil patch of given density (compaction level) may exhibit, over each cycle of the drum vibrator, two or more often three distinct phases, which are described below:

i. Soil compression, dynamic "loading" ($F_{s\,Tot} > 0$ and $\dot{z}_d > 0$): the soil possesses finite plastic stiffness and elastic stiffness values k_{sp} and k_{se}, which may vary with the degree of compaction of the soil and changes in the soil density. As the machine performs repeated passes of compaction over the given soil, both k_{sp} and k_{se} increase following a trend that leads to higher value of ε. The soil becomes more elastic due to propagation of the dynamic force to the subsequent layers of the soil (Adam & Kopf, 2000).

ii. Soil recovery, "unloading" ($F_{s\,Tot} > 0$ and $\dot{z}_d < 0$): The soil recovers only the elastic deformation as the drum moves upward i.e. $k_{sp} \to \infty$.

iii. Loss of drum-soil contact, "drum-hop" ($F_{s\,Tot} = 0$): the soil - drum link is broken as the soil cannot exert any tension on the drum, thus $k_{sp} = 0$. This phase appears in the compaction cycle as soon as the soil has reached a certain elementary level of compaction. It is actually a behaviour sought for a better compacting in soil applications (Anderegg, 2000; Briaud & Seo, 2003).

The time differentiation of Eq. (2.20) can be written as:

$$\varepsilon \gamma m_d \dddot{z}_d + \varepsilon c_{se} \ddot{z}_d - \varepsilon c_{se} \dot{z}_{se} - \varepsilon \gamma \dot{F}_d^z = \varepsilon \gamma \dot{F}(t)$$

(2.28)

where γ is proposed as the damping to plasticity ratio, given by:

$$\gamma = \frac{c_{se}}{k_{sp}}$$

(2.29)

The summation of Eq. (2.20) and (2.28) yields the following third order differential equation in coupled motion of the drum z_d and the soil z_{se} :

$$\varepsilon \gamma m_d \dddot{z}_d + m_d \ddot{z}_d + \varepsilon c_{se} \dot{z}_d + k_{sp} z_d - \varepsilon c_{se} \dot{z}_{se} - k_{sp} z_{se} - \varepsilon \gamma \dot{F}_d^z - F_d^z$$
$$= \varepsilon \gamma \dot{F}(t) + F(t)$$

(2.30)

Pre-multiplying Eq. (2.23) by ε, yields:

$$\varepsilon c_{se} \dot{z}_{se} + k_{sp} z_{se} = \varepsilon k_{sp} z_d$$

(2.31)

The above two equations yield a third-order differential equation in z_d alone:

$$\varepsilon \gamma m_d \dddot{z}_d + m_d \ddot{z}_d + \varepsilon c_{se} \dot{z}_d + \varepsilon k_{se} z_d - \varepsilon \gamma \dot{F}_d^z - F_d^z = \varepsilon \gamma \dot{F}(t) + F(t)$$

(2.32)

Substituting for F_d^z from Eq. (2.16) and $F(t)$ from (2.24), the previous is rewritten as:

$$\varepsilon \gamma m_d \dddot{z}_d + (m_d + \varepsilon \gamma c_d^z) \ddot{z}_d + (\varepsilon c_{se} + c_d^z + \varepsilon \gamma k_d^z) \dot{z}_d + (\varepsilon k_{se} + k_d^z) z_d$$
$$- \varepsilon \gamma c_d^z \dddot{z}_b - (c_d^z + \varepsilon \gamma k_d^z) \dot{z}_b - k_d^z z_b$$
$$+ \varepsilon \gamma c_d^z l_d \dddot{\varphi}_b + (c_d^z l_d + \varepsilon \gamma k_d^z l_d) \dot{\varphi}_b + k_d^z l_d \varphi_b$$
$$= \varepsilon \gamma m_v e \omega_v^3 \cos(\omega_v t) + m_v e \omega_v^2 \sin(\omega_v t)$$

(2.33)

The above equation relates the motions of the drum and the vehicle body to the vibratory excitation of the drum and elasto-plastic soil properties.

2.3.2. **Integration of the compaction model to the vehicle models**

The vehicle compaction model is built by assembling the previously described drum-soil model characterized by a 3rd order differential equation of motion and the ride dynamic model of the vehicle. The soil compaction tends to cause predominant vibration in the vicinity of the angular frequency of the rotating mass (near 30 Hz), as observed in preliminary field measurements. Since this vibration frequency is effectively attenuated by the W_k-weighting filter, the integration was performed for the seven-DOF ride model described in section 2.2.2. The integration of the drum-soil model introduces an additional DOF, leading the general coordinate vector $\{Z\}$, as:

$$\{Z\} = \{z_d \quad z_b \quad \varphi_b \quad z_e \quad \varphi_e \quad z_c \quad \varphi_c \quad z_h\}'; \qquad n = 8$$

where " $'$ " designates the transpose of the vector. The governing equations of motion may be expressed in the matrix form by a set of third-order differential equations as:

$$[A_3]\{\dddot{Z}\} + [A_2]\{\ddot{Z}\} + [A_1]\{\dot{Z}\} + [A_0]\{Z\} = \{U(t)\}$$

(2.34)

where $[A_0]$, $[A_1]$, $[A_2]$ and $[A_3]$ are $(n \times n)$ matrices of the vehicle and soil parameters, and $\{U(t)\}$ is the $(n \times 1)$ vector containing time derivatives of the excitation forces. In compaction mode, terrain elevations (z_{of}, z_{or}) are marginal, since soil compaction is performed on previously graded layers of construction material and surfaces at very low speed (near 3 km/h), and their contribution is considered negligible since it would yield

50

considerably lower magnitudes of low-frequency vibration when compared to the predominant vibration in the vicinity of the angular frequency of the rotating mass.

As described earlier, the drum-soil interactions constitute three distinct phases, namely:

- The loading phase of the elasto-plastic soil as the drum moves downward (sinkage and shearing) into the elasto-plastic soil;

- The unloading phase of the soil as the drum moves upward while retaining contact with the soil as it recovers (soil elasticity); and

- The phase in which the drum potentially looses contact with the soil towards the end of the unloading phase when the soil is considered to have recovered its elastic deformation, while the drum continues its upward motion.

The coefficient matrices $[A_3]$, $[A_2]$, $[A_1]$ and $[A_0]$ in Eq. (2.34) are determined corresponding to each of the above three phases of drum-soil interactions. These coefficient matrices comprise the $(n - 1 \times n - 1)$ mass, damping and stiffness $[M]$, $[C]$ and $[K]$ matrices, and the vector $\{U(t)\}$ includes $\{F(t)\}$.

Loading Phase

In the loading phase, the drum moves downward in the vertical direction and a compressive load is applied to the soil. Figure 2-9 illustrates the loading action of the compactor drum while moving downward into an elasto-plastic patch of the soil. This phase is characterised by both elastic and plastic deformations of the soil leading to soil compaction. The total force imparted on the soil and the necessary conditions for this loading phase are given by:

$$F_{s\,Tot} = F_s + m_1 g > 0; \qquad \text{and} \qquad \dot{z}_d > 0$$

The third-order differeantial equation describing the motion of the drum, presented in Eq.(2.33), is arranged in the following manner:

$$\varepsilon\gamma m_d \dddot{z}_d + (m_d + \varepsilon\gamma c_d^z)\ddot{z}_d - \varepsilon\gamma c_d^z\, \ddot{z}_b + \varepsilon\gamma c_d^z l_d \ddddot{\varphi}_b$$

$$+ (\varepsilon c_{se} + c_d^z + \varepsilon\gamma k_d^z)\dot{z}_d - (c_d^z + \varepsilon\gamma k_d^z)\,\dot{z}_b + (c_d^z l_d + \varepsilon\gamma k_d^z l_d)\dot{\varphi}_b$$

$$+ (\varepsilon k_{se} + k_d^z)z_d - k_d^z\, z_b + k_d^z l_d\, \varphi_b$$

$$= \varepsilon\gamma m_v\, e\, \omega_v{}^3 \cos(\omega_v t) + m_v\, e\, \omega_v{}^2 \sin(\omega_v t)$$

$$(2.35)$$
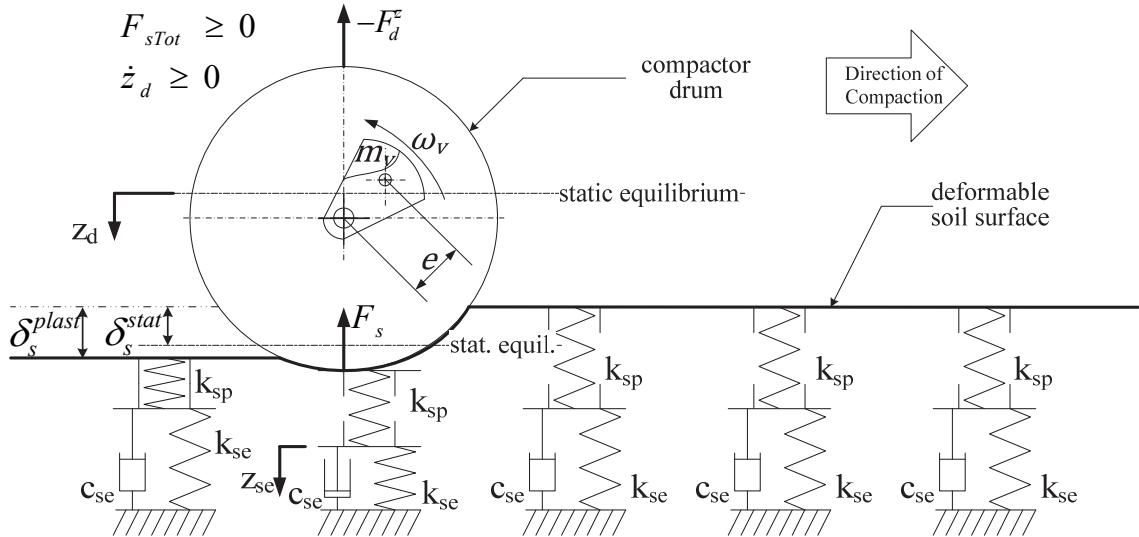
Figure 2-9: Drum-soil interaction model corresponding to elasto-plastic deformation of the soil under downward motion of the drum

The reaction force due to soil, $F_{s\,Tot}$, is derived as:

$$F_{s\,Tot} = -m_d \ddot{z}_d + F_d^z + F(t) + m_1\, g$$

$$(2.36)$$

Upon substituting for the forces due to drum mounts and excitation, the above equation may be expressed as:

52

$$F_{s\,Tot} = -m_d \ddot{z}_d - c_d^z \dot{z}_d + c_d^z \dot{z}_b - c_d^z l_d \dot{\varphi}_b - k_d^z z_d + k_d^z z_b - k_d^z l_d \varphi_b$$

$$+ m_v\, e\, \omega_v{}^2 \sin(\omega_v t) + m_1\, g$$

<div align="right">(2.37)</div>

The remaining equations of motion of the coupled drum-soil-vehicle model are identical to those presented in Eq. (2.5) to (2.7) and Eq. (2.19). Subsequently, the coefficient matrices $[A_0]$, $[A_1]$, $[A_2]$ and $[A_3]$ are formulated as:

$$[A_0] = \begin{bmatrix} (\varepsilon k_{se} + k_d^z) & \{A_0^{n1}\}' \\ \{A_0^{n1}\} & [K] \end{bmatrix}; \qquad [A_1] = \begin{bmatrix} (\varepsilon c_{se} + c_d^z + \varepsilon \gamma k_d^z) & \{A_1^{1n}\} \\ \{A_1^{n1}\} & [C] \end{bmatrix};$$

$$[A_2] = \begin{bmatrix} (m_d + \varepsilon \gamma c_d^z) & \{A_2^{1n}\} \\ \{0\} & [M] \end{bmatrix}; \qquad \text{and} \qquad [A_3] = \begin{bmatrix} \varepsilon \gamma m_d & \{0\} \\ \{0\} & [0] \end{bmatrix}.$$

where $[M]$, $[C]$ and $[K]$ are $(n-1 \times n-1)$ mass, damping and stiffness matrices, respectively derived for the $(n-1)$-DOF ride dynamic model and $\{A_0^{n1}\}$, $\{A_1^{n1}\}$, $\{A_1^{1n}\}$ and $\{A_2^{1n}\}$ are $(n-1 \times 1)$ or $(1 \times n-1)$ vectors containing the drum mounts and soil properties, given by:

$$\{A_0^{n1}\} = \begin{Bmatrix} -k_d^z \\ l_d k_d^z \\ 0 \\ 0 \\ 0 \\ 0 \\ 0 \end{Bmatrix}; \qquad\qquad \{A_1^{n1}\} = \begin{Bmatrix} -c_d^z \\ l_d c_d^z \\ 0 \\ 0 \\ 0 \\ 0 \\ 0 \end{Bmatrix};$$

$$\{A_1^{1n}\} = \{-(c_d^z + \varepsilon \gamma k_d^z) \quad (l_d c_d^z + \varepsilon \gamma l_d k_d^z) \quad 0 \quad 0 \quad 0 \quad 0 \quad 0\};$$

$$\text{and} \quad \{A_2^{1n}\} = \{-\varepsilon \gamma c_d^z \quad \varepsilon \gamma l_d c_d^z \quad 0 \quad 0 \quad 0 \quad 0 \quad 0\}.$$

The forcing vector $\{U(t)\}$ in Eq. (2.34), in a similar manner is formulated as:

$${U(t)} = \begin{Bmatrix} \varepsilon\gamma m_v \, e \, \omega_v^3 \cos(\omega_v t) + m_v \, e \, \omega_v^2 \sin(\omega_v t) \\ {F(t)} \end{Bmatrix}$$

where ${F(t)}$ is the $(n - 1 \times 1)$ forcing vector derived for the $(n - 1)$-DOF ride model.

The equations of motion of the vehicle model, described in the matrix form in Eq. (2.34), comprise $n - 1$ second-order linear differential equations and a nonlinear third-order differential equation. The system of equations may also be expressed by n third-order differential equations by taking the time derivatives of the equations of motion described in Eq. (2.19), resulting in:

$$[B_3]{\dddot{Z}} + [B_2]{\ddot{Z}} + [B_1]{\dot{Z}} + [B_0]{Z} = {V(t)}$$

(2.38)

Where $[B_0]$, $[B_1]$, $[B_2]$ and $[B_3]$ are $(n \times n)$ matrices of the system parameters and ${V(t)}$ is the $(n \times 1)$ forcing vector, given by:

$$[B_0] = \begin{bmatrix} (\varepsilon k_{se} + k_d^z) & {A_0^{n1}}' \\ {0} & [0] \end{bmatrix}; \qquad [B_1] = \begin{bmatrix} (\varepsilon c_{se} + c_d^z + \varepsilon\gamma k_d^z) & {A_1^{1n}} \\ {A_0^{n1}} & [K] \end{bmatrix};$$

$$[B_2] = \begin{bmatrix} (m_d + \varepsilon\gamma c_d^z) & {A_2^{1n}} \\ {A_1^{n1}} & [C] \end{bmatrix}; \qquad [B_3] = \begin{bmatrix} \varepsilon\gamma m_d & {0} \\ {0} & [M] \end{bmatrix}; \qquad \text{and}$$

$$\{V(t)\} = \begin{Bmatrix} \varepsilon\gamma m_v \, e \, \omega_v^3 \cos(\omega_v t) + m_v \, e \, \omega_v^2 \sin(\omega_v t) \\ \dot{F}(t) \end{Bmatrix}.$$

Unloading Phase

In the unloading phase of the soil, the drum moves upward while a contact between the drum and soil surface is retained. Figure 2-10 illustrates the action of the drum moving upward permitting the relaxation of the previously loaded soil. In this phase the soil

recovers its elastic deformation, while the plastic deformation represents the soil compaction. The soil stiffness associated with its plastic behaviour (k_{sp}) is thus assumed infinite. The soil reaction force and the necessary conditions for this phase are given by:

$$F_{s\,Tot} = F_s + m_1 g > 0; \qquad \text{and} \qquad \dot{z}_d < 0$$

As $k_{sp} \to \infty$, the plasticity factor $\varepsilon \to 1$ and the soil damping to plasticity ratio $\gamma \to 0$; The equation of motion of the drum Eq. (2.35), thus reduces to the form of a second-order differential equation:

$$m_d \ddot{z}_d + (c_{se} + c_d^z)\dot{z}_d - c_d^z \dot{z}_b + l_d c_d^z \dot{\varphi}_b + (k_{se} + k_d^z)z_d - k_d^z z_b + l_d k_d^z \varphi_b$$

$$= m_v \, e \, \omega_v{}^2 \sin(\omega_v t)$$

$$(2.39)$$
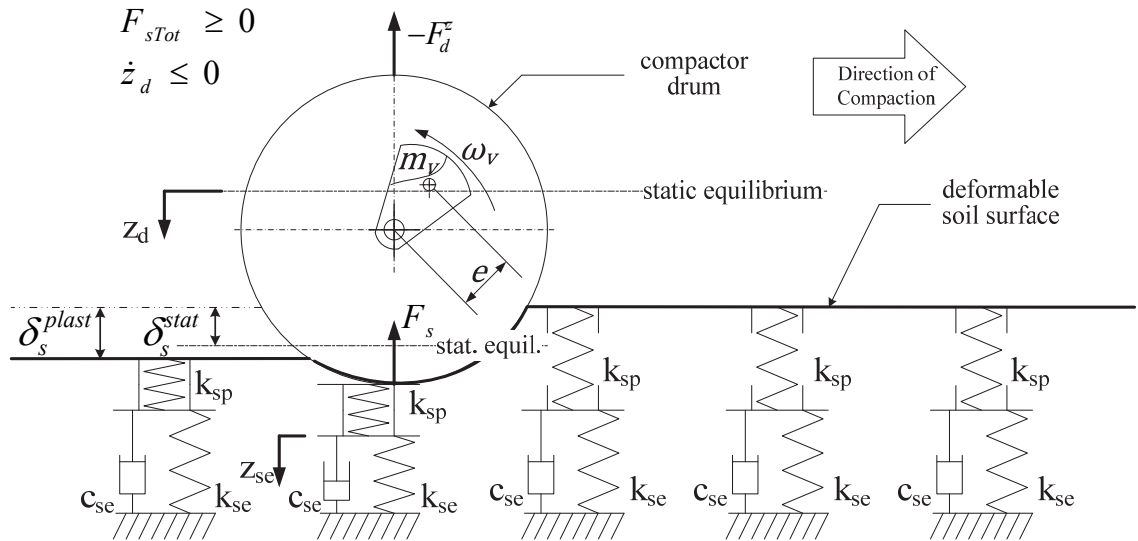
Figure 2-10: Drum-soil interaction model corresponding to soil relaxation under upward motion of the drum

The reaction force due to the soil ($F_{s\,Tot}$) is identical to that derived under the loading phase, presented in Eq. (2.36) and (2.37). The equations of motion of the coupled soil-drum-vehicle model are then described in the following matrix form:

55

$$[A_2]\{\ddot{Z}\} + [A_1]\{\dot{Z}\} + [A_0]\{Z\} = \{U(t)\}$$

<div align="right">(2.40)</div>

Where the $(n \times n)$ coefficient matrices $[A_0]$, $[A_1]$ and $[A_2]$, and $(n \times 1)$ excitation vector $\{U(t)\}$ are defined as follows:

$$[A_0] = \begin{bmatrix} (k_{se} + k_d^z) & \{A_0^{n1}\}' \\ \{A_0^{n1}\} & [K] \end{bmatrix}; \qquad [A_1] = \begin{bmatrix} (c_{se} + c_d^z) & \{A_1^{n1}\}' \\ \{A_1^{n1}\} & [C] \end{bmatrix};$$

$$[A_2] = \begin{bmatrix} m_d & \{0\} \\ \{0\} & [M] \end{bmatrix}; \qquad \text{and} \qquad \{U(t)\} = \begin{Bmatrix} m_v \, e \, \omega_v{}^2 \sin(\omega_v t) \\ F(t) \end{Bmatrix}.$$

With the $(n - 1 \times 1)$, $\{A_0^{n1}\}$ and $\{A_1^{n1}\}$ vectors being:

$$\{A_0^{n1}\} = \begin{Bmatrix} -k_d^z \\ l_d k_d^z \\ 0 \\ 0 \\ 0 \\ 0 \\ 0 \end{Bmatrix}; \text{ and} \qquad \{A_1^{n1}\} = \begin{Bmatrix} -c_d^z \\ l_d c_d^z \\ 0 \\ 0 \\ 0 \\ 0 \\ 0 \end{Bmatrix}.$$

The equations of motion of the coupled model in this phase of drum-soil interaction could also be written in the state variable form as:

$$\begin{Bmatrix} \{\ddot{Z}\} \\ \{\dot{Z}\} \end{Bmatrix} = \begin{bmatrix} (-[A_2]^{-1}[A_1]) & (-[A_2]^{-1}[A_0]) \\ [I] & [0] \end{bmatrix} \begin{Bmatrix} \{\dot{Z}\} \\ \{Z\} \end{Bmatrix} + \begin{bmatrix} [A_2]^{-1} \\ [0] \end{bmatrix} \{U(t)\}$$

<div align="right">(2.41)</div>

Drum-Hop Phase

In this phase, the drum with its continued upward motion tends to lose contact with the soil surface. Figure 2-11 illustartes the drum-soil interaction model involving loss of contact between the drum and the soil surface. This condition arises when the drum

continues its motion upward at the end of the unloading phase as the soil reaches its full elastic recovery. The resulting soil reaction force thus vanishes, defining the necessary condition for this phase of drum-soil interaction:

$$F_{s\,Tot} = 0$$

Furthermore, the soil stiffness associated with its plastic behaviour vanishes ($k_{sp} = 0$), which yields $\varepsilon = 0$. The drum-soil contact being now broken, the front axle static load is not balanced by any static reaction force of the soil. The gravity component of the forcing function ($m_1\,g$) is now to be considered in the equation of motion for the drum, presented in Eq. (2.35), which reduces to:

$$m_d \ddot{z}_d + c_d^z \dot{z}_d - c_d^z\,\dot{z}_b + l_a c_d^z \dot{\varphi}_b + k_d^z z_d - k_d^z\,z_b + l_a k_d^z\,\varphi_b$$

$$= m_v\,e\,\omega_v{}^2\,sin(\omega_v t) + m_1\,g$$

(2.42)
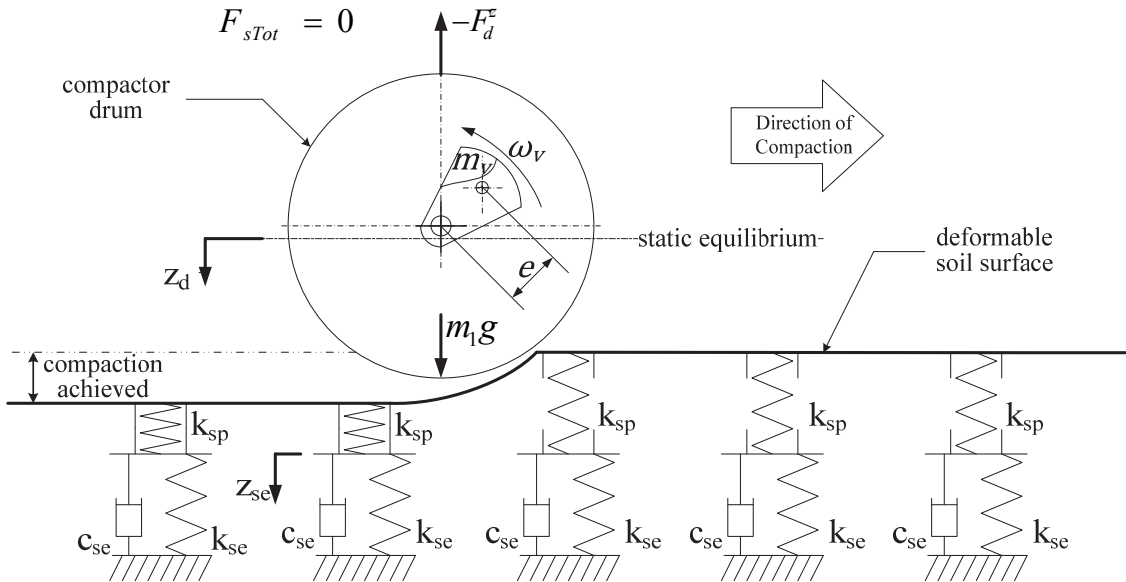
Figure 2-11: Model corresponding to drum-hop, the drum continuing its motion upward at the end of the unloading phase as the soil reaches its full elastic recovery

The equations of motion of the drum-vehicle system in this phase are described in the matrix form as in Eq. (2.40), where the $(n \times n)$ coefficient matrices and the $(n \times 1)$ excitation vector are given by:

$$[A_0] = \begin{bmatrix} k_d^z & \{A_0^{n1}\}' \\ \{A_0^{n1}\} & [K] \end{bmatrix}; \qquad [A_1] = \begin{bmatrix} c_d^z & \{A_1^{n1}\}' \\ \{A_1^{n1}\} & [C] \end{bmatrix};$$

$$[A_2] = \begin{bmatrix} m_d & \{0\} \\ \{0\} & [M] \end{bmatrix}; \text{ and} \qquad \{U(t)\} = \begin{Bmatrix} m_v \, e \, \omega_v^2 \sin(\omega_v t) + m_1 \, g \\ F(t) \end{Bmatrix}.$$

With the $(n - 1 \times 1)$, $\{A_0^{n1}\}$ and $\{A_1^{n1}\}$ vectors being:

$$\{A_0^{n1}\} = \begin{Bmatrix} -k_d^z \\ l_d k_d^z \\ 0 \\ 0 \\ 0 \\ 0 \\ 0 \end{Bmatrix}; \text{ and} \qquad \{A_1^{n1}\} = \begin{Bmatrix} -c_d^z \\ l_d c_d^z \\ 0 \\ 0 \\ 0 \\ 0 \\ 0 \end{Bmatrix}.$$

2.4. Summary

A vibratory soil compactor exhibits distinctly different dynamic behaviour in the transit and the compaction operating modes due to different excitations during the two operations. Two types of in-plane dynamic models of the vehicle are thus formulated to describe its ride vibration responses in the transit and compaction modes. For the transit mode, three different ride dynamic models of varying complexities are presented for further analysis of the vibration responses to excitations arising from randomly distributed roughness of the undeformable terrains. The compaction model is formulated by integrating the drum-soil interaction model to a ride dynamic model. The drum-soil

interaction model involves elasto-plastic soil model under three different interaction phases: (i) soil loading phase, (ii) soil unloading phase; and (iii) the drum-hop phase. The excitations and methods of solution are presented in CHAPTER 4, together with the model validations on the basis of the measured responses presented in the next chapter.

CHAPTER 3 – Field Measurements of Ride Vibrations

3.1. Introduction

The ride vibration environments of off-road vehicles and operators' exposure to whole-body vibration (WBV) are generally assessed through field measurements under representative operating conditions, (Daniere, et al., 1987; Boulanger, Donati, & Galmiche, 1996; Paddan & Griffin, 2002; Cann, Salmoni, Vi, & Eger, 2003; Beck, Bloswick, & Sesek, 2004). Such assessments, however, are considered valid under the operating conditions considered during the field measurements. The results attained from field measurements, generally exhibit considerable variability among the repeated measures. This is particularly applicable for off-rad vehicles that may operate on widely varying terrains at different speeds and load conditions. The field measurements, however, are vital for characterizing the vibration behaviour of the vehicle and verification of the analytical ride dynamic models. The performance analysis of an off-road vehicle system or a subsystem design concept through simulation of an analytical model necessitates thorough understanding and field characterization of the system properties under reasonably known excitation. The validity of the ride dynamic models, presented in section 2.2, is vital to gain confidence and to develop a reliable design tool for seeking effective design of vibration isolators.

Furthermore, the analytical model to be proposed has been formulated to describe the pitch-plane ride dynamics, assuming negligible roll and lateral motion. A few reported studies on the vibration properties of compactors (Boulanger, Donati, & Galmiche, 1996) and similar 2-axle articulated-steer construction equipment (Bovenzi, et al., 2006)

60

however, have shown considerable magnitude of lateral vibration. The field assessments are therefore considered essential to assess the WBV exposure and the environments in all the important axes.

This chapter discusses the field measurements performed on soil compactors including the methodology, data acquisition and analysis, and ride vibration responses of the candidate vehicles.

3.2.   Field Test Program

Field measurements were undertaken to characterize the whole-body vibration properties of soil compactors under two distinct operating modes: (i) transit mode (vibration off) on un-deformable surfaces at quasi-constant forward speeds; (ii) compaction mode (vibration on) on elasto-plastic graded soils at quasi-constant forward speed. The operators of soil compactors are trained to vary vibrator settings such as nominal amplitude and frequency (if several available) during the compaction process. These drum vibrator variations cause considerable change in the vibration properties and may pose complexities in interpretations of the measured data. Consequently, the experiments were performed under controlled conditions (speed and vibration amplitude) on the test courses at the manufacturer's site. The experiments involved two different vehicles. The descriptions of test vehicles and the test program are presented in the following sections.

3.2.1. Description of Test Vehicles

Two typical soil compactors were selected through consultations with the most important road building contractor in Quebec (Sintra of the Colas group), a leading global

manufacturer of road building equipment and the Quebec research institute of occupational health and safety (IRSST). The gross weight of these machines was in the range of 10 tons, which represents the greatest population of this type of equipment in North America. The selected machines were 10-ton class soil compactors powered by an in-line 4 or 6 cylinder engines. Both the vehicles were equipped with an open platform featuring an operator seat without a vertical suspension. Figure 3-1 presents a pictorial view and a schematic illustration of soil compactors equipped with a cabin and an open platform, respectively. The vehicles comprise a drum on the front axle and pneumatic tires on the rear axle. The drum features a vibratory system based on rotating eccentric masses. It is mounted to the front frame (vehicle body) though a number of rubber-mounts, while the cabin / open-platform and the engine group are supported on the rear frame (vehicle body) through four rubber mounts. The equipment can generate at least two so called nominal amplitudes of vibration by varying the eccentric moment within the drum group.
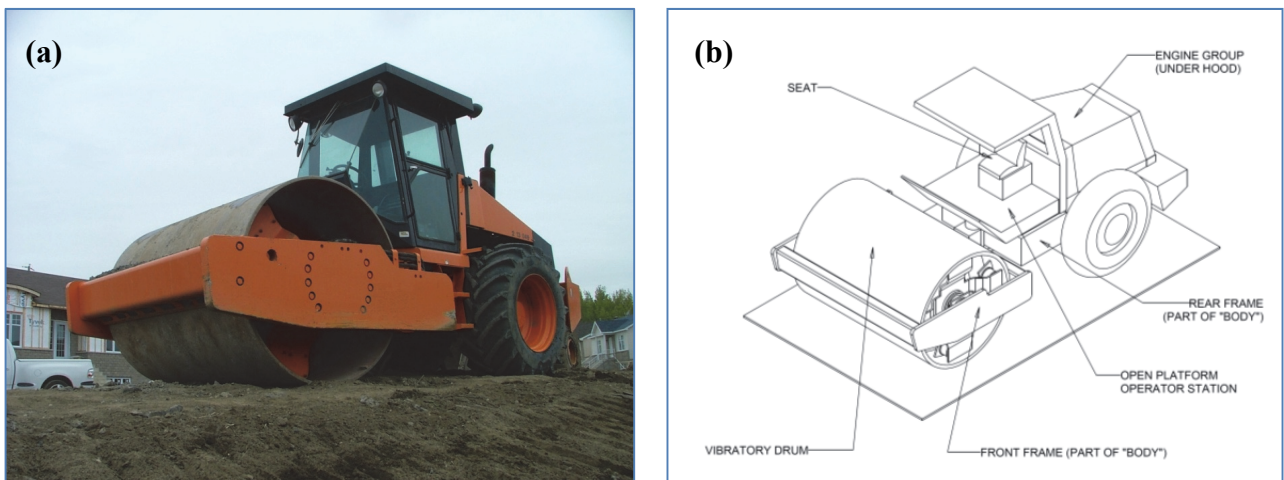
Figure 3-1: (a) A pictorial view of a cabin equipped; and (b) a schematic illustration of an open platform equipped vibratory compactors

3.2.2. **Description of the Program**

A soil compactor may be considered to comprise four primary bodies for characterization of its vibration properties. These include:

a) Operator-seat subsystem for characterization of whole-body vibration (WBV) exposure of the operator, and attenuation of vertical vibration by the seat;

b) Operator station (cabin or open platform), whose motions generally characterize the vibration transmission properties of the vehicle and its mounts; Considering that the seat mostly alters the transmission of the vertical vibration alone, the horizontal and angular vibration of the cabin/platform structure can fully characterize the vibration exposure along these axes;

c) Vehicle body comprising the front frame, rear frame and rear axle (rigidly bolted to the rear frame) and supporting the engine. Its motions characterize the transmission of drum-terrain and tire-terrain dynamic interactions to the vehicle body; and

d) Drum with the rotary eccentric mass characterizes the primary excitation during the compaction mode together with the dynamic drum-soil interaction in transit mode.

The soil compactor can thus be represented by a multi-body system illustrated in Figure 3-2, which comprises the above-mentioned four rigid bodies in addition to the engine mounted on the chassis through rubber mounts. The figure also illustrates the rotating eccentric mass within the drum, which is mounted to the main body through elastic mounts. The rear axle is represented as rigidly connected to the vehicle body and

supported by the fore-aft and vertical visco-elastic properties of the tires. The field test

program was designed to measure the vibration responses of each of the bodies in order

to fully characterize the ride vibration properties of the vehicles.
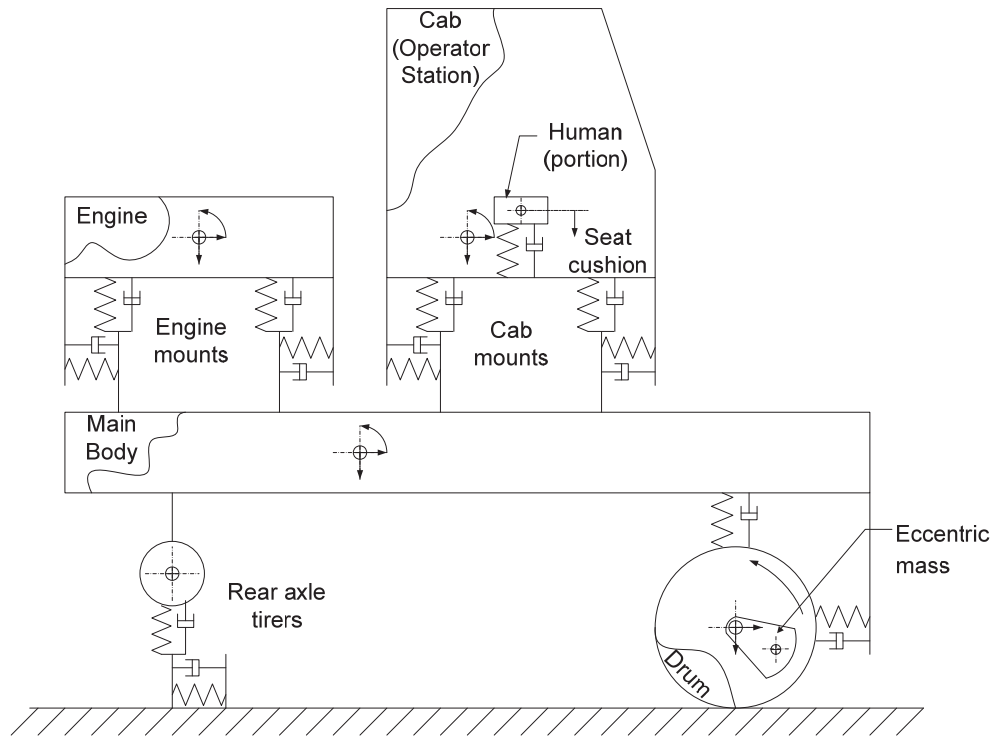
Figure 3-2: Multi-body schematic diagram of a typical soil compactor

The field measurements were performed at the manufacturer's test facility that offered

the desired courses for simulated transit and compaction tasks. In the compaction mode,

the vehicles were operated on levelled deformable soils. The vehicles were operated

forward and backward at a quasi-constant speed of 3 km/h. Compactions were performed

on selected soils of different densities featuring different levels of soil stiffness, at two

different nominal amplitudes of vibration. It should be noted that the compactor vibrator

consists of two nominal amplitude settings, denoted as "low" and "high". The majority of

the compaction runs, however, were performed with the vibrator set at high amplitude but

several runs were also performed with the vibrator set at low amplitude. Each compaction

run corresponding to low and high amplitude settings on the selected soil was repeated a few times, depending upon the weather condition and deformability of the surface.

In transit mode, compactors were driven on tracks longer than 100 m on a non-deformable road surface. The vibrator was set to the "off" position. The road surface was judged to be "average". Figure 3-3 illustrates the layouts of the transit and compaction tracks.
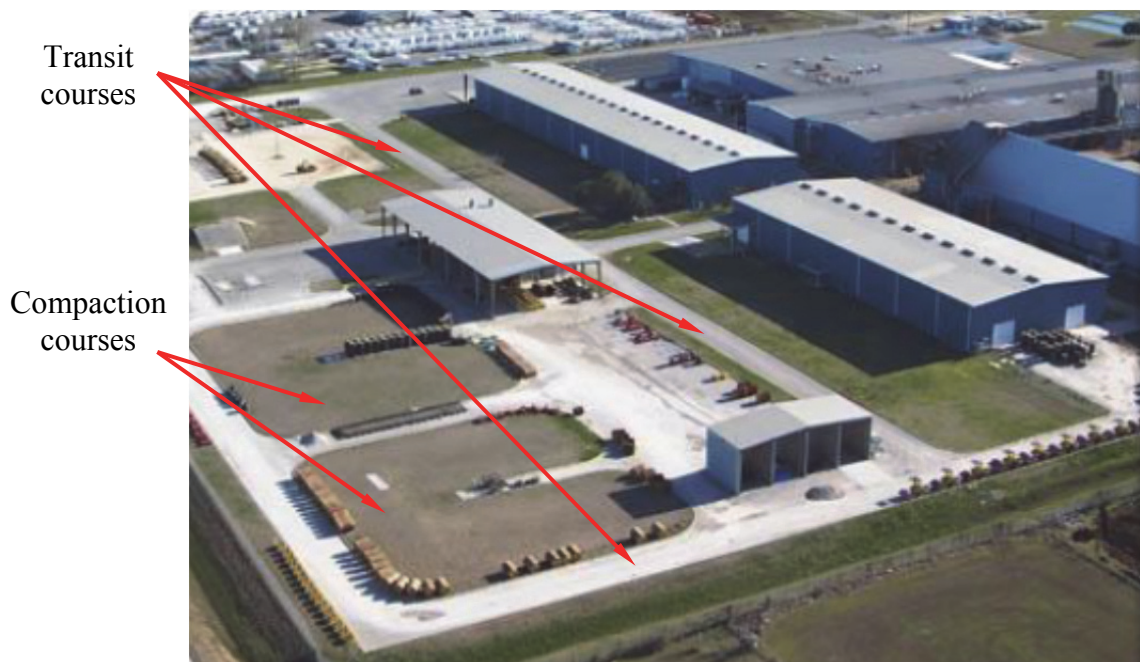
Figure 3-3: Illustration of the test tracks used in the transit and compaction modes

Apart from the transit on the tracks, the transient responses of the vehicles were also measured while operating over discrete obstacles. For this purpose, a discrete obstacle was synthesized by 5 cm × 10 cm wooden planks placed on the road surface. The vehicle was driven over the planks in the forward and reverse modes and the responses were acquired to measure the fundamental mode frequencies. Both these transit modes were

conducted at two constant speeds (6 and 10 km/h) and each test was repeated at least 3 times.

Table 3-1: Test runs for the 6-cylinder compactor

Run #	Operation	Soil Density	Vibrator amplitude	Approximate Speed (km/h)	Driving Direction
1	Transit #1	Non-deformable	Off	10	Forward
2	Engine idling #1	Non-deformable	Off	0	N/A
3	Compaction/humid soil #3	Low density	High	3	Forward
4	Compaction/humid soil #3	Low density	High	3	Backward
5	Compaction/humid soil #1	Low density	High	3	Forward
6	Compaction/humid soil #1	Low density	High	3	Backward
7	Compaction/humid soil #2	Low density	High	3	Forward
8	Compaction/humid soil #2	Low density	High	3	Backward
9	Transit #2	Non-deformable	Off	10	Forward
10	Compaction / gravel	Very high density	High	3	Forward
11	Compaction / gravel	Very high density	Low	3	Backward
12	Transit over obstacles	Non-deformable	Off	10	Forward
13	Transit over obstacles	Non-deformable	Off	10	Backward
14	Transit over obstacles	Non-deformable	Off	6	Forward
15	Transit over obstacles	Non-deformable	Off	6	Backward
16	Transit #3	Non-deformable	Off	10	Forward
17	Compaction/ dry soil #1	Over-compacted	High	3	Forward
18	Compaction/ dry soil #1	High-density	High	3	Forward
19	Compaction/ dry soil #1	High-density	High	3	Backward
20	Compaction/ dry soil #1	Over-compacted	High	3	Backward
21	Engine idling #2	Non-deformable	Off	0	N/A
22	Compaction/ dry soil #2	Over-compacted	Low	3	Forward
23	Compaction/ dry soil #2	High-density	Low	3	Forward
24	Compaction/ dry soil #2	High-density	High	3	Backward
25	Compaction/ dry soil #2	Over-compacted	High	3	Backward
26	Engine idling #3	Non-deformable	Off	0	N/A
27	Transit #4	Non-deformable	Off	10	Forward

The test program involved a total of 27 and 23 runs with the two compactors, which are denoted by "6-cylinder compactor" and "4-cylinder compactor", respectively. These also included runs with engine idling for verifications of the sensors signals. Table 3-1 and Table 3-2 summarize the various runs and the corresponding conditions such as operating mode, ground type, vibrator setting, speed and direction of transit.

Table 3-2: Test runs for the 4-cylinder compactor

Run #	Operation	Soil Density	Vibrator Amplitude	Approximate Speed (km/h)	Driving Direction
1	Compaction / gravel	Very high density	High	3	Forward
2	Compaction / gravel	Very high density	Low	3	Backward
3	Transit #1	Non-deformable	Off	10	Forward
4	Transit #2	Non-deformable	Off	10	Forward
5	Compaction/humid soil #1	Low density	High	3	Forward
6	Compaction/humid soil #1	Low density	High	3	Backward
7	Compaction/humid soil #2	Low density	High	3	Forward
8	Compaction/humid soil #2	Low density	Low	3	Backward
9	Transit #3	Non-deformable	Off	10	Forward
10	Transit over obstacles	Non-deformable	Off	10	Forward
11	Transit over obstacles	Non-deformable	Off	10	Backward
12	Transit over obstacles	Non-deformable	Off	6	Forward
13	Transit over obstacles	Non-deformable	Off	6	Backward
14	Transit #4	Non-deformable	Off	10	Forward
15	Compaction/ dry soil #1	Over-compacted	High	3	Forward
16	Compaction/ dry soil #1	High-density	High	3	Forward
17	Compaction/ dry soil #1	High-density	High	3	Backward
18	Compaction/ dry soil #1	Over-compacted	High	3	Backward
19	Compaction/ dry soil #2	Over-compacted	Low	3	Forward
20	Compaction/ dry soil #2	High-density	Low	3	Forward
21	Compaction/ dry soil #2	High-density	High	3	Backward
22	Compaction/ dry soil #2	Over-compacted	High	3	Backward
23	Transit #5	Non-deformable	Off	10	Forward

3.2.3. Instrumentation

Each test vehicle was instrumented to measure the vibration of the responses of the four primary bodies, namely the seat, operator station, drum, and the vehicle body. In the current design, soil compactors wheel axles are rigidly bolted to the rear-frame; the vertical vibrations of the rear frame at the axle location were acquired. The sensors employed at different locations are summarized below:

- A 3-axis seat accelerometer per ISO recommendations (ISO 2631-1, 1997) was installed on the seat cushion for measurements of fore-aft (x), lateral (y) and vertical

vibrations at the operator / seat interface. For this purpose, the seat pad was designed with a micro-accelerometer (ADXL05JH ±5g). Figure 3-4 illustrates the seat accelerometer mounted on the seat cushion. It needs to be emphasized that the vibration measured at the seat could not be generalized since these vehicles can as well employ genuine or "after-market" suspension seats.

Figure 3-4: Seat accelerometer

- A 3-axis gyro coupled with a 3-axis accelerometer (IMU400CC) was installed on the platform floor near the operator seat to measure the translational and rotational vibration of the operator-station structure.

- A 3-axis gyro together with a 3-axis (IMU400CC) accelerometer attached to the rear frame, close to the center of mass of the vehicle body for measurements of translational and rotational vibration of the vehicle body.

- A 3-axis accelerometer (Crossbow CXL4GP3) was mounted on the rear frame above the bolted joint of the rigid axle, although the vertical acceleration only was acquired, since the horizental vibrations were expexted to be similar to that of the vehicle body.

68

- A 3-axis accelerometer (PCB Piezotronics) was attached to the drum-propelling side (hydrostatic transmission) of the front frame in-plane with the drum axis for measurements of translational vibrations transmitted by the drum to the front frame through the elastic mounts. Figure 3-5 illustrates the location of this accelerometer. It should be noted that only x- and z-axis acceleration signals of the front frame were acquired.

- And a 3-axis accelerometer (PCB Piezotronics) was also attached to the vibrator motor bracket of the drum to measure the drum radial accelerations along the x- and z-axis. Figure 3-6 illustrates the location of this accelerometer.

Figure 3-5: Front frame accelerometer   **Figure 3-6: Drum group accelerometer**
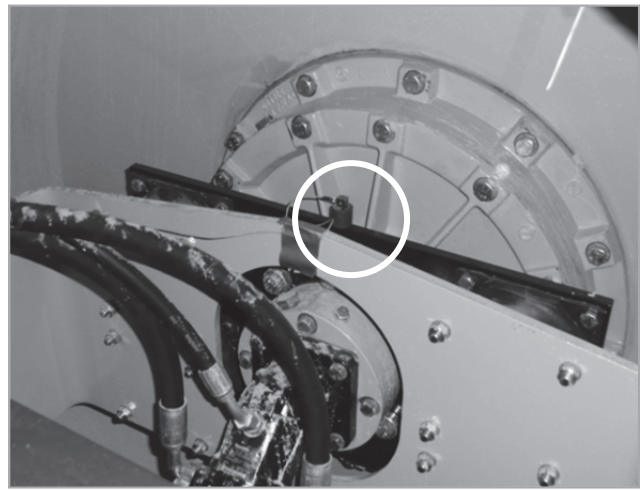
The signals from the PCB accelerometers were conditioned using the signal conditioner/amplifier, while those from the gyros and micro-accelerometers (ADXL and Crossbow) were directly acquired in a multi-channel data recorder (TEAC). It should be noted that the gyros provided the measures of the angular velocities, which were subsequently differentiated during data analysis tasks to derive the angular accelerations.

Each sensor was calibrated in the laboratory prior to their installations. Table 3-3 summarizes the location, ranges and sensitivities of various sensors together with the coordinate measured.

Table 3-3: Specifications of the sensors and their locations

Channel	Measurand	Sensor	Sensitivity	Range	Gain	Comments
1	Drum X	PCB Piezotronics ±50g	95.7mV/g	±5V	1	vib motor plate
2	Drum Z	PCB Piezotronics ±50g	99.0mV/g	±5V	1	vib motor plate
3	Front frame X	PCB Piezotronics ±50g	100.8mV/g	±5V	1	drum propel side
4	Front frame Z	PCB Piezotronics ±50g	96.3mV/g	±5V	1	drum propel side
5	Body X	Crossbow CXL10GP3 ±10g	0.200V/g	5V	1	close to hitch
6	Body Y	Crossbow CXL10GP3 ±10g	0.204V/g	5V	1	close to hitch
7	Body Z	Crossbow CXL10GP3 ±10g	0.197V/g	5V	1	close to hitch
8	Platform X	Crossbow CXL10GP3 ±10g	0.201V/g	5V	1	close to cab c.g.
9	Platform Y	Crossbow CXL10GP3 ±10g	0.204V/g	5V	1	close to cab c.g.
10	Platform Z	Crossbow CXL10GP3 ±10g	0.204V/g	5V	1	close to cab c.g.
20	Body roll	IMU400CC-200 ±200°/sec	0.782V/rad/s	±4V	1	close to hitch
12	Body pitch	IMU400CC-200 ±200°/sec	0.782V/rad/s	±4V	1	close to hitch
13	Body yaw	IMU400CC-200 ±200°/sec	0.782V/rad/s	±4V	1	close to hitch
14	Platform roll	IMU400CC-100 ±100 °/sec	1.565V/rad/s	±4V	1	close to cab c.g.
15	Platform pitch	IMU400CC-100 ±100 °/sec	1.565V/rad/s	±4V	1	close to cab c.g.
16	Platform yaw	IMU400CC-100 ±100 °/sec	1.565V/rad/s	±4V	1	close to cab c.g.
17	Seat X	ADXL05JH ±5g	0.551V/g	5V	1	seat pad
18	Seat Y	ADXL05JH ±5g	0.565V/g	5V	1	seat pad
19	Seat Z	ADXL05JH ±5g	0.485V/g	5V	1	seat pad
21	Axle Z	Crossbow CXL4GP3 ±4g	0.500V/g	5V	1	Frame over axle
22	AUDIO	micro	-	-	-	-

3.3. Data Analysis Method

The acquired data segments for each machine (4 or 6 cylinder) were grouped for each operation including the transit, compaction of lower density soil and compaction of higher density soil. Each operation comprised between 3 to 6 data segments of varying lengths as summarized below:

- 4-cylinder machine in transit mode (10 km/h): 5 segments of 120 seconds each
- 6-cylinder machine in transit mode (10 km/h): 4 segments of 120 seconds each
- 4-cylinder machine in compaction (high density): 3 segments of 60 seconds each
- 6-cylinder machine in compaction (high density): 3 segments of 60 seconds each
- 4-cylinder machine in compaction (low density): 3 segments of 120 seconds each
- 6-cylinder machine in compaction (low density): 6 segments of 120 seconds each

The vast majority of compaction runs employed high amplitude unbalance excitation. The measured analog data were processed through a 0.7 Hz cut-off frequency high-pass filter to eliminate the signal bias, if any, and digitised using Brüel & Kjær PULSE Analyser Platform. The data were subsequently analyzed using different analysers, namely:

i. Time capture analyser to study the transient responses to discrete obstacles;

ii. Fast Fourier Transform (FFT) analyser to derive the vibration spectra in terms of power spectral density (PSD) ; and

iii. Constant Percentage Bandwidth (CPB) analyser to derive the rms acceleration spectra and the overall rms acceleration values.
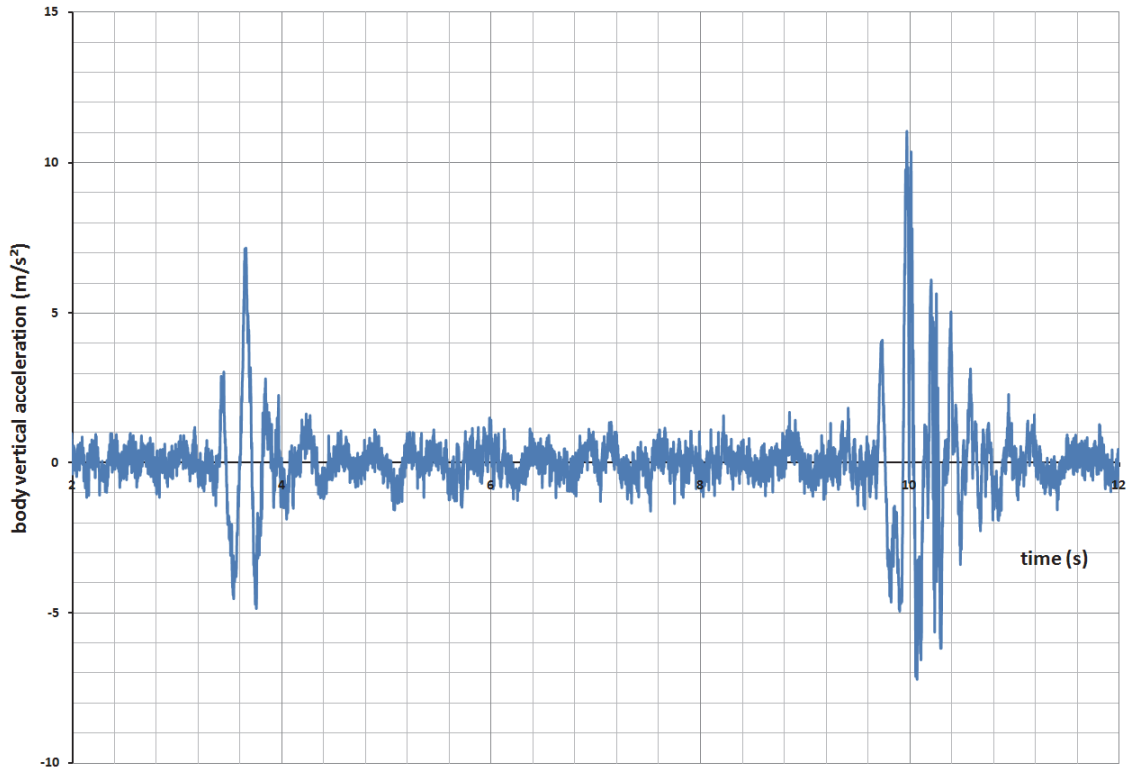
Figure 3-7: Time history of vertical acceleration measured at the main body of the 4-cylinder compactor during forward transit over the discrete obstacles at 10 km/h

The time history of each signal was recorded through the Time capture analyzer. As an example, Figure 3-7 illustrates the transient vertical acceleration response measured at the main body of the 4-cylinder machine in the transit mode over discrete obstacles. The transient measured data were acquired with vehicle traversing over two discrete obstacles. Two distinct oscillations in the figures correspond to each of the oscillations. The second oscillation, near $t \approx 10\ s$, exhibits vertical vehicle vibration caused by the interactions of the drum and the rear axle tire with one of the obstacles. This particular segment was zoomed to identify the fundamental natural frequencies of the vehicle corresponding to the bounce and pitch modes of the vehicle. The measured data revealed

a distinct frequency near 4.8 Hz, which was believed to correspond to the vertical, pitch or a coupled vertical/pitch mode of the vehicle.
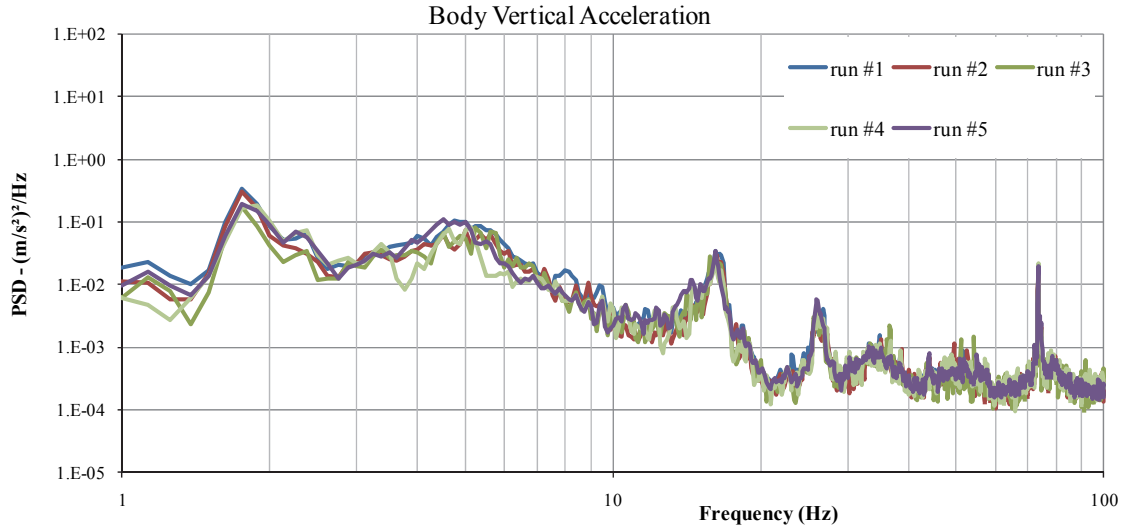
Figure 3-8: PSD of the vertical acceleration measured at the vehicle-body of the 4-cylinder compactor during 5 transit runs at a forward speed of 10 km/h

FFT analyzer processed each data segment at a sampling rate of 256 with a resolution of 0.125 Hz over a range of 100 Hz. The analysis also utilized a 75% overlap and a Hanning time-weighting function. The CPB analyzer was configured to one-third-octave bands with center frequencies of the lower and upper bands of 0.5 Hz and 100 Hz, respectively. The acquired data were analyzed to derive the acceleration spectra corresponding to each test compactor in each segment corresponding to the different operating modes considered. The results were obtained in terms of PSD and ⅓-octave band rms values of accelerations along all the translational and rotational axes. The results attained for the related segments or repeated trails for each operating mode were grouped and averaged. The repeated measures for each operation generally revealed good repeatability in the

resulting acceleration spectra. As an example, Figure 3-8 illustrates comparisons of vertical acceleration PSD measured at the vehicle body of the 4-cylinder compactor over five different transits at a forward speed near 10 km/h. the comparison suggests good repeatability of the runs particularly in predominant frequencies of vibration, while considerable deviation in the magnitude are also evident. These are attributable to local road roughness variation and possible variations in the actual speed. The data obtained during different runs of each operation were subsequently grouped and presented by their mean, minimum and maximum PSD magnitudes. The resulting envelop spectra could be applied for model verification, vibration dosage assessments and design or turning of second suspension at the operator-station and seat.

3.4. Ranges of measured responses

The measured data were analyzed to describe the ranges of acceleration response along each axis corresponding to each mode of operation. The yaw acceleration responses of both the vehicles were found to be quite small and therefore not presented in the dissertation. The ranges of acceleration grouped for each mode of operation are discussed below for both the machines considered in the study.

3.4.1. In compaction mode on lower density soil

The soil compaction is invariably preformed at very low speeds (nearly 3 km/h). The resulting whole body vibration amplitudes caused by tire/drum –terrain interactions

would thus be expected to be small. The unbalance vibrator, however, tends to introduce high magnitude acceleration at a relatively higher frequency near 30 Hz. The frequency weighting defined in ISO-2631-1 tend to greatly suppress the contribution due to such higher frequency vibration. The vehicle vibration during compaction, particularly involving low density soil or low amplitude vibrator operation, may thus not be of concern in view of the risks associated with vibration exposure of the operator.

Figure 3-9 illustrates the ranges of vertical vibration measured at the operator seat, operator-station and the vehicle body of the two machines, respectively while performing low density soil compaction tasks. The results clearly show a sharp high magnitude peak near 30 Hz, irrespective of the location of the measurement and the machine. The acceleration spectra also reveal peaks at frequencies multiples of the fundamental unbalance frequency of 30Hz. These are clearly evident in the spectra of vibration measured at the operator-station floor and at the vehicle body near 15, 60 and 90 Hz. The results in general exhibit low magnitude vertical vibration in the low frequency range (<15 Hz) to which human body is known to be more sensitive (Griffin M. J., 1990). The spectra exhibit a number of peaks in the lower frequency range, which would be of primary interest in study of WBV exposure of the operator, if the magnitudes of vibration were of concern. The peaks and the corresponding frequencies in the low frequency range, however, relate to particular vehicle vibration modes, while the peak magnitudes would be expected to be more prominent during the transit operations. These frequencies are thus examined and discussed on the basis of the transit mode of operation responses in the following section.

The results also show that magnitudes of vehicle vibration in the low frequency range are higher for the 6-cylinder machine compared to the 4-cylinder machine. Furthermore, the drum mounts and operator-station mounts tend to attenuate the high frequency vibration caused by the vibrator. The longitudinal and lateral vibration of the vehicles measured at the vehicle body, operator-station and seat, also show relatively low magnitude vibration in the lower frequency range, and high magnitude peaks corresponding to the vibrator motion, as seen in Figure 3-10 and Figure 3-11. For the 6-cylinder machine, the operator-station and the drum mounts appear to be more efficient in reducing the translational vibration (along all the three axis) transmitted to the operator-station floor compared to the 4-cylinder machine. This is most likely attributed to differences in inertial and mass distribution properties of the two vehicles.

The roll and pitch vibration of both the vehicles are also quite low in the low frequency ranges, as shown in Figure 3-12 and Figure 3-13, respectively. Both the roll and pitch accelerations, however, tend to increase with frequency at frequencies above 7 Hz. This was initially believed to be caused by integration of the velocity signal that may comprise slight dc offset. A further examination of the velocity signals, however, revealed negligible dc offset. The increasing acceleration at high frequencies however, corresponds to only low levels of displacements that are most likely attributed to the bending and torsion of the frames and the operator-station structure.
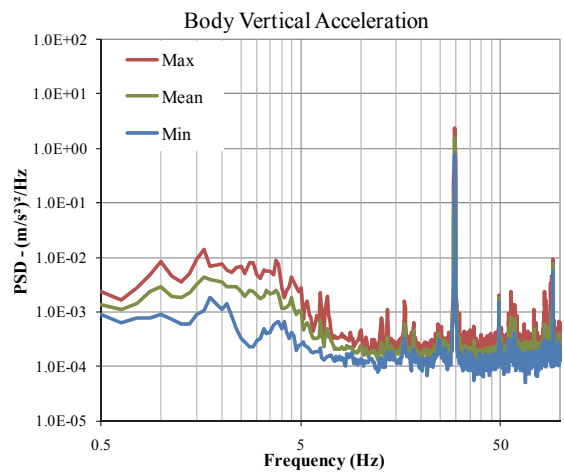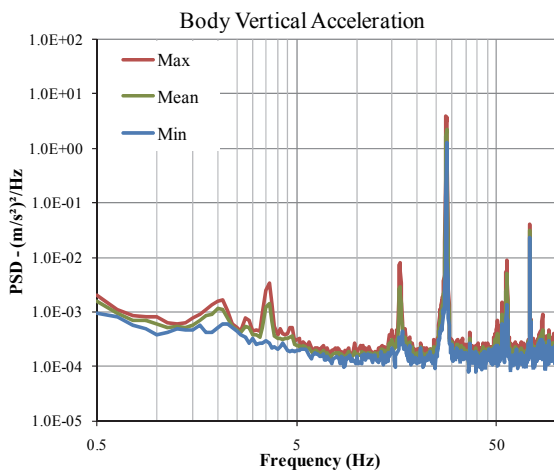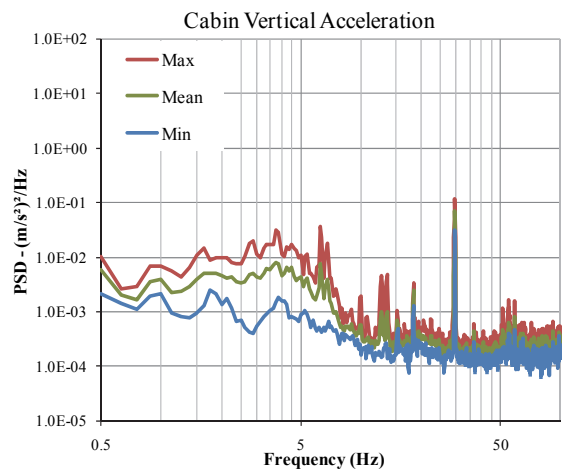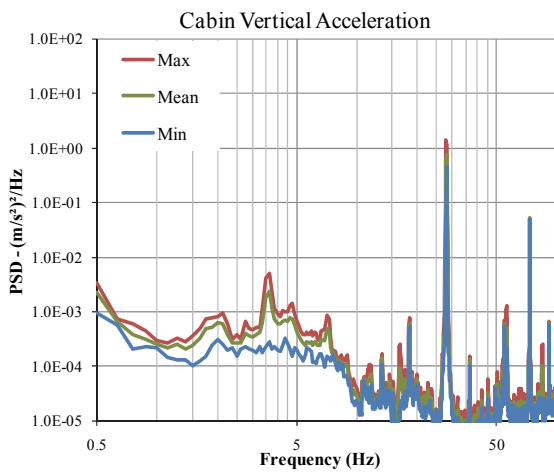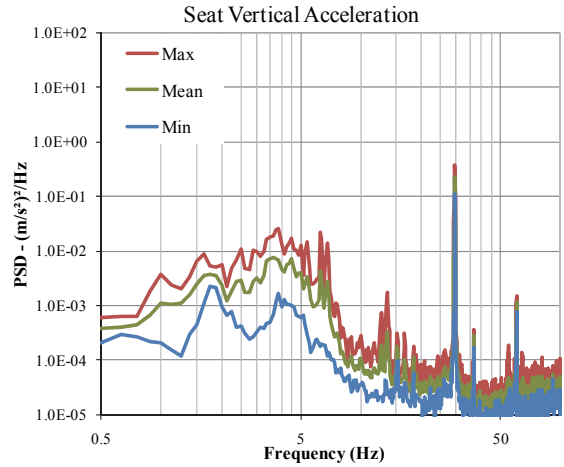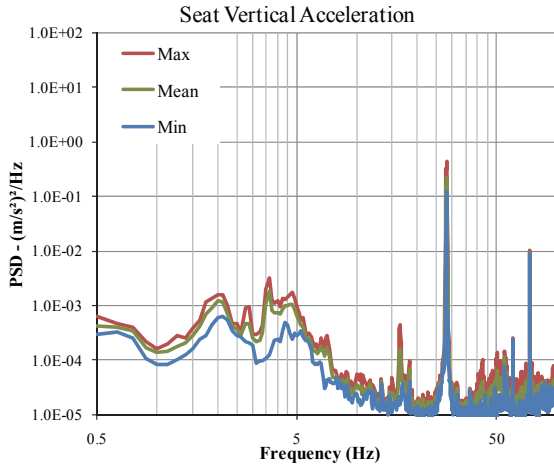
Figure 3-9: PSD of vertical acceleration measured at the vehicle body, the operator-station floor and the seat during compaction of low density soil (vibrator set at "high amplitude"): (a) 4-cylinder machine; (b) 6-cylinder machine
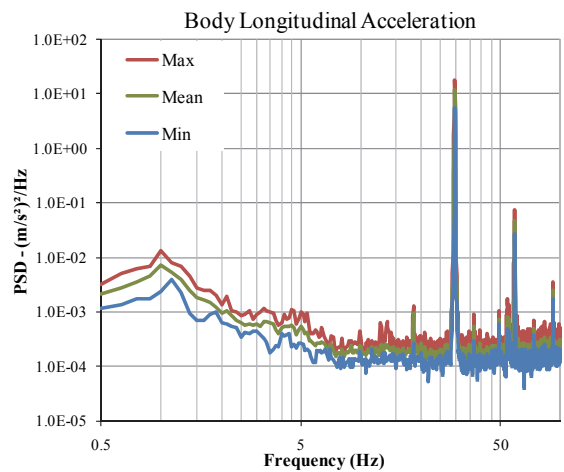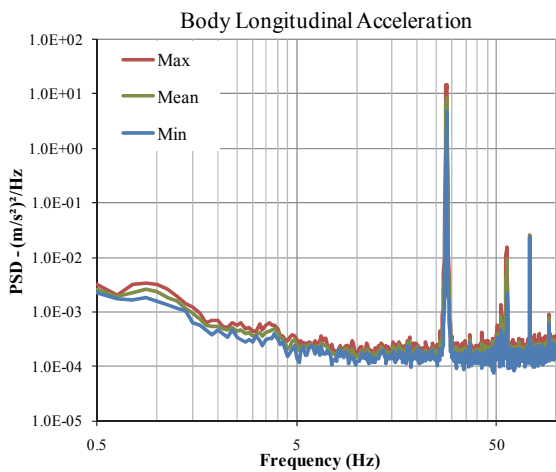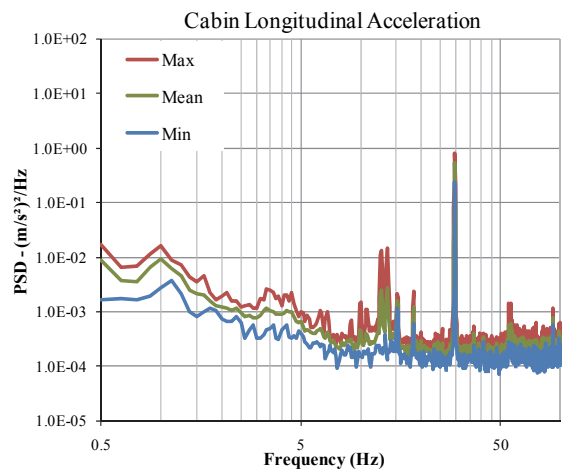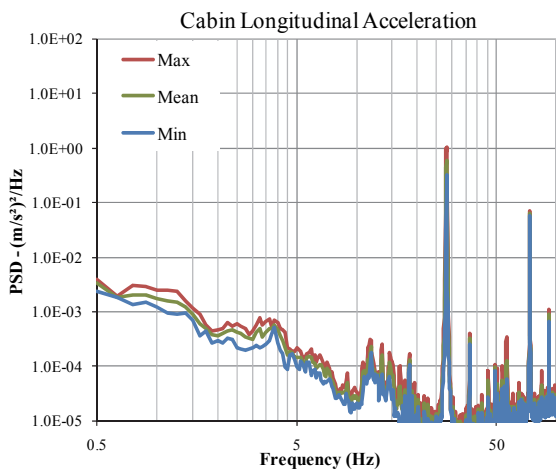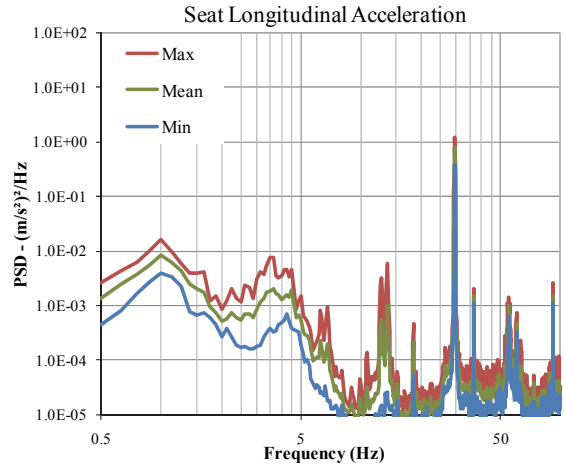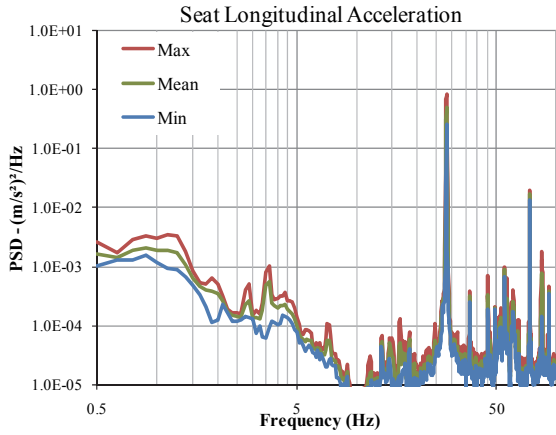
Figure 3-10: PSD of longitudinal acceleration measured at the vehicle body, the operator-station floor and the seat during compaction of low density soil (vibrator set at "high amplitude"): (a) 4-cylinder machine; (b) 6-cylinder machine
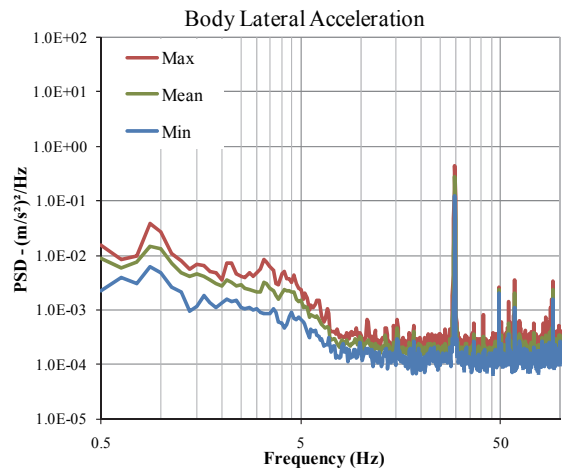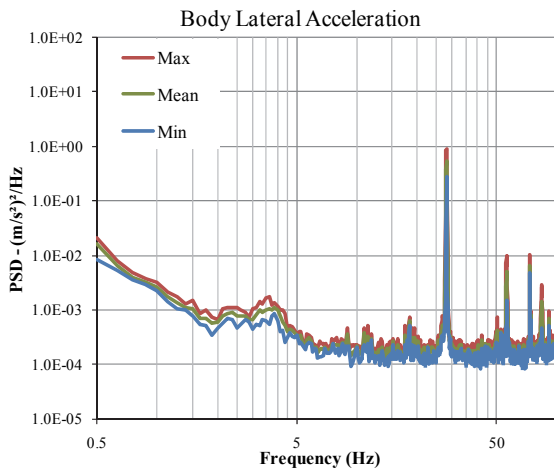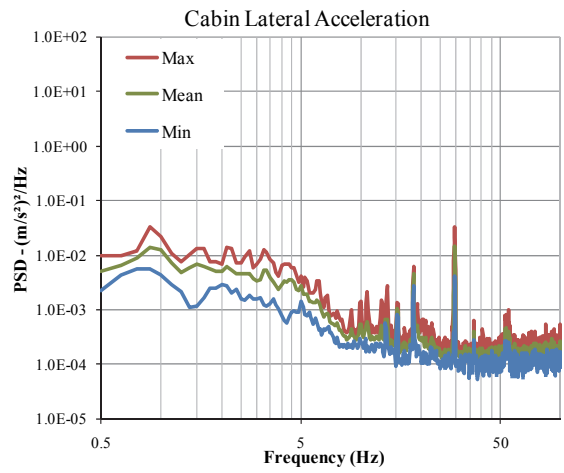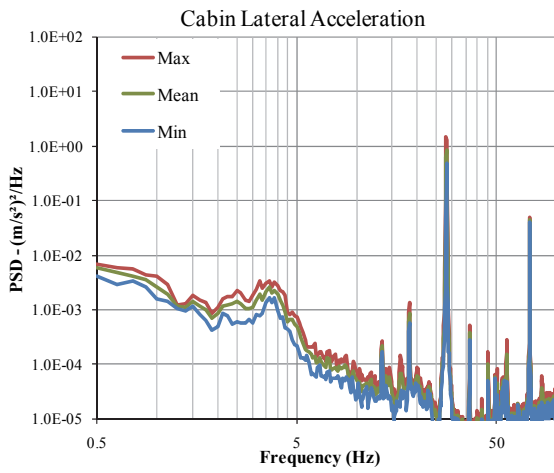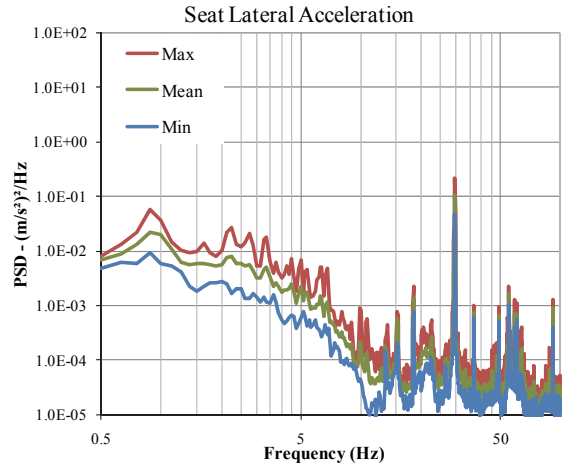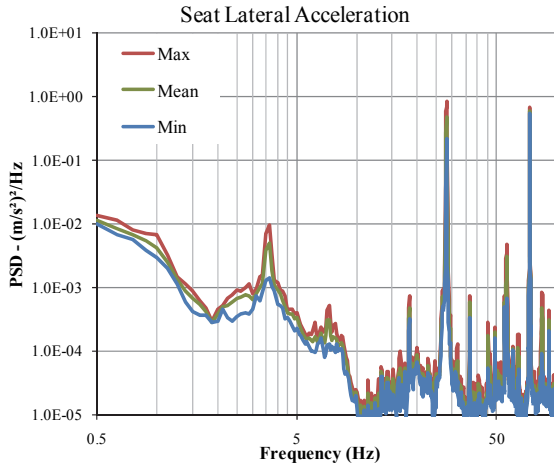
Figure 3-11: PSD of lateral acceleration measured at the vehicle body, the operator-station floor and the seat during compaction of low density soil (vibrator set at "high amplitude"): (a) 4-cylinder machine; (b) 6-cylinder machine
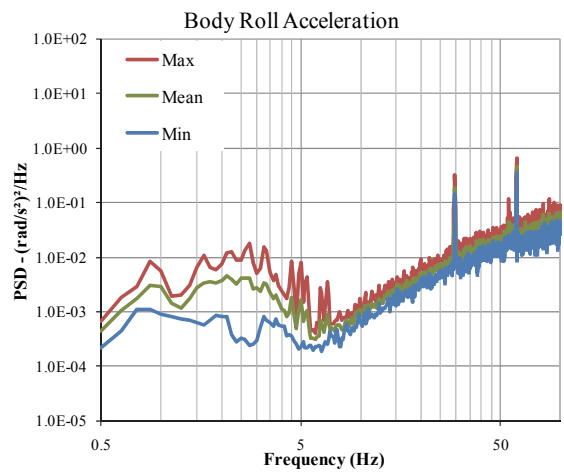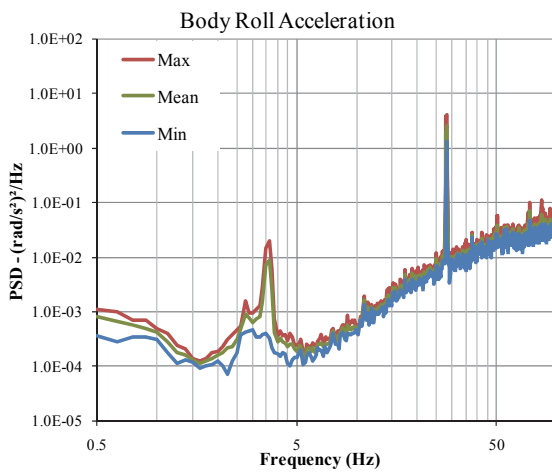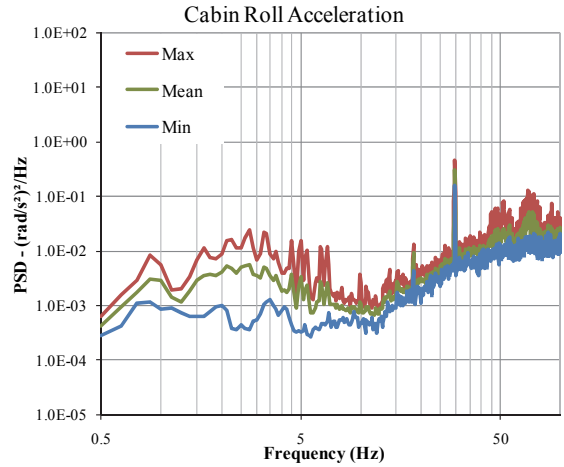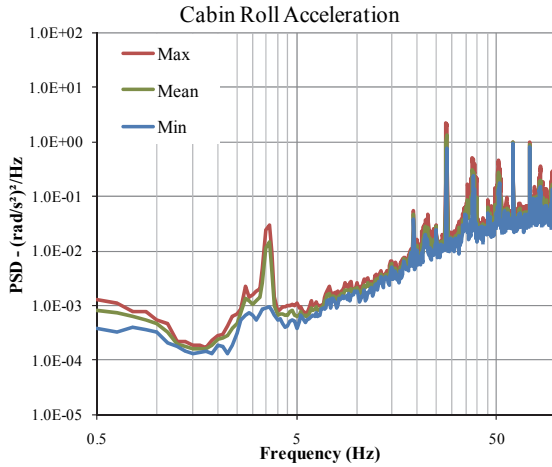
Figure 3-12: PSD of roll acceleration measured at the vehicle body and the operator-station floor during compaction of low density soil (vibrator set at "high amplitude"): (a) 4-cylinder machine; (b) 6-cylinder machine
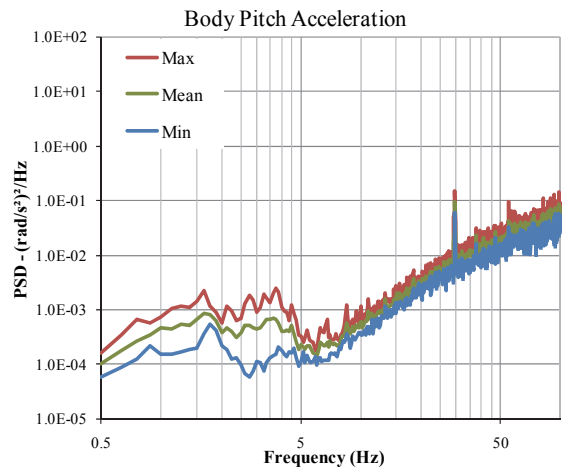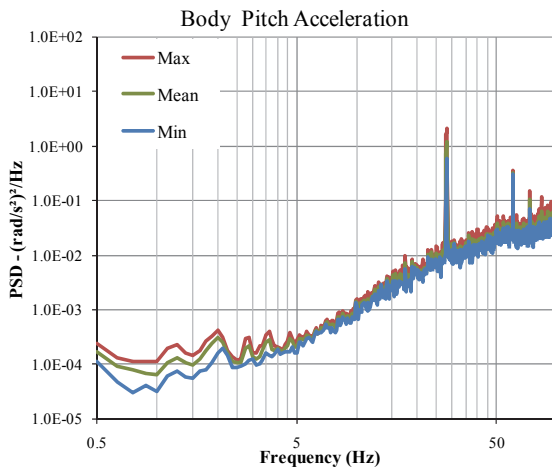
Figure 3-13: PSD of pitch acceleration measured at the vehicle body and the operator-station floor during compaction of low density soil (vibrator set at "high amplitude"): (a) 4-cylinder machine; (b) 6-cylinder machine
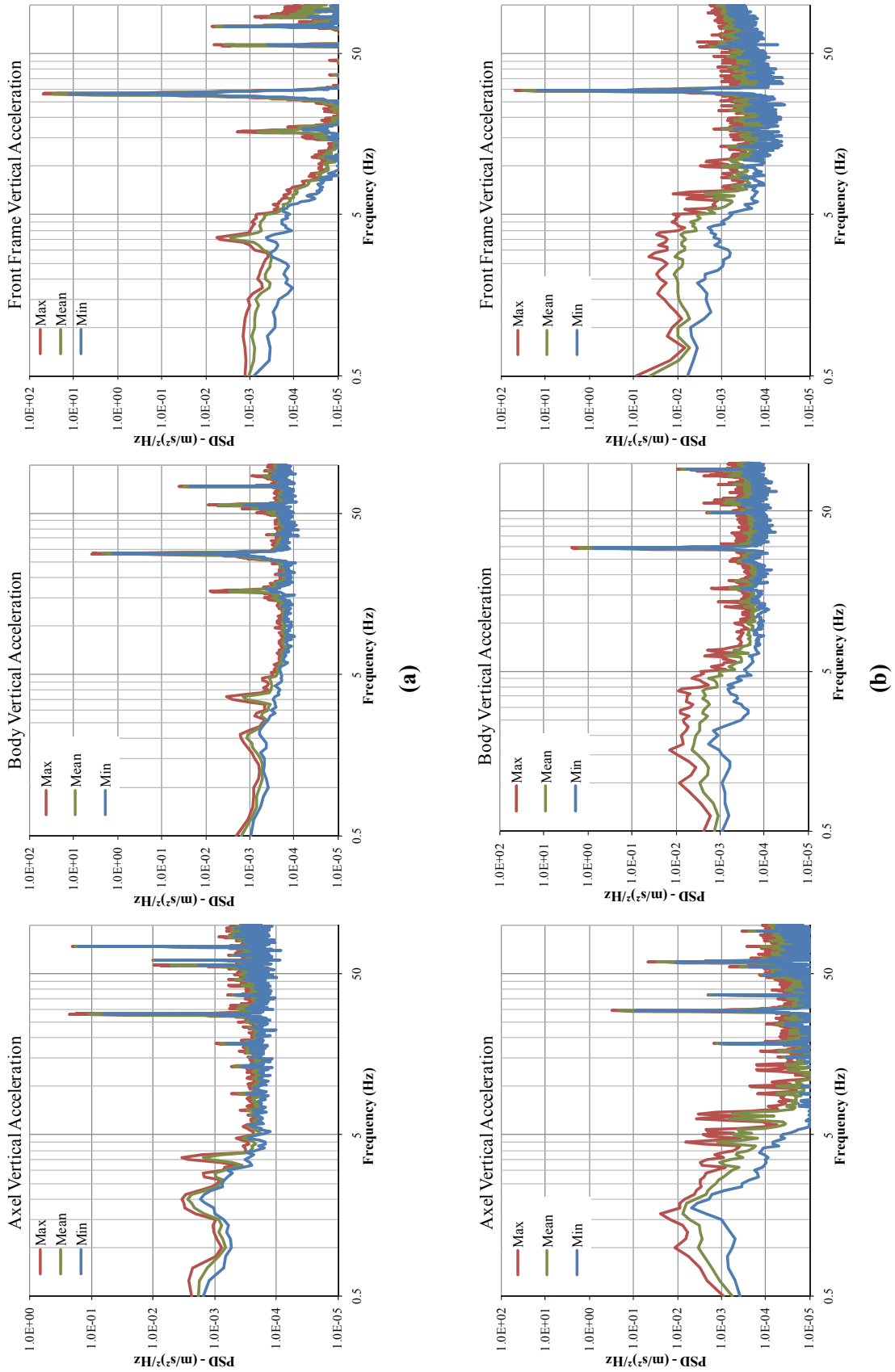
Figure 3-14: PSD of vertical acceleration measured at the axle (rear frame), center of vehicle body and at the front frame during compaction of low density soil (vibrator set at "high amplitude"): (a) 4-cylinder machine; (b) 6-cylinder machine

3.4.2. **In compaction mode on higher density soil**

The compaction of higher density soil causes greater interactions of the drum and the tire with the terrain due to greater stiffness of the soil. This operation may also yield hopping of the drum under certain conditions (Pietzsch & Poppy, 1992; Adam & Kopf, 2000; Andereg, 2000) leading to higher magnitudes of transmitted vibration. The magnitudes of low frequency vibration along the z, x and y-axis are thus higher than those observed under low density soil compaction, as evident from the spectra in Figure 3-15, Figure 3-16 and Figure 3-17, respectively. The spectral components of low frequency vibration, however, are quite similar to those observed under low density soil compaction. The compaction of higher density soil tends to emphasize the peaks corresponding to 15 Hz (one-half the frequency of the rotating unbalance), as seen in the figures. This is believed to be caused by the hopping motion of the drum on the relatively hard soil. The magnitudes of longitudinal and lateral vibration near 15 Hz tend to be higher than those observed at the fundamental frequency of approximately 30 Hz. The hopping motion of the drum may also contribute to excitations of some of the low frequency modes. The magnitudes of low frequency vibration peaks in the 1.4 – 6.5 Hz, 12-17 Hz and 18.4 – 19.9 Hz are thus higher than those observed in Figure 3-9 to Figure 3-11. Similar trends are also observed in the PSD of the roll and pitch accelerations of the vehicle body and the operator-station as seen in Figure 3-18 and Figure 3-19, respectively.
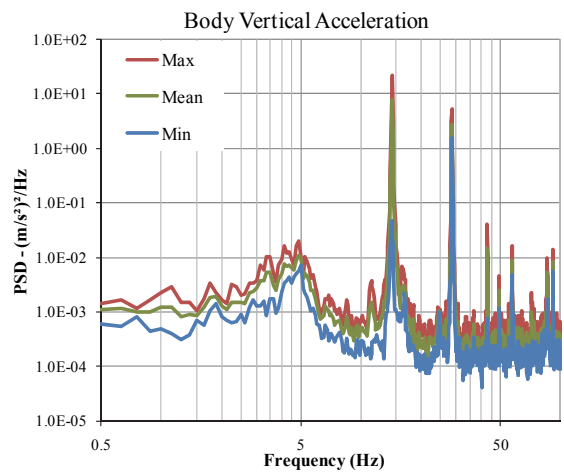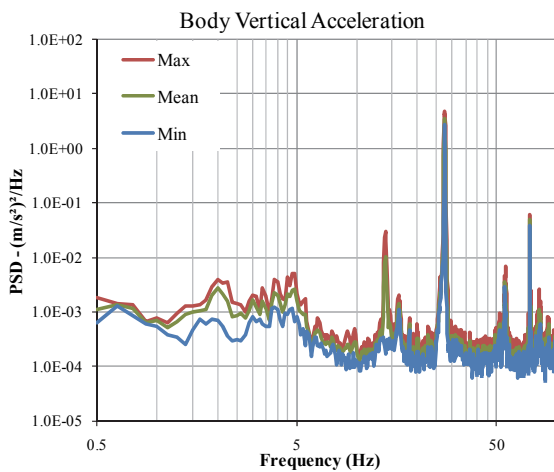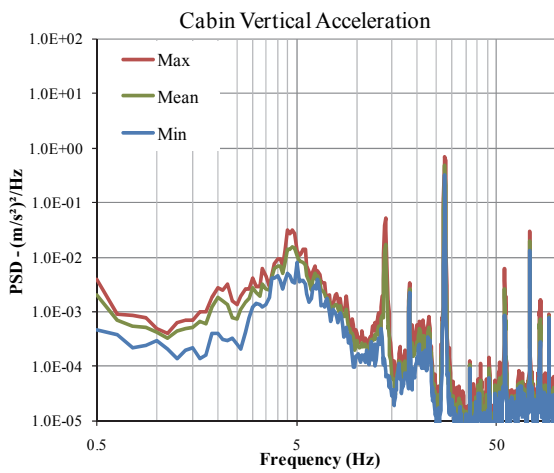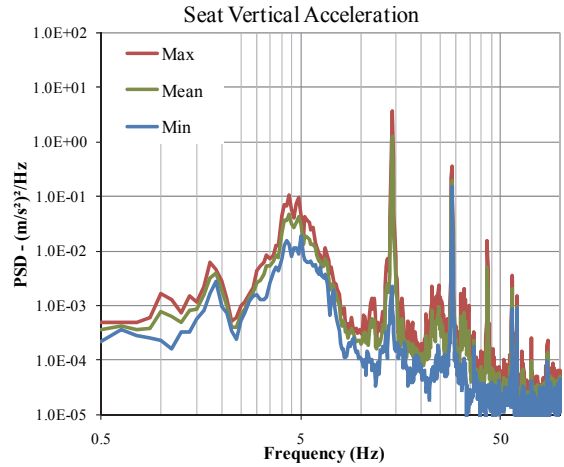
Figure 3-15: PSD of vertical acceleration measured at the vehicle body, operator-station floor and the seat during compaction of high density soil (vibrator set at "high amplitude"): (a) 4-cylinder machine; (b) 6-cylinder machine
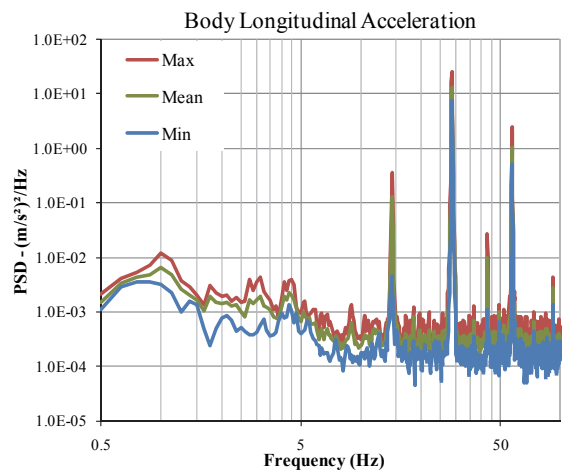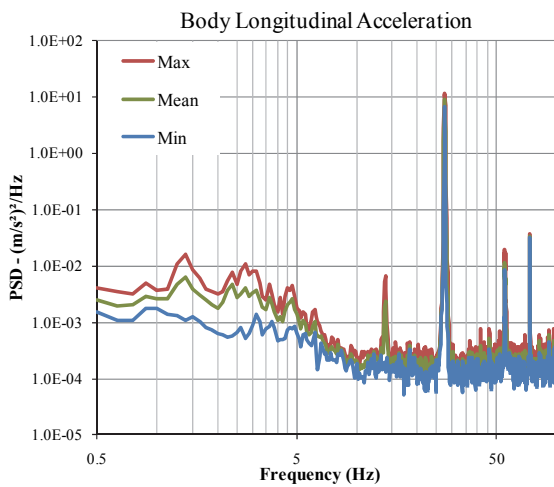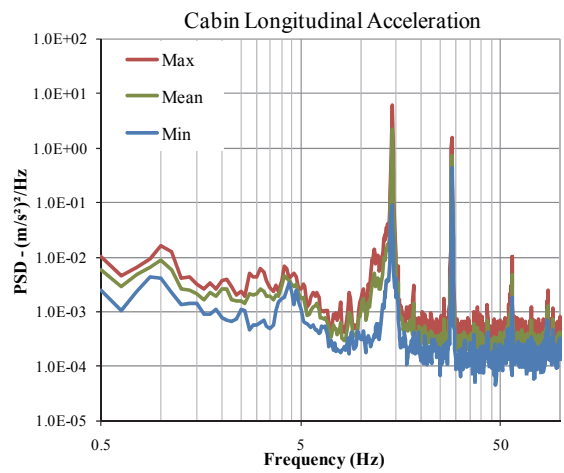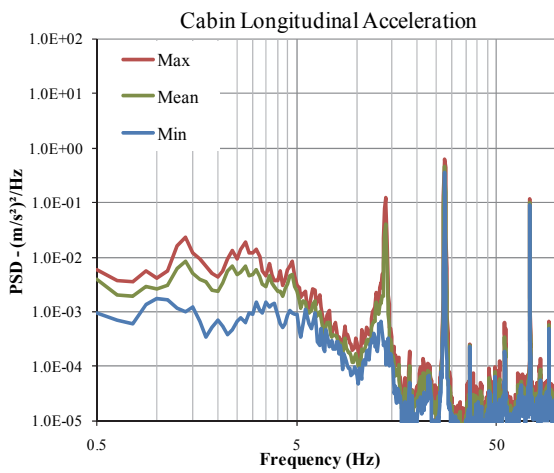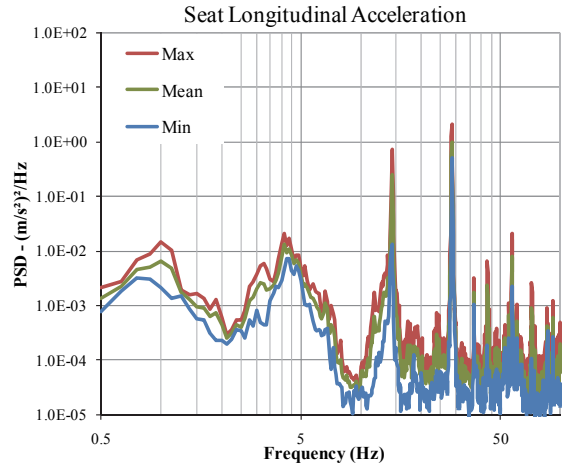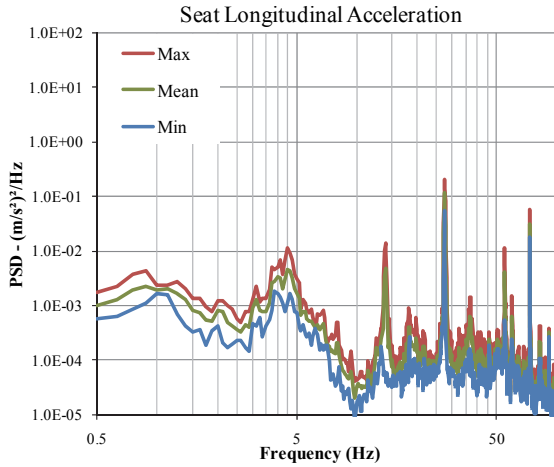
Figure 3-16: PSD of longitudinal acceleration measured at the vehicle body, operator-station floor and the seat during compaction of high density soil (vibrator set at "high amplitude"): (a) 4-cylinder machine; (b) 6-cylinder machine
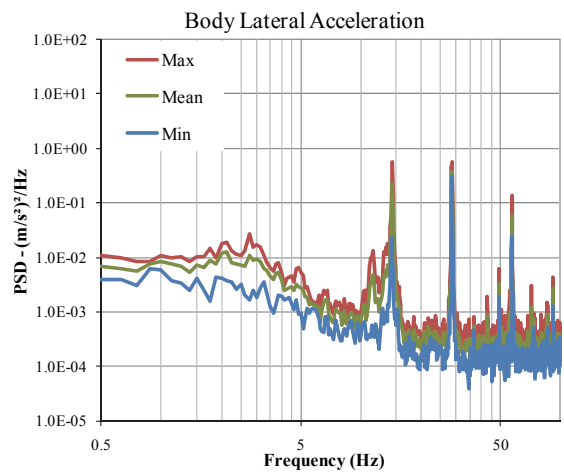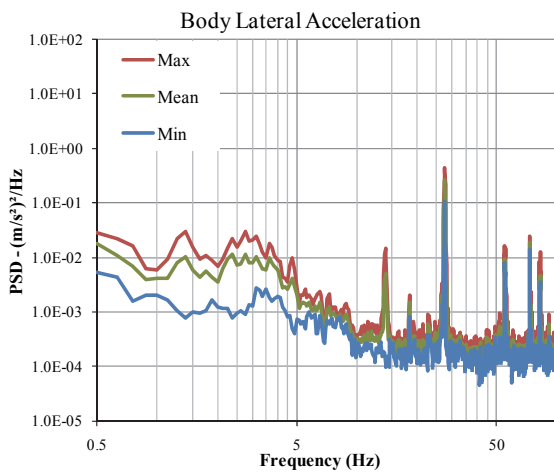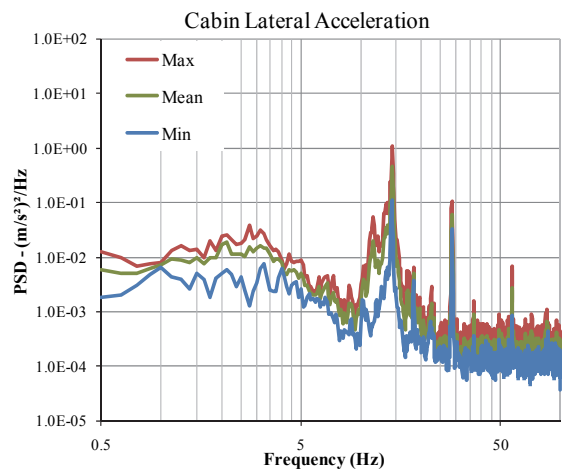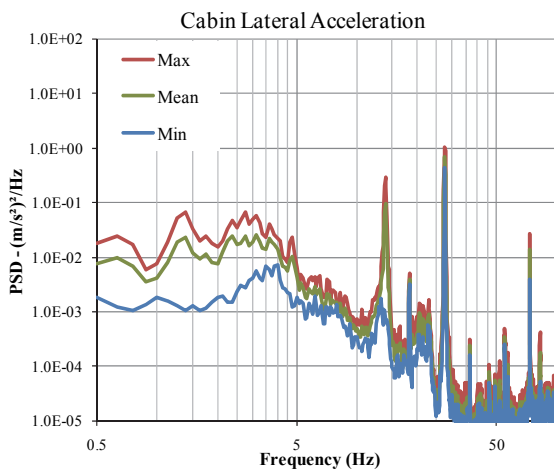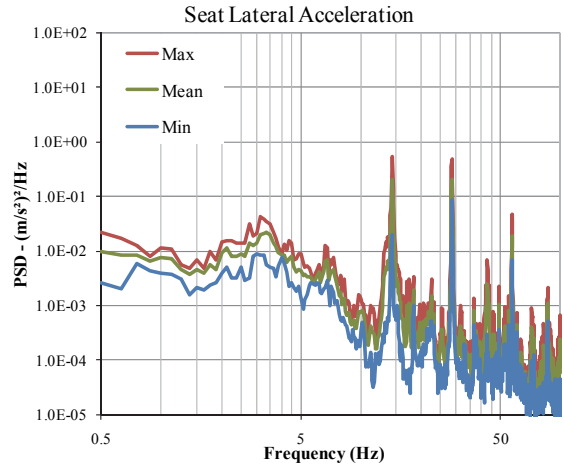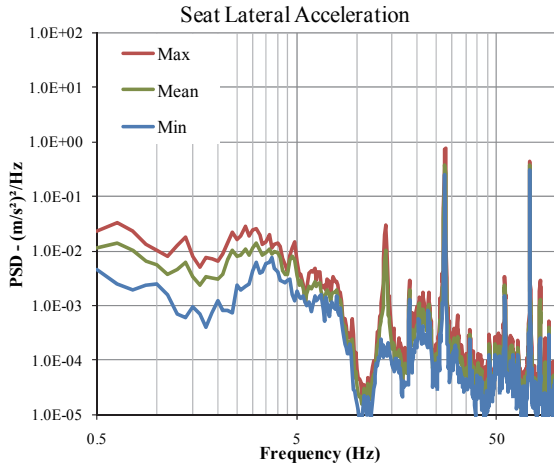
Figure 3-17: PSD of lateral acceleration measured at the vehicle body, operator-station floor and the seat during compaction of high density soil (vibrator set at "high amplitude"): (a) 4-cylinder machine; (b) 6-cylinder machine
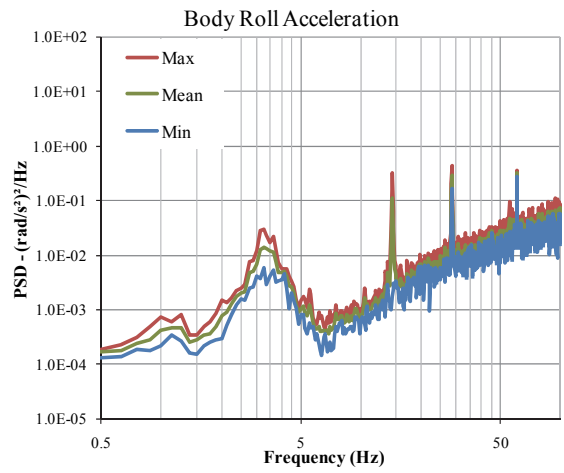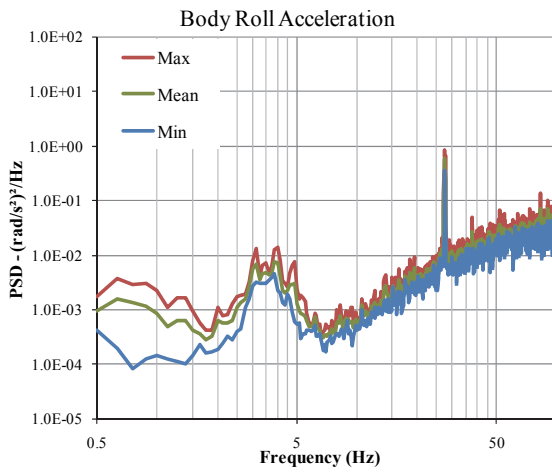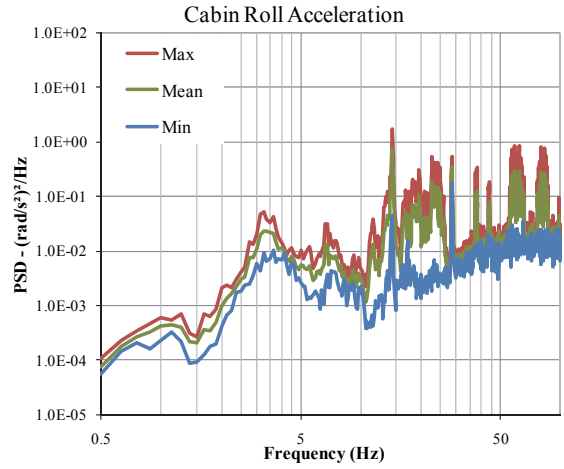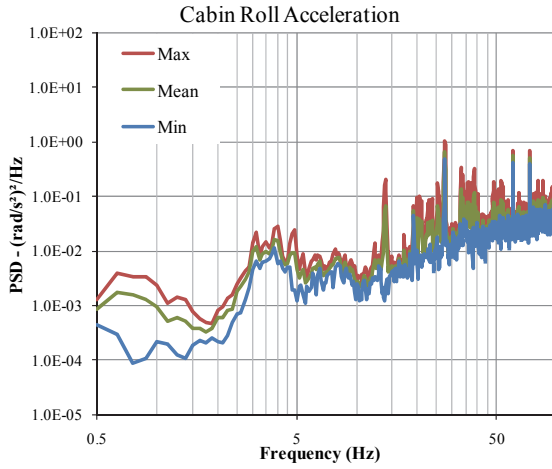
Figure 3-18: PSD of roll acceleration measured at the vehicle body and the operator-station floor during compaction of high density soil (vibrator set at "high amplitude"): (a) 4-cylinder machine; (b) 6-cylinder machine
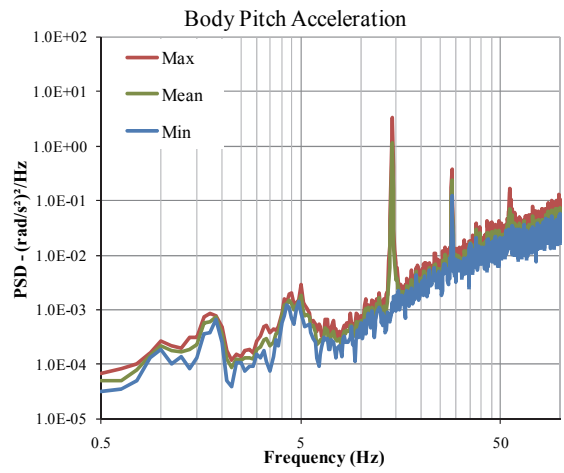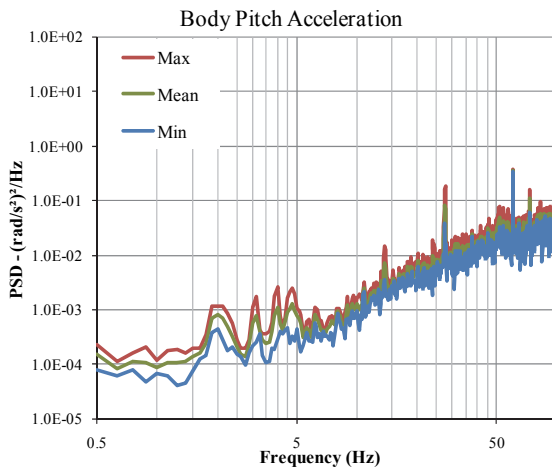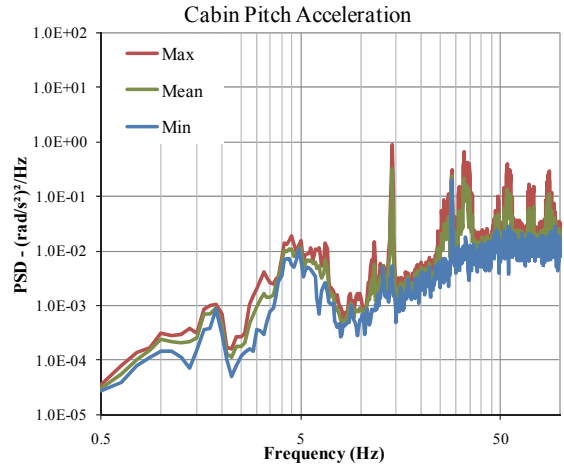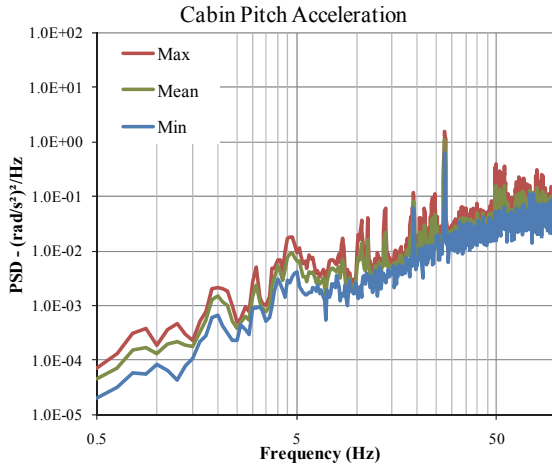
Figure 3-19: PSD of pitch acceleration measured at the vehicle body and the operator-station floor during compaction of high density soil (vibrator set at "high amplitude"): (a) 4-cylinder machine; (b) 6-cylinder machine
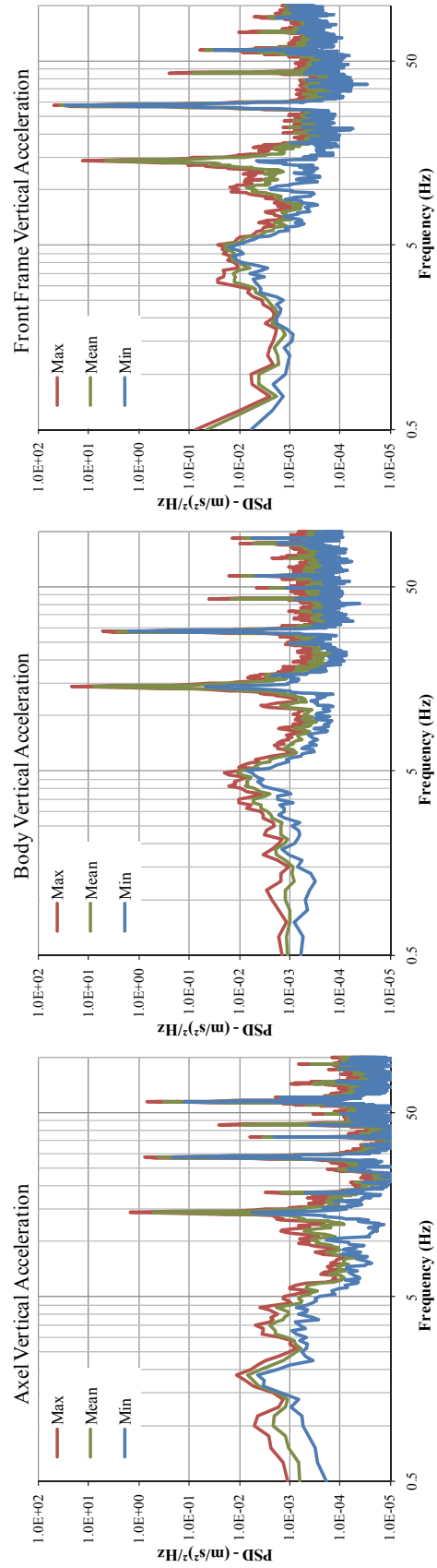
Figure 3-20: PSD of vertical acceleration measured at the axle (rear frame), center of vehicle body and at the front frame during compaction of high density soil (vibrator set at "high amplitude"): for 6-cylinder machine

3.4.3. **In transit mode**

In the transit mode of operation, the vehicle operates with the vibrator turned off. The vibration behaviour of the vehicle is mostly determined by the drum/wheel interactions with the road surface. Furthermore, the vehicle speed is significantly higher than that in the compaction, which would yield considerably higher magnitudes of vibration, particularly in the low frequency range. The ranges of measured vibration spectra in this case are thus used to identify the range of frequencies of dominant vibration and the probable corresponding modes. These frequencies of dominant vibration observed from the spectra of vibration encountered during the transit mode of operation were generally quite comparable with these observed in the data during the compaction modes.

Figure 3-21 to Figure 3-25 illustrate the ranges of spectra of vertical (z), longitudinal (x), lateral (y), roll (θ) and pitch (φ) accelerations, respectively measured at the operator-station floor and vehicle body of the two machines considered in the study. Figure 3-21 to Figure 3-23 also show the spectra of translational vibration measured at the seat. The results show considerably higher magnitudes of low frequency vibration in all the axes compared to those observed during the compaction modes. Furthermore, the high frequency vibrations attributed to the vibrator are not evident, although the results also show significant levels of high frequency vibration. These are attributable to bending and torsional deflections of vehicle and operator-station structures. The acceleration spectra show peaks in the 1.4-2.2, 2.9-3.6, 3.9-7.0, 12-17 and 18.4-19.9 Hz. These peaks can be generally observed from the responses along all the axes, while the corresponding

frequencies could be associated with particularly modes of vibration of the vehicle. Furthermore, the ranges of vibration frequencies observed from spectra of vibration of the two vehicles are quite comparable.

The ranges of pitch plane vibration spectra (x, z and φ) consistently reveal a distinct peak in the vicinity of 4.9 Hz. The magnitude of this peak is particularly pronounced in the pitch responses, but is also evident from the vertical and longitudinal acceleration spectra of the operator-station and the seat. This peak is thus believed to be attributed to the pitch vibration mode of the vehicle body. Considering that the mass and mass moment of the vehicle body are significantly larger than those of the operator-station and the engine, the participation of its pitch mode in the responses of the other bodies would be expected.

The pitch plane vibration spectra also exhibit high magnitude peaks near 1.7 and 3.2 Hz in the vertical and fore-aft responses measured at the vehicle body. The operator-station pitch spectra exhibit large peak near 4 Hz, while the operator-station vertical vibration peaks near 5.5 Hz. The operator-station acceleration spectra also exhibit peak longitudinal acceleration in the 12-13 Hz range, although this could also be associated with coupled lateral/yaw modes as the operator-station sensor was mounted with some noticeable off-set from the vertical symmetry plane of the vehicle due to space constraints in the vicinity of the operator. The results clearly show coupled pitch plan vibration (x, z and φ) with peaks occurring near 1.7, 3.2, 4, 4.9 and 5.5 Hz. From the observed peaks, it is believed that the frequencies 1.7, 3.2 and 4.9 Hz are associated with

the bounce, fore-aft and pitch modes of the vehicle body respectively. The operator-station pitch and bounce modes are speculated to occur near 4 and 5.5 Hz.

The measured acceleration spectra also show peaks at comparable frequencies in the bounce, roll and lateral axes suggesting the coupling in the roll plane. The vehicle body roll acceleration spectrum exhibits distinct peak near 3.4 Hz, which is also evident in the operator-station pitch roll response. The roll mode of the rear frame of the vehicle is thus believed to occur near this frequency. The roll acceleration spectra of the operator-station of both the vehicle also exhibit distinct peaks near 6.8 Hz and in the 12-13 Hz. These frequencies are attributed to the roll mode of the operator-station and its coupled lateral/yaw modes, respectively. Peaks near 2.2 and 3 Hz are also evident in the lateral acceleration spectra of the vehicle body. These peaks corresponding to its coupled lateral/yaw mode frequencies are also evident in the lateral acceleration spectra of the operator-station.

The acceleration spectra also show peaks near 73 Hz, which seems to correspond to the second harmonic of engine speed of 2200 rpm.
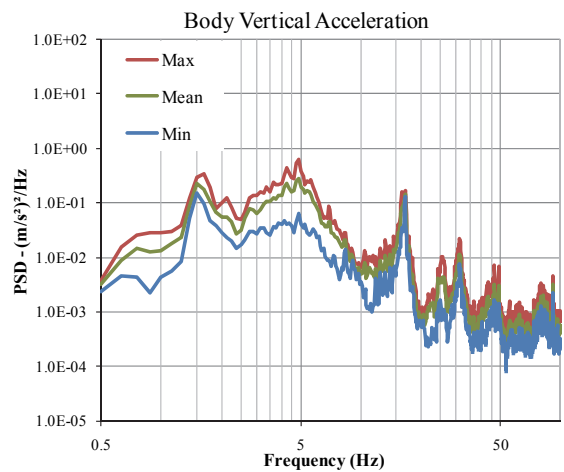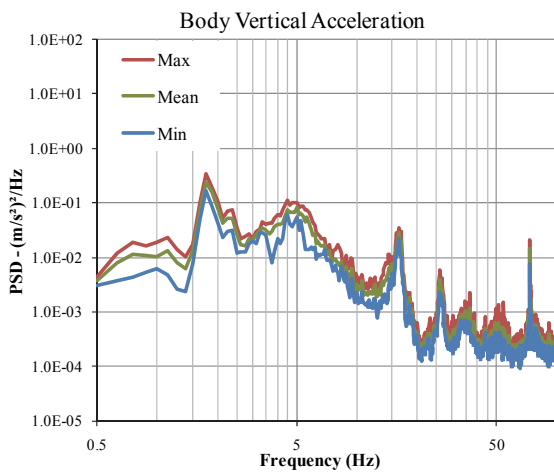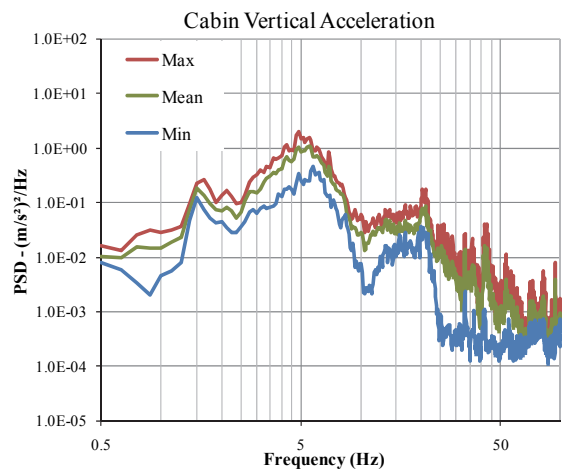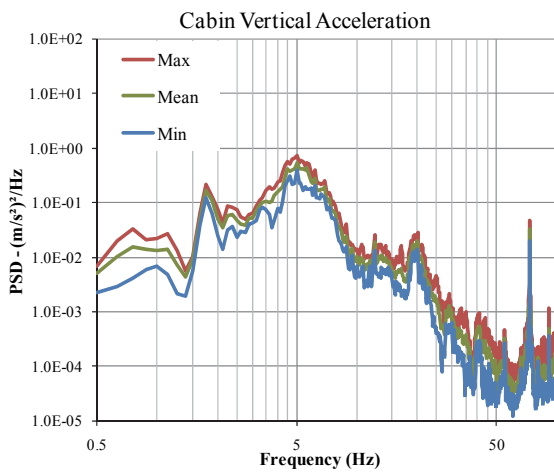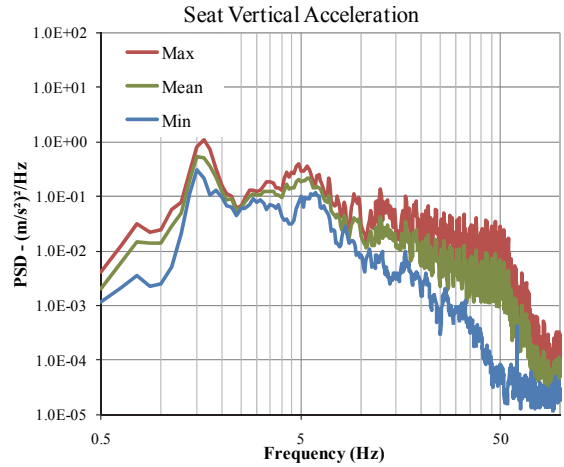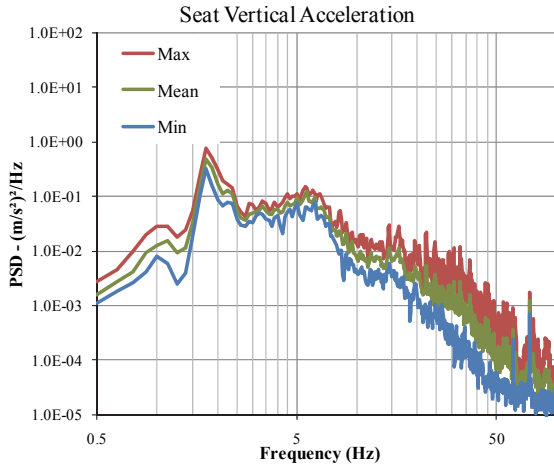
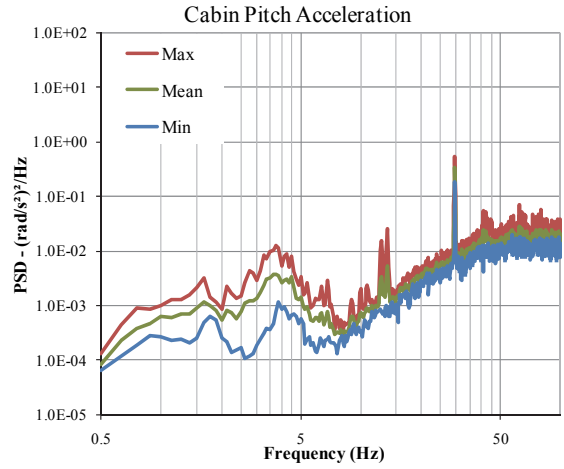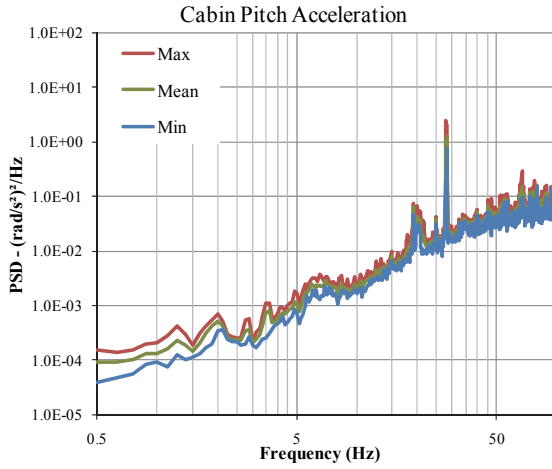**Figure 3-21: PSD of vertical acceleration measured at the vehicle body, the operator-station floor and the seat during transit mode (speed≈10km/h): (a) 4-cylinder machine; (b) 6-cylinder machine**
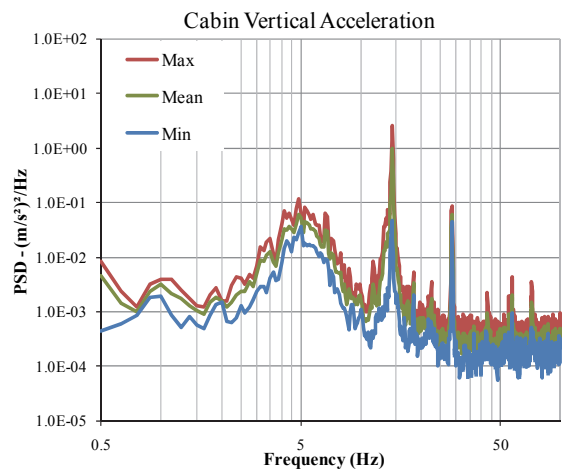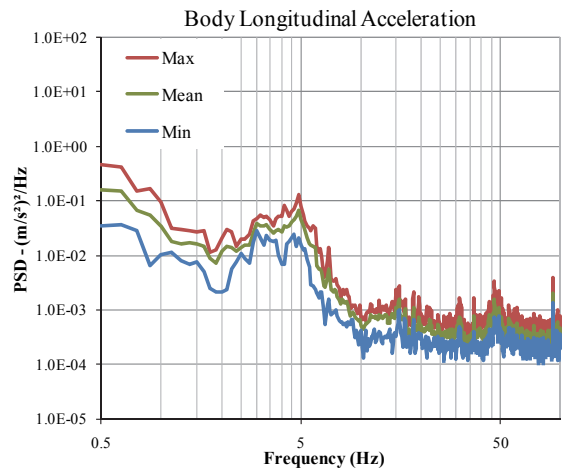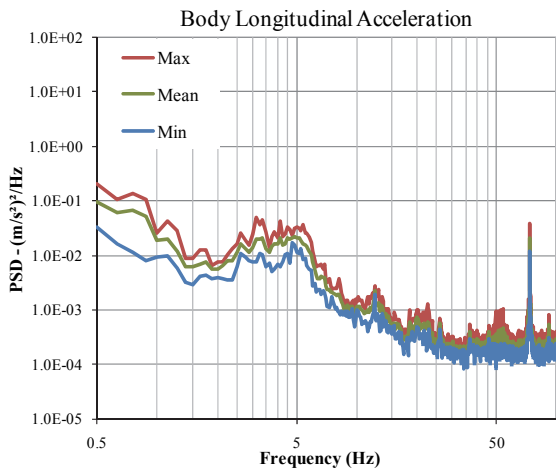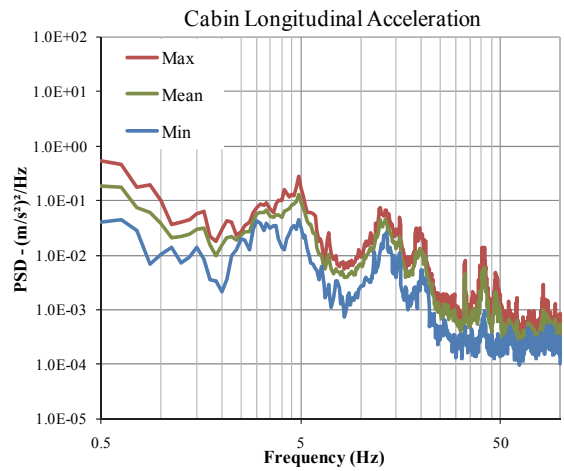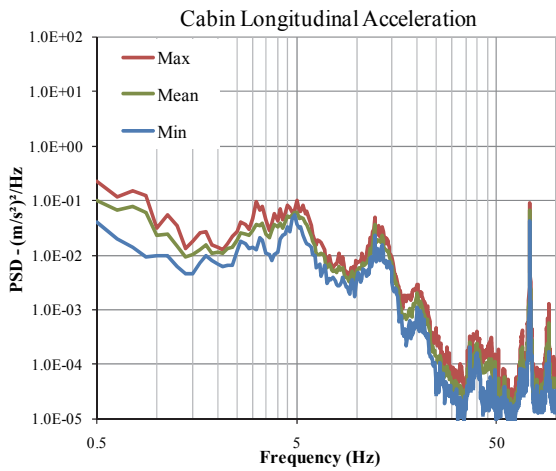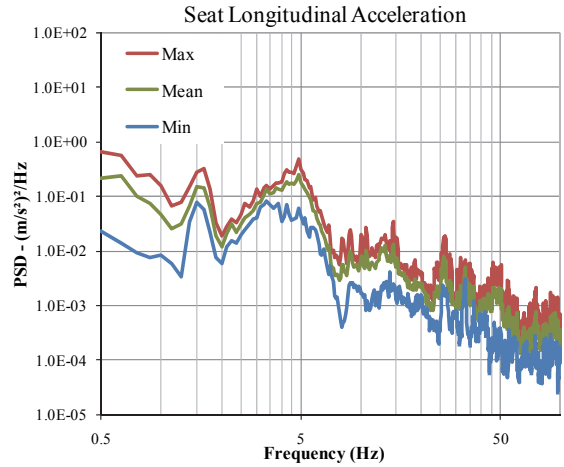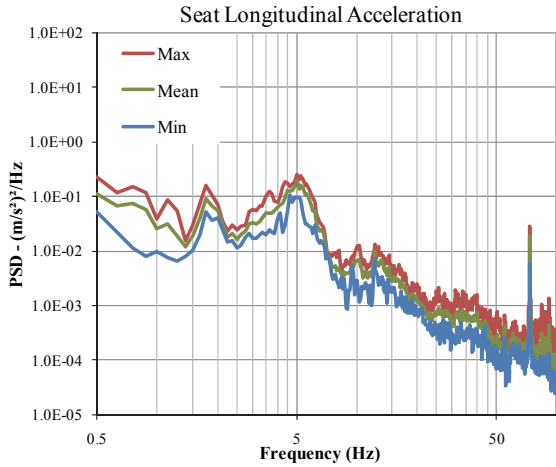
Figure 3-22: PSD of longitudinal acceleration measured at the vehicle body, the operator-station floor and the seat during transit mode (speed≈10km/h): (a) 4-cylinder machine; (b) 6-cylinder machine

94
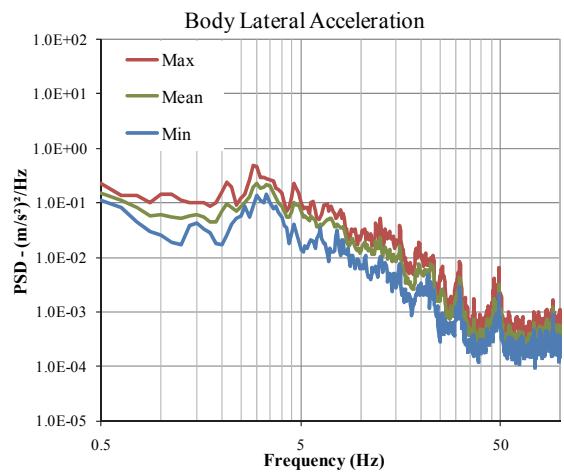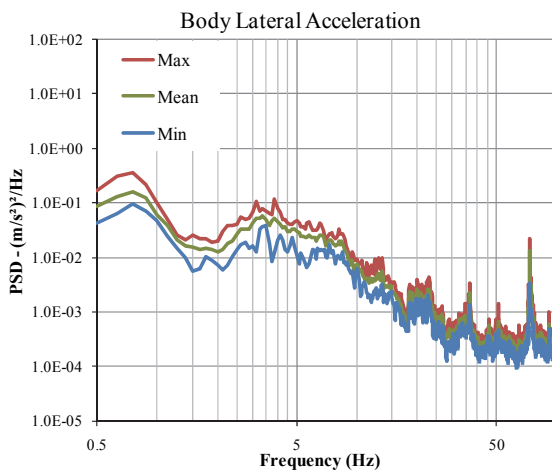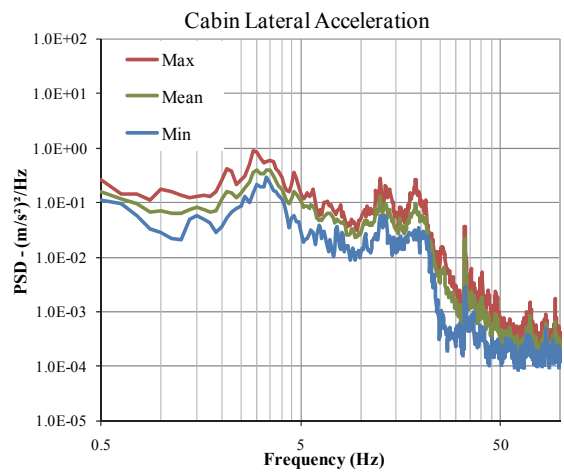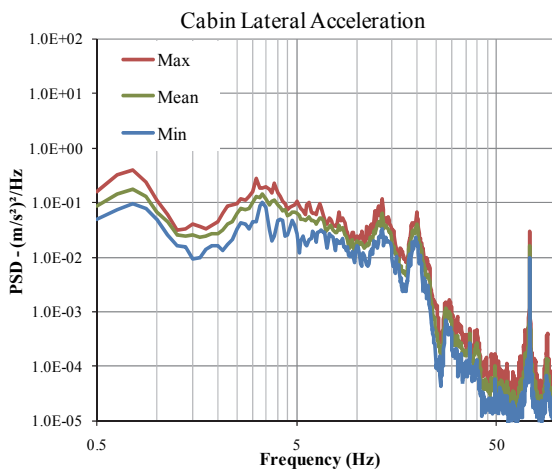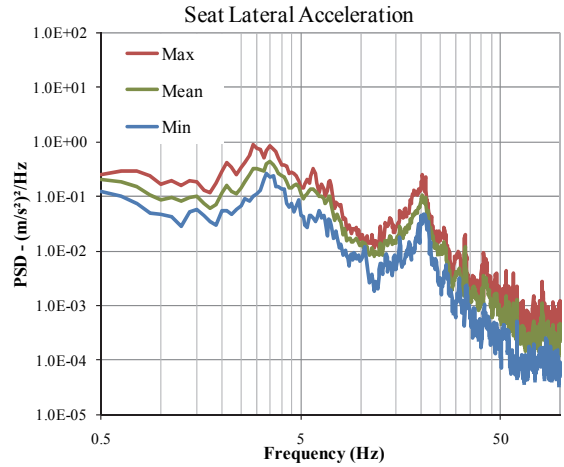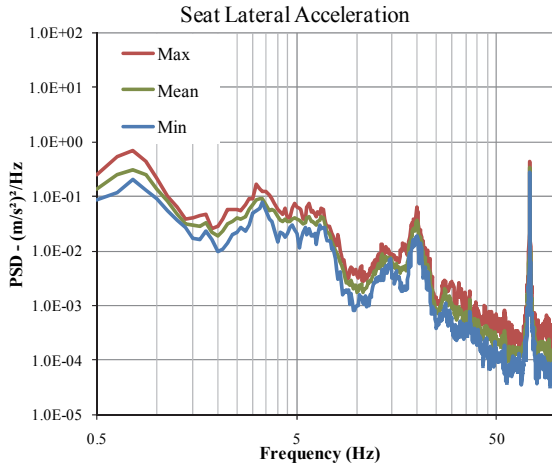
Figure 3-23: PSD of lateral acceleration measured at the vehicle frame, the operator-station floor and the seat during transit mode (speed≈10km/h): (a) 4-cylinder machine; (b) 6-cylinder machine

95
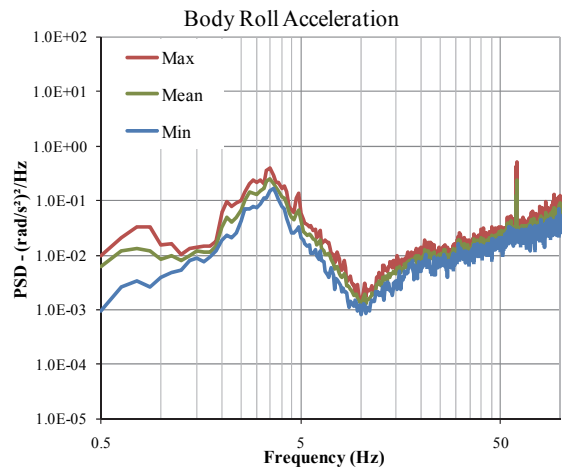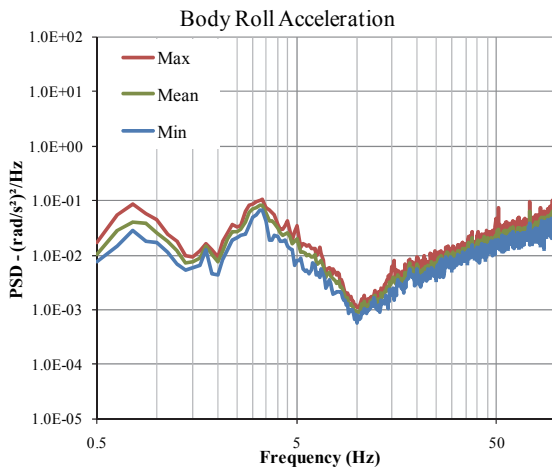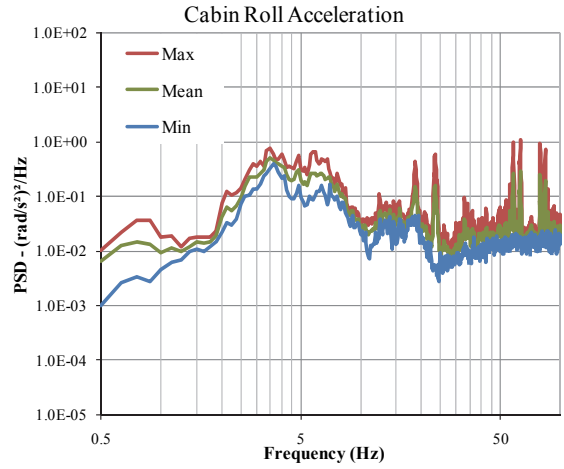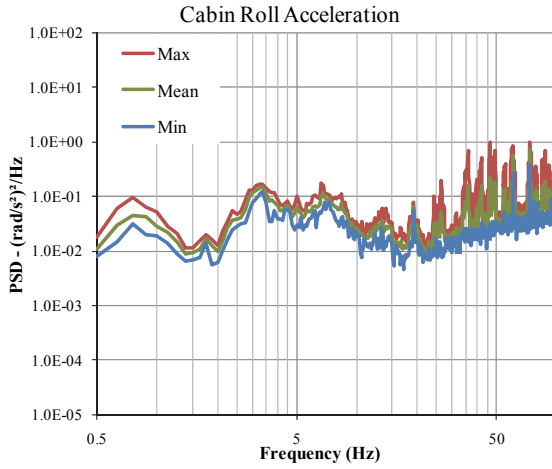
Figure 3-24: PSD of roll acceleration measured at the vehicle body and the operator-station floor during transit mode (speed≈10km/h): (a) 4-cylinder machine; (b) 6-cylinder machine
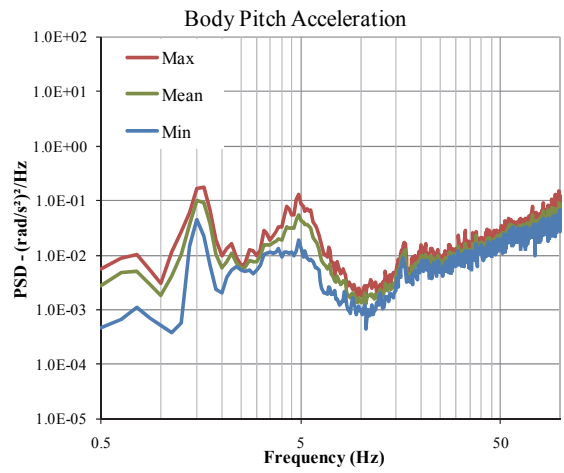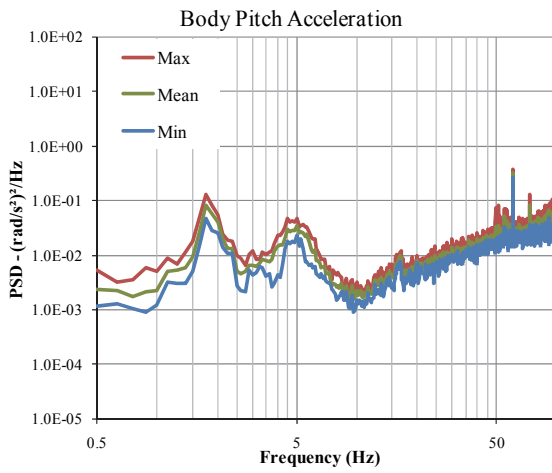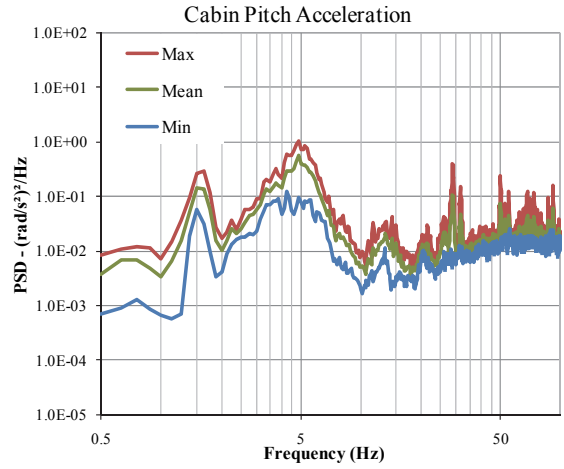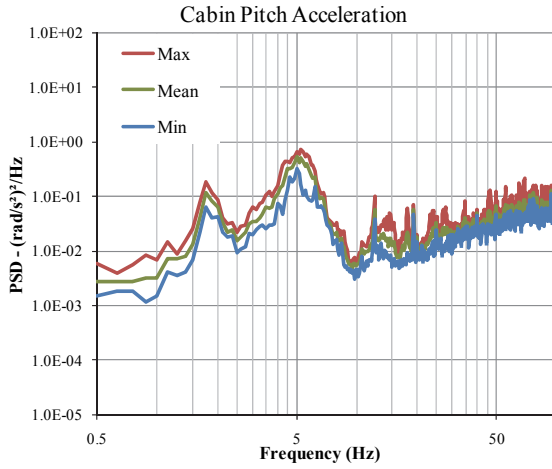
Figure 3-25: PSD of pitch acceleration measured at the vehicle body and the operator-station floor during transit mode (speed≈10km/h): (a) 4-cylinder machine; (b) 6-cylinder machine

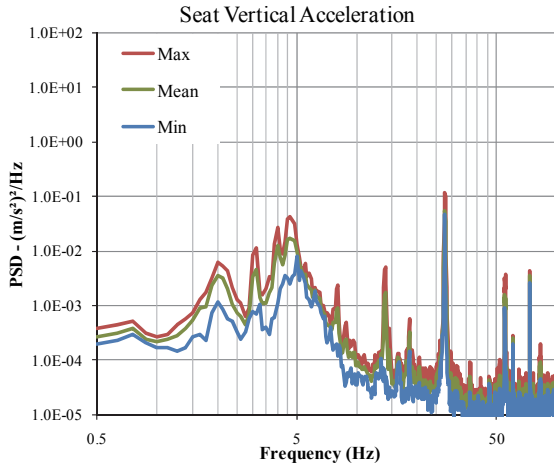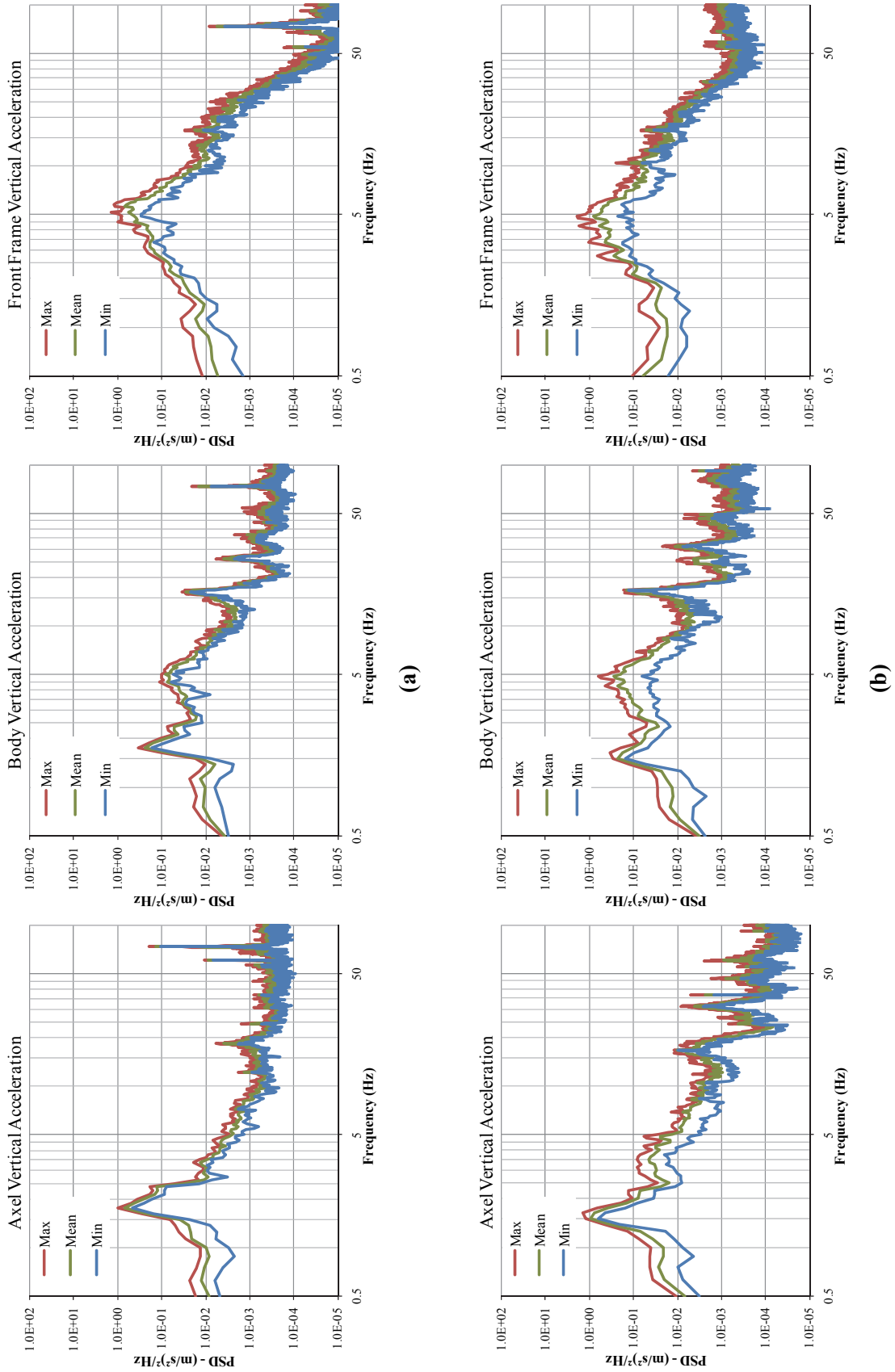**Figure 3-26: PSD of vertical acceleration measured at the axle (rear frame), center of vehicle body and at the front frame during transit mode (speed≈10km/h): (a) 4-cylinder machine; (b) 6-cylinder machine**

Table 3-4 summarizes the frequency ranges of the peaks observed from the ranges of measured acceleration spectra of both the machines and different operating modes (transit, compaction of low and high density soils). The table lists the frequency ranges observed from the vertical, fore-aft and pitch acceleration spectra, which appeared to be strongly coupled. The table also presents the overall frequency ranges of peaks observed in the ranges of measured acceleration spectra. Similarly Table 3-5 further lists the frequency ranges corresponding to the peaks observed in the spectra of vibration measured during different modes of operation together with the overall frequency ranges. The results suggest that a number of frequency ranges corresponding to vibration peaks observed during the compaction mode coincide with those observed in the transit mode.

Table 3-4: Frequency ranges of PSD peaks in all operating modes for each signal

Acceleration spectra	Peaks corresponding to observed peaks (Hz)						
$\ddot{z}_s$	1.5 ~ 2.1	3.0~ 3.5	3.9 ~ 6.5	14.0 ~ 14.5		27.3 ~ 29.4	73.2 ~ 73.3
$\ddot{z}_c$	1.5 ~ 2.0		4.0 ~ 7.0	14.0 ~ 14.5	18.9 ~ 19.9	27.5~ 29.4	73.3 ~ 73.4
$\ddot{x}_c$	1.5 ~ 1.9	2.9~ 3.5	4.0 ~ 5.5	12.3 ~ 14.5	18.4 ~ 19.9	27.5~ 29.5	73.3 ~ 73.4
$\ddot{\varphi}_c$	1.4 ~ 1.9		3.9 ~ 6.2	12.0 ~ 14.5	19.1 ~ 19.9	28.0 ~ 29.5	
$\ddot{z}_b$	1.5 ~ 2.2		3.9 ~ 5.5	15.8 ~ 17.0		27.5 ~ 29.5	73.3 ~ 73.4
$\ddot{\varphi}_b$	1.4 ~ 1.9	2.9~ 3.6	3.9 ~ 6.2	15.6 ~ 16.5		27.5 ~ 28.1	
Overall Range	**1.4 ~ 2.2**	**2.9~ 3.6**	**3.9 ~ 7.0**	**12.0 ~ 17.0**	**18.4 ~ 19.9**	**27.3 ~ 29.5**	**73.2 ~ 73.4**

Table 3-5: Frequency ranges of PSD peaks for all signals in each operating mode

PSD	Peaks frequency range (Hz)						
Transit	1.4 ~ 2.2	2.9~ 3.6	3.9 ~ 7.0	12.0 ~ 17.0	18.4 ~ 19.9		73.3 ~ 73.4
Compaction (Low density)					19.1 ~ 19.9	27.3 ~ 29.5	73.2 ~ 73.3
Compaction (High density)			3.9 ~ 6.5	14.0 ~ 14.5	19.1 ~ 19.9	27.3 ~ 29.5	73.3 ~ 73.4
Overall Range	**1.4 ~ 2.2**	**2.9~ 3.6**	**3.9 ~ 7.0**	**12.0 ~ 17.0**	**18.4 ~ 19.9**	**27.3 ~ 29.5**	**73.2 ~ 73.4**

3.5.   Summary

This chapter presented the measurements of ride vibration responses of two 10-ton compactors performing the transit and compaction tasks; the latter on low and high soil densities. The measured data were analysed to derive spectra of acceleration along the translational and rotational axis. Different runs performing the same tasks revealed good repeatability of the measurements. Various data segments corresponding to each mode of operation were thus grouped together to determine the mean and ranges of vibration spectra for both the vehicles. The ranges of resulting vibration spectra revealed strongly coupled motions in the pitch and roll planes, while the magnitudes of yaw motion were very small. The frequencies corresponding to the observed peaks in the acceleration spectra were identified and associated with probable vibration modes of vehicle. The range of acceleration spectra and the frequencies will be applied in the following chapter to examine the validity of the ride dynamic model of the vehicle.

CHAPTER 4 – METHODS OF ANALYSIS AND MODEL VALIDATIONS

4.1. Introduction

The differential equations of motion derived for the vehicle model for the transit and compaction modes of operation are solved for excitations arising from the road roughness and soil model, respectively. The evaluation of ride dynamics and compaction responses of the vehicle necessitates identifications of vehicle inertial and dimensional properties, and static and dynamic properties of the vehicle subsystems. Furthermore, it is essential to characterise the roughness properties of the road surface for ride response analysis in the transit mode, and the soil properties for analysis of compaction response. It is also vital to examine the validity of the model using the ranges of field measured responses presented in CHAPTER 3. The validated model could then serve as an important tool not only for assessment of WBV exposure under different operating conditions but also for design and/or tuning of primary and secondary suspensions.

Although the field measured responses revealed comprehensive magnitudes of vibration in the vertical, for-aft, lateral, roll and pitch directions, the ride dynamic model developed in this study is limited to pitch-plane dynamics alone. Furthermore, the assumption of constant forward speed and lack of consideration of the tire- and drum-terrain shear mode properties does not permit accurate predictions of the fore-aft vibration response. The validity and applicability of the proposed model is thus limited to vertical and pitch ride vibration responses. The measured responses, however, suggest the need for development

in three-dimension ride dynamic model of the vehicle. The model presented in this study thus represents a preliminary effort in this direction.

In this chapter, the measured data acquired at the drum is analysed to obtain estimate of the road profile. The linear ride dynamic models are subsequently analysed to evaluate the ride responses. The validity of the ride dynamic models is initially examined by comparing their natural frequencies with the dominant ride frequencies identified from the measured data of the vehicle in the transit mode. The ride models are further validated by comparing the vertical, longitudinal and pitch acceleration responses of the vehicle body, the operator-station, and the vertical and longitudinal responses at the operator-seat interface with the measured data presented in CHAPTER 3. The validity of the nonlinear compaction model is also examined by comparing, in a qualitative manner, the vibration response spectra of different bodies with the ranges of the field-measured responses, and the force – deflection response of the soil and the drum displacement response of the model with those reported in the published studies (Adam & Kopf, 2000; Floss & Kloubert, 2000; Krober, Floss, & Wallrath, 2001; Kloubert, 2004) which have been discussed in Section 1.2.2. The compaction model validity is further investigated with respect to the compaction characteristic of the soil using the trends reported in a few published studies (Anderegg & Kaufmann, 2004; Tateyama, Ashida, Fukagawa, & Takahashi, 2006; Scherocman, Rakowski, & Uchiyama, 2007; Akesson, 2008).

4.2. Ride Response Analysis in the Transit Mode

The ride dynamics of the compactor is of significance in the transit mode of operation due to its occurrence at relatively higher speeds. The ride dynamic responses of the

compactor model can be conveniently evaluated in the frequency domain to determine the ride acceleration responses of the operator station and the seat. Owing to the constant speed assumption and in-plane dynamics, the ride dynamic models can predict the ride response along the vertical and pitch axes alone, while the longitudinal acceleration at the driver's location arising from vehicle pitch may also be estimated. In this study, the ride responses of the models are evaluated in terms of PSD and overall rms values of the accelerations of the vehicle body, operator-station and the seat along the vertical, pitch and longitudinal axes. The models are also analysed to determine the natural frequencies and the corresponding deflection modes, which are expected to yield some design guidance for the primary and secondary suspensions.

The ride dynamic responses of road and off-road vehicles are known to strongly depend upon the terrain roughness and forward speed apart from the weights and dimensional, and suspension properties of the vehicle. It is thus-vital to identify the weights and dimensional, and suspension properties, and the terrain roughness. While the vehicle properties have been obtained from the manufacturer, the terrain roughness is characterised from the measured data, as discussed in the following subsections.

4.2.1. Vehicle Model Parameters

The parameters of the 4-cylinder and 6-cylinder soil compactors were obtained from the vehicle manufacturer. These included the weights and dimensional properties of the vehicle and its subsystem, stiffness and damping properties of the engine, operator-station and the drum mounts, and the vibrator parameters. Some of these parameters are

summarized in Table 4-1. Very high stiffness was assumed for the seat suspension and the rear axle suspension, since these are not present in the test vehicles.

Table 4-1: Vehicle Model Parameters

Parameter	6-cylinder compactor	4-cylinder compactor	Parameter	6-cylinder compactor	4-cylinder compactor
m_d	3,300 kg	3,300 kg	k_d^z	3,000 kN/m	3,000 kN/m
m_w	400 kg	400 kg	k_t^z	500 kN/m	500 kN/m
m_b	6,100 kg	5,700 kg	k_a^z	∞	∞
m_e	600 kg	470 kg			
m_c	350 kg	350 kg	k_{ef}^z	1,000 kN/m	800 kN/m
m_s	10 kg	10 kg	k_{er}^z	1,000 kN/m	800 kN/m
m_h	53 kg	53 kg			
			k_{cf}^z	300 kN/m	300 kN/m
I_b	16,000 kg m^2	14,000 kg m^2	k_{cr}^z	220 kN/m	220 kN/m
I_e	100 kg m^2	65 kg m^2	k_s^z	∞	∞
I_c	80 kg m^2	80 kg m^2	k_h^z	22 kN/m	22 kN/m
c_d^z	22 kNs/m	22 kNs/m	l_d	1.6 m	1.5 m
c_t^z	4 kNs/m	4 kNs/m	l_t	1.3 m	1.4 m
			l_e	1.2 m	1.4 m
h_d	0.1 m	0.1 m	l_c	0.0 m	-0.1 m
h_t	0.9 m	0.9 m	l_s	0.0 m	0.0 m

The parameters of the soil model, which serves as the primary input to the compaction model, are identified from the reported studies. They are summarised, together with the vibrator parameters, when covering the compaction model validation later in this chapter.

4.2.2. **Test-track profile**

The analysis of ride vibration properties of a vehicle necessitates characterization of the roughness properties of the tracks, apart from the reliable vehicle parameters. The surface roughness properties of various road and off-road tracks have been widely measured and expressed in terms of the spatial power spectral density of the terrain profile as a function

of its spatial frequency or the wavelength (Wong, 2001). The measured roughness profiles of various roads have also been grouped in order to characterize the average roughness of different roads classified by a relative ranking on the basis of roughness magnitudes. The International Standardization classification (ISO 8608, 1995) presents the average spatial spectral density of roads ranked from A to H, where the road "A" relates to a very smooth road surface and "H" to a very rough road surface. The average road roughness properties, defined in the ISO document, however, may not correspond to those of a typical road in the entire range of wavelengths. Furthermore, it is quite difficult to assign a particular ranking, defined in the standard (ISO 8608, 1995), to a given road on the basses of mere observations. It is thus desirable to characterize the roughness properties of the test track traversed by the vehicle. This is particularly important, where validity of a ride dynamic model needs to be investigated, as in the case of the present study. The test track used in the road measurements revealed considerable waviness in the surface but was generally observed to be smooth. It was thus expected to reveal greater magnitudes of low frequency components.

In this study, the roughness properties of the test track used in field measurements are identified from the measured data. From the review of the published studies, it was evident that many road profile surveying techniques have been based on the principal of a rigid wheel rolling on the road at a low speed, while pulled by a vehicle (Bogdanoff, Kozin, & Cote, 1966; Bekker, 1969). A soil compactor is equipped with a rigid steel drum and it operates at relatively low speeds (maximum speed near 10 km/h). In the field measurements, the compactor drum was equipped with an accelerometer to capture the longitudinal and vertical motions of the drum. The measured vertical motion could be

used to establish the road profile provided a continuous drum-ground contact could be ensured.

The measured drum acceleration data over various test segments were thus examined to ensure continuous drum-road contact. This condition was considered to be satisfied when the measured upward peak acceleration over the entire segment was inferior to 1g. The data acquired over majority of the tests revealed sufficiently long data sub-segments with peak acceleration less than 1g. The measured data over these sub-segments were thus considered to represent the acceleration of the drum due to road roughness alone. A total of 11 data sub-segments were extracted from the measured acceleration data, where each sub-segment was at least 30 s long. The acceleration data of the selected sub-segments were analysed to compute the PSD of the displacement, which were subsequently presented in the spatial domain using the quasi-constant forward speed, such that:

$$S_g(\Omega) = vS_d(f)$$

$$\Omega = {}^f\!/_v$$

(4.1)

where $S_g(\Omega)$ is the spatial power spectral density of the terrain profile in m^3/cycle, v is the forward speed, $S_d(f)$ is the measured displacement temporal PSD at the drum and f and Ω are the temporal and spatial frequencies, respectively.

Figure 4-1 compares the mean spectral densities of the selected segments obtained for the two test vehicles (4 and 6 cylinder compactors). The results show comparable road profile for both the vehicles at spatial frequencies exceeding 0.4 cycle/m. The mean

spectra however, show notable differences at lower frequencies, which were believed to be partly attributed to changes in the lateral vehicle position with respect to the centerline of the track, and in part to possible variations in the forward speed, during transit over different segments. Furthermore, data segments selected for the two machines differed considerably.
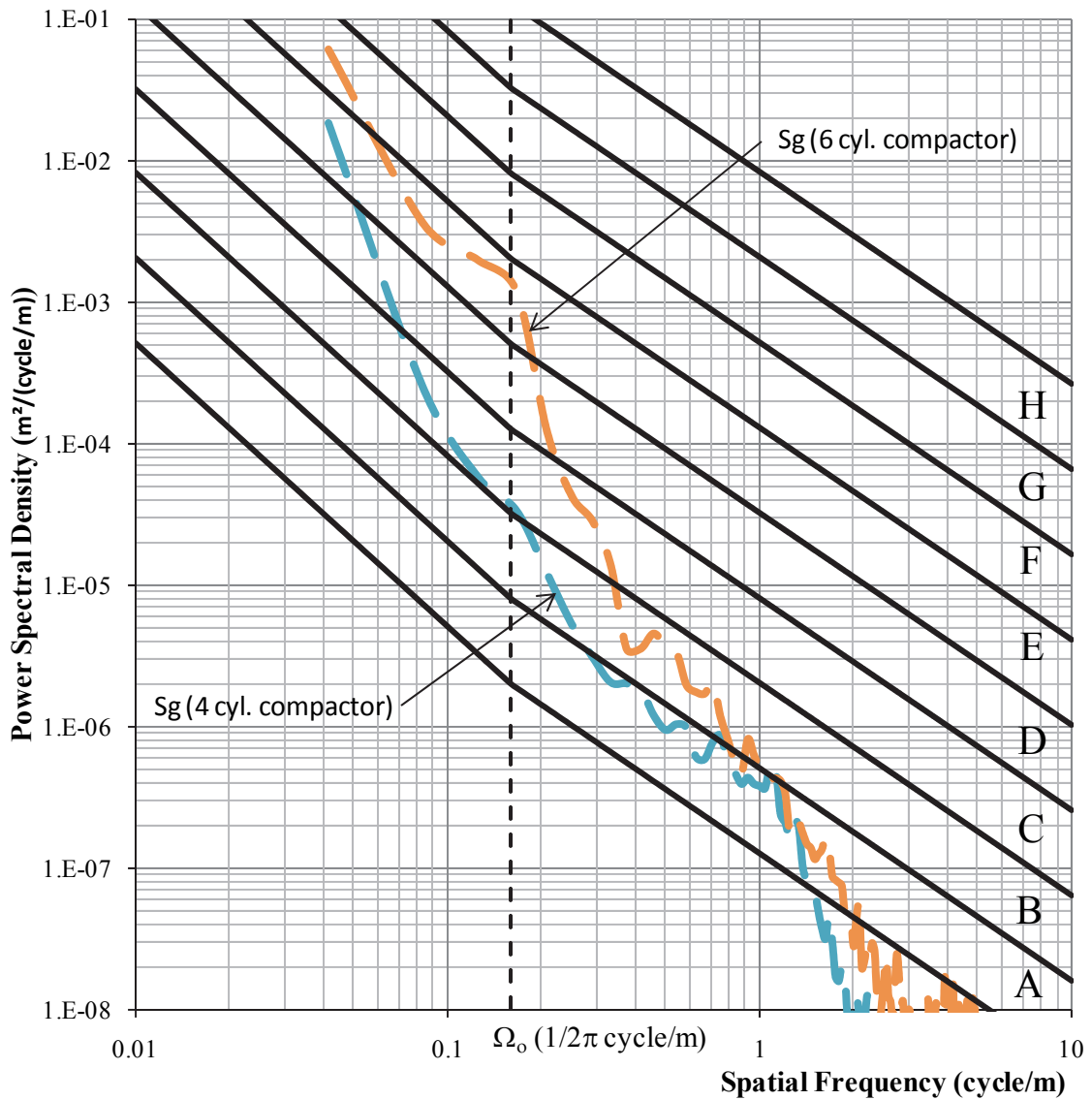
Figure 4-1: Comparison of mean spatial spectral density of the test track profile extracted from the measured drum responses of the 4- and 6-cylinder compactors

The mean of mean spatial PSDs was thus considered to describe the roughness profile of the test track used in the study. The spatial spectral density of various road profiles has been expressed by the following regression model:

$$S_g(\Omega) = \begin{cases} S_g(\Omega_o) \, (\Omega/\Omega_o)^{-2.0} & ; \quad \Omega \leq \Omega_o \\ S_g(\Omega_o) \, (\Omega/\Omega_o)^{-1.5} & ; \quad \Omega > \Omega_o \end{cases}$$

(4.2)

where $\Omega_o = \frac{1}{2\pi}$, and the range of values of $S_g(\Omega_o)$ has been defined for various roads classified by their roughness property (ISO 8608, 1995). To have the test track profile in the ISO format with the same transition frequency $\Omega_0 = \frac{1}{2\pi}$, the mean of means spectrum was logarithmically linearised by determining the average logarithmic slopes as $N_1 = 3.0$ and $N_2 = 4.0$, and estimating the transition PSD value as $S_g(\Omega_o) = 4.0 \times 10^{-4} \, m^2/Hz$. The identified test track profile is compared with the standardized road profiles (ISO 8608, 1995) in Figure 4-2. The comparison suggests that the medium- and high-frequency components of the road profile correspond to good to very good (C to A) roads, while the lower frequency components correspond to rougher roads (D to E). This also corroborated with the observation of the waviness of test track by the experimenters.

Assuming constant vehicle velocity $v \, (m/s)$, the spatial power spectral density is expressed by the temporal power spectral density of the ground surface profile $S_g(\omega)$ in $(m^2 s/rad)$:

$$S_g(\omega) = \frac{S_g(\Omega)}{2\pi \, v}$$

(4.3)
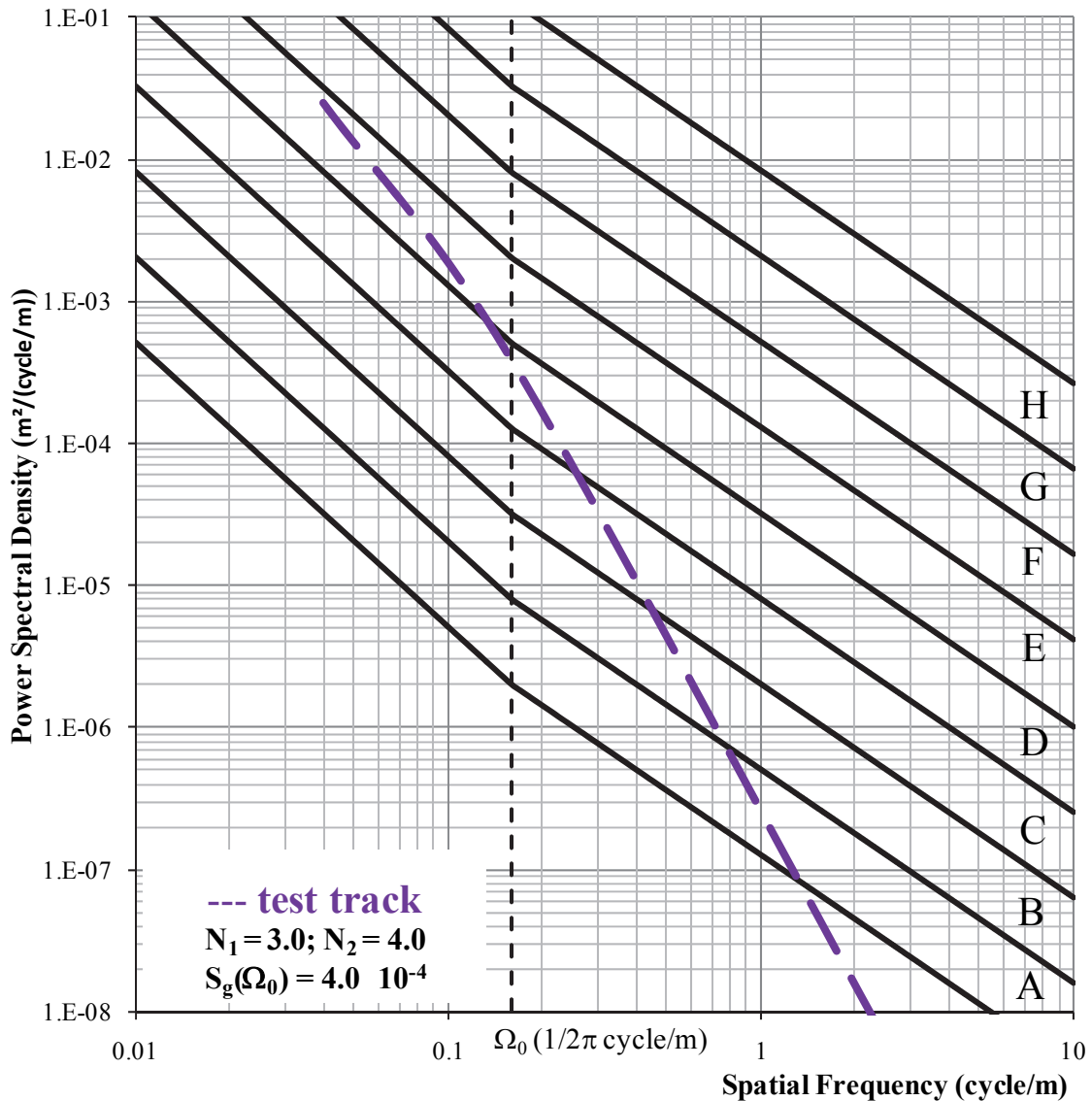
Figure 4-2: Mean of mean spatial PSDs of the road profile extracted from the measured drum responses of the 4- and 6-cylinder compactors

4.3. Methods of Analysis (Ride Response)

The ride dynamic models of the compactor are solved to determine the ride vibration responses of the vehicle in the transit mode. The compaction model, on the other hand, is solved to determine the soil compaction response characteristics. This section describes the methods of analysis of the linear ride dynamic models, while the analysis of the

nonlinear compaction model is discussed in a subsequent section. The linear ride dynamic models are solved to determine the ride accelerations due to a given ground surface profile. The responses obtained under the identified test track profile are used to examine the model validity on the basis of the ranges of the field measured responses. The dominant ride frequencies of the ride dynamic models are also identified through free vibration analysis of the vehicle model. For this purpose, an eigenvalue eigenvector problem is formulated and solved to determine the frequencies of damped oscillations and the natural modes. The eigenvalue problem is formulated as:

$$([D] - \lambda[I])\{Q\} = 0$$

(4.4)

where $\{Q\} = \begin{Bmatrix} \{\dot{Z}\} \\ \{Z\} \end{Bmatrix}$ is the eigenvector, λ are the eigenvalues, and

$$[D] = \begin{bmatrix} (-[M]^{-1}[C]) & (-[M]^{-1}[K]) \\ [I] & [0] \end{bmatrix}$$

(4.5)

is the dynamic matrix.

The above eigenvalue problem was solved using MATLAB. The natural frequencies ω_{ni} and the frequencies of damped oscillation ω_{di} were computed from the complex eigenvalues, $\lambda_i = \alpha_i \pm j\beta_i$, such that:

$$\omega_{ni} = |\lambda_i| \; ; \qquad \text{and} \qquad \omega_{di} = \beta_i \quad ; \quad i = 1, 2, 3, \dots, n$$

(4.6)

The damping ratios ζ_i associated with each mode were also determined from:

110

$$\zeta_i = \frac{-\alpha_i}{\omega_{ni}} \; ; \quad i = 1, 2, 3, \dots, n$$

<div align="right">(4.7)</div>

The deflection modes of the vehicle models were also identified from the eigenvectors. The frequencies corresponding to different modes were considered as the dominant ride frequencies, which are compared with those observed from the field measured data in section 3.4.3.

The frequency response and responses to random road excitation of the ride dynamic models are obtained assuming constant forward speed, and the lag between the excitations at the drum and the rear axle tire. The lag τ is related to the compactor wheelbase $(l_d + l_t)$ and the speed v, such that

$$\tau = \frac{(l_d + l_t)}{v}$$

<div align="right">(4.8)</div>

The frequency response characterization of the vehicle models could be derived assuming harmonic excitations at the drum and rear axle tires, such that:

$$z_{0f}(t) = Z_0 e^{j\omega t} \; ; \quad and \quad z_{0r}(t) = Z_0 e^{j\omega(t-\tau)}$$

<div align="right">(4.9)</div>

where Z_0 is the amplitude of harmonic excitation and τ is the speed-dependent delay, as defined in Eq. (4.8).

The linear equations of motion of the vehicle can thus be expressed as:

$$(-\omega^2[M] + j\omega[C] + [K])\{Z\} = (j\omega[C_0] + [K_0])\{Z_0\}$$

<div align="right">(4.10)</div>

where $[K_0]$ and $[C_0]$ are the forcing stiffness and damping matrices, respectively, and $\{Z_0\}$ is the excitation vector, comprising the vertical displacement excitations at the front drum and the rear axle wheel.

The above equation may be solved to determine frequency response characteristics or the transmission of terrain-induced vibration to the vehicle different bodies, such that:

$$\{T\} = {\{Z\}}/{Z_0}$$

(4.11)

where $\{T\}$ is the vibration transmissibility vector that defines the ratio of vertical and pitch vibration magnitudes of different model bodies (such as the vehicle body and operator-station) with respect to the vertical displacement excitation magnitude, Z_o. The frequency response characteristics of the vehicle could provide considerable insight into the dominant ride frequencies and the contributions due to various design and operating factors. It should be noted that the vibration responses of vehicles operating at low speeds invariably exhibit the wheelbase filtering effect, which is expected to influence the transmissibility responses and the frequencies of dominant responses (Sharp, 2002).

The ride dynamic responses to a random terrain excitation are evaluated by considering both the identified spectral density of the road profile and reported road profiles (ISO 8608, 1995). The excitation to a two-axle vehicle can be defined considering the temporal PSD of the ground surface profile, as described in Eq.(4.3), and the lag between the two axles, as described in Eq. (4.8):

112

$$[S_0(j\omega)] = S_g(\omega) \begin{bmatrix} 1 & e^{-j\omega\tau} \\ e^{j\omega\tau} & 1 \end{bmatrix}$$

<div align="right">(4.12)</div>

where $[S_0(j\omega)]$ defines the excitation displacement matrix.

The displacement responses of the vehicle model to random road excitations can be derived from the frequency response function of the linear model, such that:

$$[S(j\omega)] = [H(j\omega)]^*[S_0(j\omega)] [H(j\omega)]'$$

<div align="right">(4.13)</div>

where $[S(j\omega)]$ is $(n \times n)$ matrix of spectral densities of the response displacements, featuring non-complex diagonal elements, and $[H(j\omega)]$ is the complex frequency response function of the ride dynamic model, which is derived from:

$$[H(j\omega)] = (-\omega^2[M] + j\omega[C] + [K])^{-1}(j\omega[C_o] + [K_o])$$

<div align="right">(4.14)</div>

The superscripts " $*$ " and " $'$ " in Eq. (4.13) denote the complex conjugate and the transpose, respectively. The non-complex acceleration responses of the vehicle model corresponding to the generalized coordinates are subsequently derived from:

$$\{S^{acc}(\omega)\} = \omega^4 \, Diag([S(j\omega)])$$

<div align="right">(4.15)</div>

Where $\{S^{acc}(\omega)\}$ is the acceleration response vector. The acceleration responses at coordinates, other than the generalized coordinates (e.g. beneath the driver's seat) are computed using the coordinate transformations.

4.4. Validation of the ride dynamic models

The ride acceleration data for the test vehicles were gathered by means of sensors placed at selected locations. Although attempts were made to locate sensors near the centers of mass, considerable differences between the coordinates of the sensors and the respective mass centers were observed for many rigid bodies. Consequently, a coordinate transformation matrix $[R]_{sens}$ was formulated to determine the transfer function matrix $[H]_{sens}$ describing the acceleration response at the measurement locations, such that:

$$[H]_{sens} = [R]_{sens}[H(j\omega)]$$

(4.16)

The acceleration responses of the model at the sensors location were subsequently determined from:

$$\{S^{acc}(\omega)\}_{sens} = \omega^4 \, Diag([H(j\omega)]^*{}_{sens} \, [S_o(j\omega)] \, [H(j\omega)]'{}_{sens})$$

(4.17)

where $\{S^{acc}(\omega)\}_{sens}$ is the vector of PSDs of acceleration responses of the model at the sensors locations.

The above equations were solved for the 7-DOF bounce-pitch and a 12-DOF bounce-pitch-fore/aft ride models. The 12-DOF ride model is the one detailed in CHAPTER 2, where the virtual axle suspension and the optional seat suspension were set with very high stiffness values, since these were not present in the test vehicles. The validity of the 7-DOF and the 12-DOF vehicle ride models is examined by comparing their responses with the ranges of the field-measured data corresponding to the transit mode.

The models validity was also examined by comparing the resonant frequencies with the observed dominant ride frequencies. For this purpose, the eigenvalue problems were solved to determine the resonant frequencies and deflection modes of the ride dynamic models. The solution of eigenvalue problem for the simplified 2-DOF ride dynamic model revealed pitch and bounce mode frequencies near 1.6 and 4.8 Hz, respectively. These were also confirmed through the results attained for the 7- and 12-DOF models, which revealed these modes at 1.7 and 4.8 Hz for the vehicle body for the 4-cylinder compactor, and 1.6 and 4.8 Hz for the 6-cylinder vehicle. Table 4-2 and Table 4-3 compare the natural frequencies and probable modes of the vehicle models with the dominant ride frequencies observed from the measured data for the 4- and 6- cylinder compactors respectively.

Table 4-2: Comparisons of natural frequencies of the models with the observed dominant ride frequencies in the case of the 4-cyl compactor

Mode	Observed	7-DOF Model	12-DOF Model
z_w	bolted	-	∞
x_b	3.2 Hz	-	3.3Hz
z_b	1.7 Hz	1.7 Hz	1.7 Hz
φ_b	4.9 Hz	4.9 Hz	4.9 Hz
x_e	16.5 Hz	-	16.3 Hz
z_e	8.5 Hz	9.1 Hz	8.8 Hz
φ_e	9.5 Hz	9.8 Hz	9.8 Hz
x_c	-	-	11.2 Hz
z_c	5.5–5.6 Hz	5.6 Hz	5.6 Hz
φ_c	3.9 Hz	4.2 Hz	3.5 Hz
z_s	bolted	-	∞
z_h	6.15 Hz	6.1 Hz	6.1 Hz

Table 4-3: Comparisons of natural frequencies of the models with the observed dominant ride frequencies in the case of the 6-cyl compactor

Mode	Observed	7-DOF Model	12-DOF Model
z_w	bolted	-	∞
x_b	3.2 Hz	-	3.3Hz
z_b	1.60 Hz	1.65 Hz	1.65 Hz
φ_b	4.85 Hz	4.85 Hz	4.85 Hz
x_e	16.3 Hz	-	17.0 Hz
z_e	8.5 Hz	8.2 Hz	8.1 Hz
φ_e	13.7 Hz	13.4 Hz	12.9 Hz
x_c	-	-	11.1 Hz
z_c	5.5–5.6 Hz	5.6 Hz	5.6 Hz
φ_c	4.0 Hz	4.2 Hz	3.5 Hz
z_s	bolted	-	∞
z_h	6.15 Hz	6.1 Hz	6.1 Hz

The Figure 4-3 and Figure 4-4 show the PSD of vertical accelerations measured at the seat, operator-station and vehicle body of the 4- and 6-cylinder vehicles, respectively. The PSDs of pitch accelerations of the operator-station and vehicle body of the two vehicles are presented in Figure 4-5 and Figure 4-6. Each figure illustrates the range of measured acceleration response together with the mean acceleration PSD. The bounce and pitch mode frequencies of the operator-station of the vehicle models, were identified near 5.6 and between 3.5 – 4.2 Hz, respectively, which correspond with those identified from the measurements: While the ranges of the measured data do not show clear peaks around these frequencies, significant acceleration levels could be observed at frequencies near 5.5 – 5.6 and 3.9 – 4.0 Hz. The measured responses also exhibit additional peaks at low frequencies, which were not observed from the eigenvalues. These frequencies were attributed to the couplings between vertical / pitch and the lateral and roll modes of the vehicle. As discussed in section 3.4.3, the measured data revealed noticeable roll

acceleration peaks of the main vehicle body near 3.4 – 3.6 Hz and 4.5 – 4.6 Hz, which were believed to be attributed to the rear-frame and the front-frame roll modes. The same field measurements also revealed peaks in the main vehicle body responses in the horizontal plane at about 2.1 – 2.2 Hz and 3.0 – 3.1 Hz, which are most likely due to coupled lateral and yaw modes of the vehicle.

The PSDs of vertical and pitch acceleration responses of the 7-and 12-DOF vehicle models are compared with the ranges of the measured data in Figure 4-3 to Figure 4-6. The models responses generally exhibit trends similar to those observed in the measured data, although considerable differences in the magnitudes are also evident. The acceleration response of the models at the seat and the operator-station are generally significantly lower that the measured data at frequencies above 6 Hz and at frequencies below 1 Hz. The higher frequency responses are attributed to the operator-station structure bending and torsion modes, which were neglected in the lumped parameter models. Furthermore, the articulated steering hydraulic system is also expected to yield frequency components of the ride vibration. The higher magnitudes of measured data at lower frequencies could be partly caused by the dc shift in the acceleration signals. The measured signals were processed using a high-pass filter with cut-off frequency of 0.707 Hz, which perhaps should have been relatively higher for a number of data segments that resulted in higher low frequency magnitudes.

Apart from the above, the model responses exhibit distinct valleys near 2 and 8 Hz in the vertical acceleration responses, and many low magnitude peaks at higher frequencies. These are attributed to the wheelbase filtering effect that has been described in a number of reported studies (Best, 1984; Sharp, 2002; Cao, Rakheja, & Su, 2008).

117
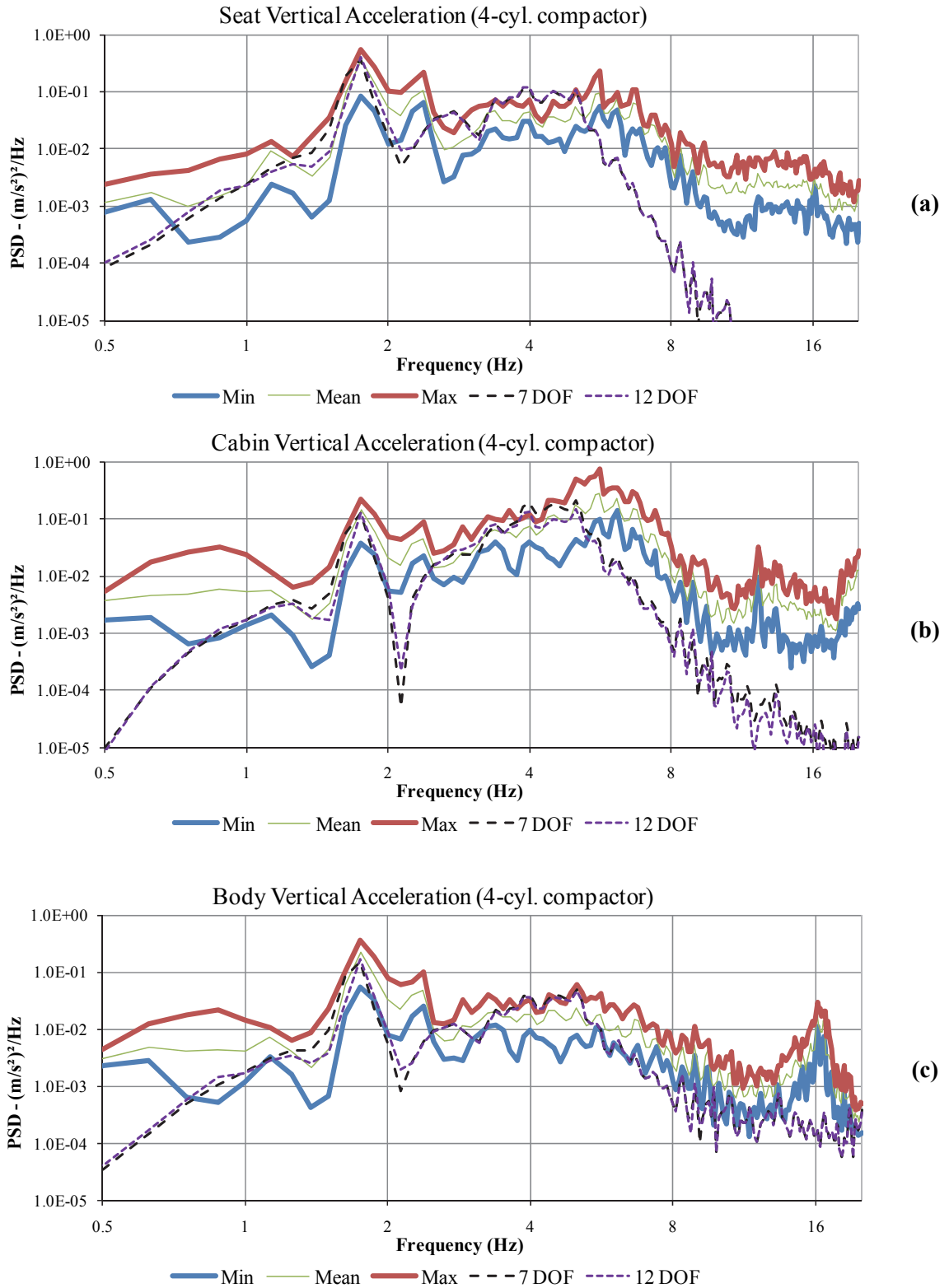
Figure 4-3: Comparison of vertical acceleration PSD responses of the 7- and 12-DOF models with the measured acceleration PSD: (a) seat; (b) operator-station; and (c) vehicle body (4-cylinder compactor in transit mode; speed≈10km/h)

118
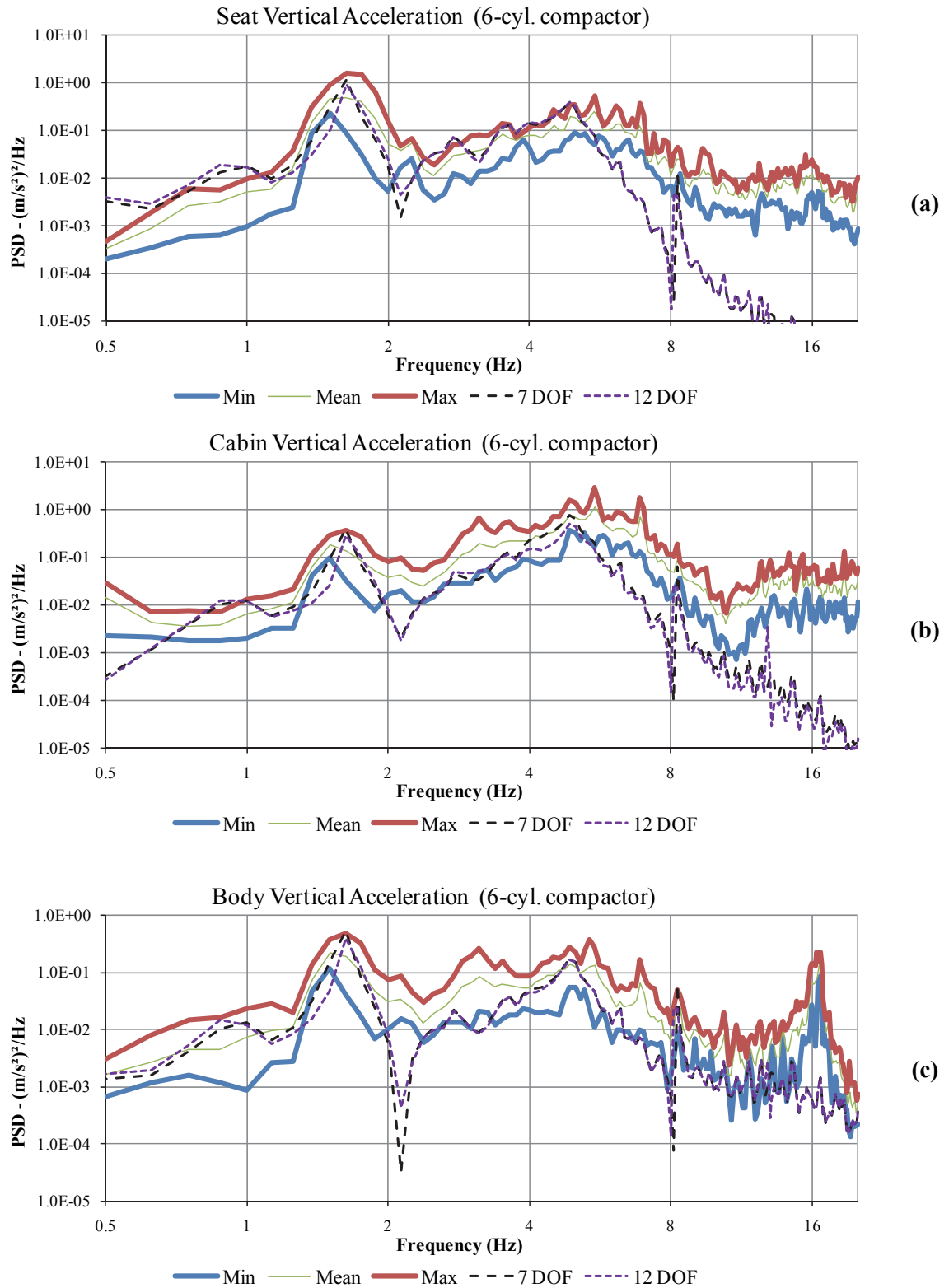
Figure 4-4: Comparison of vertical acceleration PSD responses of the 7- and 12-DOF models with the measured acceleration PSD: (a) seat; (b) operator-station; and (c) vehicle body (6-cylinder compactor in transit mode; speed≈10km/h)

119

Despite these differences, the model responses correlate reasonably well with the ranges of the measured data in the frequency range of primary interest, namely below 6 Hz. This is evident from the comparisons of the vertical acceleration responses of both the vehicles presented in Figure 4-3 and Figure 4-4, and the pitch acceleration responses presented in Figure 4-5 and Figure 4-6. The results also show that both the 7- and 12-DOF ride dynamic models yield quite comparable bounce and pitch mode responses in the frequency ranges considered.

(a)

(b)
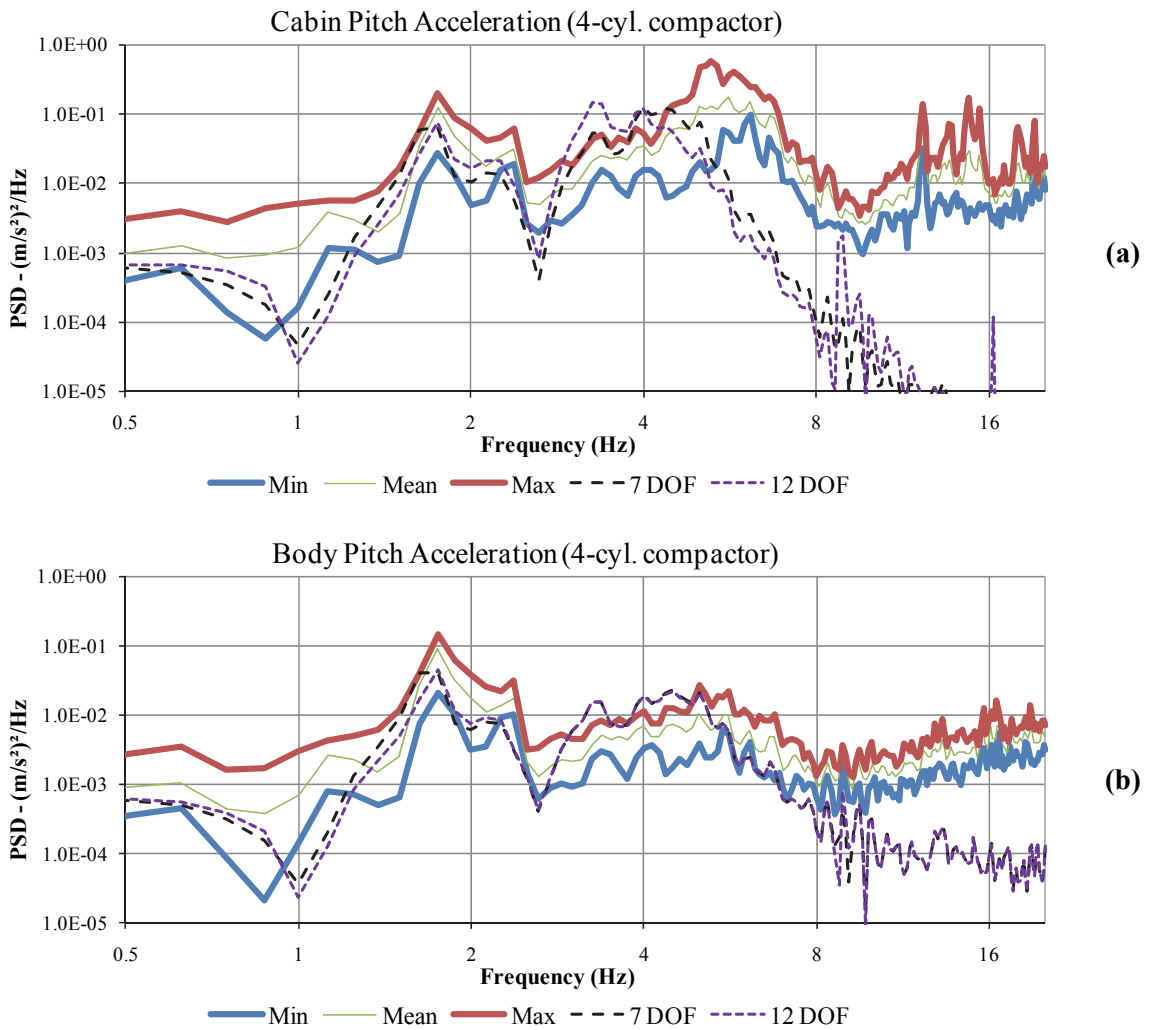
Figure 4-5: Comparison of pitch acceleration PSD responses of the 7- and 12-DOF models with the ranges of the measured acceleration PSD: (a) operator-station; and (b) vehicle body (4-cylinder compactor in transit mode; speed≈10km/h)

Figure 4-7 and Figure 4-8 compare the longitudinal acceleration responses of the two compactors, derived from the 7-DOF and 12-DOF ride dynamic models, with the ranges of the measured data. The figures show the longitudinal acceleration responses at the seat, operator-station floor and the vehicle body. It needs to be emphasized that the drum and tires interactions with the soil in the longitudinal shear mode contribute greatly to the longitudinal ride response. The modeling of the longitudinal mode interactions, however, is quite complex and thus ignored in the ride dynamic models.
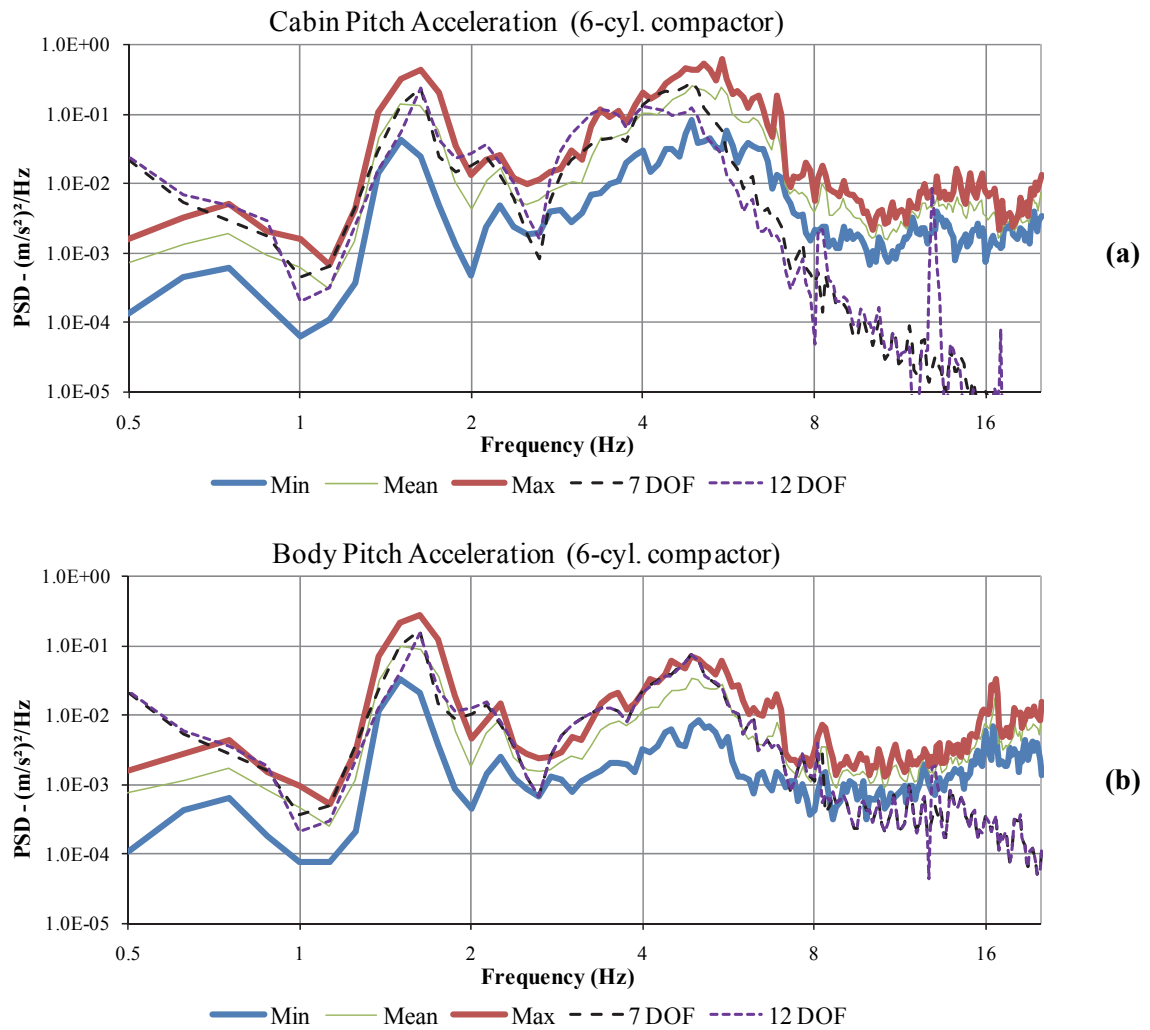
Figure 4-6: Comparison of pitch acceleration PSD responses of the 7- and 12-DOF models with the ranges of the measured acceleration PSD: (a) operator-station; and (b) vehicle body (6-cylinder compactor in transit mode; speed≈10km/h)

121

The proposed ride dynamic models cannot yield accurate prediction of the longitudinal mode ride responses. The results shown in the figures merely reflect the contributions due to the pitch mode of the vehicle body and the operator-station masses. The magnitudes of acceleration of the model responses are thus considerably lower than those of the measured data. An examination of the video records of the test vehicle revealed a stick-slip type longitudinal behaviour of the drum on the hard ground while in transit mode at a higher speed. The model responses, however, exhibit spectral components comparable to those of the measured data. Furthermore, the 12-DOF model yields higher longitudinal acceleration response compared to the 7-DOF model at lower frequencies, which is attributed to consideration of the longitudinal dynamics of the drum and the tires, while both models yield comparable responses at higher frequencies.

Figure 4-9 and Figure 4-10 further illustrate the comparisons of PSDs of vertical acceleration responses of the front frame and the wheel-axle (rigidly bolted to the rear-frame), respectively, derived from the models with the ranges of the measured data. These figures also show good agreements between the model and measured responses, except for the wheelbase filtering effect observed in the wheel-axle response.The wheel-axle response exhibits peak around the first coupled bounce/pitch mode (1.6 – 1.7 Hz) and coupled lateral/yaw mode (2.1 – 2.2 Hz) of the vehicle body, while the front-frame surrounding the rigid roller drum shows dominant ride magnitude near the second coupled bounce/pitch mode (4.8 – 4.9 Hz) of the vehicle body and the operator-station bounce mode (5.5 – 5.6 Hz). The ride responses at the two axles differ most significantly and clearly show the effect of the first suspension stage in the form of soft tires at the rear-axle versus the relatively stiff drum mounts.
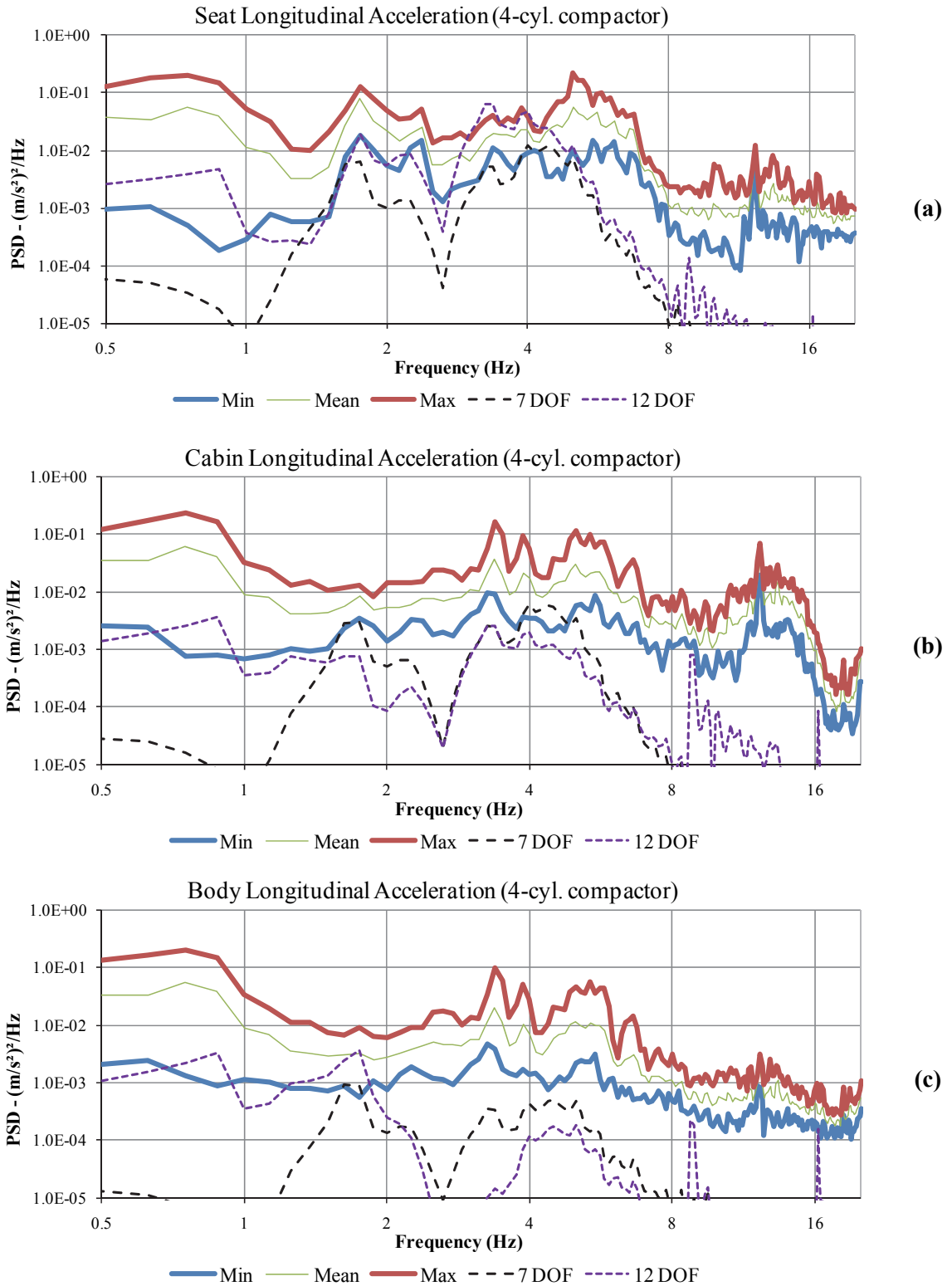
Figure 4-7: Comparison of longitudinal acceleration PSD responses of the 7- and 12-DOF models with the measured acceleration PSD: (a) seat; (b) operator-station; and (c) vehicle body (4-cylinder compactor in transit mode; speed≈10km/h)

123
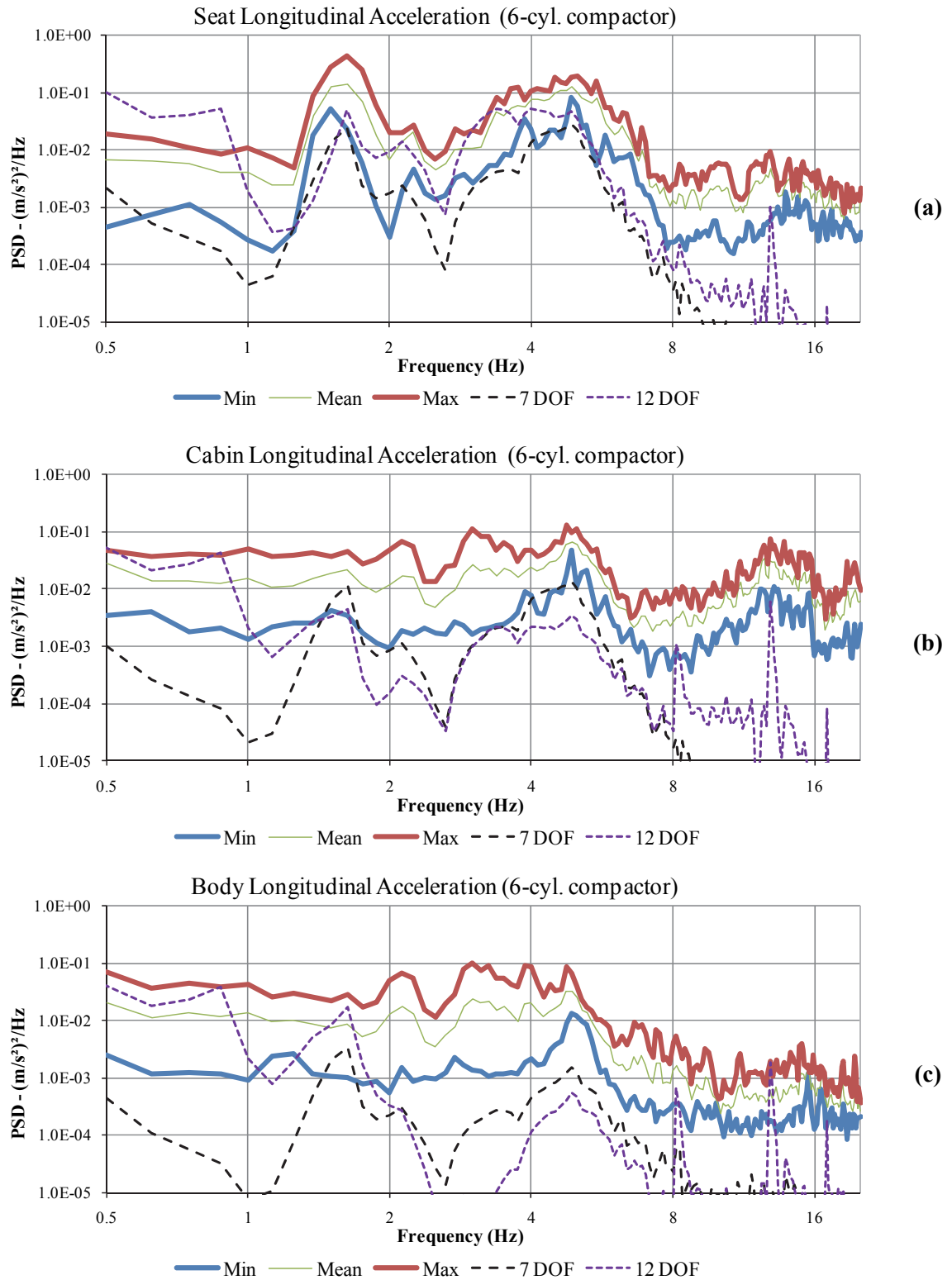
Figure 4-8: Comparison of longitudinal acceleration PSD responses of the 7- and 12-DOF models with the measured acceleration PSD: (a) seat; (b) operator-station; and (c) vehicle body (6-cylinder compactor in transit mode; speed≈10km/h)

124

The ride dynamic responses of the model were further evaluated in terms of overall rms values of the longitudinal, vertical and pitch accelerations. The overall rms values were computed over the 0.5Hz and 20Hz frequency range for the purpose of model validation. The rms values of the acceleration responses of the two models are compared with those derived from the mean measured data in Table 4-4 and Table 4-5 for the 4- and 6-cylinder compactors, respectively.
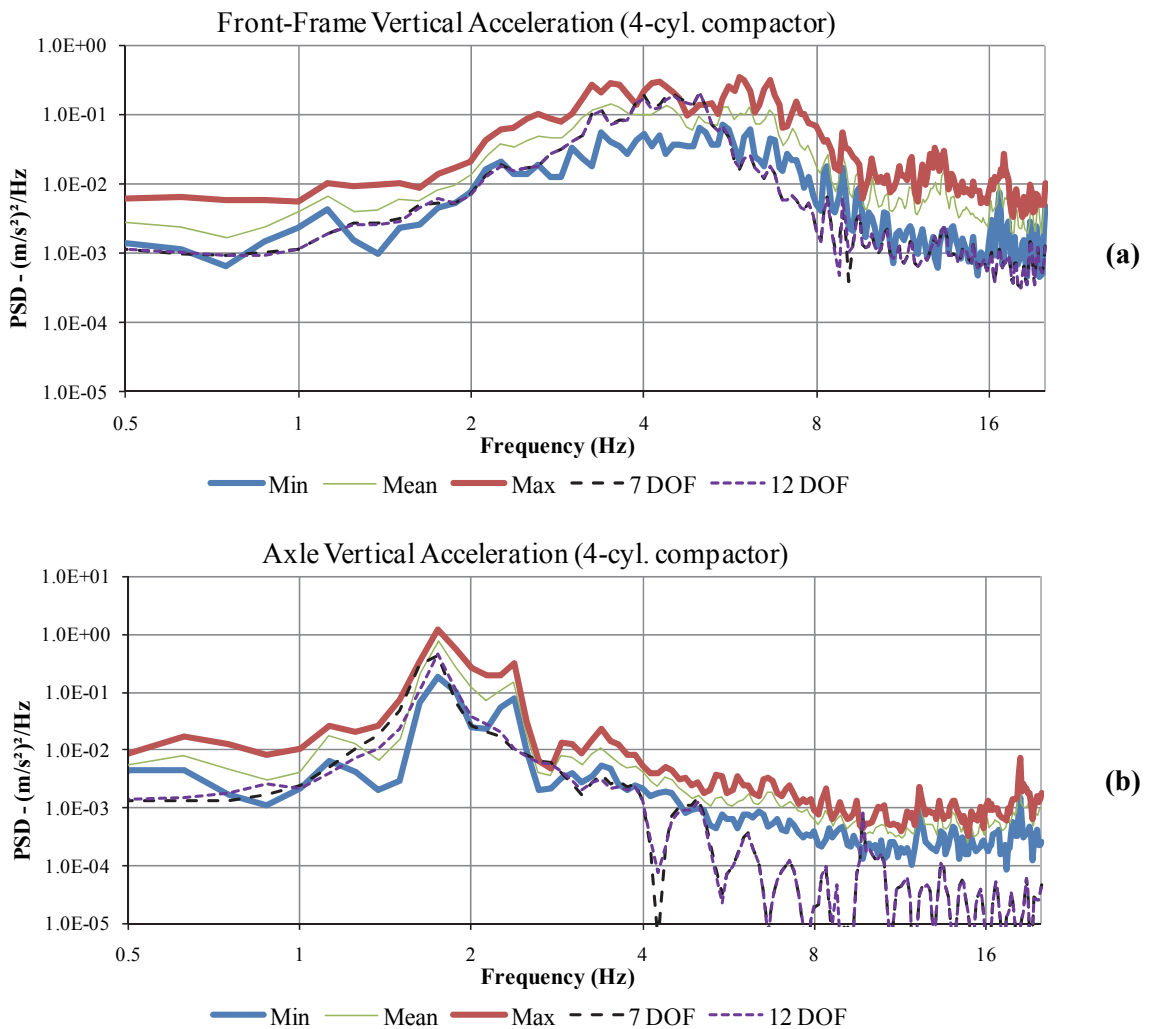
Figure 4-9: Comparison of vertical acceleration PSD responses of the 7- and 12-DOF models with the ranges of the measured acceleration PSD: (a) front frame; and (b) axle (4-cylinder compactor in transit mode; speed≈10km/h)

The rms acceleration values of the measured data were extracted from the data segments where the peak drum acceleration was less than 1g. The values listed in the Table 4-4 and Table 4-5 may thus be lower than the mean values derived from the entire set of segments. The tables also present the percent deviations of the model response with respect to the measured values. The notations x_{ff} and z_{ff} refer to the fore-aft and vertical responses of the front frame (part of the main vehicle body), respectively.
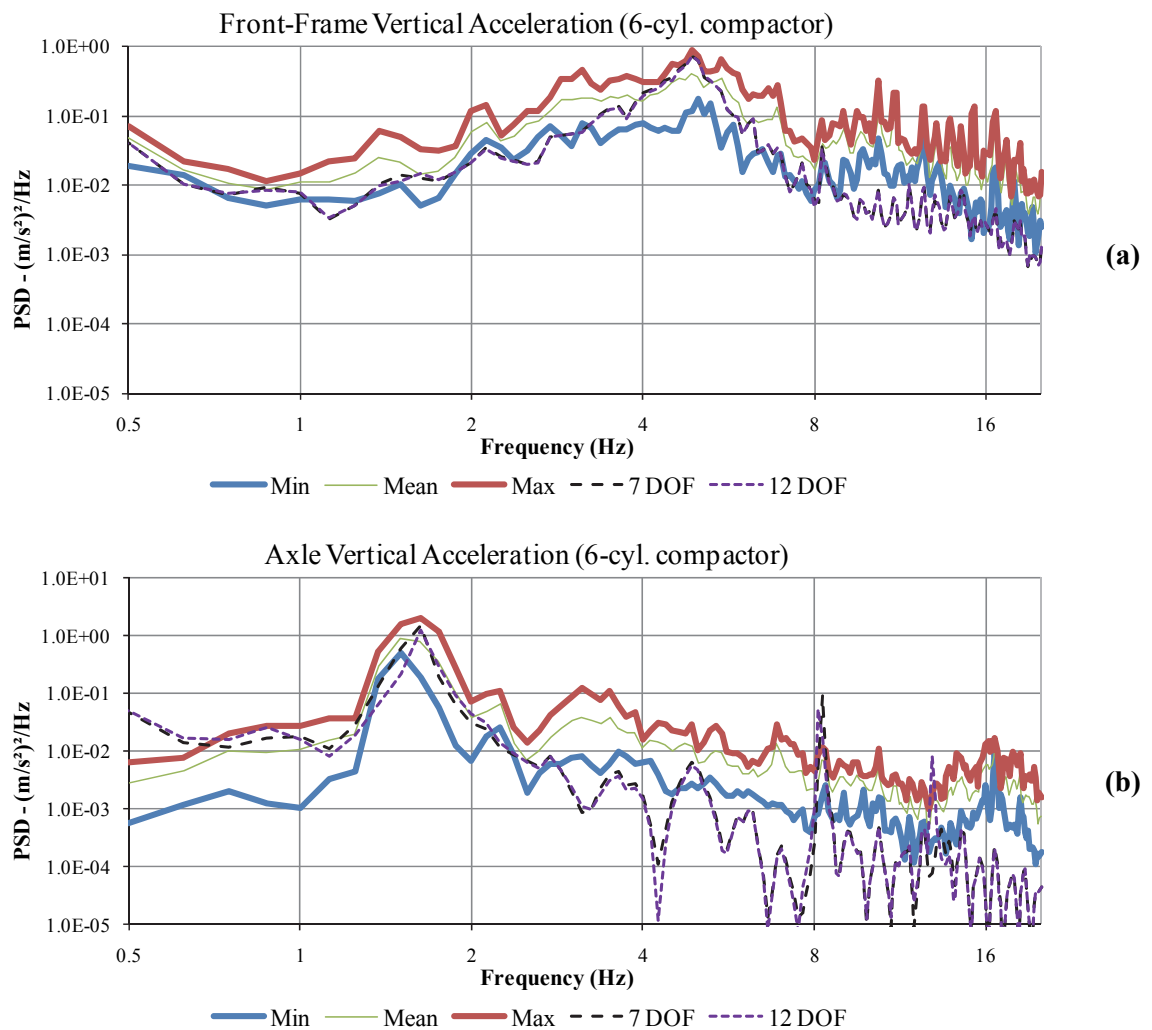
Figure 4-10: Comparison of vertical acceleration PSD responses of the 7- and 12-DOF models with the ranges of the measured acceleration PSD: (a) front frame; and (b) axle (6-cylinder compactor in transit mode; speed≈10km/h)

The results in general suggest good correlations between the rms acceleration responses values of the model and the measured data in the vertical and pitch direction. Considerable discrepancy, however, is observed in the longitudinal acceleration values.

Table 4-4: Measured and simulated overall rms acceleration responses of the 4-cylinder 10-ton soil compactor in transit mode (10km/h) on sample test tracks

Sensor	Measured	7-DOF Model	Δ	12-DOF Model	Δ
z_{ff}	0.74	0.62	17%	0.61	18%
z_a	0.50	0.35	29%	0.33	33%
z_b	0.41	0.35	14%	0.34	17%
z_c	0.78	0.60	23%	0.51	34%
z_h	0.58	0.54	7%	0.53	8%
φ_b	0.30	0.24	20%	0.23	22%
φ_c	0.70	0.44	38%	0.43	39%
x_{ff}	0.44	0.03	93%	0.05	88%
x_b	0.25	0.04	86%	0.05	79%
x_c	0.37	0.10	75%	0.07	80%
x_h	0.42	0.14	67%	0.27	34%

The results also show considerable difference in the rms values of the vertical operator-station acceleration. The measured data resulted in considerably larger values of the operator-station vertical rms acceleration than that predicted by the model. This was believed to be caused by the contribution due to roll, and lateral motions of the operator-station and the vehicle body. The roll acceleration spectra of both the operator-station and the vehicle body reveal significant roll vibration, as seen in Figure 3-24. Although, the longitudinal acceleration responses of both the models are significantly lower than the measured values, the longitudinal acceleration responses at seat is observed to be closer to that of the measured values, particular for the 12-DOF model. This can be attributed to consideration of the longitudinal properties of the operator-station and drum mounts in

the model. Furthermore, this suggests greater contribution of the operator-station pitch to the fore-aft motion at the seat.

Table 4-5: Measured and simulated overall rms acceleration responses of the 6-cylinder 10-ton soil compactor in transit mode (10km/h) on sample test tracks

Sensor	Measured	7-DOF Model	Δ	12-DOF Model	Δ
z_{ff}	1.13	0.96	15%	0.95	17%
z_a	0.66	0.61	8%	0.54	18%
z_b	0.76	0.57	25%	0.54	29%
z_c	1.49	0.94	37%	0.80	47%
z_h	0.88	0.82	7%	0.80	10%
φ_b	0.36	0.37	-3%	0.36	1%
φ_c	0.74	0.64	13%	0.56	25%
x_{ff}	0.63	0.05	93%	0.14	77%
x_b	0.29	0.05	81%	0.15	50%
x_c	0.49	0.14	72%	0.17	66%
x_h	0.54	0.20	63%	0.38	30%

The comparison between the overall rms acceleration responses of the 7-DOF and the 12-DOF yields to several conclusions: Although the additional sophistication of the 12-DOF, attempting to model the longitudinal behaviour of the vehicle does bring an insight into the longitudinal responses, the approximation in this aggregating modeling effort results in a general underestimating of these very same longitudinal responses magnitudes and furthermore, even contributes to some slight deterioration of the vertical and pitch responses. The 12-DOF modeling approach would be a good tool for identifying the resonance frequencies of the vehicle in the vertical plane but the simpler 7-DOF actually gives more accurate result when it comes to vertical and pitch responses magnitudes.

4.5. Response Characteristics during Compaction

The validity of the proposed models in the compaction mode could be evaluated both in terms of drum-soil interaction in time domain and in terms of bounce and pitch responses of the main body or the operator-station (cabin) in the frequency domain. Since the excitation frequency due to vibratory compactor is significantly higher than the resonance frequencies of the vehicle model, the whole-body vibration due to rotating inertia would be expected to be in the negligible order. The attenuation of the compaction vibration exposure of the operator may thus be of minimal concern. The primary interest in developing a compaction model of the equipment thus lies in enhancing the fundamental knowledge on the drum interactions with the soil and for building a tool to identify desirable design and operating factors that may help achieve improved work (compaction) performance of the equipment.

A review of the published studies revealed wide variations in the soil parameters (Krober, Floss, & Wallrath, 2001; Popa & Nicoara, 2002; Anderegg & Kaufmann, 2004; Mooney & Rinehart, 2007). The observed diversity in the soil model parameters was mostly attributed to the desired application and geographical location of a jobsite. The soil model parameters are known to vary considerably with the local soil properties such as density and cone index and the moisture content. Furthermore, the properties of deformable soil tend to change during the compaction tasks, particularly under repeated passes of the vehicle. Despite such variations and the wide ranges of the reported model parameters, the reported values are considered to serve as a reasonably good benchmark for the average soil conditions. Soil model parameters have been proposed on the basis of

measurements and simulation results (Adam & Kopf, 2000; Anderegg & Kaufmann, 2004; Mooney, Gorman, & Gonzalez, 2005). These parameters are taken as the baseline simulation parameters in this study and summarized, alongside the parameters of the compactor vibrator considered, in Table 4-6.

Table 4-6: Compaction Model Parameters

Parameter	Symbol	Value		
Drum static load	m_1	6100 kg		
Vibrator rotating mass	m_v	28.5 kg		
Vibrator mass eccentricity	e	0.20 m		
Vibrator frequency	f_v	33 Hz		
Vibrator centrifugal force	F_{cent}	245 kN		
Static deflection of the soil	δ_s^{stat}	14.4 mm	2.7 mm	1.7 mm
Soil plasticity parameter	ε	0.34	0.72	0.87
Soil plastic stiffness	k_{sp}	6.44 MN/m	82.1 MN/m	283 MN/m
Soil elastic stiffness	k_{se}	12.5 MN/m	31.9 MN/m	42.3 MN/m
Soil damping	c_{se}	70 kNs/m		
Vehicle parameters		6-cylinder compactor (see Table 4-1)		

4.6. Methods of Analysis (Compaction Response)

The equations of motion of the compaction model, described in section 2.3.2, are solved to determine the soil deformation responses. The simulations are performed only for the most common 6-cylinder machine (parameters indicated in Table 4-1), since both the machines were equipped with identical drum, front frame and vibrators. A constant magnitude of unbalance excitation (5.7 kg.m) at 33 Hz (2000 rpm) was also considered for the simulation that was computed from the design data of the compactors.

It needs to be emphasized that the studies reporting the soil compaction by a rolling vibratory drum, have considered widely varying soil properties, to derive the soil compaction under repeated passes of the roller (Yoo & Selig, 1979; Pietzsch & Poppy, 1992; Andereg, 2000; Tateyama, Ashida, Fukagawa, & Takahashi, 2006). These studies do not consider the dynamics of the vehicle, while the compaction is caused by an idealised axle load coupled with the unbalance excitation. The validity of the proposed compactor model for the compaction task could thus be examined only in the qualitative sense. The model simulations are performed for different soil properties, particularly the plasticity parameter (ε), which are considered to simulate the variations in soil properties over repeated passes or the density of different soils. It has been reported that ε varies with repeated passes on a soil segment (Adam & Kopf, 2000). It is shown that plasticity of soil increases with number in passes and tends to saturate after certain number of passes, as shown in Figure 4-11. The reported variations in ε are considered to study the compaction response over repeated roller passes, although it is recognised that different soils and different compaction equipments would yield different patterns in variations in ε. Furthermore, the soil density is related to the number of passes performed (Quibel & Corte, 1994; Floss & Kloubert, 2000; Krober, Floss, & Wallrath, 2001).

In this study, the simulations are performed to determine the force-deflection response of the soil by considering three different values of the plasticity parameter. These include: (i) $\varepsilon = 0.34$, representing a soft soil or the soil properties during the initial passes; (ii) $\varepsilon = 0.72$, represents a medium-dense soil or the properties during intermediate passes; and (iii) $\varepsilon = 0.87$, represents a dense soil or the soil properties during the final passes.
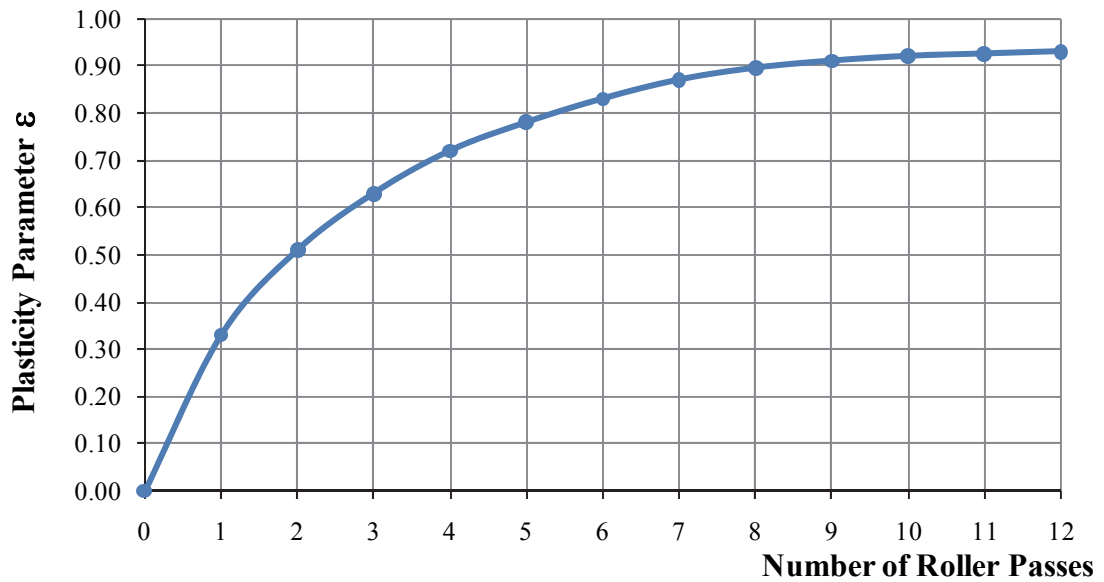
Figure 4-11: Measured plasticity parameter as function of compaction passes (Adam & Kopf, 2000)

The vertical dynamics of the drum is expected to be strongly influenced by the soil properties. A continuous contact between the drum and the soil would be expected during initial passes, when the soil is relatively soft. The "partial up-lift" or hopping motion of the drum could be observed during intermediate and final passes due to the drum interaction with the dense soil. This phenomenon has been reported in a few studies (Pietzsch & Poppy, 1992; Adam & Kopf, 2000; Andereg, 2000).

4.7. Compaction Simulation Results and Model Validation

The simulations are performed to determine the soil deformation and the total compaction force imparted by the drum on the soil for the selected soil density or the chosen pass.

The soil deformation is determined from the relative displacement of the drum with respect to the vertical coordinate of the soil surface prior to compaction. The total compaction force is derived from the static roller weight and the force developed by the elasto-plastic soil model, as described in Eq. (2.26). Figure 4-12 to Figure 4-14 illustrate the time-histories of the steady-state soil deflection and compaction force for the three plasticity parameters (levels of compaction) considered in the study. The results exhibit most significant effects of the plasticity parameter and thereby the compaction response with increasing number of passes. The results also show elastic as well as plastic deformations of the soil, irrespective of the ε value. The drum interactions with the soft soil ($\varepsilon = 0.34$) yield continuous contact with the ground, and result in the most significant soil deflection observed. This is representative of the soil deformation during the initial passes, where the magnitude of the compaction force is relatively small as seen in Figure 4-12 (b) and Figure 4-12 (c). The soil behaviour exhibits hysteretic properties, as seen from the force-deflection response shown in Figure 4-12 (c). The results further show oscillations in the deflection and the force responses at 33 Hz, the speed of the eccentric vibrator. The results suggest max soil deflection in the order of 18 mm, while the peak compaction force approaches 80 kN, which is approximately 30% of the centrifugal force due to the eccentric vibrator.

The magnitude of the compaction force increases significantly in the subsequent passes, which is mostly attributed to increase in the soil density and stiffness property, as seen in Figure 4-13(b) for the medium-dense soil ($\varepsilon = 0.72$). The max deflection of the soil and its plastic deformation, however, decrease due to higher soil density, as seen in Figure 4-13(a) and Figure 4-13(c). The peak compaction force approaches approximately 50%

of the centrifugal force. The greater force imparted on the denser soil surface causes intermittent hopping motion of the drum, as seen in the compaction force response and hysteresis loop of the soil response in Figure 4-13(b) and Figure 4-13(c). This permits certain relaxation of the soil during the unloading cycle as the compaction force diminishes. The results suggest max soil deflection in the order of 5 mm and plastic deformation in the order of 2.3 mm. For deformable soils this operating condition is considered as most efficient compaction (Andereg, 2000; Briaud & Seo, 2003), which may be attributed to impact caused by the roller as it regains the contact.

A further increase in the soil density in the subsequent passes ($\varepsilon = 0.87$) causes most significant increase in the compaction force. The peak compaction force approaches the centrifugal force, which tends to cause more significant hopping motion and loss of drum-soil contact, as seen in Figure 4-14(a) and Figure 4-14(b). The greater soil stiffness tends to transfer portion of the compaction energy to the drum leading to "double-jump" or "rocking" motion of the drum, as seen in Figure 4-14(a). This phenomenon of "double-jump" has been reported in a number of studies (Adam & Kopf, 2000; Anderegg & Kaufmann, 2004) as illustrated by Figure 4-15 depicting a case where the phenomenon is not much accentuated. The soil deflection and the compaction force responses thus exhibit an additional frequency component at 16.5 Hz. This is the sub-harmonic of the frequency associated with the eccentric vibrator, namely 33 Hz, and is due to "double-jump" of the drum. The lower frequency response can be attributed to two different impacts during a cycle: a deep impact followed by a low magnitude impact, unlike a single impact observed for medium-dense soil. This results in a major and a minor hysteresis loop as seen in Figure 4-14(c).
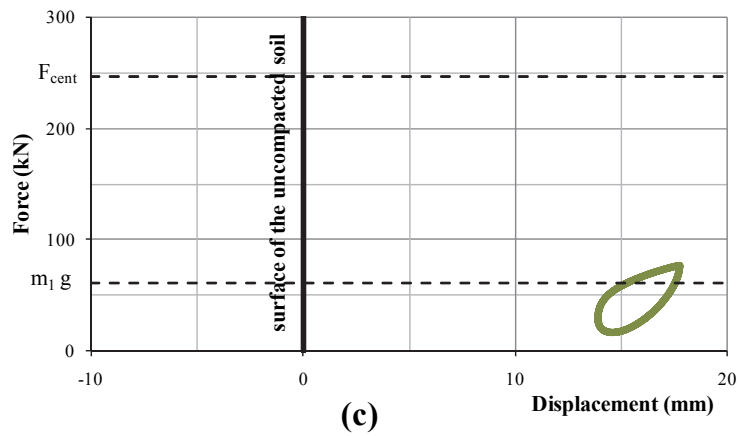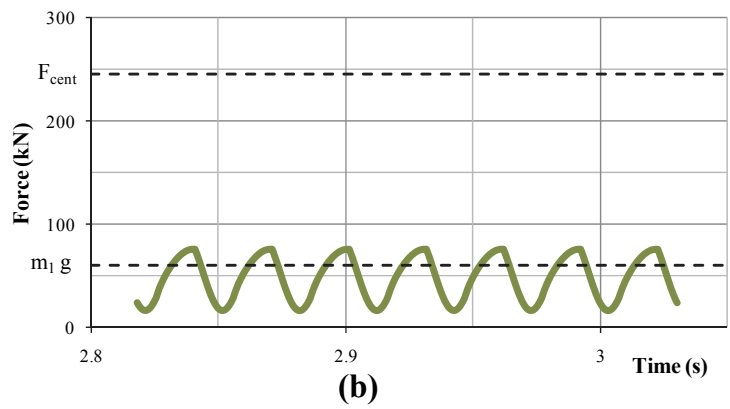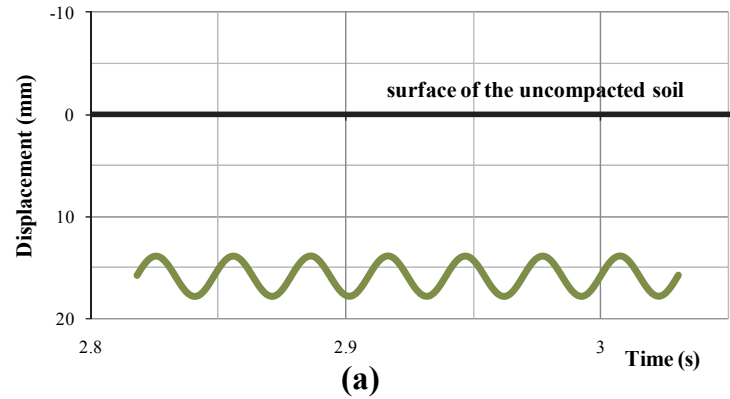
Figure 4-12: Time-histories of drum displacement (a) and the total compaction force (b), and force-deflection properties of the soil (c). ($\varepsilon = 0.34$)

135
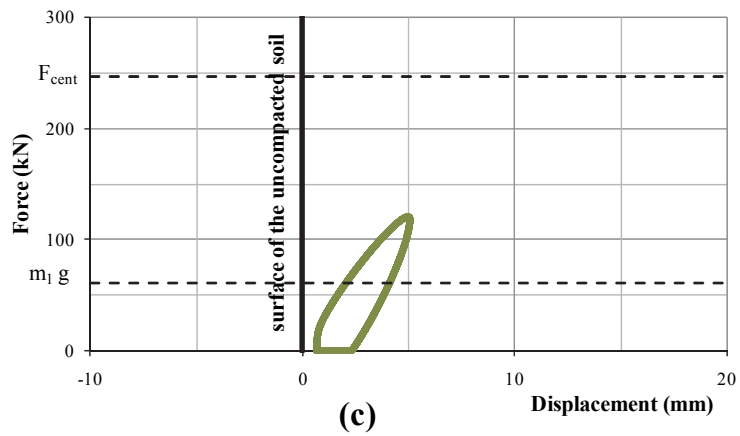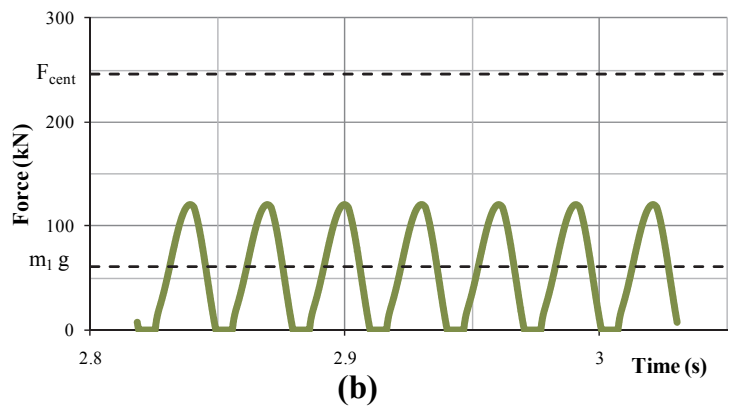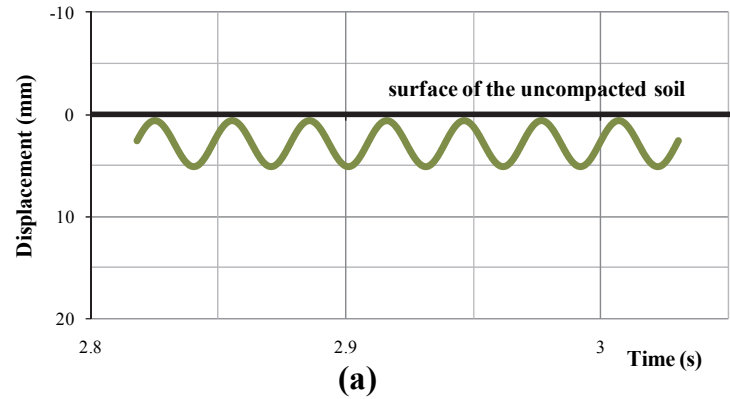
Figure 4-13: Time-histories of drum displacement (a) and the total compaction force (b), and force-deflection properties of the soil (c). ($\varepsilon = 0.72$)
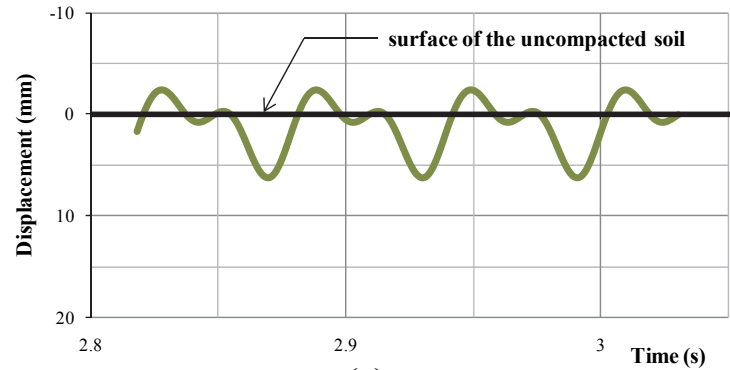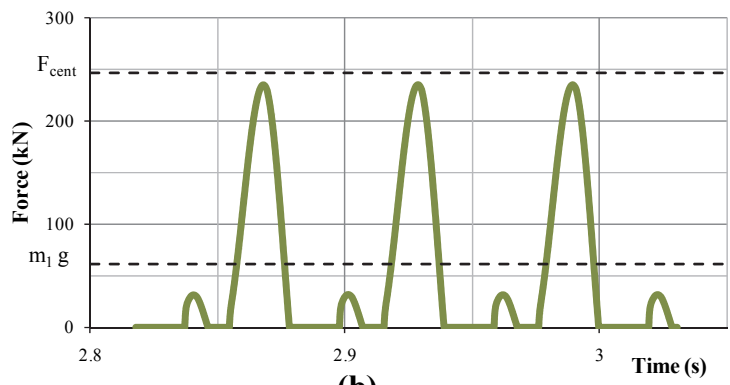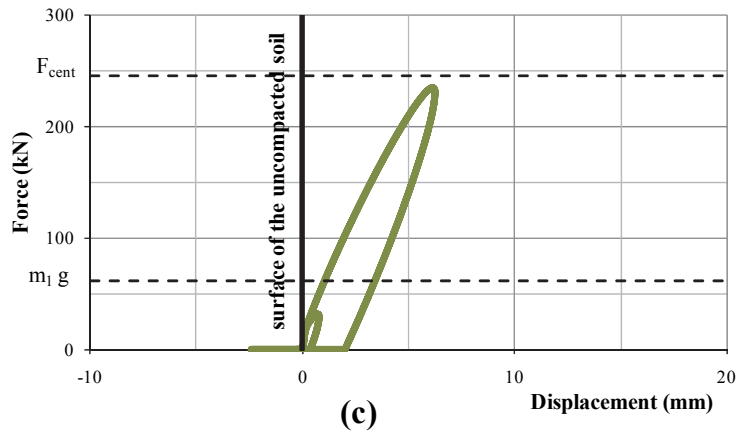
Figure 4-14: Time-histories of drum displacement (a) and the total compaction force (b), and force-deflection properties of the soil (c). ($\varepsilon = 0.87$)

137

Owing to the considerably higher frequencies of drum displacement and the compaction forces, the magnitudes of resulting ride accelerations of the vehicle bodies are significantly small in the lower frequency range. Figure 4-16, as an example, illustrates the PSD of vertical acceleration responses of the operator-station, main vehicle body, and the drum. The results are presented for the adverse case of final vibratory passes on a high density soil ($\varepsilon = 0.87$), which clearly show the sub-harmonic spectral component of vibration attributed to the "double-jump" of the drum. The hopping motion of the drum together with the eccentric excitation cause very high acceleration of the drum, as seen in Figure 4-16(c). The acceleration response invariably shows dominant response near 16.5 and 33 Hz, which is effectively attenuated by the drum and cab mounts as seen in Figure 4-16(b) and Figure 4-16(a).
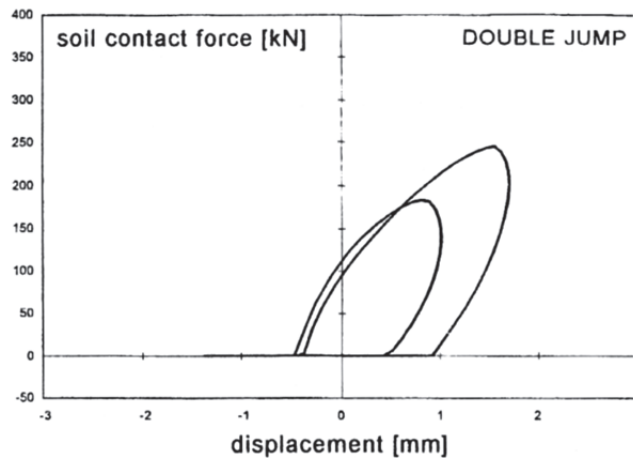
Figure 4-15: Reported energy cycle illustrating the "double-jump" phenomenon (Adam & Kopf, 2000)

The simulated force-deflection response of the soil and the drum displacement responses as depicted in Figure 4-12 to Figure 4-14 are qualitatively in good agreements with the reported trends (Adam & Kopf, 2000; Floss & Kloubert, 2000; Krober, Floss, & Wallrath, 2001; Kloubert, 2004) as illustrated in Figure 1-6 and in Table 1-1 as well as in

Figure 1-5 depicting the expected energy cycles. It may be noticed that reported energy cycles take the static drum/soil equilibrium position as the reference point for the drum displacement whereas in the present study the vertical coordinate of the soil surface prior to compaction constitutes the reference. The differences of shape that could be observed, in the transition zones between the different phases of the energy cycle, in the different works presented are due to the considered geometry of the drum/soil contact. In this study a point contact has been considered whereas a more precise cylindrical contact would result in a nonlinear elastic stiffness of the soil (Adam & Kopf, 2000).

The simulated vibration response spectra of the operator-station, the vehicle body and the drum indicate good agreements with the mean of the related field-measured responses, for example for a high density soil as illustrated in Figure 4-16. They also agree with the reported trends depicting the forcing frequency harmonics and first sub-harmonic as seen in section 1.2.2 and illustrated in Figure 1-6. The forcing frequency harmonics in the measured response are lower compared to those of the simulations. This is due to the increase in the soil stiffness causing higher loading/resistance for the vibrator from the ground that would require higher engine power. The engine rpm drops below the nominal setting to supply higher torque and resulting power which results in a reduction in hydraulic oil flow and subsequently in vibrator motor rpm. In the illustrated example (Figure 4-16) the vibrator frequency has dropped from a nominal 33 Hz to 28.5 Hz. The presence of the sub-harmonics is justified by the "double-jump" occurring at high soil densities. It is to be noticed that both the simulation and the measured responses are based on usage of the highest available eccentric moment of the vibrator (the so called "high amplitude"). Furthermore, the simulation results do not feature the lower frequency

response spectra visible in the measured data as the compaction model did not include terrain profile input as in the ride models, the surface being graded prior to compaction. Yet, the measurement results tend to highlight lower frequency ride components that seem to arise from terrain deformation in process of compaction.
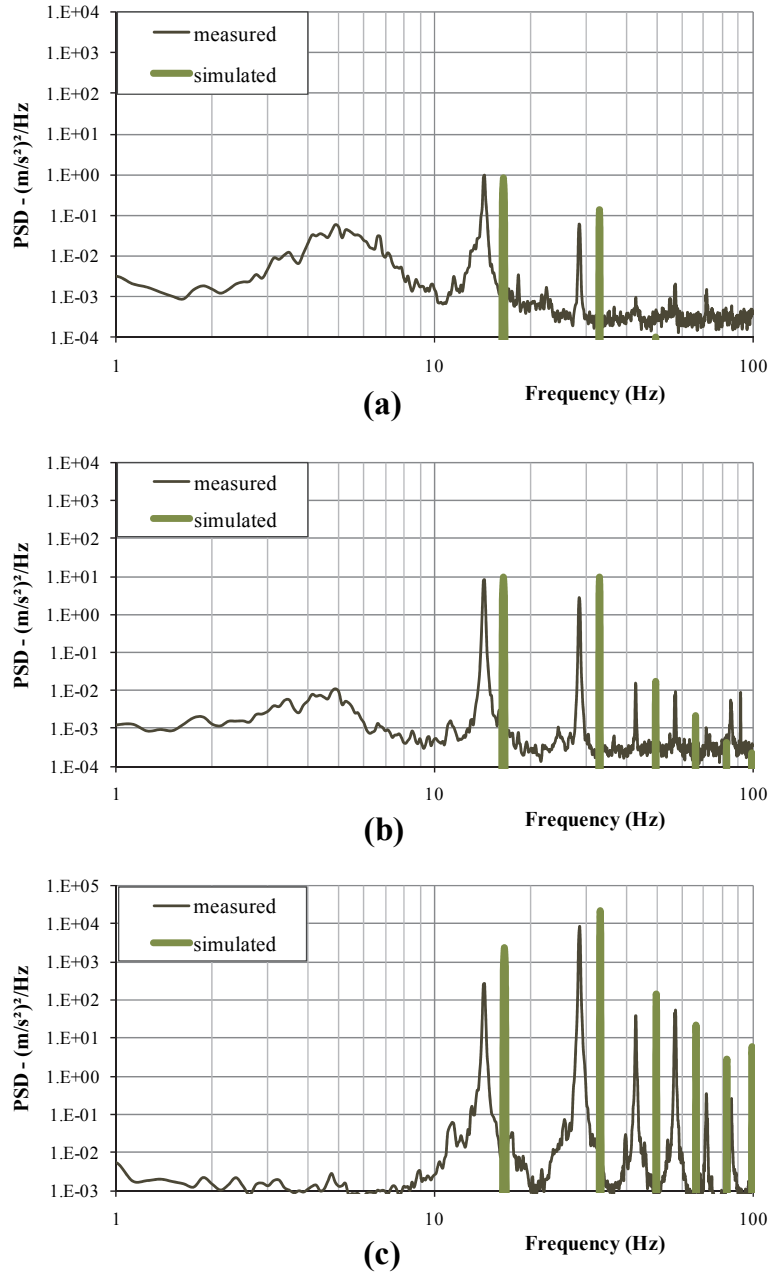
Figure 4-16: measured and simulated PSD of the (a) operator-station; (b) the vehicle body; and (c) the drum during a vibratory pass on a high density soil ($\varepsilon = 0.87$)

140

4.8. Summary

The simulation results present evident similarities with measured data although considerable deviations exist when it comes to longitudinal responses. These deviations could be attributed to various modeling simplification that in particular do not include any stick-slip phenomena at the contact between the drum and the hard ground when it comes to the vehicle operating in transit mode. Despite the observed deviations in longitudinal direction, the results in general suggest reasonably good validity of the model for predicting vertical and pitch ride responses of the vehicle. The model may thus be considered applicable for identifying desirable suspension design parameters for enhanced attenuation of the terrain-induced whole-body vibration. The non-linear time-domain compaction model leads to results that are in compliance with the roller – soil behaviour published in the soil mechanics literature. The present work brings the novelty of a complete bounce-pitch model integrating the mobile equipment dynamics, as a multi-body system, into the compaction model.

CHAPTER 5 – SENSITIVITY ANALYSIS

5.1. Introduction

The dynamic responses of a soil compactor are related to many design factors and operating conditions, irrespective of the mode of operation. In the transit mode, the ride quality of the vehicle is of primary concern; while in the compaction mode, equipment's compaction effectiveness is of interest. Both the ride quality and the compaction capability could be related to better choice of design factors and operating conditions. In This chapter, the validated models of the compactor are analysed to study the sensitivity of the ride responses and compaction properties to variations in different design and operating factors. The results are interpreted to explore different design concepts for enhancement of the vehicle performance. For the transit mode, the 12-DOF ride dynamic model of the 6-cylinder machine is employed for the sensitivity analysis. The compaction properties of the vehicle are evaluated using the 7-DOF vehicle dynamic model together with the third-order formulation of the drum-soil interaction, as described in section 2.3.1. For the ride quality analysis, the stiffness properties of the axle and seat suspensions are considered to be very high in order to simulate the existing compactors that encompass un-suspended rear axle and often un-suspended operator seat. The effect of vehicle weight and its distribution however, is investigated by also considering the inertial properties of the 4-cylinder machine which exhibits lower weight and shorter rear frame. The results of the study are discussed in view of two distinct goals: (i) improving the vehicle ride quality (transit mode), and (ii) increasing the tool capability (compaction mode).

5.2. Analysis of Ride Quality in the Transit Mode

The ride quality of the vehicle is expected to be influenced by a number of design parameters. Among these, the properties of drum and cab suspensions, vehicle weights and dimensions, suspension seat and additional primary suspension are considered to be of primary interests. In addition to these, the variations in operating conditions, such as vehicle speed and ground roughness, are also considered for the sensitivity analyses. The sensitivity of the ride quality to variations in selected design and operating parameters are evaluated using a set of performance measures, which are described below.

5.2.1. Performance measures

The ride quality of a vehicle has been directly related to acceleration due to vibration at the driver-seat interface. The vast majority of the small to medium size soil compactors used in North America are equipped with un-suspended operator seats and relatively stiff cab mounts. The vibration responses of the cab near the operator seat may thus be used to assess the vehicle ride performance. Furthermore, such levels could serve as the basis for tuning / design of an adequate suspension seat, particularly the vertical vibration levels.

The International Standard (ISO 2631-1, 1997) recommends the use of frequency-weighted rms accelerations at the operator's station for assessing the human vibration perception and potential health risks. Consequently, the sensitivity analyses are initially performed on the basis of overall rms accelerations, which are computed over the 0.5Hz to 80Hz range:

$$\{a\} = \sqrt{\int_{0.5}^{80} \{S^{acc}(f)\} \, df}$$

(5.1)

Where $\{a\}$ is overall rms acceleration vector and $\{S^{acc}(f)\}$ is the vector containing PSD of the response accelerations of the ride dynamic model.

The frequency weighted overall rms accelerations are computed by applying the weighting filters recommended by the international standard (ISO 2631-1, 1997). For this purpose, the response acceleration PSD vector is expressed by the third-octave rms acceleration spectra (IEC 61260, 1995):

$$\{\bar{a}(f_i)\} = \sqrt{\int_{fl}^{fu} \{S^{acc}(f)\} \, df}$$

(5.2)

Where $\{\bar{a}(f_i)\}$ is the rms acceleration magnitude corresponding to the center frequency f_i of the third-octave band, and f_l and f_u define the lower and upper limits of the frequency band f_i .

The frequency-weighted spectra of rms accelerations $\{\bar{a}_w(f_i)\}$ are determined by applying the frequency weightings which include W_k for the vertical axis, W_d for the horizontal (x and y) axis, and W_e for the pitch axis (ISO 2631-1, 1997), such that:

$$\{\bar{a}_w(f_i)\} = \{W_j(f_i)\}\{\bar{a}(f_i)\}$$

(5.3)

Where $\{\bar{a}_w(f_i)\}$ is the vector of frequency-weighted rms accelerations, $W_j(f_i)$, defines the weighting factor corresponding to the one-third octave band center frequency f_i , with $j = k, d, e$ referring to the appropriate weighting function. The overall frequency-

weighted rms acceleration over the 0.5 Hz and 80 Hz range is then computed from the following summation:

$$\{a_w\} = \sqrt{\sum_{i=1}^{N} \{\bar{a}_w(f_i)\}^2}$$

(5.4)

Where N defines the number of third-octave frequency bands considered.

5.2.2. Influence of variations in operating conditions

The sensitivity of the ride quality measures to variations in operating conditions is analysed by considering the variations in forward speed and the road roughness. While in transit the compactor is usually driven at relatively higher speeds. The maximum speed of most of the currently used compactors ranges from 9 to 12 km/h. A forward speed of 10 km/h is thus chosen as the nominal speed during the transit operation. Considering the drive towards higher speeds, the analyses are performed considering a higher speed of 15km/h, in addition to a lower speed of 5 km/h. The analyses are also performed by considering three different road roughness to study the influence of road excitations on the ride quality. The road roughness properties and model defined in the international standard (ISO 8608, 1995), presented in Figure 1-11, were considered for the analysis. These included the class B, C and D roads denoted as "good", "average" and "poor", respectively.

The 12-DOF ride dynamic model of the 6-cylinder compactor was analysed under different combinations of the three roads excitations and three different forward speeds (5, 10 and 15 km/h). The response acceleration spectra were subsequently expressed by

145

the overall rms and the frequency-weighted rms accelerations to assess the effects of variations in operating parameters. Table 5-1 summarises the influence of speed and the road roughness on both of the ride quality measures, in terms of cabin fore-aft, vertical and pitch accelerations. As expected, the magnitudes of weighted as well as un-weighted vibration along all the axes increase with speed and a deterioration of the road surface quality. The results also show that both the un-weighted and weighted vibration magnitudes along all the three axes increase substantially as the road roughness increases: The magnitudes of cabin vibration on the class C road are nearby twice those attained for the good quality road (class B). The magnitudes over the poor road (class D) tend to be nearly twice those obtained for the average road, irrespective of the vehicle speed. From the results, it may be concluded that the forward speeds of the vehicle traversing a rough road must be limited to limit the WBV exposure of the operator (and is often so by the operator her/himself).

Table 5-1: Influence of variation in the operating conditions (road roughness and forward speed) on the acceleration responses of the operator- station

Speed (km/h)	Road surface	Class B		Class C		Class D	
	Axis	a	a_w	a	a_w	a	a_w
5	Fore-aft	0.20	0.08	0.39	0.17	0.79	0.34
	Vertical	1.35	1.36	2.70	2.73	5.41	5.46
	Pitch	0.81	0.22	1.62	0.43	3.24	0.87
10	Fore-aft	0.23	0.09	0.44	0.18	0.90	0.36
	Vertical	1.59	1.61	3.21	3.24	6.38	6.44
	Pitch	0.96	0.26	1.93	0.51	3.84	1.02
15	Fore-aft	0.23	0.13	0.46	0.25	0.93	0.50
	Vertical	1.76	1.77	3.51	3.54	7.02	7.09
	Pitch	1.05	0.28	2.10	0.57	4.21	1.13

The results further show that frequency-weighted rms acceleration magnitudes along the fore-aft and pitch axes are substantially smaller than the respective un-weighted values. The W_k-weighted vertical acceleration magnitudes, however, tend to be slightly larger than the un-weighted values for the ranges of speed and road roughness conditions considered. This is attributed to the frequency characteristics of the W_k-, W_d- and W_e-weighting filters. The W_k-weighting emphases the human perception of vibration in the vicinity of the vertical mode resonance of the seated body (around 5 Hz) and thus yields slight amplification of vibration around 5 Hz. Considering the vertical mode resonance of the cab near 5.5 Hz, the W_k-weighted rms acceleration magnitude tends to be higher. The W_d- and W_e-weightings, on the other hand, tend to attenuate the vibration at frequencies above 2 Hz and thereby yield relatively lower values of the frequency weighted fore-aft and pitch accelerations.

5.2.3. Influences of variations in design factors

A systematic sensitivity analysis to variations in the design parameters could offer attractive design modification alternatives to enhance the ride performance of the compactor during the transit mode. In particular, different stages of vibration isolation in the vehicle could be subject to design modifications such as the suspension at the seat, cabin, and drum, and potentially at the rear axle. Such design modifications, however need to be further scrutinised in view of the performance measures related to the compaction, their feasibility and the design constraints. This is particularly true in the case of the compactor tires, which must be selected in consideration of various other design constraints such as traction, tire wear and ground pressure.

In this section, the sensitivity of the ride quality measures is investigated for the 10t-class 6-cylinder machine operating at a speed of 10 km/h over a class C ("average") road surface. The design parameters include the drum suspension, seat and cab suspensions, axle suspension and mass distribution (in which case the possibilities of a lighter 4-cylinder rear unit and a heavier front unit are considered).

Drum suspension

As indicated in the previous chapters, the drum rubber mounts are the primary suspension of the compactor and contribute greatly to the dynamic response of the vehicle. Owing to symmetric properties of the drum mounts, the fore-aft and vertical stiffness of the mounts are varied identically. The analyses are performed by considering $\pm$ 25% variations in the mounts stiffness (k_d^x and k_d^z) about the nominal values (Table 5-2). Furthermore, an analysis is performed by considering the drum stiffness equal to the rear axle tires stiffness. The concept of such a drum suspension is discussed, while the equivalent stiffness is taken as 16% of the nominal drum suspension stiffness. The effects of variation in the damping properties of the mounts are also explored, although such modifications in the mounts require considerations of additional design constraints: The isolation mounts employed in the drum suspension are known to be of natural rubber, which offer low damping; The use of material with relatively high damping may lead to greater heat generation and subsequently rapid failure. In this section, the damping coefficients due to the drum mounts (c_d^x and c_d^z) are varied in proportion to the mounts stiffness.
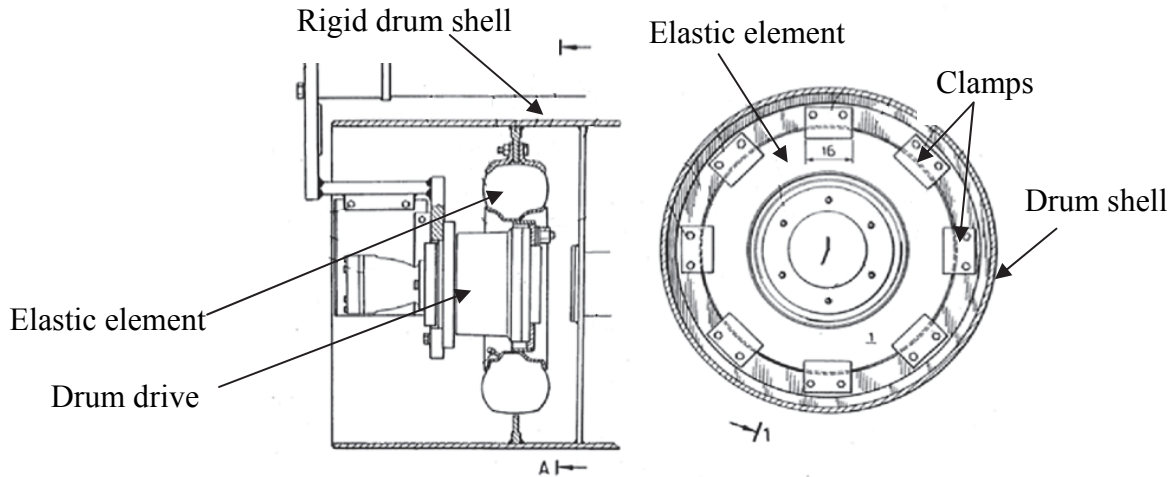
Figure 5-1: A schematic of the drum pneumatic suspension (Domenighetti, 1985)

Table 5-2 summarises the effects of variations in stiffness and damping coefficients of the drum suspension on the un-weighted and frequency weighted rms acceleration responses of the operator-station (cabin). The variation, 0.16 k_d^z / c_d^z, would be considered to be too soft when applied to the rubber mounts, and would yield excessive deflection between the drum and the front-frame and thus rapid failure. Such a variation, however, could be realised by introducing a pneumatic element, such as tires, supporting the rigid drum shell on the outer periphery. This concept of a pneumatic-tire drum suspension was proposed by (Domenighetti, 1985) and is illustrated in Figure 5-1. The proposed concept was also implemented in a number of machines in the 80s in Europe by SIMESA and Hamm. The proposed design integrates automotive tires within the drum. The tires are clamped to the drum ribs at their periphery (unsprung side) while the wheel rim is coupled to the sprung frame. The chosen stiffness value of the suspension is comparable to that of the rear axle tires, while the damping coefficient in this case was also taken as that of the rear axle tires.

149

Table 5-2: Influence of variations in the drum suspension stiffness and damping on the rms acceleration responses of the model at the operator-station floor

Drum mounts	$0.16\ k_d^z\ (= k_t^z;\ c_t^z)$		$0.75\ k_d^z / c_d^z$		$1.00\ k_d^z / c_d^z$		$1.25\ k_d^z / c_d^z$	
Axis	a	a_w	a	a_w	a	a_w	a	a_w
Fore-aft	0.24	0.12	0.40	0.18	0.44	0.18	0.52	0.18
Vertical	0.82	0.59	2.57	2.49	3.21	3.24	3.73	3.82
Pitch	0.69	0.31	2.00	0.57	1.93	0.51	1.88	0.48

The results suggest that softer drum mounts would help reduce the fore-aft and vertical acceleration of the operator-station (cabin). A 25% reduction in the present design stiffness would result in nearly 20% reduction in vertical vibration magnitude at the operator-station. While the effect of mount stiffness on the fore-aft acceleration is very small, the pitch acceleration tends to increase slightly with softer mounts. This is attributable to the pitch dynamics of the vehicle suspended on soft tires only at the rear axle. A major design constraint, however, exists for the lower limit of the drum mounts. Softer rubber mounts would undergo higher deflections particularly under the drum torque (applied on approximately 60% of the mounts on one side of the drum), leading to rapid failure of the rubber mounts. A reduction in the drum mounts stiffness may thus not be considered feasible. The pneumatic tire drum suspension, however, could be an attractive alternative for reducing the transmitted vibration most significantly. The results suggest that the pneumatic tire suspension can reduce the frequency-weighted fore-aft, vertical and pitch rms acceleration to nearly 66%, 20% and 60% of those obtained with the current designs of rubber mounts. Due to increased displacements resulting from the softer suspension, the vibrator hydraulic motor would be mounted onto the sprung front-frame and linked to the eccentric masses by means of universal joints.

Operator-station (Cabin) suspension

The operator-station suspension constitutes a major vibration attenuation stage when the equipment is operated in compaction mode. The current suspensions comprise relatively stiff cab mounts that are considered to be quite effective in attenuating high frequency vibration encountered during the compaction mode. The cabin suspension, however, yield limited performance in attenuation of low frequency ride vibration. The candidate vehicle considered in this study revealed predominant vertical vibration of the operator's platform near 5.5 Hz, which is attributed to the vertical mode resonance of the cabin suspension. The human operator exhibits greatest sensitivity to vertical vibration in the vicinity of this frequency, as evidenced from the W_K filter characteristics (ISO-2631-1, 1971). The current design of the operator-station suspension may thus be considered inadequate in limiting the exposure to WBV along the vertical axis. In this study, the stiffness due to the cab mounts (k_{cj}^x and k_{cj}^z, $j = f, r$) are varied $\pm 25\%$ and -50% of the nominal value. The variation in the damping coefficients are also considered to be proportional, as in the case of the drum suspension. The sensitivity analyses are performed assuming a constant forward speed of 10 km/h while traversing an average road surface (Class C).

Table 5-3 summarises the effect of operator-station suspension parameters on the un-weighted and frequency-weighted rms acceleration responses of the cabin. The results suggest that a softer platform suspension would be beneficial in limiting the vertical and pitch vibration. A 25% decrease in the present design stiffness yield nearly 10% reduction in the un-weighted longitudinal and vertical acceleration and nearly 25% reduction in the pitch acceleration. The soft mounts also yield lower vertical and pitch

mode frequencies of the platform, which would further affect the weighted acceleration values: A further analysis of the resulting response spectra revealed relatively lower bounce and pitch mode frequencies of the operator-station. The lower pitch frequency tends to emphasize the W_e- weighting effect, when magnitude is greater at lower frequencies. The W_K- weighting magnitude, on the other hand, is relatively higher in the 4 - 8 Hz range. A slight reduction in the vertical mode frequency thus does not lead to substantial reduction in the frequency-weighted vertical acceleration. Consequently, the results show that a 25% reduction in the suspension parameter yields relatively smaller changes in the frequency-weighted acceleration, namely nearly 5% , 10% and 15% - reduction in the fore-aft, vertical and pitch weighted acceleration, respectively.

Table 5-3: Influence of variations in the operator-station suspension stiffness and damping on the rms acceleration responses of the model at its floor

Axis	Operator station mounts parameter / nominal value							
	0.50		0.75		1.00		1.25	
	a	a_w	a	a_w	a	a_w	a	a_w
Fore-aft	0.38	0.17	0.39	0.17	0.44	0.18	0.53	0.20
Vertical	2.25	2.22	2.87	2.88	3.21	3.24	3.34	3.38
Pitch	1.03	0.39	1.43	0.43	1.93	0.51	2.54	0.62

A further reduction in the mounts stiffness would be beneficial in limiting the vertical acceleration, as seen in Table 5-3. A 50% reduction in the current suspension parameter yields nearly 30% reduction in both weighted and un-weighted vertical acceleration. The implementation of such soft rubber mount, however, will impose some challenges due to large mount deflection and limited clearance between the conventional operator station

and the main vehicle body. Alternate pneumatic or hydraulic mounts that can provide lower stiffness and higher damping would perhaps be more desirable for the cabin suspension.

Suspension Seat

The medium-size compactors, most widely used in North America, employ a cushioned seat without a suspension. The natural frequency of this seat ranges from 3 to 7 Hz, which would amplify the vertical vibration of the operator station dominant in the 1.5 to 2 Hz (vehicle body vertical mode), 4 - 5 Hz (cab and vehicle body pitch modes), and near 5.5Hz (cabin vertical mode). Alternatively, a suspension at the operator seat has been proven beneficial in limiting the transmission of vertical vibration in many road and off-road vehicle (Rakheja & Sankar, 1984; Boileau, Emile, & Rakheja, 1990). The suspension seats are generally designed with low natural frequency, in the order of 1 to 2 Hz, which would be most effective in attenuating the vertical vibration of the compactor. A suspension seat, however, offers limited suspension travel (in the order of ± 50 mm), and may lead to bump-stop impact when the vehicle operates on relatively rough terrain. A suspension at the seat is thus designed with adequate damping to limit the resonant oscillation.

Table 5-4: Influence of variations in the seat suspension properties on the rms acceleration responses of the model at the operator-seat interface

Axis	Seat suspension properties							
	Nominal (soft cushion seat)		$f_{n_s}^* = 2$ $\zeta_{n\_s}^* = 0.4$		$f_{n_s}^* = 1.5$ $\zeta_{n\_s}^* = 0.3$		$f_{n_s}^* = 1$ $\zeta_{n\_s}^* = 0.2$	
	a	a_w	a	a_w	a	a_w	a	a_w
Vertical	2.72	2.65	1.78	1.58	1.35	1.15	0.88	0.78

In this study, the effect of a suspension seat on the vertical vibration of the operator is evaluated by considering different natural frequencies (1 to 2 Hz) and damping ratios (0.2 to 0.4) of the suspension. The natural frequencies and damping ratios are estimated from the uncoupled 2-DOF suspension-seat-occupant model presented in section 2.2.3, such that:

$$f_{ns}^* = \frac{1}{2\pi}\sqrt{\frac{k_s^z}{(m_h + m_s)}} \qquad (5.4)$$

$$\zeta_s^* = \frac{c_s^z}{2\sqrt{(m_h + m_s)k_s^z}} \qquad (5.5)$$

In the above equation, f_{ns}^* is the natural frequency and ζ_s^* is the uncoupled damping ratio of the seat suspension. m_h and m_s are the masses due to seated operator and the suspension taken as 53.6 and 10.0 kg, respectively (Rakheja, Afework, & Sankar, 1994; Ma, Rakheja, & Su, 2008). K_s^z and C_s^z are the linear stiffness and damping due to suspension.

Table 5-4 summarizes the influence of the seat suspension parameters on the weighted and un-weighted vertical acceleration magnitude of the human occupant mass. The table also presents the acceleration values obtained for an unsuspended seat comprising a softer cushion. The results confirm the expected benefit of a soft suspension. A typical suspension seat with natural frequency of 1.5 Hz and damping ration of 0.3 would yield nearly 50% reduction in un-weighted and 60% in weighted vertical acceleration at the human seat interface. Reduction in the natural frequency to 1 Hz would lead to nearly

70% reduction in the weighted acceleration value, but may induce intermittent shocks due to possible bump-stop impacts.

Axle Suspension

In soil compactors the rear axle is invariably rigidly bolted to the rear frame. Although a number of suspension-axles have evolved for various off-road vehicles employed in the construction sectors, the implementations in the compactors are yet to be explored. Many studies have illustrated the ride benefits of soft axle suspension (Crolla & MacLaurin, 1985; Hansson, 2002; Lehtonen & Juhala, 2005; Rehnberg & Drugge, 2008). Such suspension, however, poses complex challenge in view of the rattle space requirement and reduced effective roll stiffness. Considering the high center of mass of the vehicle and high location of the operator, it is vital to limit the ride height of the vehicle and its roll motion. A relatively stiffer axle suspension is thus considered feasible for such vehicle. Consequently, the sensitivity analysis are performed by considering the axle suspension stiffness being 1 to 3 times the vertical stiffness of the tire, while the suspension damping was selected to achieve the uncoupled vertical mode damping ratio ζ_a of 0.2, which was estimated from:

$$\zeta_a = \frac{c_a}{2\sqrt{(m_2 - m_w)k_a}}$$

(5.6)

Where m_2 is the rear axle static load and m_w the rear axle unsprung mass (wheels), k_a is the axle suspension stiffness.

Table 5-5 summarizes the influence of variations in the suspension stiffness on the fore-aft, vertical and pitch acceleration responses of the operator-station. The table also lists

the un-weighted and weighted acceleration values of the conventional vehicle with unsuspended axle. The research show insignificant effect of the axle suspension with the selected range of parameter. Greater ride benefits may be realized by introducing considerably soft axle suspension, which would yield increased roll and lateral motions and reduced roll stability. The results thus do not justify the complex axle suspension implementations. Furthermore, soft tires would also involve greater compromises in view of traction, tire service life and roll motions, although these could yield benefits in reducing the vertical acceleration.

Table 5-5: Influence of the introduction of a rear axle suspension on the unweighted and weighted rms acceleration responses of the model at the operator-station floor

Axis	Axle suspension properties							
	Unsuspended		$k_a^z = 3.0k_t^z$		$k_a^z = 2.0k_t^z$		$k_a^z = 1.0k_t^z$	
	a	a_w	a	a_w	a	a_w	a	a_w
Fore-aft	0.44	0.18	0.43	0.19	0.43	0.19	0.42	0.20
Vertical	3.21	3.24	3.20	3.24	3.19	3.24	3.19	3.24
Pitch	1.93	0.51	1.91	0.49	1.90	0.47	1.88	0.46

Vehicle wheelbase

Apart from the suspension parameters, the vehicle geometry and inertial properties may also affect the ride performance. Modification in such parameters, however, would involve complex compromises in various other performance measures such as gradeability, serviceability, traction, compaction performance, dimension envelop or material cost and more. In this study, the effect of such variations on the ride quality is assessed, while the variations are limited to somewhat practical ranges. The variation in the wheelbase of the vehicle could be realized by varying the longitudinal portion of the

wheel axle from the central articulation of the vehicle (X_a). Varying the drum position

from the articulation would not be feasible due to various design constraints such as drum

size and the clearance required for the drum scrapers to clean dirt and mud accumulations

on the drum. Furthermore the front-frame of the vehicle is designed to support the drum

with minimum admissible leverage so as to minimize the structure deformation. In terms

of vehicle design and component integration, varying X_a is nothing more than bolting the

rigid axle closer or farther from central hitch of the articulation-steer vehicle. Such a

variation, however, would alter the distribution of the chassis weight on the drum and the

rear axle. The sensitivity analysis is limited $\pm25\%$ variation in X_a about the nominal

value. This variation is equivalent to $\pm13\%$ variation in the wheelbase ($X_a + X_d$).

Table 5-6: Influence of variation in the axle position (X_a) on the unweighted and weighted rms acceleration responses of the model at the operator-station floor

Axle position	0.75 X_a		X_a		1.25 X_a	
Wheelbase ($X_d + X_a$)	0.87 WB		WB		1.13 WB	
c.g. Coordinate	0.71 l_a^*	0.97 l_d^*	l_a^*	l_d^*	1.29 l_a^*	1.03 l_d^*
	a	a_w	a	a_w	a	a_w
Axis — Fore-aft	0.50	0.23	0.44	0.18	0.38	0.17
Axis — Vertical	3.12	3.14	3.21	3.24	3.24	3.27
Axis — Pitch	1.94	0.52	1.93	0.51	1.90	0.52

Table 5-6 summarizes the effect of varying the axle location of the vehicle wheelbase on

the weighted and un-weighted rms acceleration of the operator platform. The table also

lists the resulting variation in the wheelbase and longitudinal coordinate of the mass

center of the equivalent vehicle body (l_a^*, l_d^*). The results suggest $\pm13\%$ variations in the

wheelbase and $\pm 29\%$ variations in the center of gravity coordinate with respect to the axle location. The longitudinal coordinate of center of gravity with respect to drum, however, varies only $\pm 3\%$. Such variations suggest that an increase in X_a would yield a higher load on the drum and a lower vehicle weight on the rear axle. The results presented in Table 5-6 suggest only minimal effect of variation in X_a on the ride responses. A reduction in X_a yields slightly lower vertical acceleration, due to a higher load on the axle tire, but causes slightly greater fore-aft acceleration, due to increased vehicle pitch.

Vehicle Inertias

There are many design constraints that do not allow modifying the coordinate of the machine c.g. without modifying the distribution of the machine mass. The static load on the drum is of particular importance for preservation of compaction efficiency. Modern compactors are increasingly employing modular design approach enabling different motorisations and different drum loads. Such variations in the vehicle design affect the inertial property and mass distribution of the vehicle, as it was illustrated from the simplified 2-DOF model presented in section 2.2.1.

In this study, the effect of vehicle mass/inertia and its distribution is investigated by considering the mass properties of the 4- and 6-cylinder machines, in addition to a heavier 6-cylinder. Three different configurations of the compactor with different vehicle mass distributions are considered for analysis: These configurations include the reference design (6-cylinder), a low-cost design (4-cylinder, shorter rear frame) and an added weight design (heavier front-frame for additional drum static load). These configurations are described below:

Configuration A: 2.5 cm thick and 2.13 m wide drum supported by the standard rear frame of a 6-cylinder engine compactor with standard front frame and open operator platform.

Configuration B: 2.5 cm thick and 2.13 m wide drum supported by the shorter rear frame of a 4-cylinder engine compactor with standard front frame and open operator platform.

Configuration C: 2.5 cm thick and 2.13 m wide drum supported on a standard rear frame of a 6-cylinder engine compactor with a heavier front frame and open operator platform.

Each of the configuration yields differences in the total vehicle mass (m_{tot}), drum load (m_1), and the sprung mass supported on the drum. These parameters are summarized in Table 5-7 for the three configurations. All three configurations use the same vibratory drum. Depending upon the chosen vehicle configuration, the coordinate of the drum (l_d^*) and the axle (l_a^*) with respect to equivalent vehicle body c.g. also vary. Table 5-8 lists the variations in these coordinates of the selected configurations with respect to those of the baseline configuration (l_a^*, l_d^*).

Table 5-7: Vehicle load and load distribution of three selected configurations of typical North-American soil compactors

Configuration	A	B	C
Total mass (m_{tot}), kg	10,750	10,250	11,950
Drum load (m_1), kg	6,120	6,160	7,680
Drum mass (m_d), kg	3,280	3,280	3,280
Sprung mass ($m_1 - m_d$), kg	2,840	2,880	4,400

The results show that the heavier vehicle will pose considerably larger static load on the drum. Moreover, the 4-cylinder machine also places large static load on the drum. The results suggest that a higher drum static load, as realized for the heavier vehicle configuration, would yield 11% and 18% reduction in the un-weighted and weighted vertical acceleration magnitude, respectively. This suggests that a more pronounced weight shift toward the front axle (drum) that is supported on significantly stiffer mounts than the rear axle (tires) enhances the vertical ride quality. The drum suspension natural frequency decreases from about 5 Hz to 4.5 Hz, which is advantageous considering W_k frequency weighting. The greater non-uniformity of the loads distributed on the front and rear axle, however, results in higher pitch motion of the vehicle. This is evident from the increasing pitch acceleration magnitude in Table 5-8. The results suggest nearly 5% and 15% higher un-weighted and weighted pitch acceleration magnitude, when a greater portion of the vehicle mass is supported on the drum, as in the case of the heavier vehicle configuration. The beneficial effect of the higher drum load, however, is not evident for the 4-cylinder machine. This is attributed to lower total mass of the vehicle. A further analysis of the static loads of the vehicle revealed that the drum load of the 4-cylinder machine is only 40 kg higher than that of the baseline machine.

Table 5-8: Influence of variation in the weight distribution on the unweighted and weighted rms acceleration responses of the model at the operator-station floor

Equipment configuration	A		B		C	
	$1.00\ l_a^*$	$1.00\ l_d^*$	$1.17\ l_a^*$	$0.89\ l_d^*$	$1.45\ l_a^*$	$0.72\ l_d^*$
Axis	a	a_w	a	a_w	a	a_w
Fore-aft	0.44	0.18	0.46	0.18	0.36	0.19
Vertical	3.21	3.24	3.21	3.24	2.85	2.68
Pitch	1.93	0.51	1.97	0.53	2.08	0.61

5.3. Factors Affecting Compaction Performance

In the compaction mode, the vehicle is subject to self exciting source of vibration arising from the drum internal unbalance. The total force imparted on the soil arises from the centrifugal force due to the rotating unbalance together with the static vehicle load supported on the drum. The mass unbalance and the eccentricity together with the rotational speed thus form the important design factor. The other factors that would affect the compaction include the weight of the drum (unsprung mass) and the weight distribution of the equipment (drum static load). Apart from these the unsprung/sprung mass ratio (function of drum weight and drum static load) may also affect the compaction. The soil plasticity parameter would be the primary operating condition that would affect the compaction performance. The vehicle speed is not considered as the contributory factor, since soil compaction tasks are invariably performed at very low speed, in the order of 3 km/h or less.

The compaction performance of the vehicle can be best assessed in terms of variations in the soil density (Quibel & Corte, 1994; Briaud & Seo, 2003). The compaction model developed in the present work, however, is limited to the study of dynamic properties of the soil, and is not applicable to evaluate changes in the physical properties of soil such as modulus, density, moisture content and core index. Within the frame of the present modeling effort, the most relevant compaction performance measure would be the vertical plastic deformation of the soil, δ_s^{plast}, under the vibratory drum action, during a given pass and for the soil plasticity parameter, ε. In the compaction multi-body simulation model, the drum displacement z_d is defined with respect to the static drum /

soil equilibrium position (Section 2.3.1). The total displacement of the rigid drum with respect to the initial soil surface prior to the compaction pass considered, can also be evaluated from summation of the dynamic displacement and soil static deflection, $z_d + \delta_s^{stat}$. The final value of the total displacement at the end of the soil unloading or recovery phase (as the drum moves up before a possible take off or immediate re-loading of the soil) would be of primary interest for determining the compaction effectiveness in terms of vertical plastic deformation of the soil. In case of the total recovery, attributed to total unloading caused by the drum-soil loss of contact ("partial uplift" of the drum), the total displacement $(z_d + \delta_s^{stat})$ at the end of the soil unloading would approach δ_s^{plast} for the given pass. In the event of immediate reloading of the soil that is characterized by "continuous contact" between the drum and the soil (Section 4.7), the total displacement $(z_d + \delta_s^{stat})$ at the end of the soil unloading is further reduced by additional soil recovery due to the remaining total force $(F_{s\,Tot})$ exerted on the soil at the end of the unloading phase divided by the soil elastic stiffness k_{se}. The vehicle model, developed in section 2.3, is employed to determine the effect of design parameters on the soil deformation response. It should be noted that the model incorporates the drum-soil interaction through the elasto-plastic soil model.

The study of variations in the operating conditions is limited to varying the plasticity parameter ε of the soil, ranging from 0 to 1. The soil stiffness, however, is increased with the compaction passes, which causes the soil to be more elastic (plastic stiffness increasing more significantly than the elastic stiffness) while the resulting plasticity parameter increases (Adam & Kopf, 2000). The maximum compaction, or otherwise expressed ideal elastic behaviour of the soil is characterised by $\varepsilon = 1$ as $k_{sp} \rightarrow \infty$. Thus

162

varying the plasticity parameter permits the response analysis of the coupled soil-compactor system under varying soil properties at different levels of compaction. It should be further noted that the primary objective of the soil-compaction model formulated in this study is determine the total compaction force and the soil deformation for a given soil property, while the forward motion of the vehicle at very low speed is not considered. In this desertion research, the influence of variations is selected design parameters and soil property is investigated in view of the compaction effectiveness, which is measured in terms of plastic deformation of the soil during a given pass. The results are discussed to enhance an understanding of the present design features on the compaction performance of the vehicle. The same three different configurations of the compactor with different vehicle mass distribution, as detailed in Table 5-7, are considered for analysis. All three configurations use the same vibratory drum. In the road building industry, vibratory compactors are usually characterized by their drum static load m_1, nominal vibration amplitude A_0, vibrator frequency f_v, and the centrifugal force F_{cent}. These parameters cannot be directly related to individual design factors, except for the vibrator frequency, but arise from a combination of design factors. It is thus important to study the effects of the resulting design parameters, influencing the compaction performance, such as front axle (drum) static load, sprung mass supported by the drum, drum (unsprung) mass, vibrator eccentric moment and its frequency.

5.3.1. **Effect of Drum Load**

The drum load directly influences the compaction performance. In terms of machine design, the drum static load is a combination of (i) the unsprung mass m_d or mass of the

vibratory drum including the eccentric vibrator mass; and (ii) the sprung mass ($m_1 - m_d$), which corresponds to the portion of the equipment mass supported by the drum/soil contact dynamically isolated from the vibratory drum by means of the drum suspension. Figure 5-2 illustrates the effect of drum load on the plastic soil deformation, δ_s^{plast}, for varying plasticity parameters of the soil (ε). The results show that the effect of drum load is strongly dependent upon the soil plasticity parameter, saying the degree of compaction or density of the soil. For low plasticity parameters (low density soil), a continuous drum / soil contact condition is realized, irrespective of the drum load considered in the study. This condition yields greatest soil deformation, while a larger drum load (Configuration C) causes higher soil deformation. For intermediate to high plasticity ratios, the compaction yields to partial loss of contact between the soil and the drum, irrespective of the drum load. The compaction of soils with very high plasticity ratio (very high density soil) causes the drum to experience double-jumping condition, as observed earlier in Figure 4-14. This condition yields two plastic deformation values: a lower one attributed to the minor hysteresis loop (superficial impact) and a higher one corresponding to the major loading loop (deep impact). The double-jumping of the drum also yields irregular compaction. In order to avoid this double-jump phenomenon of the drum, the compaction task for high density soils is generally conducted under lower amplitude setting of the vibrator. The finishing stages of the compaction (final passes) are thus frequently performed at lower amplitudes. The results also show that, irrespective of the drum static load, the double-jumping occurs at the same level of soil compaction ($\varepsilon \approx 0.835$).

The Figure also shows the regions of continuous contact, partial loss of contact and "double-jump" of the drum. The results clearly show that greater plastic deformation of

the soil could be achieved during the partial loss of contact or up-lift of the drum, irrespective of the drum load: For medium-density soils, the partial up-lift of the drum occurs under lighter drum load, which could yield higher plastic deformation. A higher drum static load, however, results in noticeably higher plastic deformation on softer soils, where all the machine configurations would operate under a continuous contact condition. It is also noted that all the three configurations yields comparable plastic deformation, as they get to the partial-lift condition.
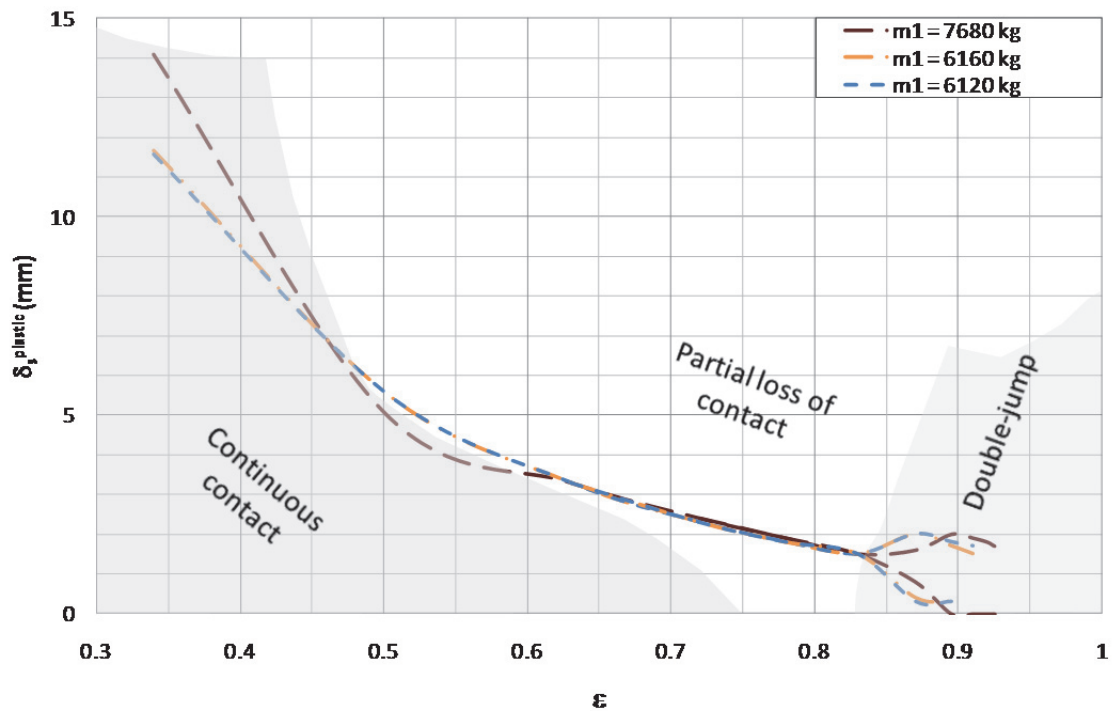
Figure 5-2: Effect of drum static load on the plastic deformation of soils as a function of the soil plasticity parameter (ε).

The results also suggest that an increase in the sprung mass supported by the drum ($m_1 - m_d$) would yield more effective compaction of the soil during the initial pass. A lower drum load, however, result in improved compaction of medium-density soils, when a partial up-lift of the drum occurs. Figure 5-3 further illustrates the influence of sprung

mass supported on the drum on the resulting plastic deformation of soil for different plasticity parameters. The results are presented for the sprung mass due to configurations A and C, which show the lowest (2,840 kg) and highest (4,400kg) sprung mass supported on the drum. As observed earlier, the drum operates in partial up-lift condition for soils of intermediate to high plasticity ratios and yields nearly constant deformation of the soil, irrespective of the available sprung mass. On the other hand, for low plasticity ratios, a higher sprung mass yields greater plastic deformation of the soil. The figure also shows that region of continuous and partial drum-soil contact. The results suggest that the region around the boundary between the two regions would be of primary interest for a plasticity ratio around 0.5. A heavier sprung mass could fall into the continuous contact region and achieve relatively less soil deformation than a lighter sprung mass that operate in the partial up-lift region, thereby offsetting some or all of the beneficial effect during previous pass (passes). Form the results, it is estimated that a sprung mass in the order of 3,700 kg could yield a better compromise, which would also yield a drum static load in the order of 6,980 kg. In some particular applications involving compaction of medium-dense materials or different grades of gravel, the initial plasticity parameter of the soil could be in the intermediate range (0.40 or higher). It would be desirable to target compaction passes in the partial up-lift operating condition, from the initial passes. This would ensure maximum plastic deformation during all the passes. This target condition could be realized with a relatively lower sprung mass in the order of 2,500 kg leading to a total drum static load of 5,780 kg. Apart from the sprung mass, the variation in the unsprung mass could also affect the dynamic behaviour of the vibratory drum, since it

would affect not only the drum static load but also the nominal amplitude of the drum. This effect is discussed in the following subsection.
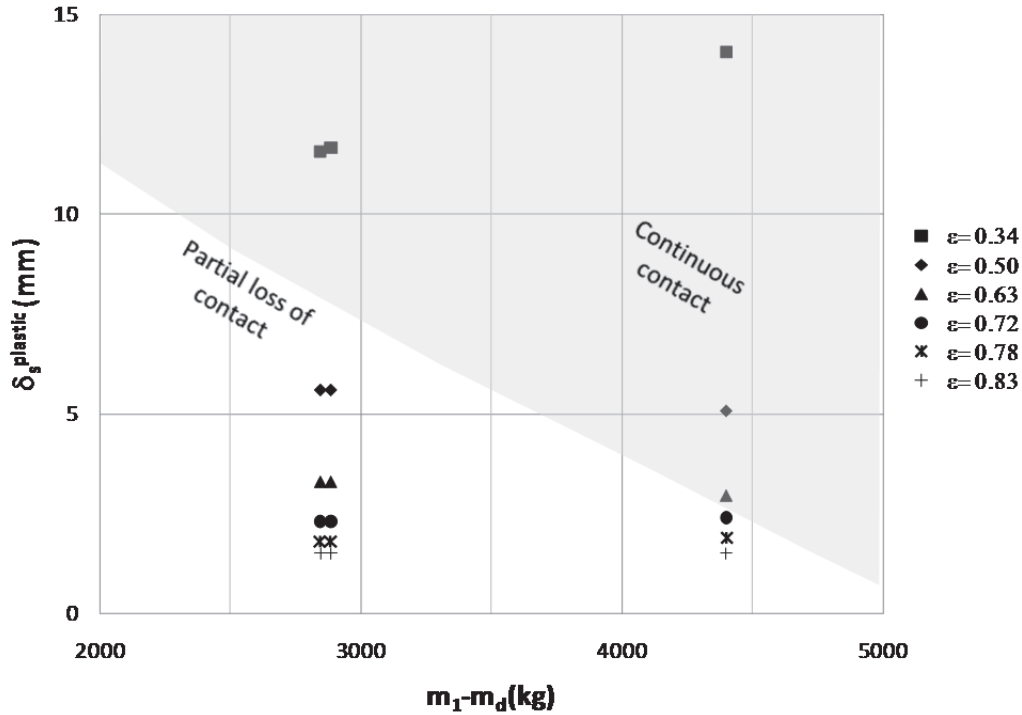
Figure 5-3: Effect of front-axle sprung mass on the plastic deformation of soils

5.3.2. Effect of Nominal Amplitude

From a dynamic standpoint, the primary compaction parameter of a vibratory compactor, as referred to in the industry, is the drum nominal amplitude A_0 (Quibel & Corte, 1994; Valeux & Feistenauer, 1995). In soil compaction, there has been a tendency to increase the compaction by increasing the nominal amplitude. The nominal amplitude has been defined and standardised (ISO 8811, 2000) by and for the construction equipment industry (CIMA, 1994). The rationale for defining nominal amplitude lies in the fact that it is practically difficult to predict the actual amplitude of compaction, which is not only a function of the equipment but also of the dynamic characteristics of the soil being

167

compacted, which itself is a function of many variables including the nature of material (particle size, shape, etc.), layer thickness, moisture content, etc. Furthermore, the dynamic characteristics of the soil being compacted will vary as its density increases with the number of passes. The concept of the nominal amplitude is based on the vibration behaviour of a single-degree-of-freedom (SDOF) system under an internal rotating unbalance. It considers the vibratory drum to be freely suspended in the air, as if the compactor body were lifted from the ground by means of solid supports. Furthermore, the damping due to natural rubber mounts constituting the drum suspension is assumed to be negligible. The drum with its suspension is thus idealized by an un-damped SDOF system subject to forced vibration due to its rotating unbalanced mass. The resulting amplitude of vibration $|z_d|$ is thus expressed as a function of the drum mass m_d, its unbalance (vibrator) eccentric moment $m_v\,e$ and the square of the ratio of the forced vibration frequency f_v and its uncoupled natural frequency $f_{n\,d}^*$, such that:

$$|z_d| = \frac{m_v\,e}{m_d}\left|\frac{1}{1 - \left(\frac{f_v}{f_{n\,d}^*}\right)^2}\right| \qquad (5.7)$$

With

$$f_{n\,d}^* = \frac{1}{2\pi}\sqrt{k_d^z/m_d} \qquad (5.8)$$

The natural frequency of the freely suspended drum, however, is generally very small compared to the vibrator frequency for soil compaction, which yields the amplitude of drum as:

$$A_0 = |z_d| \cong \frac{m_v\, e}{m_d} \tag{5.9}$$

In terms of the sensitivity analysis, the nominal amplitude of vibration could be varied through variation in two design parameters: (i) the drum (unsprung) mass, m_d; and (ii) the vibrator eccentric moment $m_v\, e$. The drum unsprung mass influences the drum static load, which affects the compaction performance of the compactor in a considerable manner, as described in section 5.3.1.
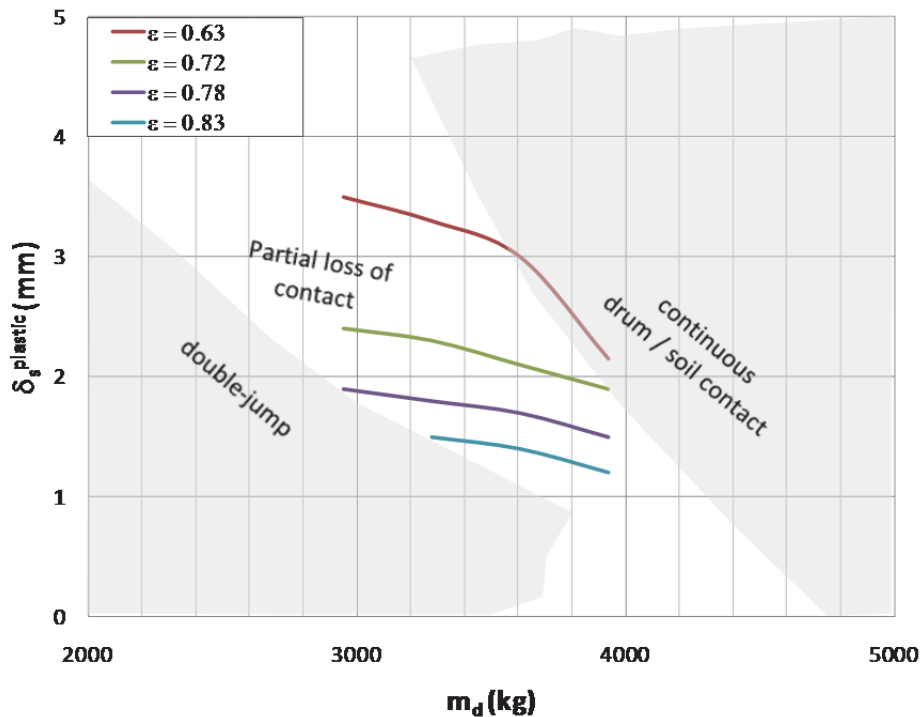
Figure 5-4: Effect of drum unsprung mass on the plastic deformation of soils

In order to study the effect of the unsprung mass alone on the compaction performances of the equipment, the drum shell thickness is varied from 15mm to 40mm for the reference 6-cylinder compactor, these variations yield variations in the drum unsprung mass and the drum static load of –350 kg to 650 kg. The eccentric moment and the frequency of the drum vibrator, however, remain unchanged. Figure 5-4 depicts the

plastic deformation achieved as a function of variations considered in the unsprung mass, for soils at different degrees of compaction. The values of plasticity parameter ε considered correspond to the core of compaction passes, typically intermediate levels of soil stiffness/compaction. The three operation condition regions (continuous contact, partial up-lift and double-jump) appear in the figure, which are shown by shading. A lower unsprung mass tend to encounter double-jumps region, while a higher unsprung mass yields significantly smaller plastic deformation in the continuous contact region. An unsprung mass in the vicinity of 3,500 kg appears to offer a better compromise, which is slightly higher than that of the current design. Furthermore, it should be noted that the compaction performance increases as drum unsprung mass decreases within the partial up-lift region. In addition, as the drum outer shell experiences wear by friction on abrasive soil, while in service, the resulting decrease in the drum unsprung mass would lead to a higher tendency toward double jumping during final compaction passes.

Apart from the unsprung mass, the nominal amplitude of drum vibration is related to drum eccentric moment. The effect of this moment is evaluated for the standard machine (6-cylinder, standard front-frame), by varying the unbalance mass eccentricity e. The unbalanced mass, m_v, however is held constant so as to retain the same total drum mass m_d. Furthermore, the vibrator frequency is also held constant. The eccentricity is varied from 50% of the current design (corresponding to the "low amplitude" setting of the vibrator available on the compaction equipment) to 200% of the current design. The resulting eccentric moment would thus vary from 2.9 kgm to 8.6 kgm.

Figure 5-5 depicts the plastic deformation achieved as a function of the vibrator eccentric moment for soils with different degrees of compaction. The figure also illustrates the

regions of continuous drum-soil contact and partial up-lift. As for the previous analysis, the ranges of plasticity parameter ε considered correspond to typical intermediate levels of soil stiffness/compaction. The results show that reducing the eccentric moment by 50% (the "low amplitude" setting of the vibrator) leads systematically, in terms of operating conditions, to continuous drum/soil contact. An increase in the eccentric moment yields partial lift. Increasing the eccentric moment by 100%, however, does not transform the usual, sought after, partial up-lift condition into double-jumping. The results clearly show that the compaction performance (plastic deformation of the soil) increases with the eccentric moment. A tendency thus exists to increase the eccentric moment. However the eccentric moment is limited due to physical constraints and the corresponding increase in the centrifugal force would require oversized bearings.
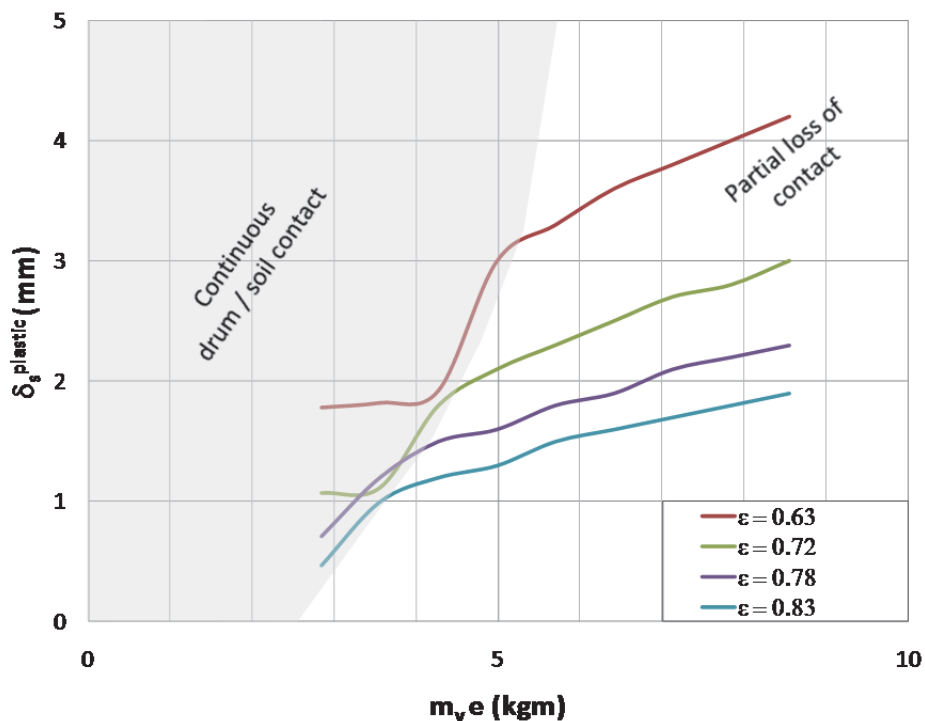
Figure 5-5: Effect of vibrator eccentric moment on the plastic deformation of soils

171

5.3.3. **Effect of Vibrator Frequency**

The vibrator frequency has been the very first design parameter considered to define the compaction performance since the beginning of the vibratory compaction. Decades of field experience and research in soil mechanics (Quibel, Froumentin, & Morel, 1981; Valeux & Feistenauer, 1995; Dynapac, 2000) have converged toward a nearly standardized vibrator frequency of soil compactors around 30Hz for the highest eccentric moment (some machines are equipped with variable frequency settings). Increase in the vibrator frequency, however, is limited due to constraints imposed on the maximum centrifugal force due to the physical constraints on the size of the bearings. It may thus be less cost effective to increase the frequency beyond 35Hz.
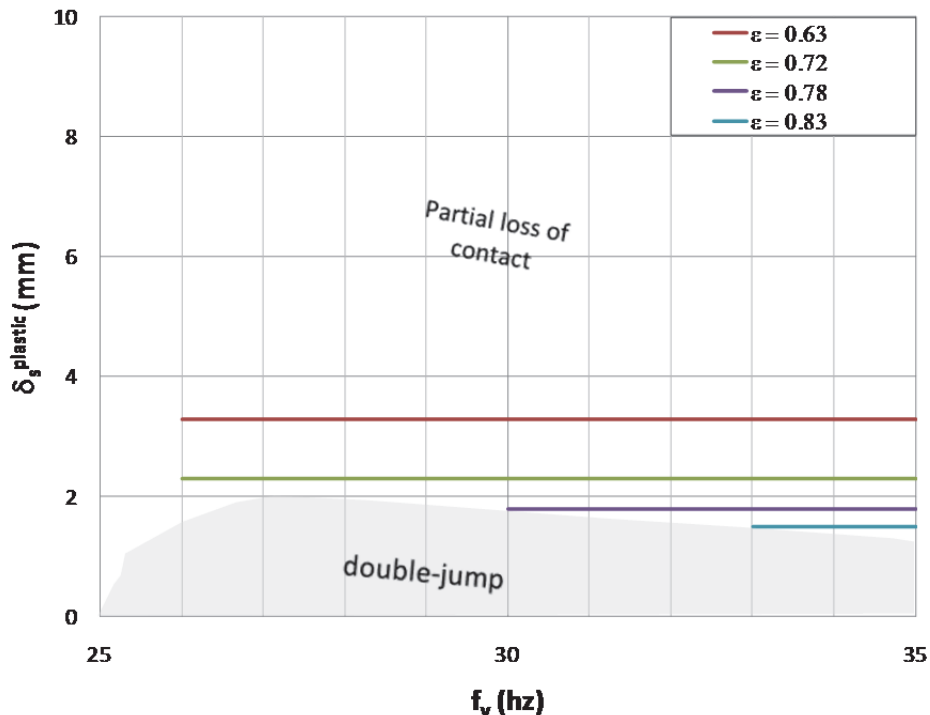
Figure 5-6: Effect of vibrator frequency on the plastic deformation of soils

In this study the impact of vibrator frequency on the compaction performances of the equipment is investigated by varying frequency from 26Hz to 35Hz. The drum (unsprung) mass and the unbalance (eccentric moment) are those of the standard 6-cylinder machine and remain constant. Figure 5-6 depicts the plastic deformation achieved as a function of the vibrator frequency for soils at different degrees of compaction. The values of plasticity parameter ε considered are the same as for the sensitivity analysis of the eccentric moment and the drum mass. It can be noticed that an increase in the soil stiffness leads to a higher tendency towards double-jumping, irrespective of the vibrator frequency. A reduction in the vibrator frequency down to 27Hz, however, yields in double-jumping arising at lower soil compaction level. This is an important fact as an increase in the soil stiffness causes higher loading/resistance for the vibrator from the ground that would require higher engine power and subsequently results in a decrease of the engine rpm, systems hydraulic flow and thus a decrease in the vibrator frequency. The drop in the vibrator frequency would be more probable for the less powerful 4-cylinder motorizations. A frequency setting close to the upper limit considered here (35 Hz) would thus seem to be adequate considering that other than the risk of double jumping the variation in vibrator frequency does not affect compaction performance greatly. The upper limit for frequency setting is governed by bearing size constraints due to the resulting increase in the centrifugal force.

5.3.4. **Effect of Centrifugal Force**

The centrifugal force due to rotating eccentric mass could also affect the compaction performance, although it is directly related to the vibrator frequency and the eccentric moment, such that:

$$F_{cent} = m_v \, e \, (2\pi f_v)^2$$

(5.5)

The effect of both the design factors have been investigated and discussed in section 5.3.2 and 5.3.3 (Figure 5-5 and Figure 5-6). The results have shown that an increase in both the performance and thus the centrifugal force would be justifiable in the context of enhanced soil compaction. Such increases, however, would be limited by the physical constraints of the drum design.

5.4.   **Summary**

The simulation results present evident similarities with measured data although considerable variations in operating conditions and in design parameters have been introduced, both in transit mode and in compaction mode.

In transit mode, the typical North-American soil compactor feature poor ride characteristics that would be hard to accept even though periods of transit of the vehicle are short in duration. If slight improvements could be expected by softening the operator station suspension, some noticeable improvement would be experienced by equipping the vehicle by suspension seats. Further investigations and analyses also led to the possibility of a major breakthrough based on an older European design of the 70s and 80s that

disappeared when its originator went bankrupted: The design involved a pneumatic tire suspension for the vibratory drum.

In compaction mode of operation the efficiency of the vibratory tool was also analysed. It seems that the design of the tool has reached optimum levels in many design aspects. The only area where room for some potential improvement was discovered is the sprung mass supported by the front axle (drum). However, the sprung mass is a global parameter of the heavy equipment and is not limited to a particular part, but is also influenced by the vehicle mass distribution and wheelbase. In terms of design, variations in the sprung mass are highly constrained by other criteria such as gradeability, serviceability, dimensions envelop and material cost.

CHAPTER 6 – CONCLUSION AND RECOMMENDATION FOR FUTURE WORK

This research dissertation permitted a better understanding of the ride and compaction dynamics of a soil compactor, which was achieved through modeling, testing, validation and analysis efforts. The results attained could be interpreted to formulate design guidance for enhancement of ride quality and compaction performance. In the present chapter, the highlights of the research work are summarized together with the major conclusions and some recommendations for future works.

6.1.   Highlights of the present work

The ride and compaction dynamics of typical vibratory soil compactors were investigated experimentally and analytically. Two planar ride dynamic models of the vehicle a 7-degrees-of-freedom bounce and pitch model and a 12 degrees-of-freedom bounce, pitch and fore-aft model, were formulated to study its ride vibration characteristics during the transit mode of operation at relatively higher speeds on undeformable terrain surfaces in the absence of the centrifugal force from the eccentric roller vibrator. These ride models considered the rigid roller drum as the extension of the terrain profile from which the rest of the vehicle was isolated by means of the drum suspension. In the compaction mode, a one-dimensional single DOF dynamic model of the vibratory roller drum interaction with deformable soil in the vertical direction was formulated in the form of a non-linear third order differential equation, the model nonlinearity arose from consideration of the elasto-plastic behaviour of the compacted soil layer and variation in its effective stiffness when loaded and unloaded by the vibratory drum, and possible drum-hop. The non linear third

order equation describing the drum-soil interactions was integrated to the in-plane ride dynamic models to study its dynamic characteristics during compaction mode of the operation at very low speed on deformable soils in the presence of self-generated vibration due to the rotating centrifugal force from the eccentric roller vibrator. The ride dynamic responses of the vehicle during the transit mode of operation were obtained through analyses of both the linear models. The responses during the compaction mode of operation were obtained using only the bounce-pitch plane model (7-DOF) ride dynamic model together with the one dimensional vertical drum-soil interaction model. Both the ride and compaction models were limited to the pitch plane dynamics. The longitudinal shear interactions of the drum and terrain/soil, and the roll/lateral dynamics of the vehicle could not be evaluated. The non-linear compaction model, however, permitted the soil compaction responses for varying soil density.

Extensive field measurement were conducted to quantify the whole-body ride vibration environment of two different compactors along the vertical, lateral, fore-aft , roll and pitch-axes, especially in the transit mode of operation. The elastic vibration isolation mounts between the drum and the chassis, and between the operator station (cabin) and the chassis, generally provided attenuation of higher frequency vibration arising from the drum vibrator in the compaction mode of operation. From the comparisons of the simulation responses and the measured data, it is shown that the models could effectively predict the low frequency vertical and pitch vibration environment, while further efforts in developing a comprehensive three-dimensional model would be desirable. Such a model, when adequately validated, could serve as an important design/assessment tool for design and tuning of the primary and secondary suspensions for enhancement of the

177

vehicle ride quality. The ride dynamic responses of the models showed very good agreements in their natural frequencies with the dominant ride frequencies observed from the measured data, and reasonably good agreements with measured vibration levels in the vertical and pitch axes. The compaction model showed very good agreements with the reported trends depicting the expected energy cycles and forcing frequency harmonics and sub-harmonic (when applicable). In the process of validating the ride dynamic model of the soil compactor in the transit mode, a method for estimating the track profile was formulated using the measured vibration of the rigid drum equipped vehicle.

The proposed pitch-plane ride models of the vehicle were subsequently applied to study the beneficial effects of primary and secondary suspension concepts for enhancement of ride properties of the soil compactors during the transit mode. The proposed pitch-plane compaction model of the equipment also served to study the beneficial effects of different static and dynamic compaction parameters for increasing soil deformation under the equipment action in the compaction mode of operation.

6.2. Major Conclusions

The major conclusions drawn from the study are summarized below:

(a) The whole body vibration levels of the vehicle in transit mode of operation were judged to be relatively high in accordance with the available assessment guidance (ISO 2631-1, 1997 and EN 2002/44/EC, 2002), which could be attributed to relatively higher speed (10 km/h) used in the study. The simulation results suggested that a reduction in the speed to 5 km/h would not yield reduction in the vertical and pitch rms accelerations.

178

(b) The vertical and pitch ride vibration of the vehicle were predominant in the 1.5-6 Hz frequency range, which could be attributed to the vertical and pitch mode resonances of the vehicle body and the operator-station (cabin). Considering that the human body is most sensitive to horizontal and angular vibration in the 0.5 to 2 Hz frequency range and to vertical vibration in the 4–10 Hz range, the adequate selection of vibration isolation stages forms an important design task.

(c) A soft drum suspension would yield most significant benefits in limiting the vertical and pitch acceleration vibrations of the operator-station. The design of a drum integrating a pneumatic tire could yield nearly 80% and 40% reductions in the frequency-weighted vertical and pitch accelerations, respectively, at the operator platform.

(d) The use of a commercially available suspension seat (natural frequency in the order of 1.5 Hz) would also reduce the operator exposure to frequency-weighted vertical acceleration by nearly 60%. A further reduction in the natural frequency to 1 Hz would lead to nearly 70% reduction in the weighted acceleration value. A low frequency suspension seat, however, would require a relatively large suspension travel and space, and may induce intermittent shocks due to possible bump-stop impacts.

(e) The variations in the platform suspension and the axle suspension concept resulted in only limited performance gains in terms of the ride vibration levels. A softer axle suspension, however, could provide enhanced ride quality at the expense of greater roll and thus the lateral motion of the occupant. The results suggest that the implementation of an axle suspension would not be justifiable for soil compactors.

(f) The most effective soil compaction could be achieved when the drum exhibit partial loss of contact with the soil.

(g) The compaction performance of the vehicle is strongly related to the static drum load, drum mass (unsprung) and the vibrator eccentric moment.

(h) An increase in the vibrator frequency resulted in lower double jumping tendencies during the final compaction passes, which could yield more uniform soil compaction.

(i) An increase in the eccentric moment also resulted in enhanced soil compaction. The use of higher eccentric moment and the frequency would, however, yield considering higher centrifugal force and thus require oversized bearing and more expensive power plants.

(j) From the simulation results attained, it is shown that a vibrator frequency of 33 Hz together with an eccentric moment that is 7% higher than that of the baseline machine considered, would offer a feasible combination in view of the soil compaction performance; In view of the static compaction parameters, the results suggest a sprung mass of about 3,700 kg supported by the drum together with the unsprung mass in the vicinity of 3,500 kg, would yield improved compaction. These represent a 30% and a 7% increases over the baseline 10-ton machine, respectively.

6.3. Recommendations for future work

Although the in-plane models developed in this study provided reasonable correlation with the measured data along the vertical and pitch axis, the models could not be applied to evaluate the fore-aft, lateral and roll vibration responses. The measured data revealed

comprehensive levels of lateral and fore-aft vibration. The models presented in this dissertation thus represent a preliminary effort towards assessment and control of whole-body vibration levels of the vehicle. It is thus recommended to develop a three-dimensional ride dynamic model by incorporating the lateral and roll degrees-of-freedom of the vehicle body, operator-station and the engine-group. Furthermore, the contribution due to articulated-frame steering to the ride vibration responses may be considered. Modeling the drum in the roll plane would also permit the consideration of the drum-soil interface by a line contact, which would permit the observation of the rocking motion and chaotic behaviour of the drum in addition to the double-jump behaviour observed in this study.

Further efforts in modeling the drum-soil dynamics would be desirable to enhance the compaction analysis. In particular, the important contribution due to the non-linear soil elastic stiffness attributed mostly to the cylindrical geometry of the drum could be effectively investigated. Considering that the stiffness of the soil depends on the size of the contact surface loaded by the drum, and thus on the drum size, it would be more convenient to express the soil stiffness as a function of its modulus which is a direct indication of soil density for more efficient compaction analyses. A major step in enhancing the modeling of the vibratory compaction process, as described in the present work, would comprise the characterization of coupling between the plastic deformation obtained during a given compaction pass to the resulting plasticity parameter in order to simulate the deformation during a subsequent pass. This would enable the compaction performance analysis in a continuous manner, starting form the first to the final pass. Furthermore, the simulation of the compaction mode of operation could include vehicle

ride dynamics with terrain profile input arising from terrain deformation in process of compaction.

Future work could also be directed towards the equipment design enhancement in enhancing the ride performance. In view of the excellent ride performance potentials of pneumatic drum suspension, it is recommended to undertake further investigation on realisation of such a design. The ride vibration responses of compactors differ most significantly with the mode of operation (transit and compaction): A cab suspension tends to amplify the low frequency transit mode vibration, while it effectively attenuates the higher frequency vibration of the compaction mode. It is thus suggested to explore a two-stage cab suspension, where the normal stage would be tuned for the compaction mode, while the transit mode would require the second stage locked suspension. This dual setting operator-station suspension could have the actual shifting between the two settings controlled by the roller vibrator and / or speed range controller(s). It would be equally interesting to investigate semi-active cabin or seat suspensions using magneto-rheological (MR) shock absorbers with damping characteristics continuously controlled to adapt to the modes of operation.

REFERENCES

EN 2002/44/EC. (2002, 06 25). Directive 2002/44/EC of the European Parliament and of the Council of 25 June 2002. *L 177 (13)* . Official Journal of the European Communities.

ISO 8608. (1995). *Mechanical Vibration - Road Surface Profiles - Reporting of Data.* Standard, ISO, TC108/SC2, Geneva.

Adam, D., & Kopf, F. (2000). Sophisticated Compaction Technologies and Continuous Compaction Control. *European Workshop Compaction of Soils and Granular Materials*, (pp. 207-220). Paris.

Adam, D., & Kopf, F. (2000). Theoretical Analysis of Dynamically Loaded Soils. *European Workshop Compaction of Soils and Granular Materials*, (pp. 3-16). Paris.

Akanda, A. (1999). *Effect of moisture content & clay fraction on the cyclic behavior of soil during compaction.* MS Thesis, University of Oklahoma, CEES, Norman.

Akesson, F. (2008). Dynapac Compaction Analyzer and Optimizer. Texas, USA: Dynapac.

Allen, G. (1978). Part II: A critical look at biodynamic modelling in relation to specifications for human tolerance of vibration and shock. *AGARD Conference Proceedings*, (pp. A25:5-15). Paris.

Andereg, R. (2000). ACE Ammann Compaction Expert-Automatic Control of the Compaction. *Le Compactage des Sols et des Materiaux granulaires*, (pp. 229-236). Paris.

Anderegg, R. (2008). Intelligent Compaction... GPS-based Compaction Control. *TPF ICS initial-TWG meeting* .

Anderegg, R., & Kaufmann, K. (2004). Intelligent Compaction with Vibratory Rollers: Feedback Control Systems in Automatic Compaction and Compaction Control. *Transportation Research Record* (1868), 124–134.

Anderegg, R., & Wehrli, C. (1995). *Optimization of Vibratory Soil Compactors and Measurement of Compaction.* Eidgenössische Technische Hochschule, Zurich.

Anderegg, R., von Felten, D. A., & Kaufmann, K. (2006). Compaction Monitoring Using Intelligent Soil Compactors. *GeoCongress 2006: Geotechnical Engineering in the Information Technology Age*, (pp. 1-6). Atlanta.

Bartlett, N., & Brown, D. (1995, June). Self-levelling suspension for streetwise tractor. *Design Engineering* , pp. 33-34.

Beck, L., Bloswick, D., & Sesek, R. (2004). Health Effects of Vibrating Equipment - A Comparative Analysis of a Caterpillar CS-433B Vibratory Compactor. *2nd Annual*

Regional National Occupational Research Agenda (NORA) Young / New Investigators Symposium. Salt Lake City.

Bekker, M. (1969). *Introduction to Terrain-Vehicle Systems.* Ann Arbor: The University of Michigan Press.

Bernard, B. (1997). *Musculoskeletal disorders and workplace factors.* Cincinnati: National Institute of Occupational Safety and Health.

Bertrand, L., Brzezinski, J., & Rocques, P. (1994). Dynamic simulation of vibratory soil compactor. *Mécanique Industrielle et Matériaux , 47* (2), 318-319.

Best, A. (1984). Vehicle ride-stages in comprehension. (15), 205-210.

Bogdanoff, J., Kozin, F., & Cote, L. (1966). *Atlas of Off-Road Ground Roughness P.S.D.'s and Report on Data Acquisition Technique.* U.S. Army , Tank Automotive Center, Warren, MI.

Boileau, P., Emile, P., & Rakheja, S. (1990). Vibration attenuation performance of suspension seats for off-road forestry vehicles. *Int J of Industrial Ergonomics* (5), 275-291.

Bongers, P. M., Boshuizen, H. C., Hulshof, C. T., & Koemeester, A. P. (1988). Back disorders in crane operators exposed to whole-body vibration. *International Archives of Occupational and Environmental Health* (60), 129-137.

Boulanger, P., Donati, P., & Galmiche, J. (1996). L'Environnement Vibratoire aux Postes de Conduite des Mini-Engins de Chantier. *Cahiers de Notes Documentaires* , pp. 33-38.

Bovenzi, M., & Hulshof, C. (1998). An updated review of epidemiologic studies on the relationship between exposure to whole-body vibration and low back pain. *Journal of Sound and Vibration , 215* (4), 595-611.

Bovenzi, M., Rui, F., Negro, C., D'Agostini, F., Angotzi, G., Bianchi, S., et al. (2006). An epidemiological study of low back pain in professional drivers. *Journal of Sound and Vibration , 298*, 514-539.

Briaud, J.-L., & Seo, J. (2003). *Intelligent Compaction: An Overview and Research Needs.* Texas A&M University. College Station: Texas A&M University.

BS 6841. (1987). British Standard Guide to measurement and evaluation of human exposure to whole body mechanical vibration and repeated shock. British Standards Institution.

Cann, A., Salmoni, A., Vi, P., & Eger, T. (2003). An Exploratory Study of Whole-Body Vibration Exposure and Dose While Operating Heavy Equipment in the Construction Industry. *Applied Occupational and Environmental Hygiene , 18* (12), 999–1005.

Cao, D., Rakheja, S., & Su, C.-Y. (2008). Heavy vehicle pitch dynamics and suspension tuning, Part I: unconnected suspension. *Vehicle System Dynamics , 46* (10), 931-953.

Cashin, E. (2007). Taking the Shakes Out of Construction Trucks. *ANSYS Advantage , I* (4), pp. 10-11.

CIMA. (1994). *vibratory roller handbook.* handbook, CPMTC & BAEB.

Claar II, P. W., Buchele, W. F., & Sheth, P. N. (1980). Off-Road Vehicle Ride: Review of Concepts and Design Evaluation with Computer Simulation. In S. Technical (Ed.), *International Off-Highway Meeting and Exposition MECCA.* Milwaukee: SAE.

Claar, P. W., Sheth, P. N., Buchele, W. F., & Marley, S. J. (1980). Agricultural tractor chassis suspension system for improved ride comfort. *SAE Preprints .* SAE.

Corcoran, P., & Fernandez, F. (2001). *Patent No. 6,188,942.* USA.

Crolla, D. A. (1980). *Vehicle System Dynamics: International Journal of Vehicle Mechanics and Mobility , Volume 9* (Issue 5), 237 – 260.

Crolla, D. A., & MacLaurin, E. B. (1985). Theoretical and practical aspects of the ride dynamics of off-road vehicles—Part 1. *Journal of Terramechanics , 22*, 17–25.

Dale, A. K. (1978). The theoretical prediction of tractor ride vibration. *Inst. of Measurement and Control Symposium "Dynamic analysis of vehicle ride and manoeuvring".* London.

Daniere, P., Robinet, D., Sueur, J., Boulanger, P., Donati, P., Galmiche, J., et al. (1987). L'environnement acoustique et vibratoire aux postes de conduite des engins de terrassement. *Cahiers de Notes Documentaires ,* pp. 63-73.

Delclos, A., Vandanjon, P.-O., Peyret, F., & Gautier, M. (2001). Estimating the degree of compaction of asphalt using proprioceptive sensor and dynamic model. *International Symposium on Automation in Road Construction.* Krakow.

Domenighetti, D. (1985). *Patent No. 4,655,636.* USA.

Donati, P. (2002). Survey of technical preventive measures to reduce whole-body vibration effects when designing mobile machinery. *Journal of Sound and Vibration , 253* (1), 169-183.

Dupuis, H., & Zerlett, G. (1987). Whole-body vibration and disorders of the spine. *International Archives of Occupational and Environmental Health* (59), 323-336.

Dynapac. (2000). *Compaction and paving, theory and practice.* Dynapac Publication.

Els, P. (2005). The applicability of ride comfort standards to off-road vehicles. *Journal of Terramechanics , 42* (1), 47-64.

Erdmann, P., Adam, D., & Kopf, F. (2006). Finite element analyzes of dynamic compaction techniques and integrated control methods. In Schweiger (Ed.), *Numerical Methods in Geotechnical Engineering: Sixth European Conference on Numerical Methods in Geotechnical Engineering* (pp. 197-203). Graz: Taylor & Francis Group.

Farzaneh, O. (1983). *Compactage par vibration des materiaux granulaires, Étude sur le comportement de l'ensemble sol-rouleau vibrant.* Paris: Laboratoire Central des Ponts et Chaussées.

Floss, R., & Kloubert, H. J. (2000). Newest Developments in Compaction Technology. *European Workshop on Compaction of Soils and Granular Materials*, (pp. 247-261). Paris.

Griffin, M. J. (1990). *Handbook of human vibration.* London: Academic Press.

Griffin, M., Howarth, H., Pitts, P., Fischer, S., Kaulbars, U., Donati, P., et al. (2006). *Guide to good practice on whole-body vibration: non-binding guide to good practice for implementing Directive 2002/44/EC on the minimum health and safety requirements regarding the exposure of workers to the risks arising from physical agents (vibrations).* Brussels: European Commission.

Guillo, E., Gautier, M., & Boyer, F. (1999). Dynamic Modelling and Simulation of a Compactor. *14th IFAC World Congress.* Beijing.

Guillo, E., Gautier, M., & Froumentin, M. (1999). Dynamic modelling and identification of a compactor. *International Symposium on Automation in Road Construction.* Madrid.

Hansson, P.-A. (1996). Rear axle suspension with controlled damping on agricultural tractors. *Computers and Electronics in Agriculture , 15*, 123–147.

Hansson, P.-A. (2002). Working Space Requirement for an Agricultural Tractor Axle Suspension. *Biosystems Engineering , 81* (1), 57-71.

Hohl, G. (1984). Ride comfort of off-road vehicles. *Proceedings of the 8th international conference of the ISTVS. 1*, pp. 413-432. Cambridge: International Society for Terrain Vehicle Systems.

IEC 61260. (1995). Electroacoustics- Octave-band and Fractional-Octave-Band Filters. *IEC 61260 .* Geneva, Switzerland: International Electrotechnical Commission.

ISO 10326-1. (1992). Mechanical vibration -- Laboratory method for evaluating vehicle seat vibration -- Part 1: Basic. Geneva: ISO.

ISO 2631-1. (1997). Mechanical vibration and shock – Evaluation of human exposure to whole-body vibration-Part 1: General requirements. Geneva: ISO.

ISO 8811. (2000). Earth-moving machinery -- Rollers and land-fill compactors -- Terminology and commercial specifications. *ISO Standards .* Geneva: ISO.

ISO. (1982). *Reporting Vehicle Road Surface Irregularities.* ISO, TC108/SC2, Geneva.

Kabré, H. (1991). *Contribution à l'étude du comportement au compactage des matériaux granulaires pour assises de chaussées.* PhD Thesis, Université de Nantes, Formation doctorale Génie Civil, Nantes.

Kittusamy, N. (2003). A checklist for evaluating cab design of construction equipment. *Applied Occupational and Environmental Hygiene , 18* (10), 721-723.

Kittusamy, N. K., & Buchholzb, B. (2004). Whole-body vibration and postural stress among operators of construction equipment: A literature review. *Journal of Safety Research* (35), 255-261.

Kloubert, H. J. (2004, January 11-15). Bomag IC System. *TRB annual meeting .* Washington D.C., Washington D.C., USA.

Krober, W., Floss, R., & Wallrath, W. (2001). Dynamic Soil Stiffness as Quality Criterion for Soil Compaction. *4th Int. Symposium "Technik und Technologie des Verkehrswegebaus" Bauma 2001*, (pp. 51-62). Munich.

Laib, L. (1995). Analysis of the vibration-excitation effect caused by deformable soil surfaces. *Journal of Terramechanics , 32* (3), 151-163.

Lay, M. G. (2009). *Handbook of Road Technology* (4th ed.). Routledge.

Lehtonen, T. J., & Juhala, M. (2005). Predicting the ride behaviour of a suspended agricultural tractor. *Int. J. Vehicle Systems Modelling and Testing , 1* (1/2/3), 131-142.

Lehtonen, T. (2005). Validation of an agricultural tractor MBS model. *International Journal of Heavy Vehicle Systems , 12* (1), 16-27.

Lemaire, C. E., Vandanjon, P. O., & Gautier, M. (2005). Dynamic Modelling of a Vibratory Asphalt Compactor and Estimation of Contact Forces Wrench. *16th International Federation of Automatic Control World Congress.* Prague.

Lemaire, C.-E., Vandanjon, P.-O., & Gautier, M. (2003). Dynamic identification of a compactor using splines data processing. *System Identification.* Rotterdam.

Lemaire, C.-E., Vandanjon, P.-O., Gautier, M., & Lemaire, C. (2006). Dynamic identification of a vibratory asphalt compactor for contact efforts estimation. *IFAC Symposium Modelling, Identification and Signal Processing (SYSID 2006) Identification and System Parameter Estimation.* Newcastle.

Lemaire, C.-E., Vandanjon, P.-O., Gautier, M., & Peyret, F. (2002). Motion planning taking into account the dynamic model of vehicles : application to the compactor. *ISARC 2002: 19th International Symposium on Automation and Robotics in Construction*, (pp. 223-228). Gaithersburg.

Lowell Beck, D. S. (2004). Health effects of vibrating equipment - a comparative analysis of a Caterpillar CS-433B vibratory compactor. *National Occupational Research Agenda (NORA)* . Salt Lake City.

Ma, X., Rakheja, S., & Su, C.-Y. (2008). Damping requirement of a suspension seat subject to low frequency vehicle vibration and shock. *Int. J. Vehicle Design , 47* (1/2/3/4), 133–156.

Mooney, M. A., Gorman, P. B., & Gonzalez, J. N. (2005). Vibration-based Health Monitoring of Earth Structures. *Structural Health Monitoring , 4* (2), 137–152.

Mooney, M., & Rinehart, R. (2007). Field Monitoring of Roller Vibration during Compaction of Subgrade Soil. *Journal of Geotechnical Geoenvironmental Engineering* (133(3)), 257–265.

Paddan, G. S., & Griffin, M. J. (2002). Evaluation of whole-body vibration in vehicles. *Journal of Sound and Vibration , 253* (1), 195-213.

Paddan, G., & Griffin, M. (2002). Effect of seating on exposures to whole-body vibration in vehicles. *Journal of Sound and Vibration , 253* (1), 215-241.

Paramythioti, M., & Girard, J. (1973). Les engins de compactage en construction routière. *Travaux La Route* (1973).

Peng, C., & Lines, J. A. (1997). Ground induced vibration on unsuspended agricultural tractors. *Heavy Vehicle Systems, International Journal of Vehicle Design , 4* (2-4), 166-182.

Pietzsch, D., & Poppy, W. (1992). Simulation of soil compaction with vibratory rollers. *Journal of Terramechanics , 29* (6), 585-597.

Popa, G., & Nicoara, S.-V. (2002). Study of a Soil − Vibratory Roller Response. *Ovidius University Annals of Constructions , 1* (3).

Pradko, F., & Lee, R. (1966). *Vibration comfort criteria.* Society of Automotive Engineers. Warrendale: SAE Technical .

Quibel, A., & Corte, J.-F. (1994). Modelisation pratique du compactage par vibration. *Bulletin de Liaison des Laboratoires des Ponts et Chaussees* (192), 27-35.

Quibel, A., Froumentin, M., & Morel, G. (1981). *Le vibrex Influence des paramètres d'un rouleau vibrant sur l'efficacité du compactage.* Paris: Laboratoire Central des Ponts et Chaussées.

Rakheja, S., & Sankar, S. (1984). Suspension design to improve tractor ride: II passive cab suspension. *SAE Transactions* (4), 1105–1112.

Rakheja, S., Afework, Y., & Sankar, S. (1994). An Analytical and Experimental Investigation of the Driver-Seat-Suspension System. *Vehicle System Dynamics , 23* (1), 501 — 524.

Rehnberg, A., & Drugge, L. (2008). Ride comfort simulation of a wheel loader with suspended axles. *Int. J. Vehicle Systems Modelling and Testing , 3* (3), 168-188.

Rinehart, R. V., & Mooney, M. A. (2008). Instrumentation of a roller compactor to monitor vibration behavior during earthwork compaction. *Automation in Construction , 17* (2), 144–150.

Sandström, Å. (1994). *Numerical simulation of a vibratory roller on cohesionless soil.* Geodynamik. Tullinge: Geodynamik.

Scherocman, J. A., Rakowski, S., & Uchiyama, K. (2007). Intelligent Compaction, Does It Exist? *Canadian Technical Asphalt Association*, (pp. 373–398). Niagara Falls.

Seidel, H. (1993). Selected health risks caused by long-term whole-body vibration exposure. *American Journal of Industrial Medicine , 23*, 589-604.

Sharp, R. (2002). Wheelbase Filtering and automobile suspension tuning for minimizing motions in pitch. *Proc Instn Mech Engrs , Vol 216* (12), 933-946.

Soliman, A. M., Monstafa, S. M., El-Sayed, F. M., & El-Gawwad, K. (1995). Experimental and analytical study of the tractor ride comfort. *Heavy Vehicle Systems , 2* (1), 58-76.

Stayner, R., Hilton, D., & Moran, P. (1975). Protecting the tractor deriver from low frequency ride vibration. *Institution of Mechanical Engineers Conference on "Off-highway vehicles, tractors and equipment".* London: Institution of Mechanical Engineers.

Tateyama, K., Ashida, S., Fukagawa, R., & Takahashi, H. (2006). Geomechatronics - Interaction between ground and construction machinery and its application to construction robotics. *Journal of Terramechanics , 43* (3), 341-353.

Terzaghi, K., Peck, R., & Mesri, G. (1996). *Soil Mechanics in Engineering Practice* (3rd ed.). New York: John Wiley & Sons, Inc.

Thurner, H. F. (2001). Quality Assurance and Self Control in Road Construction, Advanced Measurement Technology. *4th International Symposium "Infrastructure Construction Systems and Technologies"*, (pp. 73-81). Munich.

Timoney Mobility Systems. (n.d.). *Articulated Dump Truck Independent Suspension.* Retrieved 03 18, 2010, from www.timoneygroup.com

Valeux, J.-C., & Feistenauer, H. (1995). *Savoir Compacter.* Hamm Walzenfabrik GmbH.

VDI 2057. (1987). Effect of Mechanical Vibrations on Human Beings. Dusseldorf: Verein Deutscher Ingenieure.

VDI. (1963). Human exposure to mechanical vibrations - Whole-body vibration. Dusseldorf: VDI Verlag GmbH.

Weber, M. (2008). *AN21E - EC Directive 2002/44/EC.* Metra Mess- und Frequenztechnik, Human Vibration Measurement . Radebeul: Metra Mess- und Frequenztechnik.

Wikström, B. (1993). Effects from twisted postures and whole-body vibration during driving. *International Journal of Industrial ergonomics* (12), 61-75.

Wong, J. (2001). *Theory of Ground Vehicles.* New York: John Wiley & sons, Inc.

Wu, X., & Griffin, M. J. (1996). Towards the Standardization of a Testing Method for End-stop Impacts of Suspension Seats. *Journal of Sound and Vibration , 192*, 307–319.

Wu, X., & Griffin, M. (1998). The Influence of End-stop Buffer Characteristics on the Severity of Suspension Seat End-stop Impacts. *Journal of Sound and Vibration , 215*, 989–996.

Wu, X., Rakheja, S., & Boileau, P. (1999). Dynamic Performance of Suspension Seats Under Vehicular Vibration and Shock Excitations. *Proceedings of the International Congress & Exposition.* Detroit.

Yoo, T.-S., & Selig, E. T. (1979). Dynamics of Vibration-Roller Compaction. *Journal of the Geotechnical Engineering Division , 105* (10), 1211-1231.